ERDC/CHL TR-14-14

Coastal and Hydraulics Laboratory

US Army Corps of Engineers®
Engineer Research and Development Center

ERDC
INNOVATIVE SOLUTIONS for a safer, better world

Monitoring Completed Navigation Projects Program

Houston-Galveston Navigation Channel Shoaling Study

Jennifer Tate, Brittany Gunkel, Julie Rosati, Eric Wood, Alejandro Sanchez, Rob Thomas, Naveen Ganesh, and Thad Pratt

December 2014

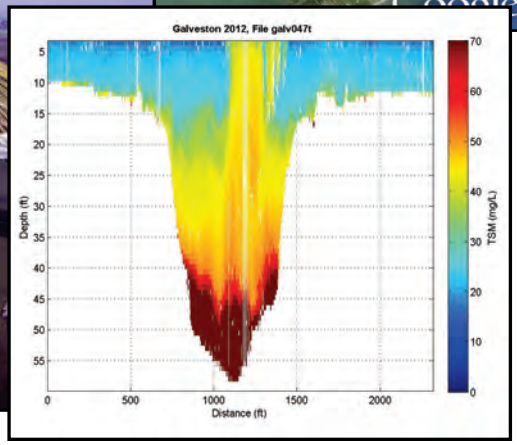

The US Army Engineer Research and Development Center (ERDC) solves the nation's toughest engineering and environmental challenges. ERDC develops innovative solutions in civil and military engineering, geospatial sciences, water resources, and environmental sciences for the Army, the Department of Defense, civilian agencies, and our nation's public good. Find out more at www.erdc.usace.army.mil.

To search for other technical reports published by ERDC, visit the ERDC online library at http://acwc.sdp.sirsi.net/client/default.

ERDC/CHL TR-14-14
December 2014

Houston-Galveston Navigation Channel Shoaling Study

Jennifer Tate, Brittany Gunkel, Julie Rosati, Alejandro Sanchez,
Naveen Ganesh, and Thad Pratt

Coastal and Hydraulics Laboratory
U.S. Army Engineer Research and Development Center
3909 Halls Ferry Road
Vicksburg, MS 39180

Eric Wood and Rob Thomas

U.S. Army Engineer District, Galveston
PO Box 1229
Galveston, TX 77553-1229

Final report

Prepared for U.S. Army Corps of Engineers
Washington, DC 20314-1000

Abstract

The Monitoring Completed Navigation Projects (MCNP) program evaluates the performance of civil works navigation projects to advance coastal and hydraulic engineering technology and guidance. Monitoring is designed to understand how well projects are achieving their design goals to ultimately develop more accurate and cost-effective engineering solutions for U.S. Army Corps of Engineers (USACE). The monitoring program also identifies where present technology is inadequate or where additional research is required.

The Houston-Galveston Navigation Channel (HGNC) MCNP study was initiated in 2009 to determine the causes of an unanticipated increase in channel shoaling that occurred after deepening and widening was completed in 2005. Recent deepening and widening of the HGNC was authorized to accommodate larger vessels and meet safety and efficiency requirements of the Port of Galveston and Port of Houston.

When designing the most recent channel improvement, the USACE, Galveston District, calculated future shoaling and the associated required placement area capacity based on historical O&M data. The final design estimated 1.42 million cubic yards per year maintenance dredging for the 45 × 530 foot channel, whereas the actual has been estimated by some methods to be much more.

Nine hypotheses were developed to explain the unanticipated increase in navigation channel shoaling after channel improvements. These hypotheses were tested through historical analysis, field data collection, and numerical modeling. Goals of the study were to determine why the HGNC is shoaling more than anticipated as well as to develop standards to aid future channel enlargement O&M plans.

Contents

Figures and Tables

Figures

Tables

Preface

This investigation was conducted from October 2009 through September 2012 at the U.S. Army Engineer Research and Development Center (ERDC) by Jennifer N. Tate, Brittany Gunkel, Dr. Julie D. Rosati, Dr. Alejandro Sanchez, Thad Pratt, and Naveen Ganesh of the Coastal and Hydraulics Laboratory (CHL), and by Eric Wood and Rob Thomas of the U.S. Army Engineers District, Galveston. The field data collection was conducted from May through June 2010, April through September 2011, and May 2012. Funding was provided by the Monitoring Completed Navigation Projects (MCNP) program, which is administered for U.S. Army Corps of Engineers, Headquarters (USACE HQ) by ERDC, CHL, Vicksburg, MS, under the Navigation Program of USACE HQ. Jeffrey A. McKee was USACE HQ Navigation Business Line Manager overseeing the MCNP. W. Jeff Lillycrop, CHL, was the ERDC Technical Director for Navigation. Dr. Lyndell Z. Hales, CHL, was the MCNP Program Manager.

The work was performed under the general direction of Dr. William D. Martin, former Director; José E. Sánchez, Director and former Deputy Director; and Dr. Kevin Barry, Deputy Director of CHL. At the time of publication, Dr. Ty V. Wamsley was Chief of the Flood and Storm Protection Division, CHL; Dr. Jackie Pettway was Chief of the Navigation Division, CHL; Mark Gravens was Chief of the Coastal Processes Branch, CHL; James Gutshall was Chief of the Harbors, Entrances, and Structures Branch, CHL; and Dr. Robert McAdory was Chief of the Estuarine Engineering Branch, CHL.

At the time of publication, Dr. Jeffery P. Holland was Director of ERDC, and COL Jeffrey R. Eckstein was Commander and Executive Director.

Unit Conversion Factors

Multiply	By	To Obtain
cubic feet	0.02831685	cubic meters
cubic yards	0.7645549	cubic meters
feet	0.3048	meters
miles (U.S. statute)	1,609.347	meters
miles per hour	0.44704	meters per second
square miles	2.589998 E+06	square meters
tons (2,000 pounds, mass)	907.1847	kilograms

1 Introduction

Overview of study

The Monitoring Completed Navigation Projects (MCNP) program evaluates the performance of civil works navigation projects to advance coastal and hydraulic engineering technology and guidance. Shallow- and deep-draft navigation projects located in rivers, reservoirs, lakes, estuaries, and the coastal zone have been monitored by the MCNP (or its predecessor, the Monitoring Completed Coastal Projects (MCCP)) program. Monitoring is designed to understand how well projects are achieving their design goals to ultimately develop more accurate and cost-effective engineering solutions for U.S. Army Corps of Engineers (USACE) coastal and hydraulic problems. Through the MCNP, design criteria and methods, construction practices, and Operation and Maintenance (O&M) techniques are improved. The monitoring program also identifies where present technology is inadequate or where additional research is required. MCNP projects are nominated by USACE District offices and selected for study by USACE, Headquarters (USACE HQ).

The Houston-Galveston Navigation Channel (HGNC) MCNP study was initiated in 2009 to determine the causes of an unanticipated increase in channel shoaling that occurred after deepening and widening was completed in 2005. Commercial traffic in Galveston Bay began in 1837 through a shallow, natural channel. Since the 1870s, expansions of the HGNC system and the Port of Houston have been inherently related to the growth of Houston as a center for national commerce, including a national center for oil and gas distribution. Recent deepening and widening of the HGNC was authorized for construction on 12 October 1996 to accommodate larger vessels and meet safety and efficiency requirements of the Port of Galveston and Port of Houston. Presently, the Galveston Harbor and Channel and Houston Navigation Channel are ranked second and third, respectively, in the nation with nearly 200 million tons of commerce for the period 2001–2005.

Project location and background

Since the early 1800s, vessels have transited Galveston Bay both to and from Galveston and Houston (Galveston Bay Estuary Program 2002).

Galveston Bay is a microtidal, diurnal, wind-dominated, lagoon-type estuary with a 1.4 f00t (ft) diurnal tide range (National Oceanographic and Atmospheric and Association (NOAA) 2014). The earliest improvements to the navigation channel were in the early 1870s to widen and deepen the channel (Alperin 1977). Presently, the HGNC extends approximately 60 miles from the 45 ft depth contour in the Gulf of Mexico to Houston, TX. The portion of the HGNC extending from offshore to the entrance is called the Galveston Entrance Channel. The Entrance Channel traverses through Galveston Inlet, also called Bolivar Roads, which is bordered by Bolivar Peninsula to the northeast and Galveston Island to the southwest (Figure 1). Two jetties approximately 6,900 ft apart were constructed in the 1880–1890s to stabilize the entrance channel. The north and south jetties are 4.9 and 6.8 miles in length, respectively. Net longshore sand transport is from north to south, although a reversal in direction occurs southwest of the Entrance, so that net transport is effectively into the inlet from both sides. Figure 2a is an image of the south jetty after Hurricane Claudette (27 July 2003) showing sand transport over and through the structure (Morang 2006).

Sand dredged offshore is placed in a beneficial use berm located southwest of the channel in depths ranging from 26–47 ft relative to mean lower low water (MLLW). Sand transport over and through the jetties, particularly the south jetty, occurs especially during energetic conditions and elevated water levels. Big Reef is often mined and sand back-passed (placed updrift) to the south (Figure 2b).

The Houston Ship Channel (HSC) continues through Galveston Bay to Houston, TX, as shown in Figure 3. Since 1903, O&M dredging has been conducted in the bay to maintain authorized channel dimensions. Sediment dredged in the bay, primarily silt and clay, has been used beneficially to create and restore islands in the bay, such as Atkinson Island.

When designing the most recent channel improvement, the USACE, Galveston District (SWG), calculated future shoaling and the associated required placement area capacity based on historical O&M data. Trawle's (1981) method was applied to estimate shoaling with the deepening and widening in which a quadratic relationship was formulated based on the cumulative New Work volumes (volume of cut) and associated historical shoaling rates. Maintenance dredging is removal of sediment that shoals in the channel, whereas New Work dredging is the quantity that is removed to

Figure 1. Galveston Entrance Channel, Big Reef, and Beneficial Use Berm.

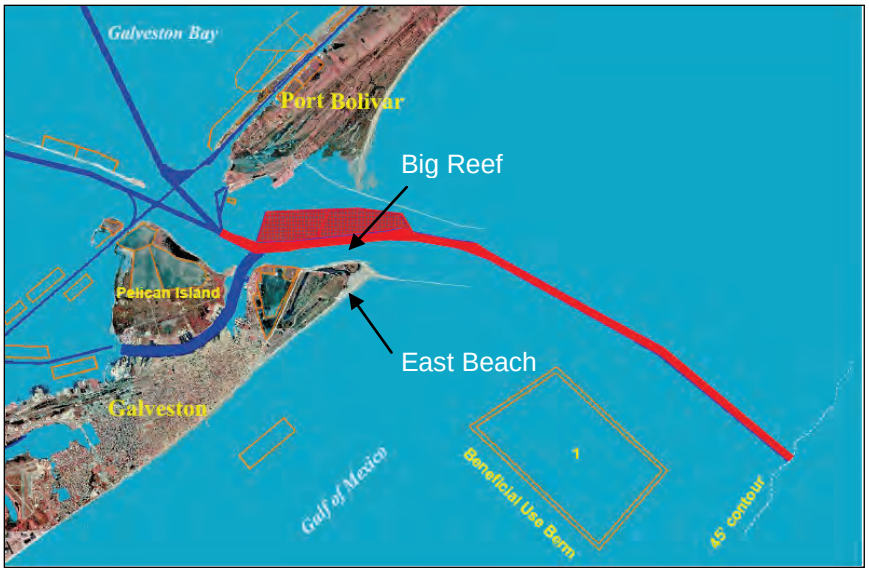

Figure 2. Sand transport and operations in the vicinity of Galveston Entrance Channel.

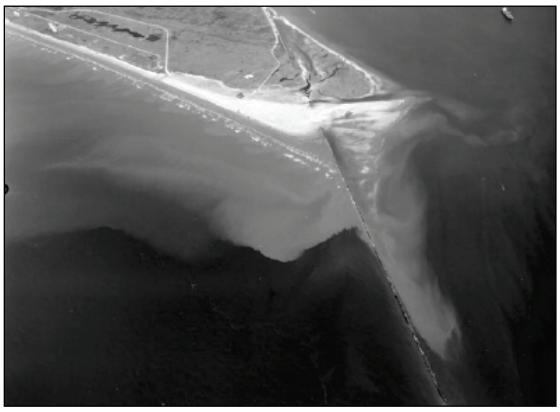

a. South jetty after Hurricane Claudette (27 July 2003), showing sand transport over and through the structure (Morang 2006).

b. Mining of Big Reef and back-passing sand to the south (20 March 2009).

Figure 3. Location map of HSC and Atkinson Island placement sites.

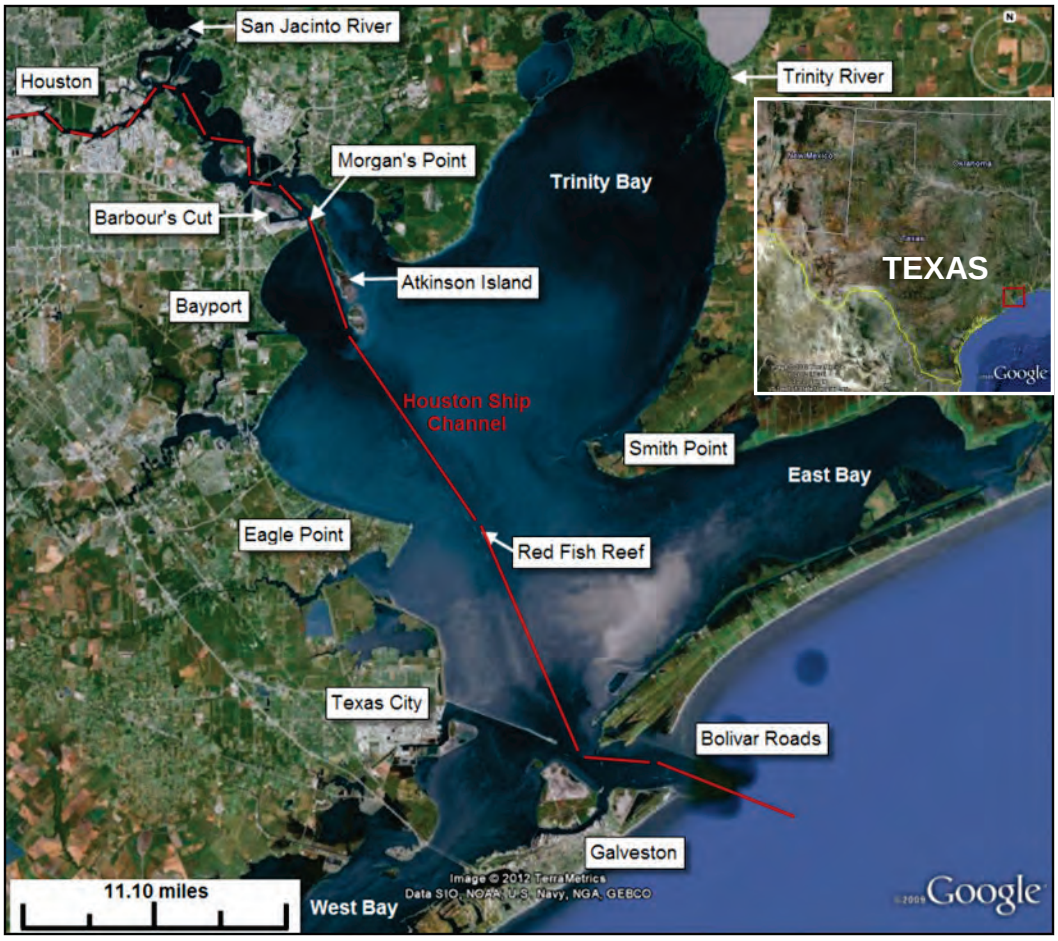

deepen, widen, and/or lengthen a channel. With Trawle's Method, each shoaling volumetric rate was weighted according to the number of O&M dredging events for that channel dimension. The District anticipated that the trends from 1948 through 1995 would continue, and the only increase in O&M dredging would be caused by the lengthening of the channel offshore. However, for the estuarine portion of the channel (the area inland of Bolivar Island up to approximately Morgan's Point, including Galveston Bay and Trinity Bay), shoaling rates were projected to *decrease* 20% because of confined dredged material practices that would reduce loss of sediment during the dredging process. The final design estimated 1.42 million cubic yards per year (myd^3/yr) maintenance dredging for the 45 × 530 ft channel, whereas the actual has been estimated at approximately 4 myd^3/yr.

Hypotheses and goals

Nine hypotheses were developed to explain the unanticipated increase in navigation channel shoaling after channel improvements. These hypotheses

were tested through historical analysis, field data collection, and numerical modeling. The hypotheses were organized by channel location:

Galveston Entrance Channel

1. Dispersion of the Beneficial Use site moves sediment into the entrance channel.
2. Sand is transported over, through, or around the Entrance Channel jetties.
3. Significant sand volume moves through Bolivar Roads and into the bay/estuary channel.

Houston Ship Channel

1. Sediment is resuspended with wind-generated waves in the bay and trapped more efficiently in the deeper/wider channel.
2. Vessel passage has increased the erosion of the bay and generates hydrodynamics that aid sediment transport into the channel.
3. Subsidence and anthropogenic effects such as shrimp trawling and disposal practices have generated more sediment, which is transported into the channel.
4. Enlargements to Atkinson Island for additional disposal sites negatively impacts channel shoaling.
5. High river flow triggers sedimentation and possible fluid mud formation in the Bay, which is not represented in numerical models and simple estimators.
6. Sediment properties differ in spring months when Gulf of Mexico salinity is lower and there are high flows on rivers.

Goals of the study were to determine why the HGNC is shoaling more than anticipated by the pre-enlargement analysis and planned disposal practices as well as to develop standards to aid future channel enlargement O&M plans. These methods were based on analytical computations, modeling, and field data analysis.

Project monitoring and analysis

Three separate field monitoring studies were conducted to collect field data on hydrodynamics, sediment properties, sediment loads into the HGNC system, and the possible existence of fluid mud which may transport into the channel and give a false indication of decreased channel

depth. The monitoring events occurred over 3 yr and focused separately on the entrance channel and the bay.

Report organization

This report is organized into seven chapters:

- Chapter 1 is this introduction, background information, and outline of hypotheses.
- Chapter 2 provides details on the history of the HSC.
- Chapter 3 details the three monitoring and data collection efforts.
- Chapter 4 describes the vessel data analysis process and findings.
- Chapter 5 provides the details of the numerical modeling of the entrance channel and the estuarine channel to include model setup and validation.
- Chapter 6 presents results of the proposed hypotheses and recommendations.
- Chapter 7 summarizes conclusions of the study.

2 History of Navigation Channel

Overview

This chapter presents the history of channel improvements and the resulting O&M of the channel. Previous studies evaluating the channel and placement sites are reviewed. Methods that have been applied in the past to estimate with-project channel shoaling are reviewed and evaluated with the available history.

Behavior of Galveston Bay

Galveston Bay is a tidal estuary such that the effect of the tide on the water surface elevation is observed from the Gulf of Mexico to locations near Houston, TX. The HSC is a deep-draft navigation channel that allows for vessel passage from the Gulf to the city of Houston, approximately 53 miles upstream. The navigation channel acts as a flow pathway for salinity to travel upstream since high-saline water is heavier than fresh water and tends to flow upchannel along the channel bottom. The net drift is flood in much of the channel (Tate and Berger 2006) (i.e., the tendency is for suspended material to move upstream into the bay.) The current magnitudes drop in the Atkinson Island reach due to tidal reflections from the bay boundary. The flow tends to stratify more as a result in this reach, and material from farther downstream in the estuary will tend to collect near Atkinson Island.

The behavior of the salinity and hydrodynamics in Galveston Bay during May through June is different than the remainder of the year due to a salinity drop in the northern Gulf of Mexico as the Mississippi, Sabine-Neches, Atchafalaya, and other northern Gulf river systems provide a significant influx of fresh water. When the salinity in the Gulf of Mexico drops, the salt water tends to evacuate from the bay. A reduction in bay salinity could result in different suspended concentrations and fresh deposit characteristics during this time period compared to data collected at other times during the year. If this is the case, sediment would tend to collect farther down the channel toward Red Fish Reef during this period.

History and previous studies

The HGNC has been deepened and widened from the natural bay depth of 4 ft and width of 70 ft in the 1800s to the present 45 ft depth (relative to mean low tide (MLT) a local navigation datum) and 530 ft width, as presented in Table 1. In this section, previous studies are reviewed that have been conducted to understand the HGNC sediment transport system.

Table 1. HGNC dimensions* and previously estimated shoaling rates.

Date	Depth, ft MLT	Width, ft	Shoaling Rates, yd^3/yr (Gahagan and Bryant 2008)		
			Bayou Reach	Bay Reach	Entrance Reach
1851	4	--	-	-	-
1870	4	70	-	-	-
1874	9	120	-	-	-
1889	12	100	-	-	-
1893	14	100	-	-	-
1903	18.5	100	-	-	-
1914	25	100	161,000	2,246,000	-
1926	30	250	751,000	2,797,000	-
1932	32	250	-	-	-
1935	32	400	1,683,000	-	-
1935	34	400	-	3,317,000	-
1948	36	400	1,963,000	1,718,000	-
1964	40	400	1,376,000	1,629,000	-
2005	45	530	2,922,000	3,102,500	1,560,200

*Combined from data in Alperin (1977), Trawle (1981), and USACE SWG.

In 2008, the USACE SWG, and the Port of Houston tasked a joint venture formed by Turner Collie & Braden, Inc., and Gahagan & Bryant Associates, Inc., to evaluate dredging histories for the HGNC considering the limited dredged material capacity and high sedimentation rates that were occurring in the channel following the 2005 channel improvements (Gahagan and Bryant 2008). In the study, the team evaluated before- and after-dredging surveys and historical dredging data, as well as calculated average annual shoaling rates for sections of the channel for the pre- and postchannel deepening time periods. Limitations in the data sets were noted and included irregularities in dates, purpose of survey (before or after dredge), and identification of new work or maintenance dredging, along with others. The sections of the channel analyzed were as follows:

- Entrance Channel, extending from Bolivar Roads offshore 14.4 miles
- Bay Channel, extending 26.1 miles from Morgan's Point to Bolivar Roads and divided into Lower- (11.0 miles), Mid- (9.6 miles), and Upper- (5.5 miles) Bay segments
- Bayou Channel, extending from Houston to Morgan's Point for 13.0 miles and divided into Lower- (5.6 miles), Mid- (3.3 miles), and Upper- (4.1 miles) Bayou segments.

Gahagan & Bryant (2008) summarized historical shoaling rates up until the 1964 channel for the Bayou and Bay segments as presented by USACE SWG (1995) (reproduced in Table 1). For the 2005 channel improvements, maintenance shoaling rates were obtained through analysis of channel condition data sets from 2004 to 2008. Figure 4 shows a comparison between the pre-and post-2005 deepening shoaling rates as a function of distance along the channel, with the exception of the Entrance Channel, for which predeepening bathymetric data were not available. Gahagan and Bryant (2008) also compared bathymetric volume data with the dredging records available for the same time period and concluded "the magnitudes of the volumes match well."

Figure 4. Shoaling rates for the pre- (40 × 400 ft) and postimprovement (45 × 530 ft) channels as a function of distance along the channel as calculated from survey data from 2004 to 2008 (data from Gahagan and Bryant 2008).

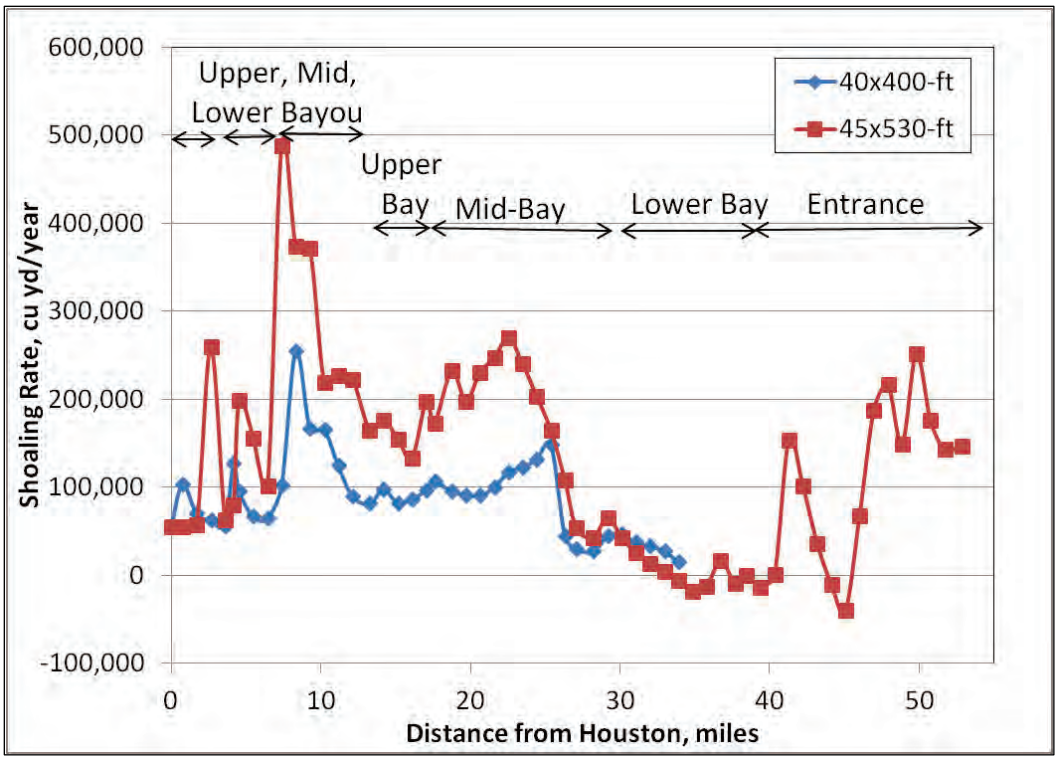

Several interesting trends can be observed in Figure 4. First, the peak in Entrance Channel shoaling at approximately 50 miles from Houston is adjacent to the beneficial use placement site, indicating that re-entry of sediment from this site back into the channel may occur. Second, another peak in Entrance Channel shoaling at approximately 41 miles is adjacent to Big Reef, which is fed by sand transport through the southwest jetty from East Beach, likely a function of degraded jetties. Next, sedimentation caused by influx of the salt water wedge appears to have moved upchannel 3 miles, from approximately 25 miles in the predeepening channel to 22 miles in the post-2005 channel. The movement of the saline wedge indicates the increased tendency of Gulf saline water to flow up the channel. Finally, the cause of the extremely high sedimentation rate in the Bayou portion of the channel was not understood but potentially could have been caused by rainfall and hurricanes, channel stabilization, or other natural processes.

Gahagan and Bryant (2008) also evaluated data after the first postdeepening maintenance dredging to determine whether there was a trend to reduce shoaling with time as the newly deepened and widened channel reached a new equilibrium. They found that the Mid-Bay, Upper-Bay, and Mid-Bayou reaches reduced in sedimentation with time. The Entrance channel increased shoaling by 24%, which was attributed to major hurricane activity during the period.

In summary, Gahagan and Bryant's (2008) analysis indicated an overall increase in channel shoaling of approximately 74%, as summarized in Table 2.

Table 2. Comparison of shoaling for pre- and postimprovement channels.

	Shoaling Rate, yd^3		
Channel Segment	40x400 ft Channel*	45x530 ft Channel**	% Change
Entrance	1,363,000	1,560,200	14.5%
Bay	1,629,000	3,102,500	90.5%
Bayou	1,376,000	2,921,700	112%
Total	4,368,000	7,584,400	73.6%

* Based on historical dredging records.

** Based on analysis of survey data from 2004 to 2008.

The Coastal and Hydraulics Laboratory (CHL) at the U.S. Army Engineer Research and Development Center (ERDC) has performed field data collection and analysis as well as numerical model studies in vicinity of the HGNC Bay Channel for approximately 20 yr. This work began with the

development of a three-dimensional (3D) numerical model of the hydrodynamics and salinity transport associated with the Bay Channel (Berger et al. 1995a, 1995b) and the effects of adding barge lanes to the HSC in the Bay (Carrillo et al. 2002). In the last 10 yr, the work has included sedimentation studies and analysis within the Bay (Tate and Berger 2006, 2008, 2009), including modeling of wind-generated currents, sediment transport, and vessel-induced flow and sedimentation. The years of research have led to an understanding of the estuarine system and a building of hypotheses as each step has progressed.

The numerical model developed in these studies has led to a better understanding of the behavior of Galveston Bay and the shoaling of the Bay Channel. The percentage increase of shoaling in segments along the channel, as computed in the model for the Bay Channel, is shown in Figure 5. As observed by measured shoaling shown in Figure 4, the numerical modeling accurately predicted movement of the peak in shoaling deposition up the channel due to the increased tidal prism and salt wedge intrusion. Also in agreement with Figure 4, the numerical model calculated a considerable increase in shoaling for the Bay. The distribution is similar to that actually observed after the deepening, but the quantity comparison is uncertain due to the continued new work and variations among dredging record sources. This model predicted a 30% average increase in Bay

Figure 5. Percentage increase in shoaling from the 40 × 400 ft channel to the 45 × 530 ft channel for the Bay Channel from Morgan's Point (station 1) to Bolivar Roads (station 33).

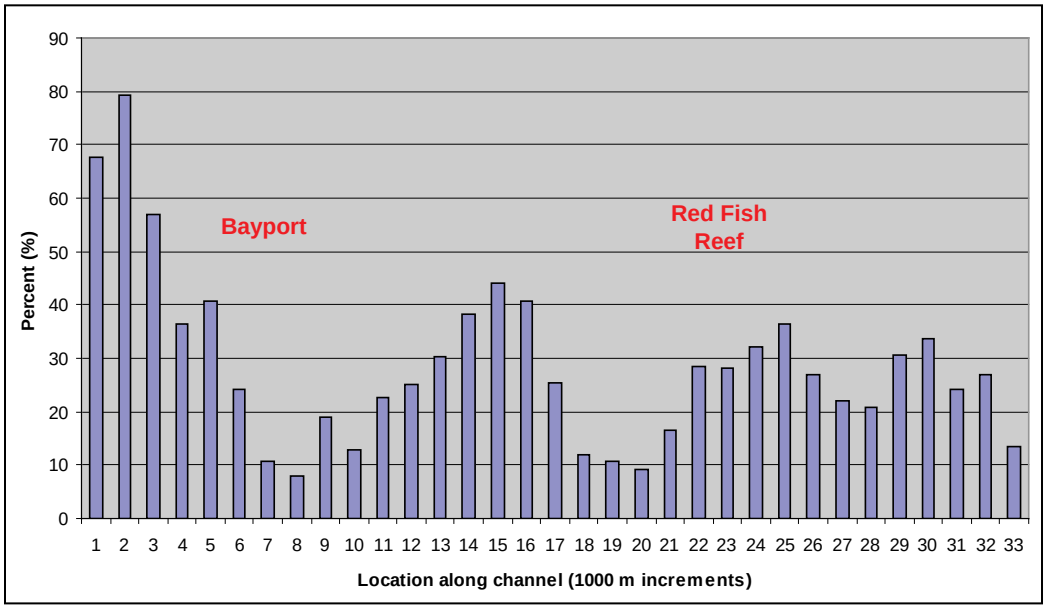

shoaling along the channel after the enlargement, or approximately one-third of the measured increase as shown in Table 2 for the Bay Channel. It is believed that fluid mud in the Bay, discrepancies between designation of new work versus maintenance dredging, continuing equilibration of the channel, and uncertainties in the sediment sources account for the differences between measured channel shoaling and numerical modeling.

In these earlier studies, CHL collected estuarine field data in the summer of 2004 and early winter of 2005. CHL validated the 3D Bay Channel model for hydrodynamics, salinity, and sediment erosion properties. The previous studies using the model and field data analysis led to certain understandings of the system, which are summarized in the following:

1. The bulk of the deposition in the Bay Channel was demonstrated to occur during large freshwater flow events. The model indicated that the flow from the San Jacinto River is a primary contributor to shoaling in the upper Bay Channel. Additional field data are needed during the spring and early summer periods when river flow rates are high to extend this numerical modeling result for representative seasons.
2. Based on field data collected during a strong wind event and on wind wave modeling in the HGNC model, the impact of wind waves on resuspension was shown to be confined to the shallower areas of the bay. This finding is not completely unexpected since wind waves have a relatively short wave-length in the Bay and therefore do not penetrate very deep in the water column. Figure 6 shows resuspension from currents combined with wind waves during a year-long simulation. The red-shaded areas experience a shear stress on the bed that is higher than the critical shear stress for erosion of the silt material, therefore eroding the bed. Blue areas have shear stresses that are high enough to limit deposition of the silts but not large enough to generate bed erosion of those materials. Bed sediment characteristics during the spring and early summer when the sediment is freshly deposited are important since the summer and early winter sediments tested in previous field campaigns would have been settled for a long period, most likely modifying the material properties over time due to bed consolidation. Thus, a time-dependent characterization of bed erosive properties may be warranted to best represent long-term suspension of bay sediments.

Figure 6. Maximum shear stress values from currents and wind waves over a 1 yr simulation to show area of resuspension (contoured between 0.1 and 0.67 Pa). Red areas experience higher-than-critical shear stress and would have potential to erode the estuary bed, and blue areas represent regions for which sediment would be kept in suspension. Erosive properties of the Bay sediments were based on summer and early winter samples; it is not known whether there is a time dependency to erosive characteristics of the estuary bed sediments.

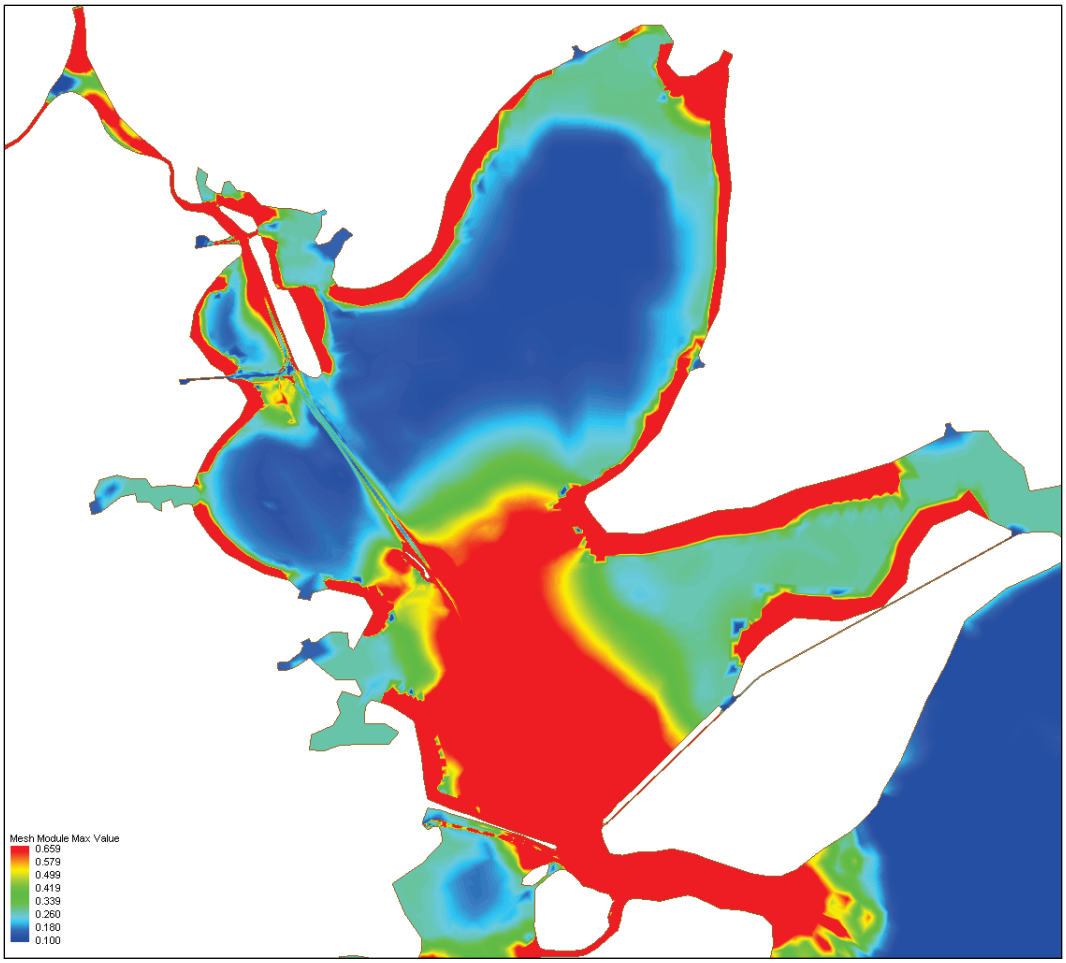

3. The model, field data, and literature (Ward and Armstrong 1993; Solis et al. 1994; White et al. 2002) have shown that the source of sediment depositing in the Bay and Bayou Channels is from the rivers entering the bay. Figure 7 shows the model results for shoaling impacts along the Bay portion of the ship channel from Morgan's Point to Bolivar Roads (Figure 3) for a representative year from 1994 to 1995. The San Jacinto River has the largest effect, especially in the upper portion of the channel along Atkinson Island; these results reinforce the need for data collection during times that freshwater flow rates are high.

Figure 7. Channel shoaling by source for the Bay Channel as calculated with the HGNC model from 1994 to 1995 for the 45 × 530 ft channel.

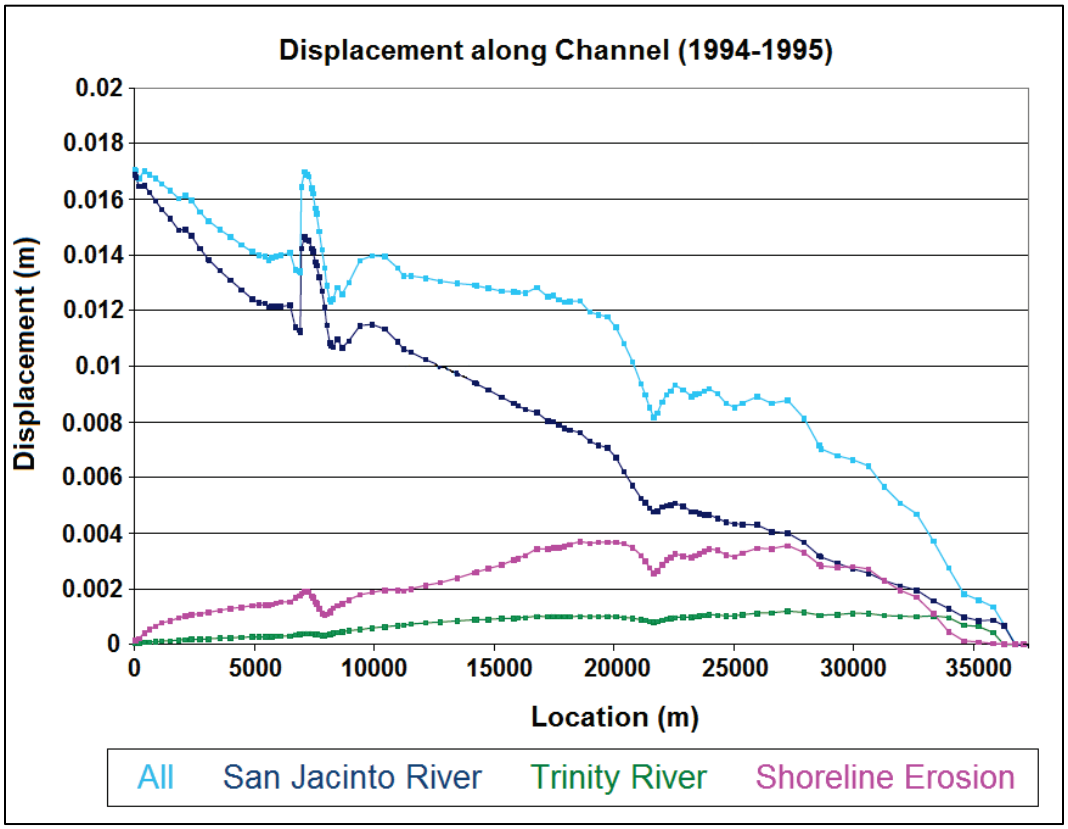

4. Vessel effects were shown to be very important in resuspension and movement of sediment. In 2005, approximately 50 deep-draft vessels per day transited the channel (U.S. Coast Guard 2006), and the vessel traffic increased 10% from 2004 to 2005. Vessels, especially fast moving, will create drawdown waves that move away from the vessel as it travels. This wave can become supercritical in the shallow regions beyond the channel and generate a bore that can be felt by the bed, creating erosion, or at least, preventing deposition in the shallow bay. Without the vessel effects on bed shear stress, the model showed deposition in the shallows near the channel. Field data have not shown deposition in the bay shallows. When the passage of these vessels was incorporated into the bed shear in the HGNC model, deposition was eliminated throughout those areas, and a shoaling pattern that better replicated nature was obtained within the model. However, field data supporting the range and magnitude of the vessel-induced waves and shoaling was quite limited.
5. The normal condition of the channel was observed to have the net drift direction near the bed to be upchannel (or flood). The net upchannel drift was true over much of the water column south of the Bayport Flare. Due to

reflection of the tide near Atkinson Island, the currents were found to be lower, and more stratification occurred. Thus, from Bayport Flare (where the Bayport Channel meets the HSC) northward, the surface water was ebb predominant, and the near-bed currents were strongly flood predominant, although the near-bed currents were observed to be very small. The model demonstrated that during the late spring, this flow pattern changes in a dramatic fashion. The Gulf salinity drops during this period, and the saltwater in the bay tends to evacuate. For the wind and flow conditions that were investigated previously, the net drift in the channel upland from Red Fish Reef was ebb predominant during the late spring. Also, the center of Trinity bay was ebb predominant. The ebb predominance is significant since sediment in the center of the bays will tend to move toward the channel, and sediment in the channel will move toward the Red Fish Reef area. Once again, data during the spring are needed to validate this pattern.

Analysis of historical dredging data

Overview

Historical dredging data were analyzed to update the Gahagan and Bryant (2008) report and provide bulk validation for the numerical models applied in the MCNP study. Three different sources of dredging data were examined. The first source was dredging records that were provided in USACE Annual Reports by channel reach and separated into New Work and Maintenance dredging. The second source was a dredging database that is maintained by the SWG for planning and historic purposes. The third source was provided by surveys that were taken after dredging cycles and recorded by channel stations. Unfortunately, for HGNC, analyses of dredging data from these three sources do not agree. Gahagan and Bryant's (2008) study also noted discrepancies with various sources of dredging data. The likely source of the discrepancy is the mistaken classification of Maintenance dredging for New Work dredging or vice versa.

USACE Annual Reports

The Annual Report data from 1873 to 2012 were obtained and are shown cumulatively for New Work and Maintenance dredging for the Bay Channel in Figure 8. Based on these data, Maintenance dredging decreased since the channel enlargement as indicated by the slope of the line from 2005 to 2012, 0.705 myd^3/yr, which is just under 23% of Gahagan and Bryant's

(2008) analysis of survey data (3.103 myd^3/yr for the 45 × 530 ft Bay channel, as shown in Table 2). Pre-improvement Maintenance dredging for the Bay Channel from 1986 to 1998 was 1.201 myd^3/yr, which is approximately 74% of Gahagan and Bryant's (2008) estimate for the 40 × 400 ft Bay Channel (1.629 myd^3/yr). New Work dredging is high during the period of the HGNC channel enlargement from 1998 to 2005, as expected. Some additional New Work was performed from 2007 to 2011, which most likely concerned mining and deepening of Barbour's Cut (Gahagan and Bryant 2008). For 1998 to 2011, the total dredging volume for Maintenance and New Work according to the Annual Reports was 65.2 myd^3, or 4.7 myd^3/yr.

Figure 8. USACE Annual Report records for New Work and Maintenance dredging for the Bay Channel.

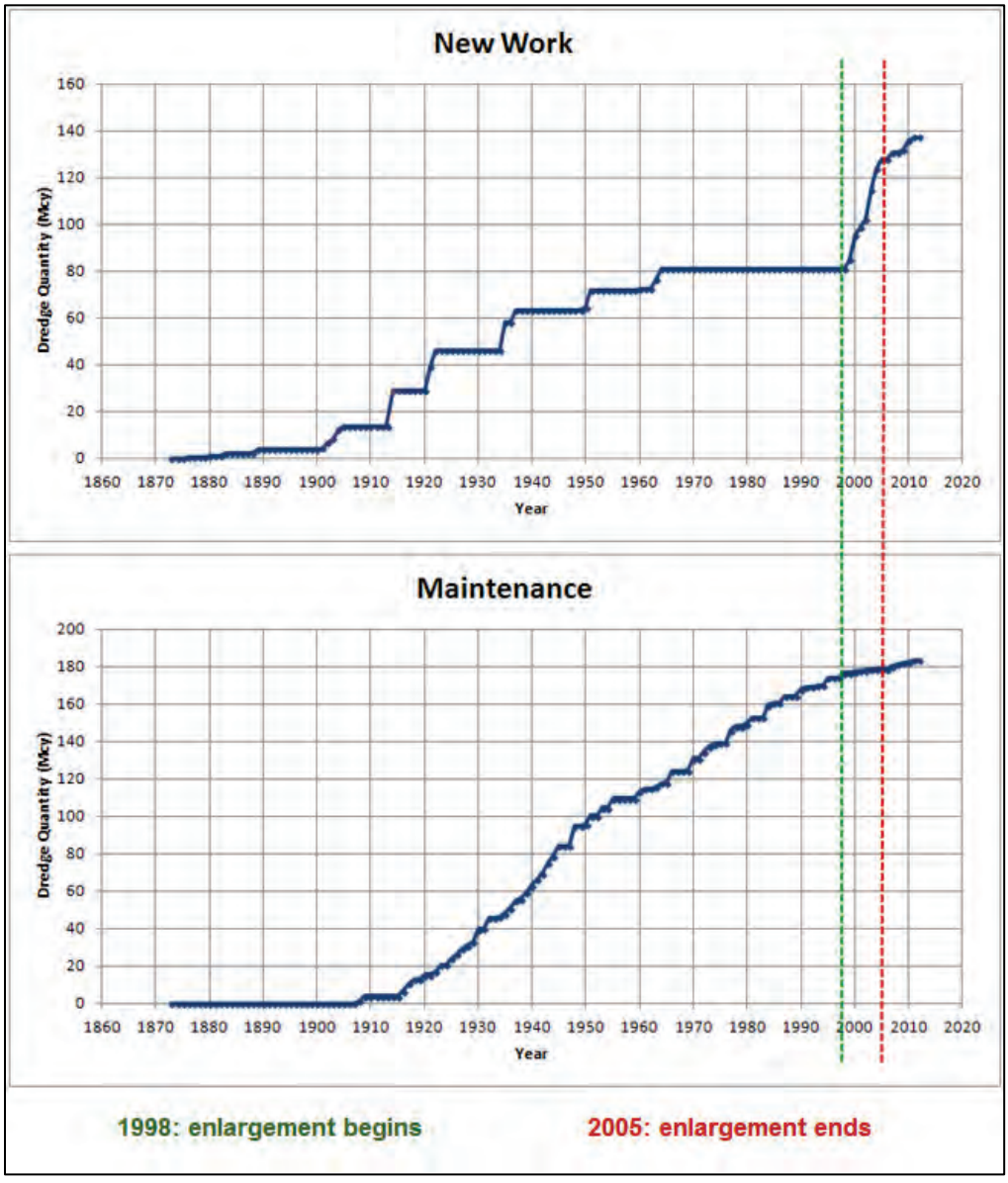

SWG dredging database

The Dredging Frequency Database maintained by SWG for the Bay Channel from 1998 to 2011 indicates a total of 29 myd^3 of dredging, or 2.1 myd^3/yr. This is for both New Work and Maintenance, 67% of Gahagan and Bryant's (2008) value for the Bay Channel from 2004 to 2008. The database includes only one Maintenance dredging of 6.4 myd^3 in September 2004.

Figure 9 shows cumulative Maintenance dredging for both the Entrance and Bay Channels since channel improvements began, based on the Annual Reports. Rates range between 75% to 104% of the historical rates shown in Table 1, with the most recent shoaling rate from 1990 to present totaling 4.38 myd^3/yr, or approximately 6% less than the sum of Entrance and Bay Channel shoaling rates in Table 1 (3.103 + 1.560 = 4.663 myd^3/yr). Overall, similar trends are observed, with a decrease in maintenance dredging requirements from 1948 through the time that the most recent improvements began in 1990 for the Entrance Channel.

Figure 9. Cumulative O&M dredging in HGNC through time for the Entrance and Bay Channels as a function of channel dimensions (combined from data in Alperin (1977), Trawle (1981), and analysis of data in USACE Annual Reports).

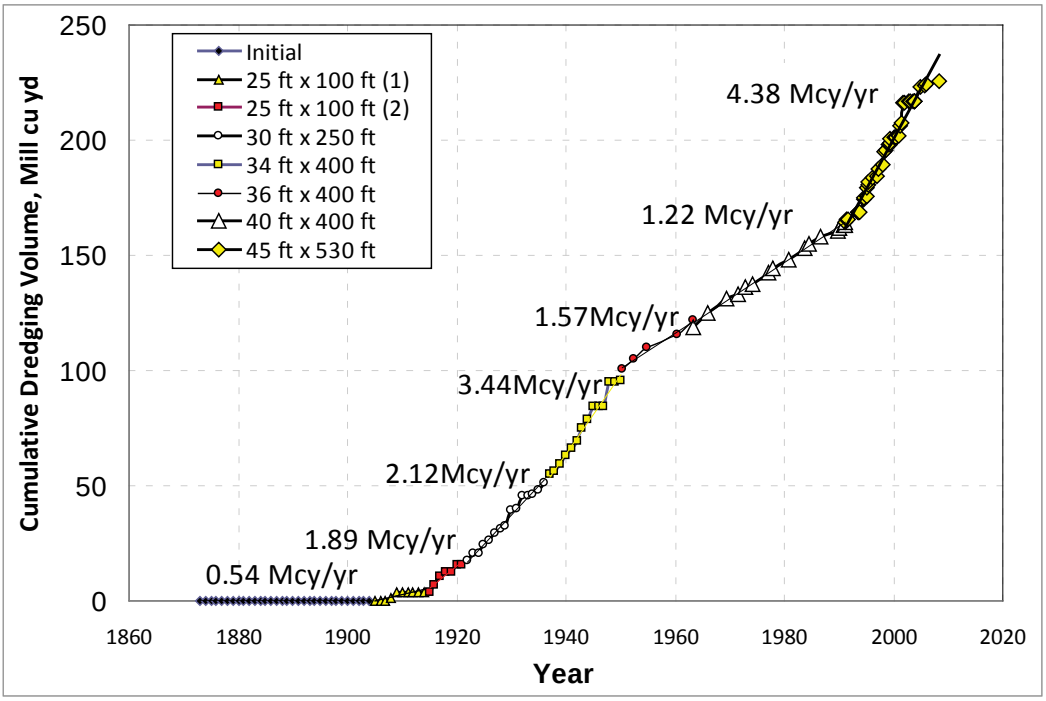

Analysis of survey data from 2004 to 2010

Station records based on pre- and postdredging surveys were provided by SWG for 2004 t0 2010 for the Bay Channel. These data indicate 10.8 myd^3 of dredging, or 1.5 myd^3/yr, which is approximately half of the value calculated by Gahagan and Bryant (2008) in Table 1.

Summary of analyses and discussion

Table 3 compares the channel shoaling rates from the various sources of data for a similar time period, from 2004 through 2010, for the Bay Channel only, and the Entrance plus the Bay Channel for 1990 through 2010.

Table 3. Comparison of channel shoaling rates from different sources for the Bay Channel and Entrance and Bay Channels.

Bay Channel		
2004–2010 (7 yr)	Total Yardage (myd^3)	Average Yearly Yardage (myd^3/yr)
Annual Reports (Maintenance only)	4.1	0.6
Dredging Database (SWG; likely Maintenance and New Work dredging)	6.4	0.9
Survey Data (Maintenance dredging)	10.8	1.5
Entrance and Bay Channels (1990–2010)		
Annual Reports (Maintenance only)		4.38

It is evident that every source of dredging data differs for this most recent time period. Unfortunately, without accurate dredging and placement data, it is difficult to understand how channel shoaling has changed since the most recent improvement. The designation of New Work versus Maintenance dredging is the most likely source of discrepancy and is critical when attempting to determine average annual shoaling rates and the volume of disposal area needed for future dredging, as well as determining how well a numerical model is replicating the field. The dredge disposal management plan for the 1998–2005 Bay Channel enlargement did not contain adequate storage capacity for the material. This could be due to changes in the planned configuration (i.e., adding barge lanes or simply not calculating the correct volume of material needing to be dredged). Given that the disposal sites have filled, understanding how the sediment moves within this very complex system is important.

3 Monitoring and Analysis

Overview of deployments

A series of three deployments were designed to address the hypotheses discussed in Chapter 1: June 2010 (Entrance Channel), April–September 2011 (Bay), and May 2012 (Bay). Data are also utilized from an additional field measurement study that was funded by the SWG for Galveston Channel in February–March 2010; this study is briefly reviewed herein, and details may be found in URS (2010). In this chapter, each deployment, the types of data collected, and results of analyses are discussed, as referenced by the year of the collection and the location.

2010 Entrance Channel deployment

The purpose of the 2010 Entrance Channel (EC) and Galveston Channel (GC) data collection study was to establish data sets with which to drive numerical models, characterize sediment type and erosion thresholds, and evaluate sediment transport pathways at the Entrance of the Houston-Galveston Navigation Channel. The 2010 data collection included two field studies which were used in calibration and validation of models. From February to March 2010, a field study funded by the SWG was conducted for GC and a portion of the EC by URS, Inc., Sea Engineering, Inc. (SEI), and Texas A&M University–Galveston (TAMUG) (URS 2010). Data collected in this study included a bathymetric survey and various types of sampling and monitoring. This study is briefly summarized herein. The MCNP funded complementary data collection with a focus in the EC in June, including three wave-and-current tripods, suspended and bedload sediment samples, cross-channel Acoustic Doppler Current Profiles (ADCPs), a multibeam survey, and sediment cores, which were later tested in the SedFlume (McNeil et al. 1996) to evaluate critical erosion thresholds.

February–March 2010 (URS 2010)

This field data collection focused on shoaling patterns and pathways within the GC, which had experienced unanticipated channel shoaling hotspots after deepening and widening. The GC traverses from the EC between Galveston Island and Pelican Island, exiting to Galveston Bay (Figure 10). Data collected during this study included detailed bathymetric surveys, current velocity transects, total suspended solids (TSS) samples,

Figure 10. February–March 2010 field study showing three shoaling hotspots in Galveston Channel (modified from URS 2010).

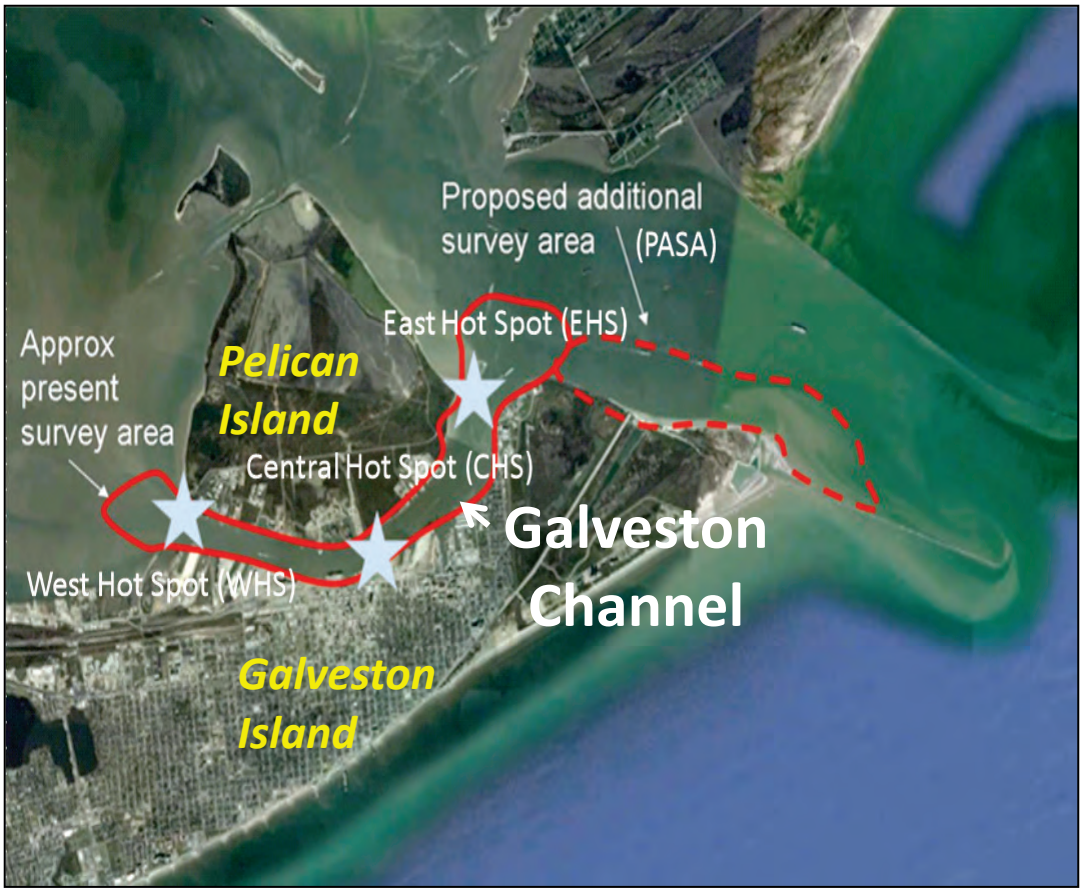

sediment samples, a ship-wake analysis, SedFlume cores, and four platforms with instrumentation located near the hotspots and one in the channel. Instrumentation included downward-looking, near-bottom-mounted ADCP, conductivity-temperature-depth (CTD) profiles, and channel-hindered settling monitoring (Figure 11) (URS 2010). Hindered settling was monitored by slowly lowering a clear, plastic polyvinyl chloride (PVC) pipe towards the bottom sediments and capturing a sample at a specified depth. Field measurements utilized in calibration of the EC model included the bathymetric surveys, water levels, and velocity measurements.

For additional information about the February–March 2010 data collection, see the URS (2010) report.

Figure 11. February–March 2010 Entrance Channel data collection instrument and sample locations.

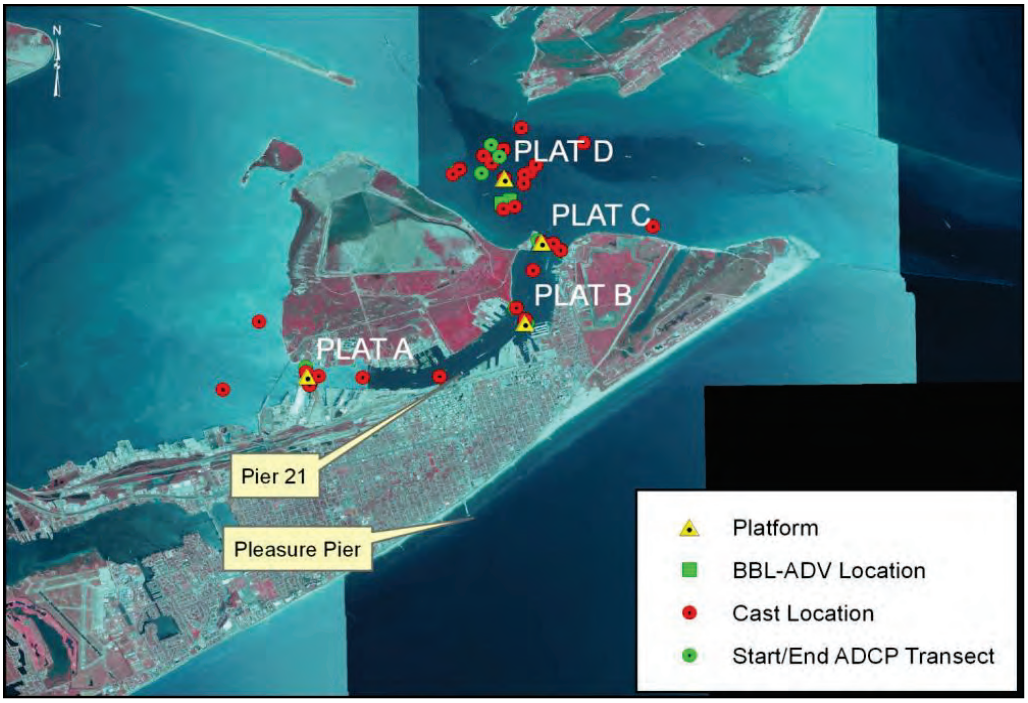

June 2010

The June 2010 deployment was designed to complement the earlier URS study, with a focus in the EC. Three tripods were deployed with wave and current gages; unfortunately, only information from POD-3 (seaward-most tripod) was recovered. Additional measurements included cross-channel ADCP transects along various ranges to measure suspended sediment (Figure 12), a multibeam bathymetric survey, point samples of suspended sediment concentration (within the water column), bed sediment samples, and cores for sediment testing in the SedFlume (Figure 13). A summary of the ADCP transects and sediment data is provided here; the bathymetric, wave, current, and water level data are discussed in the chapter documenting calibration and validation of the EC model.

Sediment grab samples

A total of 38 sediment samples were analyzed for grain size distribution and type (Table 4). Of these 38 samples, 15 had significant shell hash fraction that disproportionally skewed the distribution to larger grain sizes. Sand content ranged from 4% to 100% of the sediment composition, silt from 0% to 77%, and clay from 0% to 18%. The location of samples taken within Galveston Entrance is shown in Figure 14, with samples having more than 90% sand identified by the brown circles.

Figure 12. June 2010 ADCP range locations.

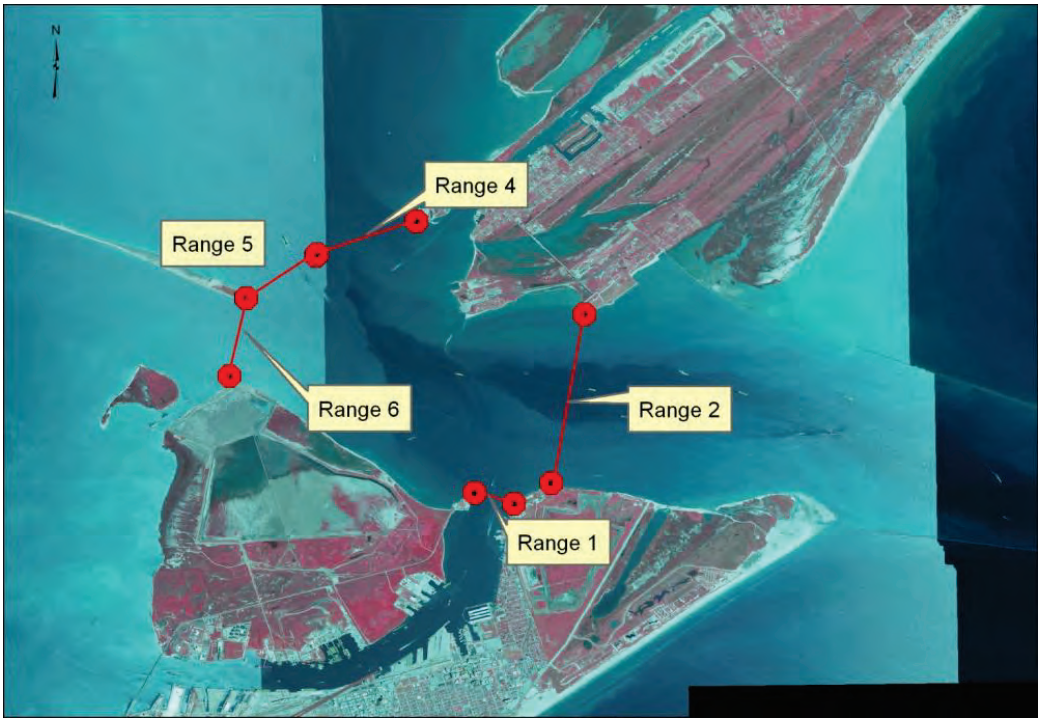

Figure 13. June 2010 Entrance Channel data collection instrument and sample locations.

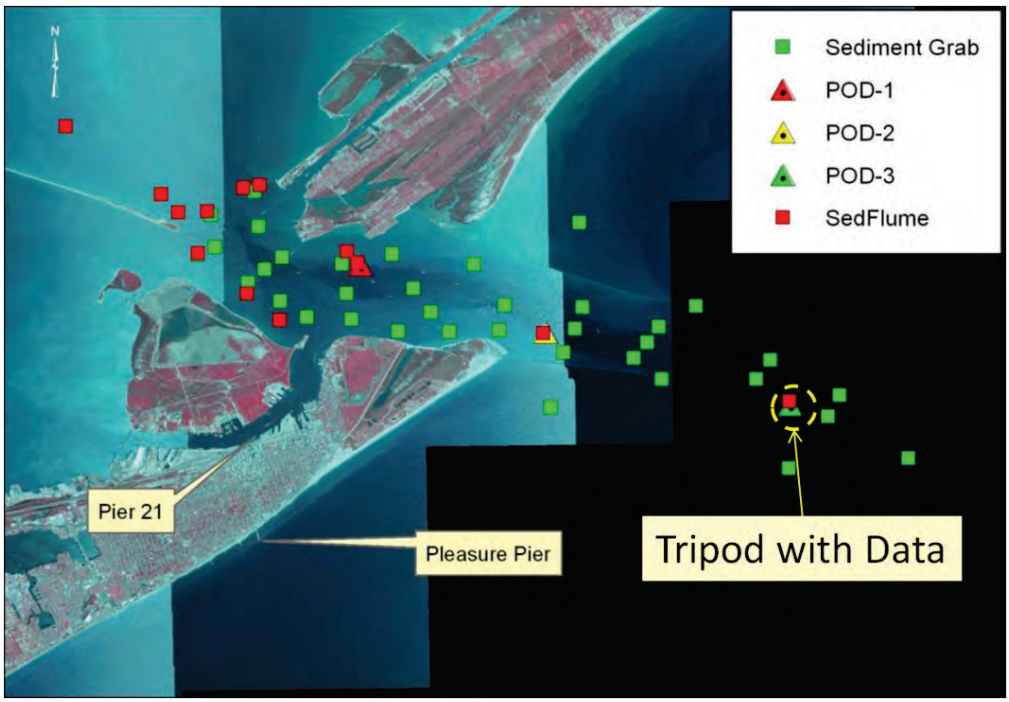

Table 4. Grain size distribution for bottom samples collected at Galveston Entrance Channel and adjacent beaches in June 2010.

Sample	% Sand	%Silt	%Clay	% very fine silt	% fine silt	%med silt	%coarse silt	%very fine sand	% fine sand	%med sand	%coarse sand	% very coarse sand	Notes
EC-1	93.92	4.39	1.69	1.20	1.66	1.53	0.01	20.10	66.03	7.79	0.00	0.00	
EC-2	94.76	3.92	1.32	1.06	1.47	1.20	0.20	19.57	41.23	18.53	8.87	6.56	shell hash
EC-3	65.38	29.84	4.78	6.42	7.80	7.58	8.04	11.80	14.80	12.62	15.70	10.46	shell hash
EC-4	70.64	23.23	6.14	6.65	6.82	4.97	4.79	19.95	26.43	12.09	8.29	3.88	shell hash
EC-5	95.57	3.20	1.23	0.79	1.22	1.19	0.01	19.65	68.31	7.60	0.00	0.00	
EC-6	92.04	5.87	2.08	1.86	2.21	1.79	0.01	19.81	64.63	7.61	0.00	0.00	
EC-7	75.64	19.69	4.68	5.32	5.65	4.71	4.02	2.93	5.15	18.06	31.48	18.02	shell hash
EC-8	75.72	16.03	8.25	4.14	4.54	3.85	3.50	10.17	19.09	18.77	18.13	9.56	shell hash
EC-9	68.57	25.41	6.03	6.76	7.43	6.00	5.22	21.25	26.47	9.44	7.63	3.77	
EC-10	69.77	24.91	5.32	6.20	7.17	6.18	5.37	16.73	26.97	14.23	7.45	4.40	shell hash
EC-10 #2	99.99	0.01	0.00	0.00	0.00	0.00	0.01	24.42	70.97	4.60	0.00	0.00	shell hash
EC-11	4.34	77.27	18.39	28.33	26.65	14.84	7.46	2.31	1.10	0.88	0.05	0.00	
EC-12	90.87	6.88	2.25	2.13	1.88	2.02	0.85	3.93	26.04	34.32	19.55	7.03	shell hash
EC-13	36.87	53.08	10.05	16.89	15.69	7.42	13.08	26.27	10.60	0.00	0.00	0.00	
EC-14	96.66	3.34	0.00	0.00	0.00	0.00	3.34	52.16	43.68	0.82	0.00	0.00	
EC-15	78.92	16.95	4.14	5.35	5.43	4.20	1.96	23.26	44.54	11.11	0.00	0.00	
EC-16	100.00	0.00	0.00	0.00	0.00	0.00	0.00	22.15	72.80	5.05	0.00	0.00	
EC-17 -- 35 ft deep	89.83	7.58	2.59	2.19	2.47	2.19	0.73	20.07	41.54	21.36	5.68	1.17	shell hash
EC-18	28.00	54.22	17.78	20.10	16.62	10.00	7.50	8.10	12.19	7.24	0.47	0.00	
EC-19	90.26	7.66	2.08	2.28	2.33	1.76	1.30	16.97	35.54	20.61	10.79	6.37	shell hash
EC-20	100.00	0.00	0.00	0.00	0.00	0.00	0.00	19.46	76.51	4.03	0.00	0.00	
EC-21	38.37	48.36	13.28	15.10	13.64	10.09	9.52	16.46	17.10	4.80	0.01	0.00	
EC-22	42.98	47.90	9.12	12.75	12.91	8.96	13.28	26.00	15.59	1.39	0.01	0.00	
EC-23	94.68	3.63	1.69	0.99	0.90	1.72	0.01	8.53	74.81	11.33	0.00	0.00	
EC-24	49.70	39.75	10.56	10.88	9.96	9.22	9.70	10.01	16.29	19.78	3.61	0.00	shell hash
EC-25 -- 57 ft deep	54.48	31.07	14.45	12.69	8.72	5.32	4.34	4.65	9.95	20.79	17.02	2.07	shell hash
EC-26	66.16	25.64	8.20	7.66	7.30	6.37	4.32	7.30	19.47	27.93	11.45	0.00	shell hash
EC-27	64.99	28.43	6.57	7.13	7.62	5.93	7.76	24.80	28.13	9.68	2.35	0.04	shell hash
EC-28	63.59	26.14	10.27	10.03	6.83	4.28	5.00	12.05	15.75	6.14	12.74	16.91	shell hash
EC-30	66.40	26.14	7.46	9.37	8.23	4.60	3.93	25.86	35.40	5.15	0.00	0.00	
EC-31	100.00	0.00	0.00	0.00	0.00	0.00	0.00	23.66	67.46	8.88	0.00	0.00	
EC-32	60.07	30.53	9.40	10.24	8.84	5.31	6.14	26.04	30.16	3.87	0.00	0.00	
EC-35	69.13	25.31	5.57	7.87	8.09	3.76	5.59	32.67	32.76	3.70	0.00	0.00	
EC-36	40.02	49.63	10.36	14.83	14.05	8.63	12.11	23.54	15.66	0.82	0.00	0.00	
EC-37	45.98	44.11	9.91	13.79	12.78	7.23	10.31	25.82	19.28	0.89	0.00	0.00	
EC-37 #2	92.61	5.69	1.70	1.60	2.60	1.13	0.36	37.61	53.25	1.76	0.00	0.00	
North Jetty Base	100.00	0.00	0.00	0.00	0.00	0.00	0.00	4.36	79.13	16.51	0.00	0.00	
North Jetty Beach Dune	99.99	0.01	0.00	0.00	0.00	0.00	0.01	25.68	64.24	10.07	0.00	0.00	
South Jetty Beach Shoreline	84.90	11.57	3.53	4.27	4.63	2.65	0.03	16.62	49.21	11.19	6.47	1.41	

* For samples that contained large amounts of coarse shell hash, reported grain size is not representative of bulk sample.

Figure 14. Location of June 2010 sediment bed samples within Galveston Entrance Channel; samples with more than 90% sand are noted.

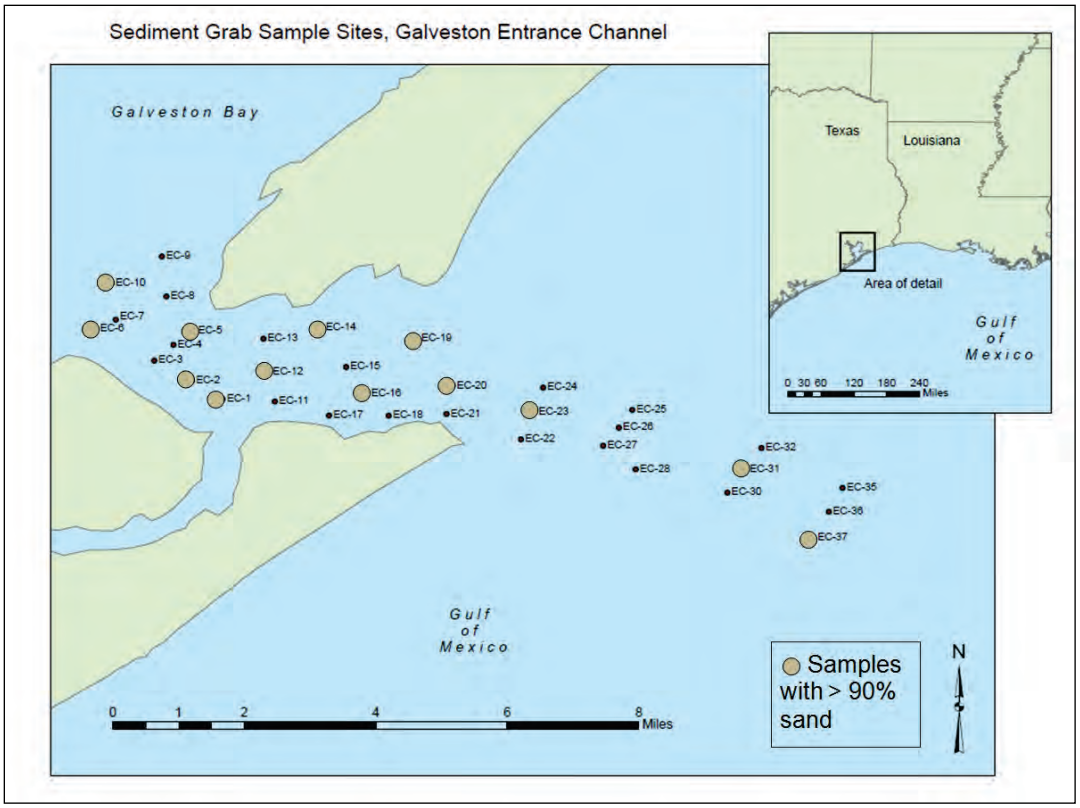

ADCP channel transects

Acoustic backscatter from the ADCP was used as a proxy for suspended sediment concentration (SSC) by calibrating to bottle samples. Measurements were made along five transects in the Entrance (Figure 12). These measurements are compared to numerical model calculations in a later chapter. Range 1 extended from bank-to-bank at the mouth of Galveston Channel, and all measurements were during high tide. In general, SSC was greater during the earlier measurements and decreased with time, with greatest values measured near the bed. ADCP summary plots (Figure 15 through Figure 19) show the time varying nature of suspended sediment in the channel. The water level is shown in the lower right corner of each (the red line indicates the observed water level; black dots correspond to the time of each ADCP frame; the blue line is the predicted tide; and the green x's are the difference between the predicted and observed tidal elevations).

Figure 15. ADCP channel transects through time (Central Daylight Time) at Range 1, 27 June 2010 (the red line indicates the observed water level; black dots correspond to the time of each ADCP frame; the blue line is the predicted tide; and the green x's are the difference between the predicted and observed tidal elevations).

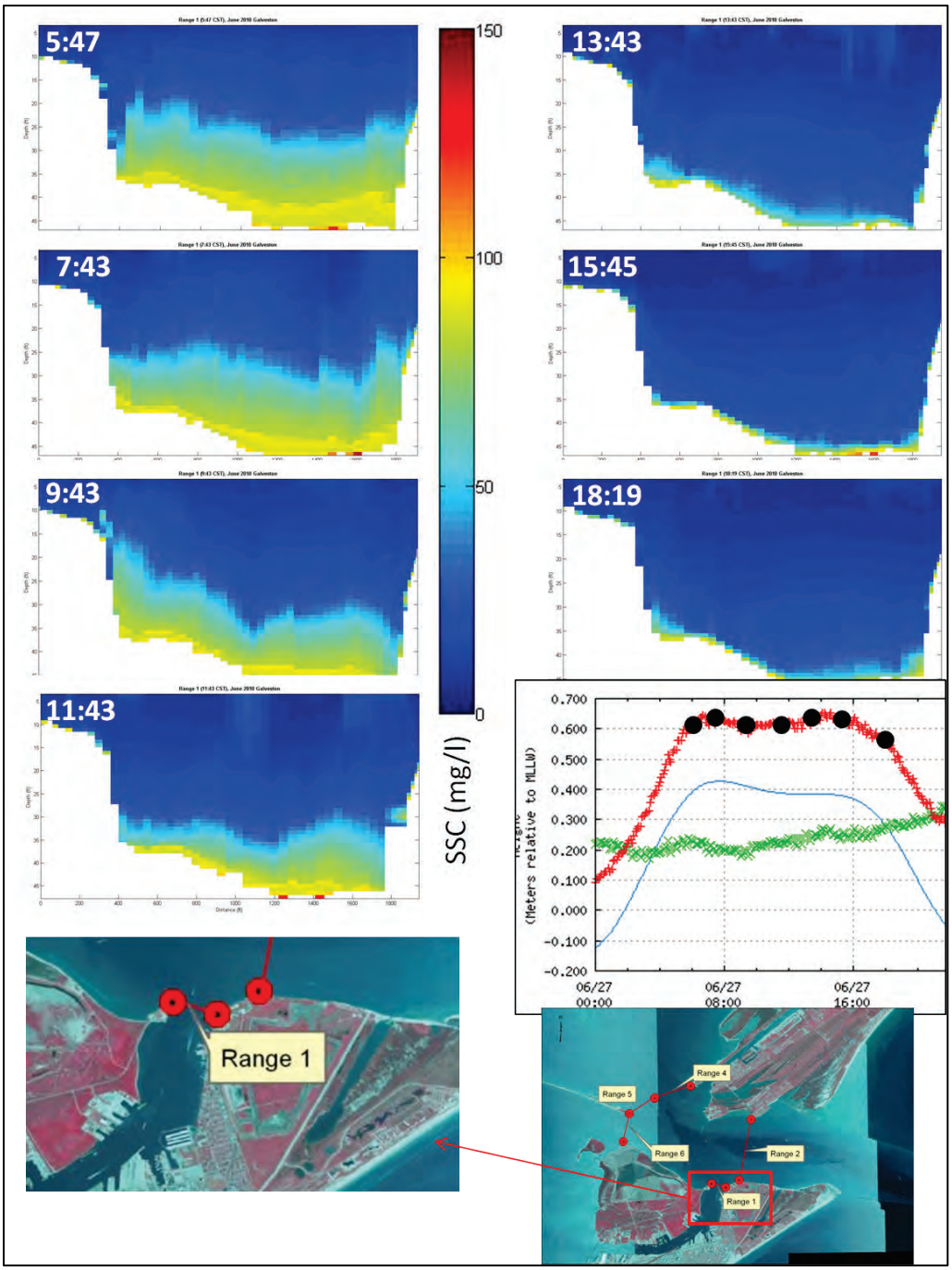

Range 2 extended from bank-to-bank facing the Gulf side of the Entrance Channel. This range had the greatest SSC of any ranges, which occurred at the start of high tide. Similar to Range 1, the magnitude of SSC decreased with time although sediment concentration along the bed remained above 100 milligrams per liter (mg/L) (Figure 16).

Figure 16. ADCP channel transects through time (Central Daylight Time) at Range 2, 27 June 2010 (the red line indicates the observed water level; black dots correspond to the time of each ADCP frame; the blue line is the predicted tide; and the green x's are the difference between the predicted and observed tidal elevations).

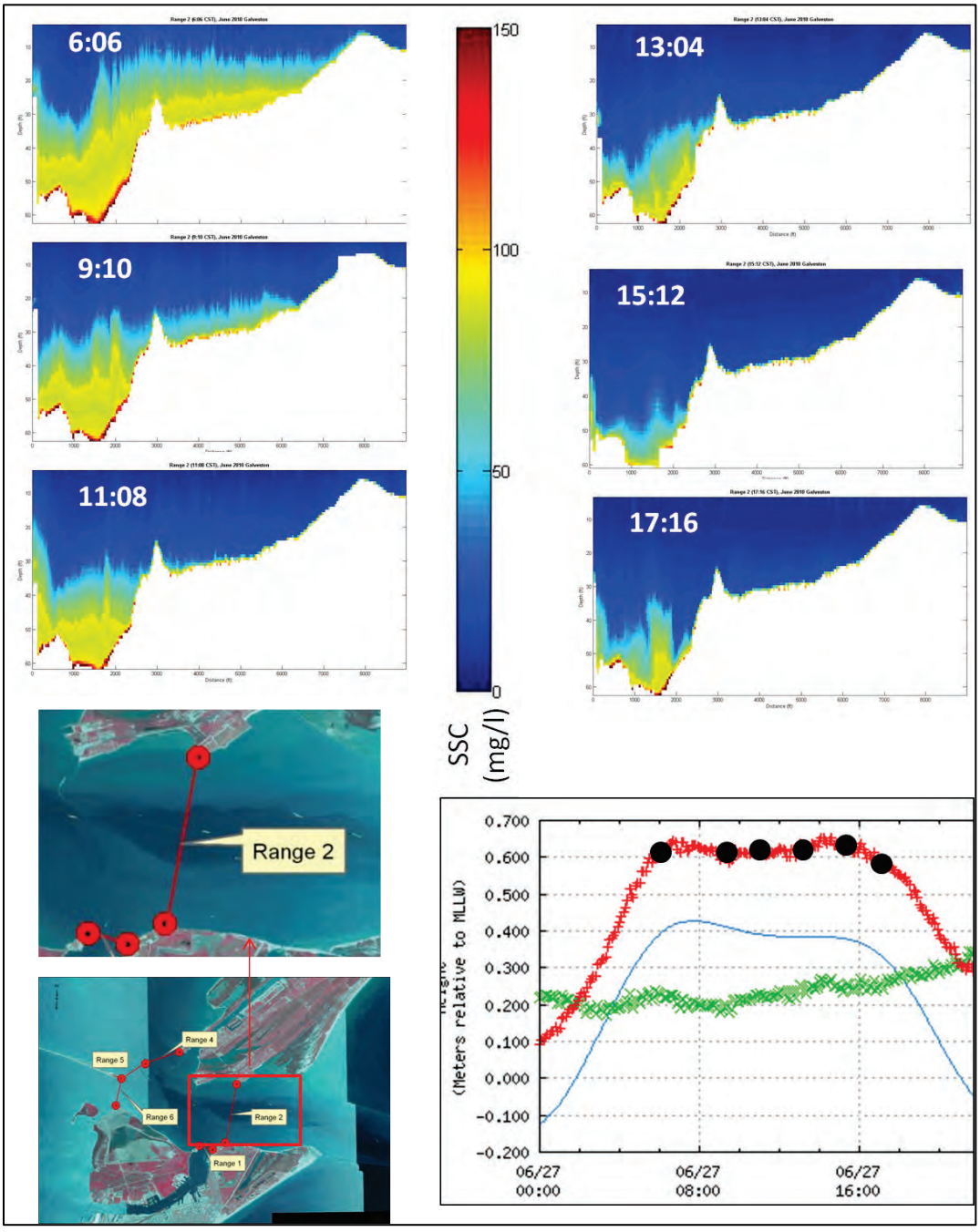

There was no Range 3 measured. Ranges 4, 5, and 6 extended across the bay side of the Entrance, beginning at the middle of high tide and continuing as the tide fell (Figures 17 - 19). Ranges 4 and 5 showed greater SSC as compared to Range 6, which has the lowest of any Range. In general, SSC decreased as the tide fell for these three Ranges.

Figure 17. ADCP channel transects through time (Central Daylight Time) at Range 4, 27 June 2010 (the red line indicates the observed water level; black dots correspond to the time of each ADCP frame; the blue line is the predicted tide; and the green x's are the difference between the predicted and observed tidal elevations).

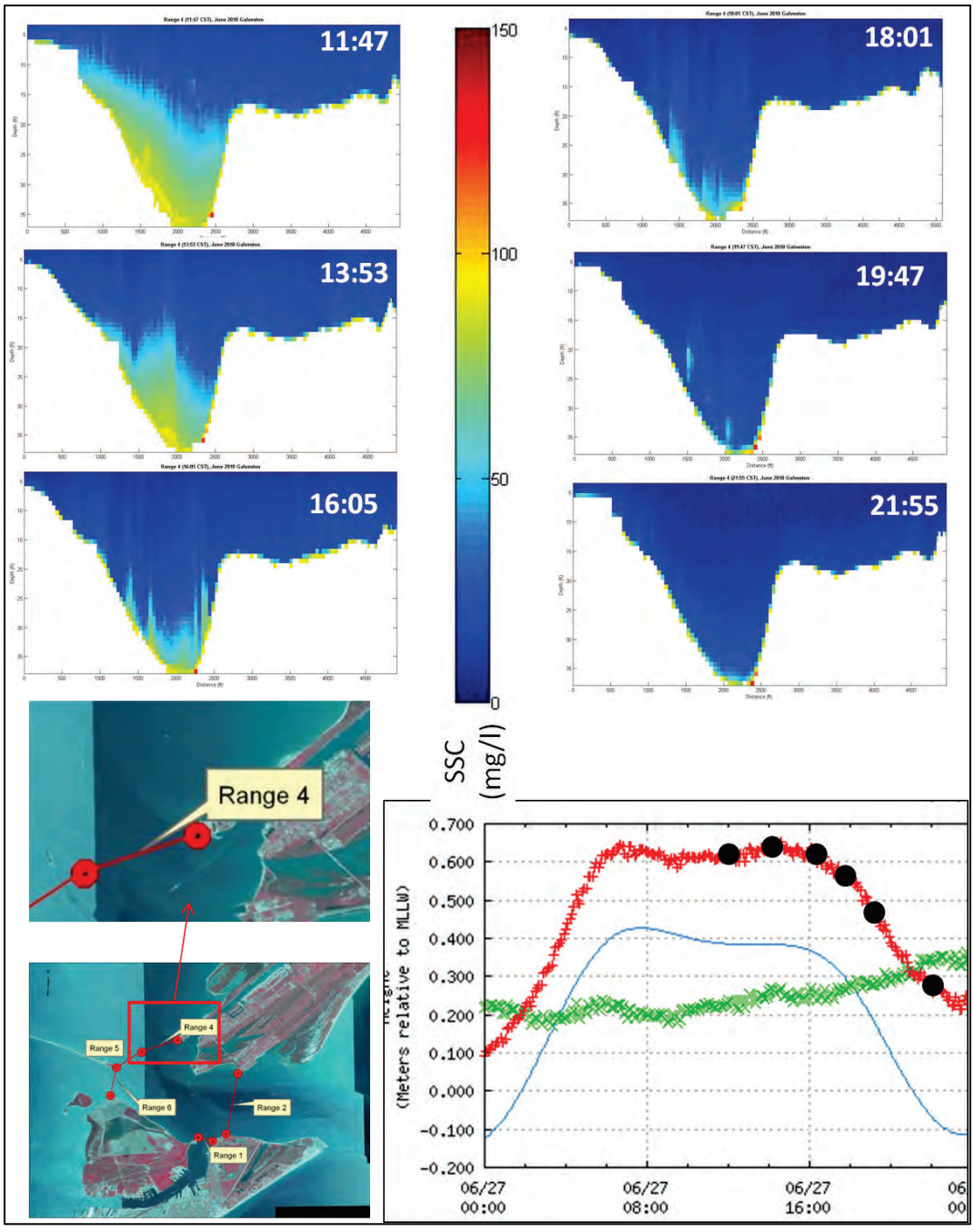

Figure 18. ADCP channel transects through time (Central Daylight Time) at Range 5, 27 June 2010 (the red line indicates the observed water level; black dots correspond to the time of each ADCP frame; the blue line is the predicted tide; and the green x's are the difference between the predicted and observed tidal elevations).

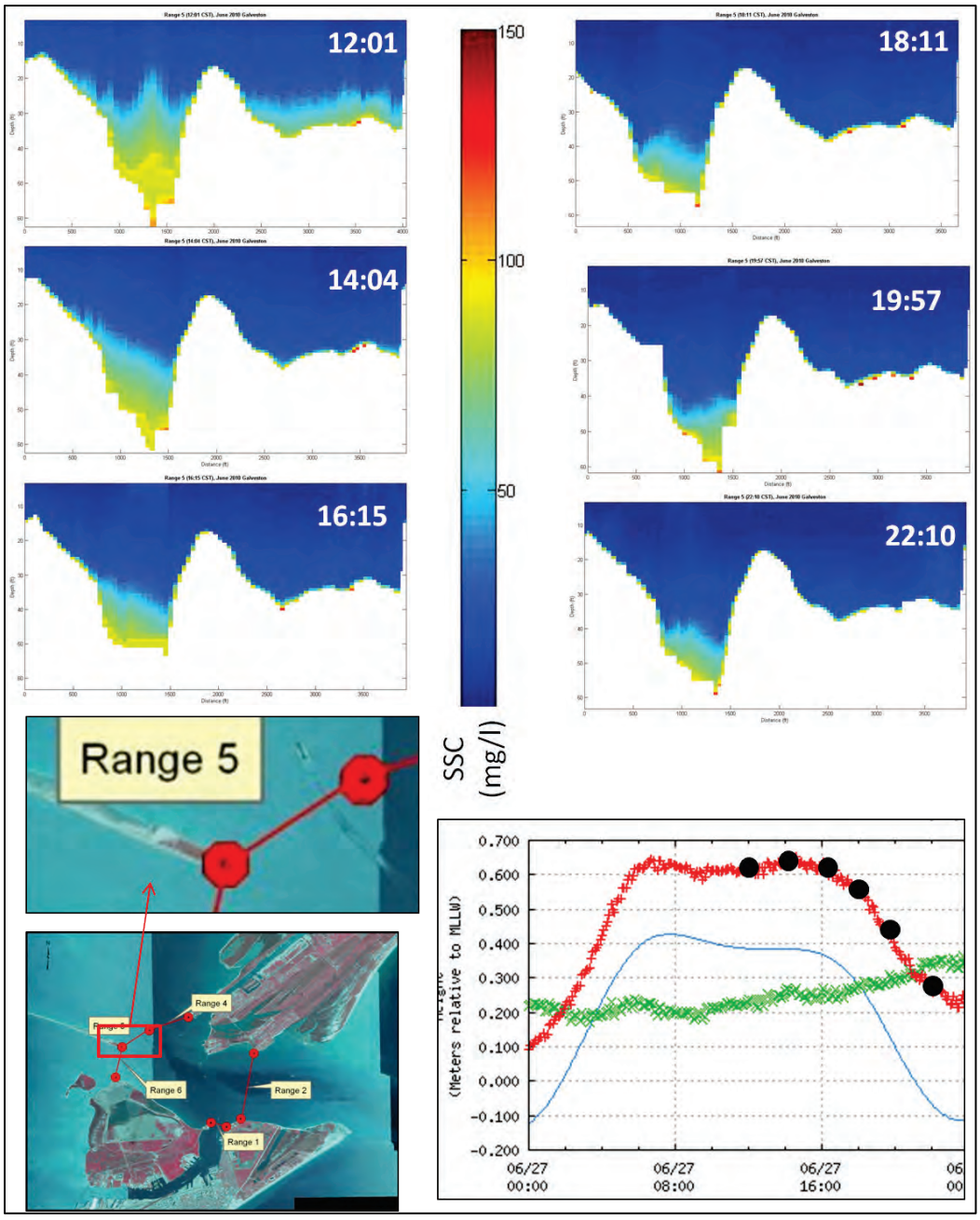

Figure 19. ADCP channel transects through time (Central Daylight Time) at Range 6, 27 June 2010 (the red line indicates the observed water level; black dots correspond to the time of each ADCP frame; the blue line is the predicted tide; and the green x's are the difference between the predicted and observed tidal elevations).

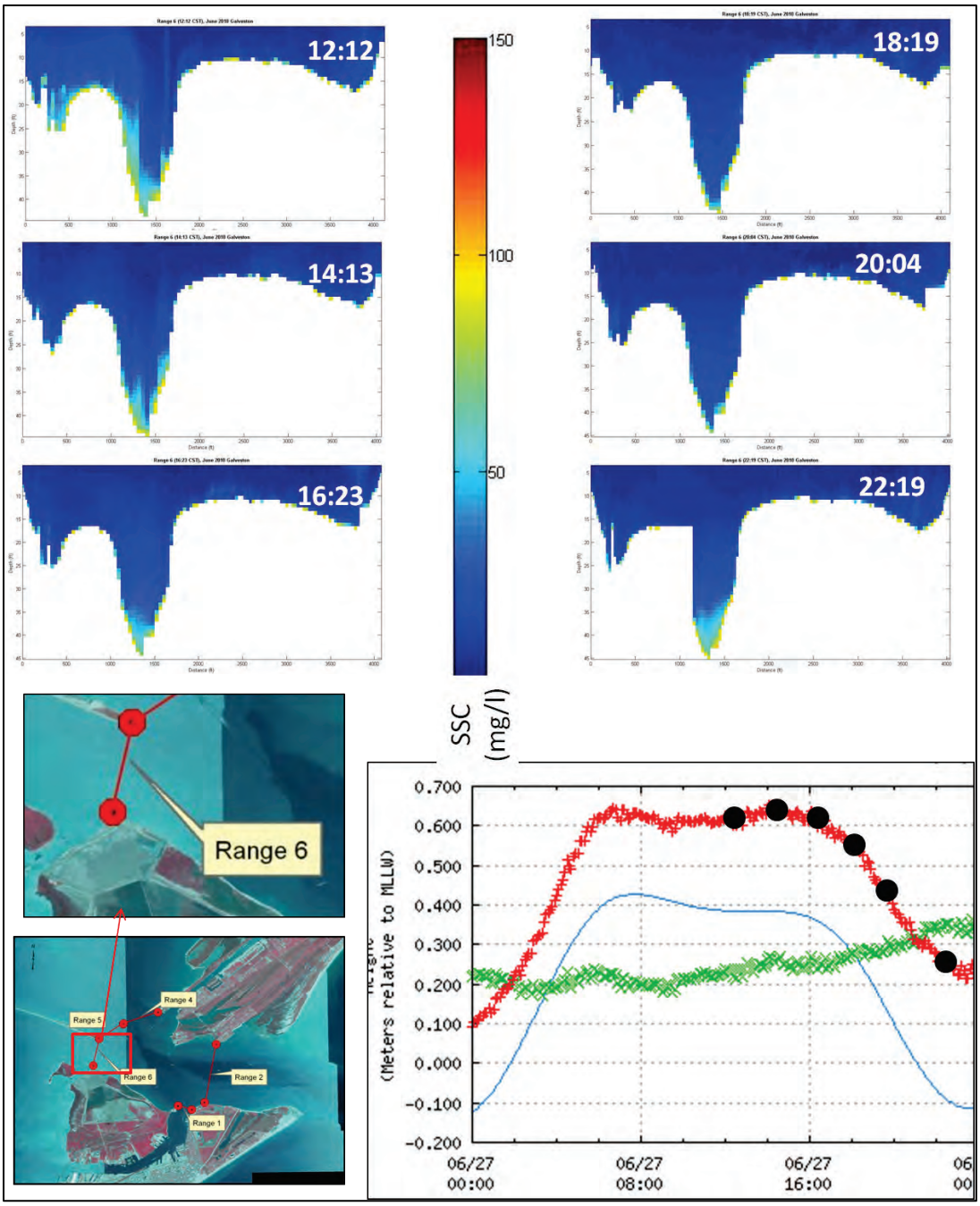

2011 Bay deployment

The purpose of the 2011 field data collection effort was to collect long-period samples during high freshwater flows. Figure 20 shows the data locations. These data include velocity, salinity, and suspended concentration at four

locations within the bay, focusing on potential sediment pathways into the navigation channel. Additional flow and sediment load data were collected to determine inflow data for the Trinity and San Jacinto Rivers. However, southeast Texas experienced a drought in the spring of 2011 making data collection of a spring flood event impossible. The river inflow data were not usable for model inputs due to the river's limited, low-flow, collection range. The salinity and velocity gage data, however, were useful for model comparisons. The total suspended load data were not compared back to field samples, so they were useful only for trend analysis but not for quantitative sediment comparisons. The gages were deployed from mid-April through late September 2011. Unfortunately, the southernmost gage was lost during the deployment, and only limited data from the first month of deployment were available for this site.

Figure 20. 2011 Bay data collection locations.

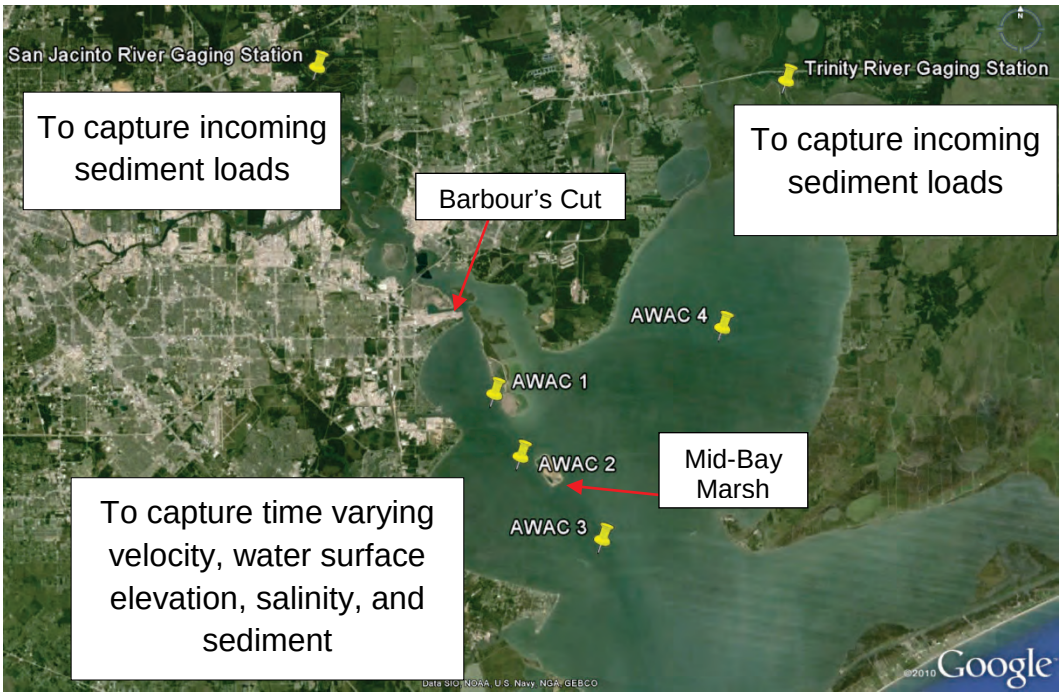

The acoustic wave and current system (AWAC) gages collected data at various points in the vertical 0.5 meters (m) apart beginning 0.4 m from the bed. The samples were collected at a 15-minute interval with a 60-second average value. There were periods of fouling obvious in some of the data, especially the salinity, which generated uncertainty in some of the data available for model comparison.

These data showed salinity values on the order of 15–22 parts per thousand (ppt) near the channel at sites 1 and 2 and 15–21 ppt in Trinity Bay. The velocity magnitudes ranged from 1.5 feet per second (fps) near the channel and 1.0 fps in the bay.

2012 Bay deployment

The purpose of the 2012 field data collection effort was to collect vessel-induced current and resuspension data as well as fluid mud and other sediment data. Given that the 2011 bay deployment did not allow for bed sampling of freshly deposited material (given that there was very little fresh deposit during the drought period), bed samples were collected in Trinity Bay during this deployment. The samples were available for grain size analysis but not for erodibility properties due to the inability to test for this immediately after the collection, allowing for bed consolidation to occur.

Fluid mud was searched out using a dual-frequency fathometer, to indicate changes in density within the water column, between Barbour's Cut and the Mid-Bay Marsh site but was not detected during the collection period. Individuals have discussed the presence of fluid mud in the area, but it has not been documented or detected over large areas or to remain longer than a few hours. The question still remains if fluid mud is a large component of the shoaling process in the HSC because it could produce large volumes of material in the channel while being very thin in the shallows. However, since it has not yet been detected on a regular basis, it is not included as a major component in the remainder of this study.

The vessel-effect data collection included four AWACs just south of Atkinson Island, with one farther east in Trinity Bay, and four acoustic doppler velocimeters (ADV) approximately halfway between the Mid-Bay Marsh site and Eagle Point. Figure 21 shows the gage locations. These collection devices measured water surface elevation, velocity, depth, and turbidity over time. Vessel data were also collected during the same period such that events due to ship passage could be cross-referenced to the vessel's size, speed, and path. This collection occurred 10–13 May 2012. In addition, a shorter, single-day sampling period included measurement of suspended material concentration immediately behind a vessel passage to determine exactly how much material gets resuspended under different vessel conditions. An example of this type of data is shown in Figure 22.

Figure 21. 2012 Bay data collection locations.

Figure 22. Vessel passage suspended material data across ship channel.

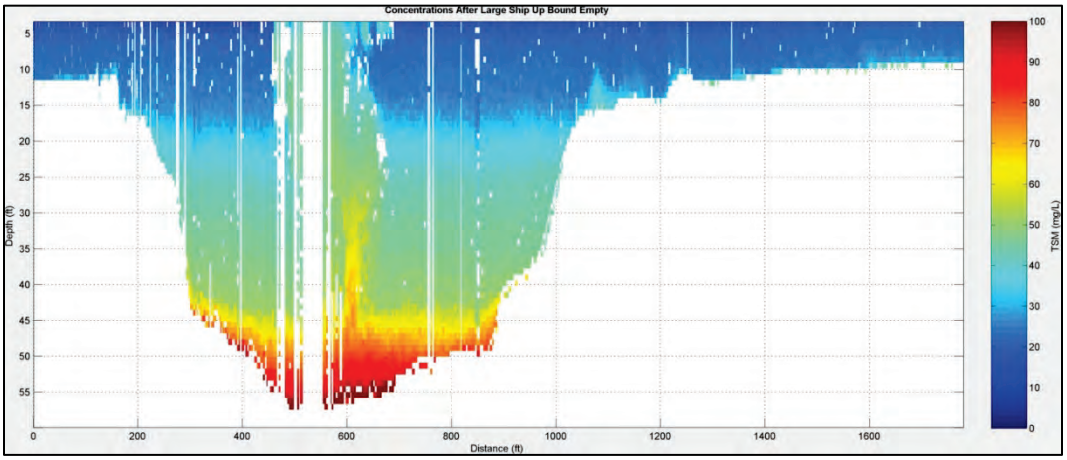

Findings

The data collection efforts occurred in three phases. The first included sampling in the HSC entrance between the jetties and through Bolivar Roads as well as in the Galveston Channel to the northwest of the entrance. The final two efforts occurred in the bay portion of the ship channel. Data were collected to determine sediment pathways and possible transport mechanisms. Sediment properties and long-term hydrodynamic data were collected for use in numerical model validation.

Sediment

Sediments in HGNC are mixed, with sands at the entrance and finer sediments upstream in the channel. Field data indicate that fine material enters the HGNC from the rivers and then slowly falls through the water column. As the material falls to the bed, grains are moved upstream with the salinity wedge that intrudes along the bottom, below the fresher water on the surface. Therefore, bed material is finer as you move upstream in the area of Atkinson Island. The bed material sampling in the bay was not able to occur during a spring flood or freshwater flow event, so the variation of sediment properties throughout the year still remains unknown. Based on the known bed properties, the bay material critical shear stresses for erosion are not reached unless under very high wind conditions such as tropical storm or hurricane force. Only the shallow bay boundaries are erodible under typical wind and wave forces; however, bores generated by passing vessels can be strong enough to erode material from the bay bottom.

The sediment in the entrance channel is primarily sand. The suspended concentration data show that the SSC dropped over time during the sampling period. This is likely due to the phase of the tidal cycle during the collection. The samples were taken at high water which corresponds to the time of low velocity. Also note that the SSC was lowest at Range 6. The reason for this decrease may be the proximity of this collection location to the Texas City Dike which reduces the flow in this area.

Fluid mud

The May 2012 data collection effort included a fluid mud component. However, no fluid mud was found in the area of the bay or channel between Barbour's Cut and the Mid-Bay Marsh site. The effort occurred on 12 May 2012, immediately after a passing front and storm, so material that may have formed fluid mud could have been washed to other areas or distributed about the bay bottom and thus undetectable. The indication from all who have detected fluid mud in the system is that it is sporadic and not a regular or cyclic occurrence. It is still possible that some event pushes this fluid material into the channel such that it is a source of large deposition volumes, but presently this hypotheses cannot be confirmed.

Vessel effects

It is known from previous work that the vessels have a large impact on the shoaling potential in the HSC due to the hydrodynamics of the vessel movement. The vessel displaces the water such that it is pushed out and around the vessel and then moves back into the channel behind the vessel. This forcing of the water around the vessel creates waves that can become supercritical as they move to shallower areas, therefore reaching the bed and causing erosion of the bed material. Details of the vessel data collection and analysis are provided in Chapter 4.

4 Vessel Data Analysis and Modeling

Overview

The vessel data were collected 10–13 May 2012 in the vicinity of the HGNC using the deployed AWACs shown in Figure 21. The vessel characteristics obtained from the Lock Operations Management Application (LOMA) include the vessel call sign (unique to the individual vessel), draft, length, and beam. Each AWAC recorded drawdown (depth) from the water surface elevation to the top of the instrument, backscatter that was converted to sediment concentration, and the velocity of the water at depths of 1.2, 2.2, 3.2, and 4.2 m. The data at AWAC 4, farthest from the ship channel, was difficult to interpret. The drawdown and concentration data did show peaks due to passing waves, but determining which vessel produced them was problematic as was the magnitude of the variations at times. Therefore, the analyses to follow often do not include AWAC 4. The time in which the vessel was passing was recorded at locations POS1 (coincides with AWAC 1) and POS2 (following the channel, farther south of AWAC 2) as shown in Figure 23. Since the time and distance were known between these positions, the velocity of each vessel was calculated and used in the analysis.

Figure 23. POS1 and POS2: Locations of passage data recording.

The purpose of the analysis was to address the following questions:

1. Does the speed of a vessel impact a larger spatial area of the bay than the size of a vessel?
2. Do the deep draft vessels (over 9 m (27 ft)) keep the channel center from shoaling?
3. What impact, if any, do barges have on the shoaling?

The vessels were initially separated into different class ranges based on the length and draft ranges listed in Table 5. A subset of the available data was extracted to analyze only those vessels recorded on 12 May 2012. The number of vessels for each class range is listed in the table.

Table 5. Vessel class ranges for 12 May 2012.

Class	Length (m)	Draft (m)	Date	Number of Vessels
1	250–300	10–15	5/12/2012	1
2	250–300	5–9	5/12/2012	1
3	200–249	10–15	5/12/2012	5
4	200–249	5–9	5/12/2012	3
5	150–199	10–15	5/12/2012	10
6	150–199	5–9	5/12/2012	8
7	<150	5–15	5/12/2012	11

Data analysis

For this data analysis, vessels creating major events on 12 May 2012 were used. Major events consist of larger-than-average background peaks in the drawdown and concentration data. This day was chosen because it contained a variety of vessels applicable to the objectives of the study. A data analysis graphical user interface (GUI) was developed for analysis of the collected vessel data. Details of this GUI are provided in Appendix B. Plots of the depth (drawdown) and concentration were created for a 24 hr time period on the twelfth (Appendix A), and the major events were determined. These events were then sorted by the different vessel characteristics to determine if any correlations between these and the drawdown or concentration exist. A total of 32 events was considered major and used for this analysis. The other 7 events (39 total events are presented in Table 5) did not produce a measurable drawdown response. Table 6 lists the characteristic ranges of the vessels used for analysis.

Table 6. Vessel characteristics of major events.

Characteristic (units)	Values
Beam (m)	8–44
Length (m)	120–294
Draft (m)	7–13
Speed (m/s)	4.9–7.5
Blockage ratio	0.01–0.18

Blockage is a common parameter used for vessel transport analysis and is the product of the vessel's draft and beam (width) (Maynord et al. 2006). This parameter defines the area that the vessel takes away from the channel dimensions. The blockage ratio is the ratio of the vessel blockage to the channel cross section and is often used to determine the vessel's limiting speed (Tate et al. 2008). The concept of a limiting speed means that at a given throttle setting, a vessel with a larger blockage ratio will move slower than a vessel with a smaller blockage ratio because there is more resistance on the larger blockage vessel, therefore slowing it down. The vessel data analysis includes blockage ratio as a characteristic parameter using a constant channel cross section of 2413 m^2 (25,957 ft^2) based on a depth of 14.9 m (49ft (i.e., 45 ft authorized depth plus 4 ft advanced maintenance)) and a width of 161.5 m (530 ft). For instance, a vessel with a beam of 36 m and draft of 12 m would have a blockage ratio (BR) of 0.18:

$$BR = \frac{36\,m \times 12\,m}{2413\,m^2} = 0.18$$

The ranges of drawdown and concentration at each AWAC are shown in Table 7. The relative magnitude of the drawdown was determined by removing the mean from the data collected by the AWAC instruments at the different locations. The drawdown for each event was then determined by taking the difference of the drawdown before (baseline) the event and the peak. For example, at AWAC 2 the mean was 3.81 m, and the drawdown before the event (after removing the mean) was 0.021 m, and the peak was −0.27 m. Therefore, for this event the drawdown (depth) contained a magnitude of approximately 0.29 m. The same was done for the concentrations. The difference between these data for depth is shown in Figure 24 with the raw data displayed as "AWAC # field" and the demeaned data as "AWAC # field – RM". The demeaned data lie along the zero drawdown line. The demeaned data will be used for all data analyses presented.

Table 7. Drawdown and concentration ranges for the 32 events at each AWAC.

AWAC Location	Drawdown (m)	Concentration (mg/L)
AWAC 1	0.075–0.40	0–160
AWAC 2	0–0.32	0–385
AWAC 3	0–0.16	0–205

Figure 24. Raw depth field data and depth field data with removed mean (RM).

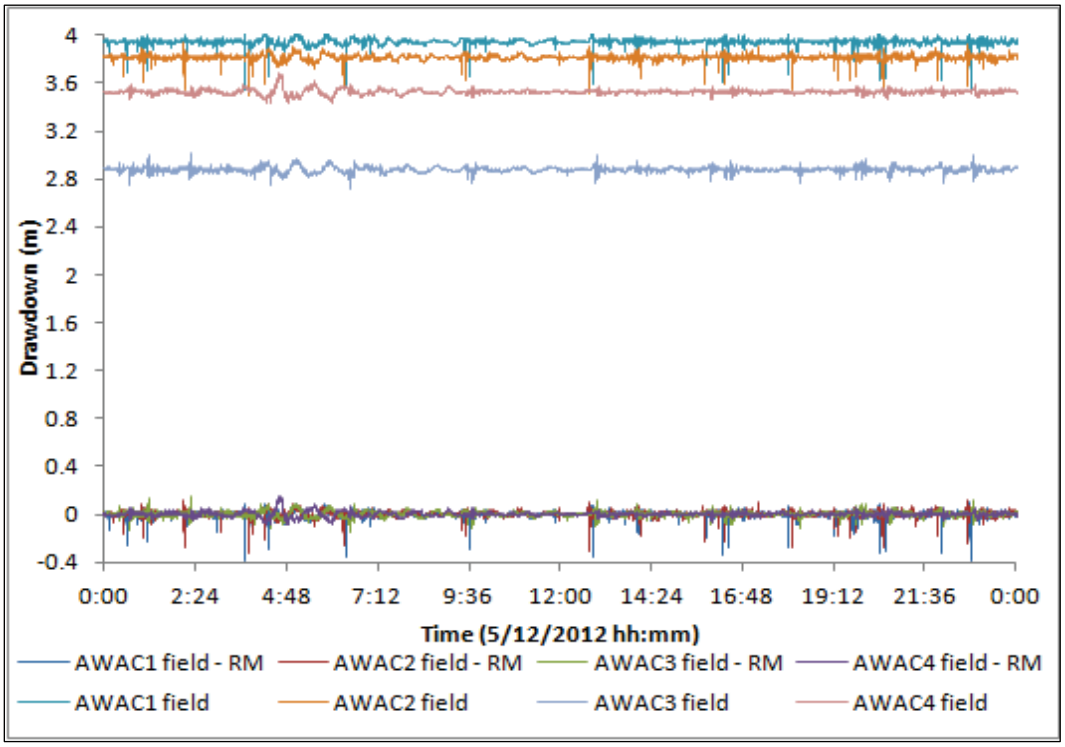

Drawdown trends

Table 8 provides a complete list of the ranges of values for drawdown and vessel characteristics for each draft and at each AWAC (A1, A2, A3). Instead of 32 vessels, 30 vessels are included in these data analysis because drafts 10 m and 13 m contained only one vessel each, so those were excluded.

Figure 25 shows the blockage ratio of the vessels included in this analysis against the drawdown at AWAC 1 (closest to the HSC) for each draft per vessel. A general trend of increasing drawdown with increasing blockage ratio is observed in the figure. There are not enough data in the set to determine trends in blockage ratio according to draft, however. It is also noticeable that with higher blockage ratio values, the spread in the drawdown data is increased, making correlations of blockage ratio to drawdown limited.

Table 8. Ranges of values organized by draft.

Draft (m)	# Vessels	Drawdown (m)	Length (m)	Speed (m/s)	Beam (m)	Blockage Ratio
7	4	0.080–0.19 (A1) 0.12–0.28 (A2) 0.080–0.12 (A3)	120–225	4.9–7.5	20–32	0.06–0.09
8	6	0.090–0.34 (A1) 0.085–0.23 (A2) 0–0.090 (A3)	135–188	5.5–6.6	16–33	0.05–0.11
9	6	0.075–0.40 (A1) 0.060–0.32 (A2) 0–0.090 (A3)	139–250	5.1–7.1	8–44	0.08–0.16
11	6	0.11–0.33 (A1) 0–0.18 (A2) 0–0.15 (A3)	158–245	6.0–6.8	25–33	0.11–0.15
12	8	0.090–0.40 (A1) 0.040–0.31 (A2) 0–0.12 (A3)	176–294	5.4–6.7	31–36	0.15–0.18

Figure 25. Vessel blockage ratio as compared to drawdown for each draft per vessel.

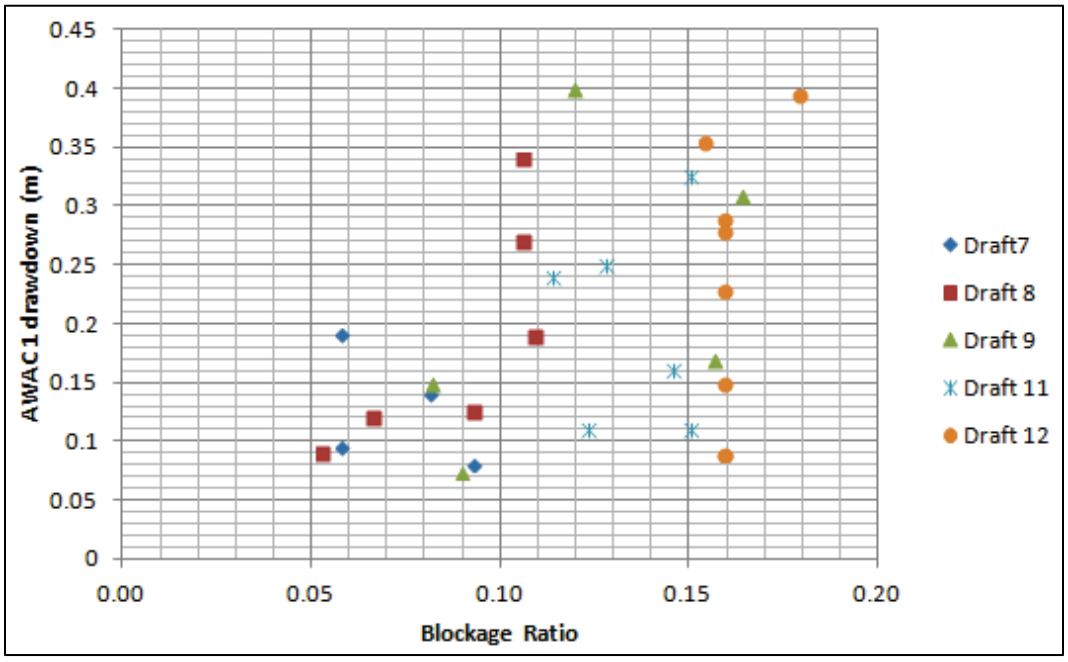

Table 9 presents the drawdown trends for each AWAC as compared to increasing length, draft, and beam. Blockage ratio has also been included since it is a commonly used parameter to describe vessel size. Increasing drawdown is highlighted in green while decreasing drawdown is highlighted in red. The values that remain relatively consistent are black. The increase

and decrease is determined from vessel to vessel with increasing characteristic—length, speed, beam, or blockage ratio. For instance, the four vessels with a draft of 7 m, the vessel with the shortest length shows a decrease in drawdown from the next vessel in length, and from the second to third vessel in length there is an increase, and so on. The general trends presented in Table 9 are for overall occurrences at each draft for each characteristic. Note that the comparison for each vessel may vary for each characteristic. In other words, the vessel with the shortest length will not necessarily have the slowest speed, etc.

Table 9. Summary of drawdown effects at AWACs 1-3.

Location	Draft	Drawdown effect for increasing...			
		Length	Speed	Beam	Blockage Ratio
A1	7	↓↑↓	↑↑↓	↓↑↓	↓↑↓
	8	↑-↑↑↑	↓↑↑↓↓	↑↑↑↓↓	↑↑↑↑↓
	9	↓↑↓↑↑	↓↑↓↑↑	↓↓↑↓↑	↓↓↑↓↑
	11	↑↓↓-↑	↑↓↑↓↓	↓↑↓↑↓	↓↑↓↓↑
	12	↓↑↑↓↑↑↓	↑↑↓↑↑↓↑	↓↑↑↓↑↓↑	↓↑↑↓↑↓↑
A2	7	↓↑↑	↓↓↓	↓↑↑	↓↑↑
	8	↑↓↑↑↓	↑↑-↓↓	↑↑↓↑-	↑↑↑↓↑
	9	↓↑↓↓↑	↑↑↓↑↑	↑↓↑↓↑	↑↓↑↓↑
	11	↓↑↓↑↓	↑↑↑↓↑	↓↑↑↑↑	↓↓↑↑↓
	12	↓↑↑↓↑↓↓	↑↑↓↑↑↓↑	↓↑↑↓↑↓↑	↓↑↑↓↑↓↑
A3	7	-↑↑	↓↓-	-↑↑	-↑↑
	8	↑-↑-↓	↓↑-↓↓	↑-↑↑-	↑-↑↓↑
	9	↑↑↓-↑	-↑↓↓↑	-↑↑↓↑	-↑↑↓↓
	11	↓↓-↑-	↑↓↑↑↓	↓↑↓↑-	↓↑↓↑-
	12	↓↓↑↓↑↓↓	↑↑↓↑↓↓↑	↓↑↑↓↑↓↑	↓↓↑↓↑↓↑

"↑" and "↓" indicate an increase or decrease, and "-" indicates the values are relatively similar.

The following general trends were observed when comparing the draft and increasing length to drawdown. Drawdown for a draft of 7 m typically decreases at AWAC 1 but increases at AWACs 2 and 3, while draft 8 m shows an average increase in drawdown at each AWAC. Draft 9 m increases at AWACs 1 and 3 and generally shows a decrease at AWAC 2. Draft 11 m has a decreasing drawdown at AWACs 2 and 3 but is split evenly between increasing and decreasing at AWAC 1 as the vessel length

increases. Similarly, for a draft of 12 m, the drawdown decreases at AWACs 2 and 3 but increases at AWAC 1.

When observing the draft and increasing speed compared to drawdown for a vessel with draft of 7 m, there is an overall increasing drawdown at AWAC 1, but a decreasing drawdown at AWACs 2 and 3 is observed as speed increases. Draft 8 m has decreasing drawdown at AWACs 1 and 3 as speed increases and is split evenly between increasing and decreasing at AWAC 2. Draft 9 m drawdown increases at AWACs 1 and 2 and is split evenly between increasing and decreasing at AWAC 3. Draft 11 m has decreasing drawdown at AWAC 1 and increasing drawdown at AWACs 2 and 3. Draft 12 m generally has increasing drawdown at AWAC 1 and decreasing at AWACs 2 and 3 as speed increases.

Trends were also observed when comparing the draft and increasing beam of the vessels. With a draft of 7 m at AWAC 1, the drawdown decreases with increasing beam, and at AWACs 2 and 3 the drawdown increases. Draft 8 m showed an overall increase at each AWAC. Draft 9m is similar to the trends for draft 7 m in which the drawdown decreases at AWAC 1 and increases at AWACs 2 and 3 as beam increases. For a vessel with draft of 11 m, the drawdown varied between decreasing and increasing at AWACs 1 and 2, respectively, and was split evenly between increasing and decreasing at AWAC 3. Draft 12 m, similar to draft 8 m, also displayed overall increases at each AWAC. The trends for increasing blockage ratio generally tend to mimic the same trends as the increasing beam, showing increasing and decreasing drawdown from vessel to vessel in the same manner.

Table 9 presents substantial variation among the impacts of the various vessel characteristics and the drawdown that is created for a given draft vessel at each analysis location. It is difficult to develop clear conclusions from the data in this manner.

Table 10 presents the general trends when comparing the drawdown with draft and increasing length, speed, and beam to the smallest characteristic value for each draft. For instance, instead of comparing the first vessel to the second, the second vessel to the third, etc., each drawdown value is compared to the vessel with the smallest characteristic value at that same draft. Therefore, when analyzing the drawdown for increasing length, all vessels with a draft of 7 m are compared back to the vessel of the smallest length to determine the overall trend of the drawdown. (The drawdown for

each vessel comparison may be either increasing or decreasing, but if the net of the drawdown showed a decrease, then the trend was recorded as negative (–)). Note that the vessel with the smallest length does not correlate to the lowest drawdown.

Table 10. Summary of drawdown effects at AWACs 1-3 compared to smallest value of characteristic for each draft.

Location	# Vessels	Draft	Drawdown effect for increasing...			
			Length	Speed	Beam	Blockage Ratio
A1	4	7	(-)	(+)	(-)	(-)
	6	8	(+)	(-)	(+)	(+)
	6	9	(+)	(-)	(-)	(-)
	6	11	(-)	(+)	(-)	(-)
	8	12	(-)	(+)	(-)	(-)
A2	4	7	(+)	(-)	(+)	(+)
	6	8	(+)	(+)	(+)	(+)
	6	9	(+)	(+)	(+)	(+)
	6	11	(-)	(+)	(-)	(-)
	8	12	(-)	(+)	(-)	(-)
A3	4	7	(+)	(-)	(+)	(+)
	6	8	(+)	(-)	(+)	(+)
	6	9	(+)	(+)	(+)	(+)
	6	11	(-)	(+)	(-)	(-)
	8	12	(-)	(+)	(-)	(-)

By analyzing the results of comparing the smallest value of vessel characteristic for each draft, trends become clearer. The drawdown response for both length and beam are similar at each AWAC and for each draft, with one exception at AWAC 1 and a 9 m draft. Once again, the blockage ratio is displaying the same trends as the beam. The previously discussed general trends for increasing or decreasing drawdown based on Table 9 correlate well to the drawdown trend when compared to the smallest value based on Table 10, although there are a few differences.

The data in Table 10 indicate that faster vessels generate larger drawdown when the draft is greater than 8 or 9 m, regardless of location. As length increases, the drawdown increases until the draft reaches 11 m, at which point the drawdown becomes less, regardless of location. Changes in drawdown with increasing beam mimic the changes with increasing length,

and the blockage ratio mimics the changes with increasing beam. There is an initial increase in the drawdown with increasing beam or blockage ratio until 11 m when the trend reverses and the drawdown becomes less.

Based on all of these trends, correlation coefficients (r) were determined to quantitatively see how each vessel characteristic is related to drawdown and sediment concentration. Table 11 presents the correlation of all vessels used in the analysis for drawdown while Table 12 presents the correlation for concentrations. For the coefficients in the following tables, positive correlations (greater than 0.1) are highlighted in green, while negative correlations (less than −0.1) are highlighted in red, and the values without any correlation (between −0.1 and 0.1) are black. Positive correlations are values close to 1 and indicate a positive linear relationship between the data sets. Values close to −1 indicate one set has a negative linear relationship to another (anticorrelation). Finally, values close to or equal to zero suggest no linear relationship.

Table 11. Correlation coefficients for drawdown on all vessels.

Variable	AWAC 1	AWAC 2	AWAC 3
Draft	0.34	0.05	0.08
Length	0.28	0.21	0.07
Speed	0.09	0.27	0.11
Beam	0.40	0.39	0.21
Blockage Ratio	0.43	0.29	0.19

Table 12. Correlation coefficients for sediment concentration on all vessels.

Variable	AWAC 1	AWAC 2	AWAC 3
Draft	0.23	0.12	−0.12
Length	0.14	0.24	0.04
Speed	0.21	0.15	0.11
Beam	0.19	0.09	0.02
Blockage Ratio	0.28	0.17	−0.06

Although the correlation coefficients for all vessels analyzed indicate no strong linear relationships between vessel characteristics and drawdown or concentration, majority positive correlations do exist. Drawdown and concentration appear to increase with increasing draft, length, speed, beam, and blockage ratio at AWAC 1, but the correlation values generally drop for

each characteristic when moving farther away from the channel. This drop indicates that the impacts of the vessel are not as strong farther away from the channel, but the trends still remain. Speed is not a large factor of the drawdown close to the channel, with a correlation coefficient of 0.09, but does have a larger impact at the other two locations. The correlation of speed with concentration at AWAC 3 is larger than any of the other characteristics at this site, indicating that it is a highly important factor in the erosion potential in the shallow areas of the bay. The draft shows a negative correlation at AWAC 3. Combining these factors indicates that a faster, shallower vessel will generate more bed erosion in the shallows that may then travel and deposit in the ship channel. Although this seems to contradict the information provided in Table 10 and Table 11 that indicate the drawdown is lower at AWAC 3, it is accurate given that the drawdown in the shallower areas will be less than in the areas closer to the ship channel. So, a lower drawdown can provide more erosion where the depth is less.

For the vessel data from 12 May 2013, the following conclusions can be drawn:

- The maximum concentration increases farther into the bay when moving from the ship channel based on the concentration ranges listed in Table 7. AWAC 1, closest to the channel, has lower maximum concentrations than AWACs 2 and 3 that are located farther away and in shallower areas.
- Given that the correlation of speed with concentration is stronger than any of the other vessel characteristics at AWAC 3 and that the draft shows a negative correlation at AWAC 3 (Table 12), it is likely that a faster, shallower vessel will generate more bed erosion in the shallows that may then travel and deposit in the ship channel.

ADCP concentration plots

The effect of the vessels on sediment concentration in the ship channel is best understood by observing the images created from the ADCP measurements collected immediately behind a passing vessel. Figure 26 through Figure 27 are a subset of all the recorded images of the total suspended material after the passing of various vessels. All figures of the ADCP measured concentration can be found in Appendix C. Down-bound or up-bound and loaded or empty ships and tows (barges) are discussed. Loaded ships will have a deeper draft than empty ships. The parameters for each vessel in this set of figures are given in Table 13. The ADCP concentration

figures present a cross section of the channel with concentration magnitude contours in mg/L over the water column at that location.

Figure 26. Down-bound, slower and loaded ship *Boxtrader* (left) and up-bound, faster and loaded ship *WH Blount* (right)

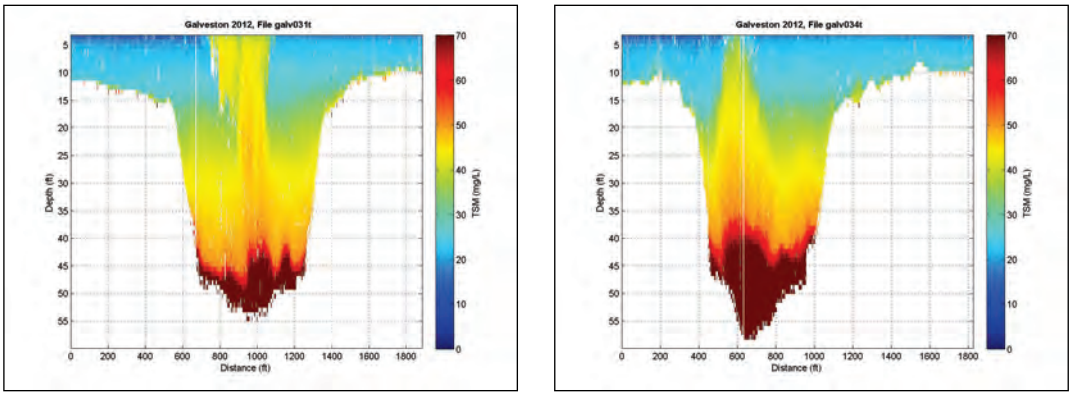

Figure 27. Down-bound ship *MSC Brianna.*

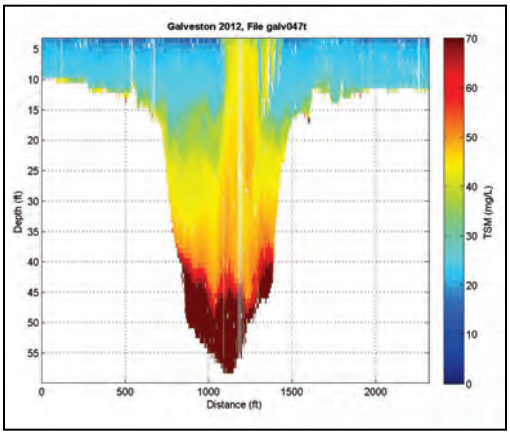

Table 13. ADCP vessel characteristics

Vessel Name	Type	Length (m)	Beam (m)	Draft (m)	Speed (avg, m/s)	Travel Direction
Box Trader	Container ship	228	32	10	4.5	Down
WH Blount	Bulk carrier	225	32	8	6.6	Up
MSC Brianna	Container ship	245	33	7	5.6	Down
Lorette	Pusher tug	20	8	3	3.6	Down

As shown in Figure 26, the *Box Trader* container ship is traveling in the down-bound direction (towards the gulf) while the *WH Blount* bulk carrier is traveling up-bound (towards Houston). Both ships are loaded and are practically the same in length and beam. The only differences are the direction and the speed at which the vessels are moving, an artifact of the

2 m draft difference. The down-bound *Box Trader* is traveling at a slower speed than the up-bound *WH Blount* by 2.1 m/s. The down-bound ship appears to pull more sediment from the bottom to the surface than the up-bound. For the *Box Trader*, a higher concentration (approximately 50 mg/L) towards the surface is seen, while the faster up-bound *WH Blount* with a shallower draft seems to have a concentration of 40–45 mg/L near the surface in the 5–10 ft depth range.

The *MSC Brianna* is a large container ship with a shallow draft traveling at an average speed of 5.6 m/s. Compared to the *Box Trader* and *WH Blount*, it is shallower, longer, and at a speed between the two. Figure 27 shows the *MSC Brianna* is suspending concentrations of 14–50 mg/L to the water surface. The ADCP plot of the *MSC Brianna* shows that a large, fast vessel does not impact a larger area of the water column than a large, slow vessel. The *MSC Brianna* is traveling at a slower speed than the *WH Blount,* and by examining the ADCP plots of the two it is apparent that the *MSC Brianna* has more of an influence in suspending sediment to the water surface.

The image on the left of Figure 28 is after the passing of the tug *Lorette,* and shows that it entrains material in a small area near the surface with a concentration of approximately 40 mg/L. This vessel passed near the upper slope of the ship channel, making material available for erosion due to the reduced depth under the vessel. The image on the right of Figure 28 shows the total suspended material taken after the passing of two tows near the center of the channel. It is apparent from this figure that very little disturbance is caused by the movement of these tows (barges) when under-vessel clearance is large.

Figure 28. Down-bound ship *Lorette* (left) and very little effect seen after tows (right).

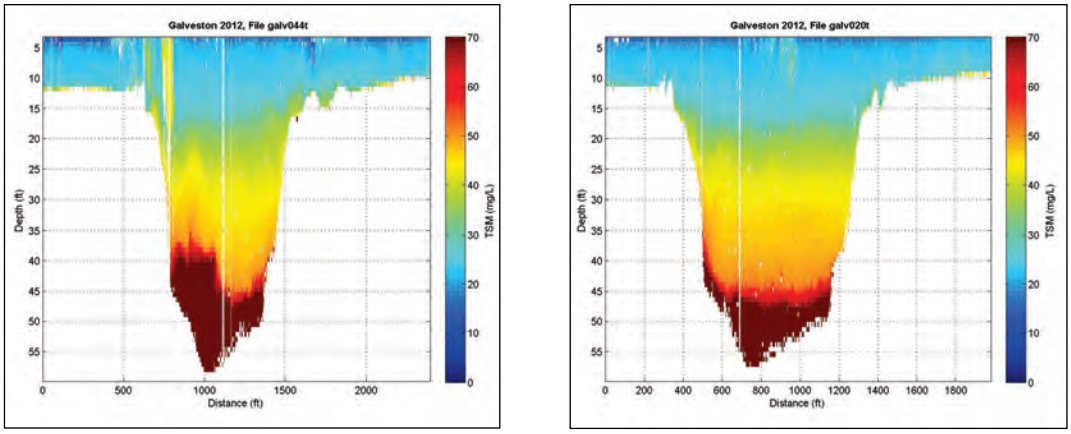

Model analysis

A numerical model of the vessel movement was developed to determine if the model can accurately duplicate the vessel effects observed in the field. Several varying runs were completed using Adaptive Hydraulics (AdH) version 4.2 (http://adh.usace.army.mil) to compare with the field data. This is a two-dimensional (2D) code that simulates the movement of a vessel—based on its size, draft, and speed—to impact the surrounding waterway. The characteristics of the vessels simulated in each run are presented in Table 14.

Table 14. Vessels used in AdH model runs.

Run	Draft (m)	Length (m)	Beam (m)	Direction	Speed (m/s)
1	12	180	32	DOWN	6.1
2	12	189	32	DOWN	5.4
	11	183	32	DOWN	6.4
	9	247	8	UP	5.1
	12	180	32	DOWN	6.1
3	9	247	8	UP	5.1

The model included only the hydrodynamics as produced by the vessel movement. No other conditions such as winds, tides, or river inflows were included in the model. Observation points were created at the location of each AWAC in order to accurately compare the model data with the field data.

The results from Run 1 are shown in Figure 29. The model results are shown with the dashed lines, and the field data are shown as solid lines.

Run 1 included one vessel. The results indicate that the model exhibits a large wave, or increase in water level, before the drawdown. Also, the model is overestimating the drawdown created from the vessel at both AWACs 1 and 2 by a factor of nearly 2.0. It was hypothesized that the model may be overestimating the water level changes because in the field there were other vessels moving in the area during the same time frame. These additional vessels could be generating a cumulative effect in the field. Run 2 was set up to include the vessels that may be collectively affecting the flow field.

Figure 29. Run 1 model results.

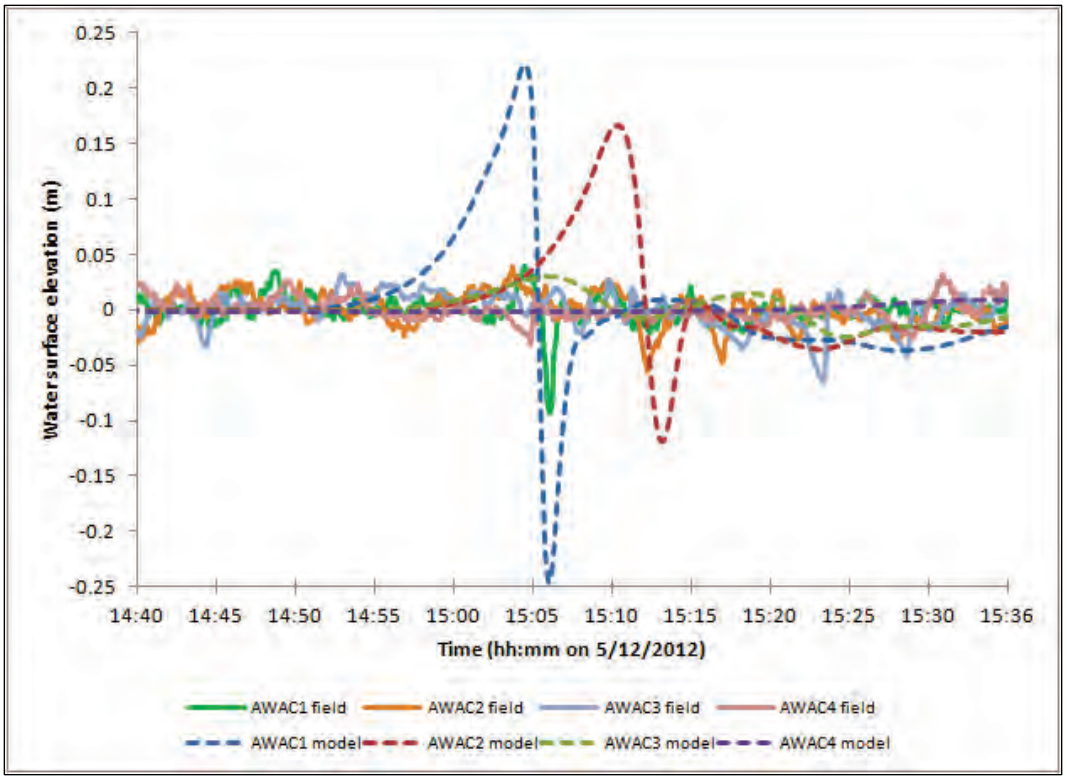

Run 2 included four vessels within approximately a 1-hour (hr) time frame. Results from this simulation are shown in Figure 30.

The results from Run 2 also show a large increase before the drawdown. The model overestimates the drawdown at AWAC 1 but varies at AWAC 2 between over- and underestimating. The model consistently underestimates the magnitude of the drawdown at AWAC 3. The differences in the model and field drawdown magnitudes are less for the first two vessel passages than for the final vessel. The third vessel is difficult to see in the model results as well as in the field data.

Run 3 is a simulation of one of the vessels included in Run 2. This vessel was run separately because, although it is present in Run 2, its effects are so minor by comparison to the other vessels that they are therefore not readily observed. This run is intended to determine how this vessel affects the waterway. Results from Run 3 are shown in Figure 31.

Figure 30. Run 2 model results.

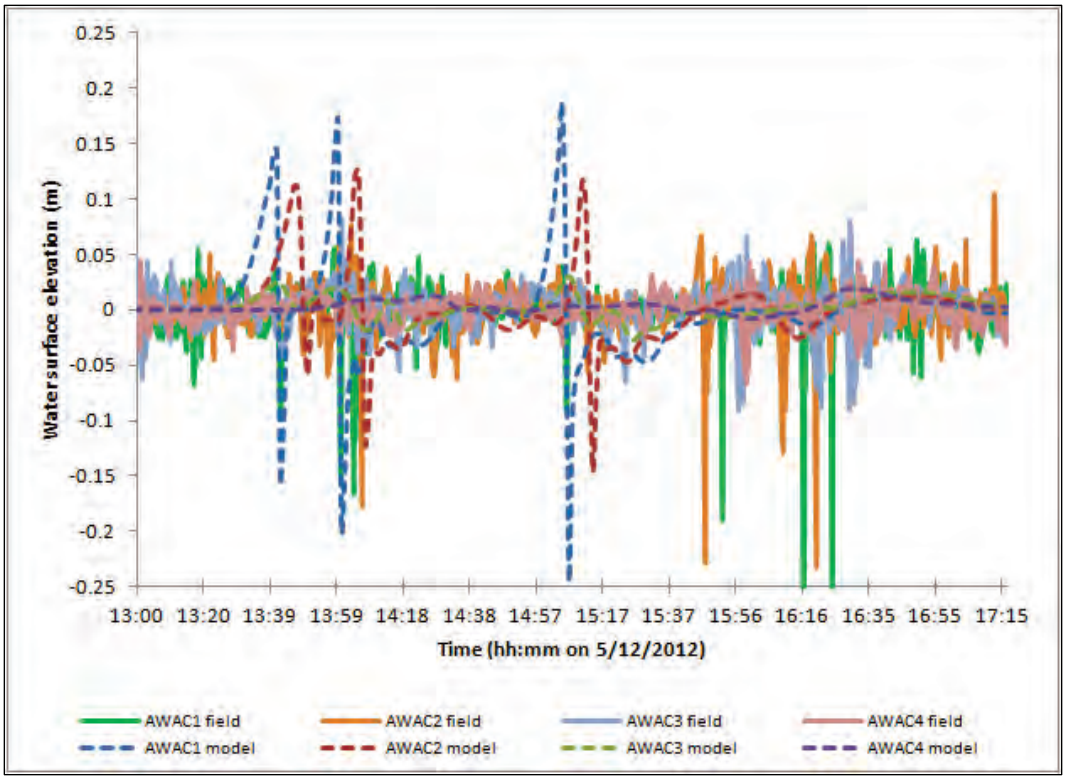

Figure 31. Run 3 model results.

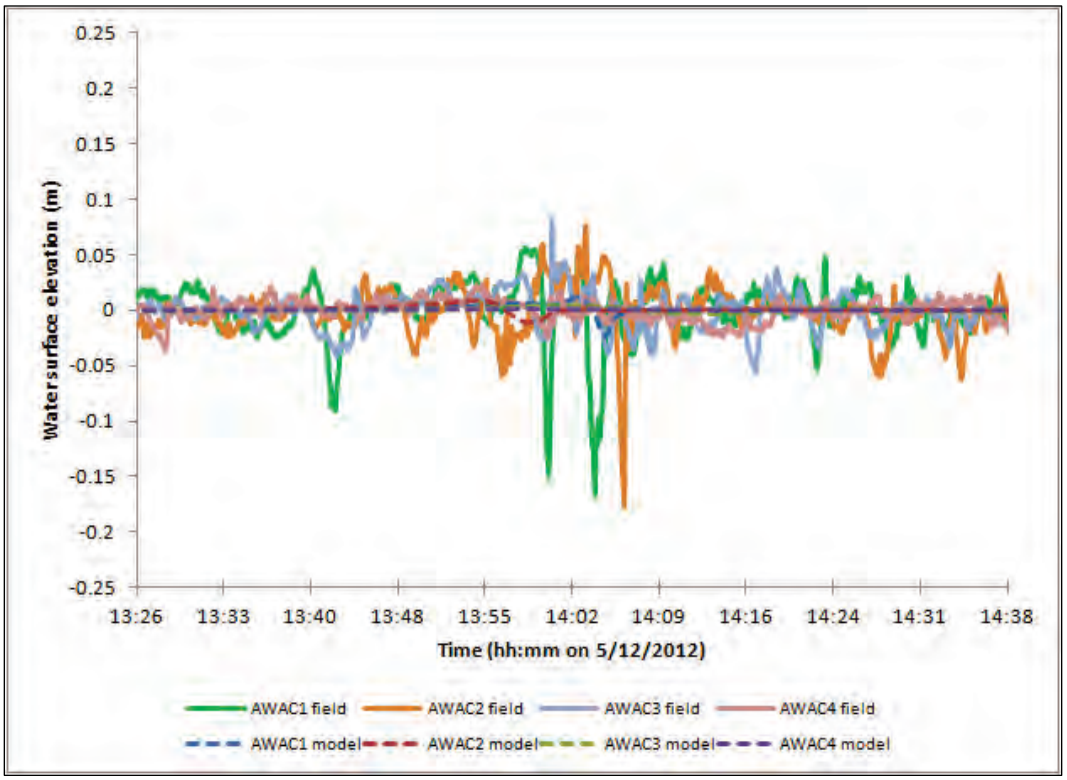

The effects of the third vessel may not be as visible as the other vessels in Run 2 because it is caught in the aftermath of the second vessel. The second and third vessels in Run 2 pass AWAC1 only 5 seconds apart. The vessel in Run 3 may be the longest vessel tested but contains the smallest beam and is traveling at the slowest speed. Therefore, the Run 3 test does verify that this vessel is being computed and that its impact is simply much smaller in magnitude than that of the other vessels. In Run 2, the second and third vessels are so close in passage time at AWAC1 that the field and the model do not show individual impacts but rather a combined impact.

Overall, the model produces a large rise in water level prior to the drawdown that the field does not show and on average, an overprediction of the drawdown magnitude. Note that the ambient conditions are not included in the model simulations, only the effects due to the vessels. Some of the inaccuracy in the comparison to the field will be due to the tide, wind, and flow conditions at the time. However, if the drawdown is overpredicted, it is likely the shear stress produced on the bed is higher, and the erosion potential is increased. This effect would produce a conservative estimate of vessel-induced bed erosion, meaning that in reality, it will likely be less than predicted.

Vessel effect summary

Based on the provided data, definitive relationships between vessel characteristics (draft, length, beam, speed) and the drawdown effect or sediment concentration are inconclusive. However, some associations can be drawn. Recall, the following hypotheses were stated:

1. The speed of a vessel impacts a larger spatial area of the bay than the size of a vessel.
2. The deep-draft vessels (over 9 m (27 ft)) keep the channel center from shoaling.
3. Barges have little impact on the shoaling at the measured locations.

The ADCP plots of the *Boxtrader* and *WH Blount* may be used to draw some conclusion for the first hypothesis in the ship channel. Based on these plots, the vessel traveling at a faster speed with a shallower draft entrained less sediment to the surface than the vessel traveling at a slower speed with a deeper draft. This result does not follow the hypothesis that a faster vessel impacts a larger area of the water column. However, the horizontal entrainment for the faster vessel appears slightly greater than

that for the slower vessel. The plots demonstrate that a slower vessel impacts the channel center longer and therefore has more time to erode material from the bed and keep it in suspension.

As for the effect of the vessel speed in the shallows away from the channel, Table 9 through Table 12 provide some insight. There is a trend that the drawdown generally increases as the speed of the vessels increases, regardless of vessel size. The correlation coefficients also indicate a trend that increasing speed will produce increasing drawdown and concentration as far away as AWAC 3. This correlation is smaller for draft or length.

The information found in Table 10 indicates that the vessels with the largest draft will produce a larger drawdown when their speed is faster. This trend is observed at all three AWACs for drafts of 11 and 12 m. At AWAC 3, the smaller draft vessels (7–8 m) actually show a decrease in the drawdown as their speed increases.

The first hypothesis is difficult to conclude due to the inability to obtain definitive drawdown and concentration data for each passing vessel at AWAC 4. The drawdown progression from the channel at AWAC 1 to the farthest, AWAC 4, was intended to help determine which vessels impacted the farthest into the shallows. Unfortunately, the time-varying data from this sampling event are difficult to interpret at AWAC 4. An additional sampling event similar to that when passing behind the vessel should be performed such that a single wave is tracked into the shallow regions of the bay to determine where its impact dissipates for various vessel characteristics.

Conclusions about the second hypothesis, shoaling of the channel center, can be drawn after analyzing the first hypothesis. The first hypothesis determined overall that a slower vessel with a deep draft entrains more sediment to the water surface in the ship channel. Although vessels with a deep draft stir up more sediment, this sediment does not necessarily move out of the channel and could redeposit. However, due to the number of vessels transiting the HSC, there is little time for material to settle and consolidate on the channel bed, allowing it to migrate up and down the ship channel based on the flow characteristics.

In the third hypothesis, the effects of barges may be analyzed by the ADCP plots created from tows (Figure 28). The plots created from tows clearly

show that a shallow draft has very little impact, if any, on the sediment in the channel. Although, if the tow is traveling near the upper slope of the channel, the potential for erosion is greater than if it is moving in the deeper areas of the channel.

The model's reproduction of vessel impacts varied between under- and overestimating these impacts. Since only vessel-induced hydrodynamics were included in the model, further studies should be conducted to include the effects of winds, tides, and river inflows. Even though the magnitude of the drawdown may not be accurate, the time in which the effect is seen at the various AWACs is close to the field time. By incorporating other hydrodynamic drivers such as winds, etc., the magnitude of the drawdown computed by the model may become more in sync with the field data.

5 Numerical Modeling

Overview

This chapter reviews the application of numerical models that were applied in this study. The purpose of these applications was to determine whether these models could be used in the future to better estimate navigation channel shoaling with improvements. The models were calibrated and validated with data measured at the site, along with other forcing information, and then applied to evaluate the accuracy of calculated shoaling for the present channel design. Two models will be presented—one for the Entrance Channel and one for the Bay.

Entrance Channel model

Model setup

The Coastal Modeling System (CMS) was applied for this investigation. The model calculates depth-averaged hydrodynamics by solving the conservative form of the shallow water equations on a uniform or telescoping Cartesian mesh (Sanchez et al. 2011a) and includes the capability to calculate waves and sediment transport. The model was applied to investigate hydrodynamics and sediment transport in the vicinity of the entrance channel.

The computational grid and bathymetry are shown in Figure 32. The grid has 121,581 cells with variable resolution from 30 to 1,920 m. A list of basic model setup parameters is presented in Table 15. The implicit CMS code was used for this study. Two time periods were modeled—February to March 2010 for calibration and June 2010 for validation.

Spatially constant water levels measured at Pleasure Pier (located on the Gulf of Mexico side of Galveston to the southwest of the inlet) was applied on the ocean boundary. A comparison of winds at Eagle Point, Pleasure Pier, and Morgan's Point was made for the modeled time periods. Based on the comparisons, temporally varying and spatially constant wind forcing measured at Eagle Point was applied. A wall boundary condition was used at all boundaries inside the bay. The Manning's coefficient was the only parameter varied for calibration in this study. Freshwater inflow from the two rivers was neglected because both time periods investigated coincided with low river flows.

Figure 32. CMS computations grid showing model bathymetry.

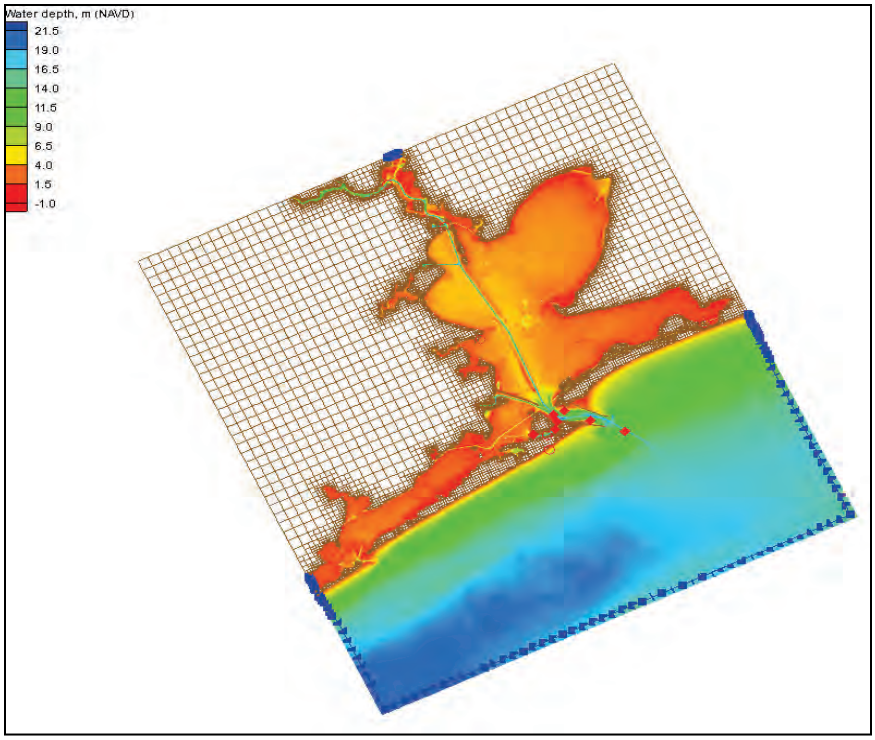

Table 15. General model parameter settings.

Parameter	Value	Default
Flow time step	360 s	None
Simulation durations	83 hr, 576 hr	None
Ramp time	0.25 hr	None
Manning's *n*	0.015 s/m$^{1/3}$	None

Circulation model

Comparison between measured and calculated water level and currents are presented for model validation at Galveston Bay, TX. Four goodness-of-fit statistics assessed how well the model matched observed values. These statistics are Normalized Root Mean Square Error (NRMSE), Normalized Mean Absolute Error (NMAE), R-squared (R^2), and Bias. Equations used to estimate goodness-of-fit are defined in Appendix A of Sanchez et al. (2011a). Results were analyzed in MATLAB and the Surface-Water Modeling System (SMS).

Calibration results (February–March 2010)

CMS was calibrated over a period of approximately 2 weeks between February–March 2010 using data previously described in Chapter 3.

Calibration was achieved by varying Manning's roughness parameter (n) until error between model results and measurements was minimized (n = 0.015 s/m$^{1/3}$ was the best fit). Figure 33 compares NOAA-measured and CMS water level at Eagle Point. Figures 34 and 35 plot measured and modeled currents along the principle axis at Platforms A and D (location shown in Figure 11). Not all physical processes present in Galveston Bay are captured by this application of CMS. Some examples of the many different factors that impact water movement are local deviation in winds, the influence of vessels berthed along channels, and unresolved bathymetric features. These factors introduce noise to the measured current speed and direction. One way to better compare model results to field data is to extract the component of the current along the principal axis (i.e., the axis along which the majority of the readings were measured). This practice can help verify the quality of the model. Statistics representing goodness-of-fit for currents at the data collection platforms and water levels at Pier 21 and Eagle Point are listed in Table 16. Overall, the model represents circulation well except for currents between Galveston and Pelican Islands.

To investigate reduced performance between the islands, x- and y-axis components of velocity were compared at Platforms A and D (Figures 36 and 37, respectively). The figures show that the flow direction is well captured in the entrance channel (Platform D) but less so in the channel between the islands (Platform A). This may be a result of the complex topography of the channel, details of which were not included to reduce model run time. Topography in the channel is complicated by the shape of the berthing facilities that can be difficult to measure due to the presence of large vessels.

Validation results (June 2010)

Field data measurements from June 2010 were used to verify model performance. Figure 38 shows measured and modeled water levels at Eagle Point. Measured current speed at POD 3 (location shown in Figure 13) was compared to model results in Figure 39, showing good agreement (although the water level shows better agreement than the velocity). Current direction was not well measured making it difficult to validate, as shown in the comparison between x- and y-axis components of velocity in Figure 40. Goodness-of-fit statistics for currents at POD 3 and water level at Pier 21 and Eagle Point are presented in Table 17.

Figure 33. Comparison between CMS and measured water level at Eagle Point.

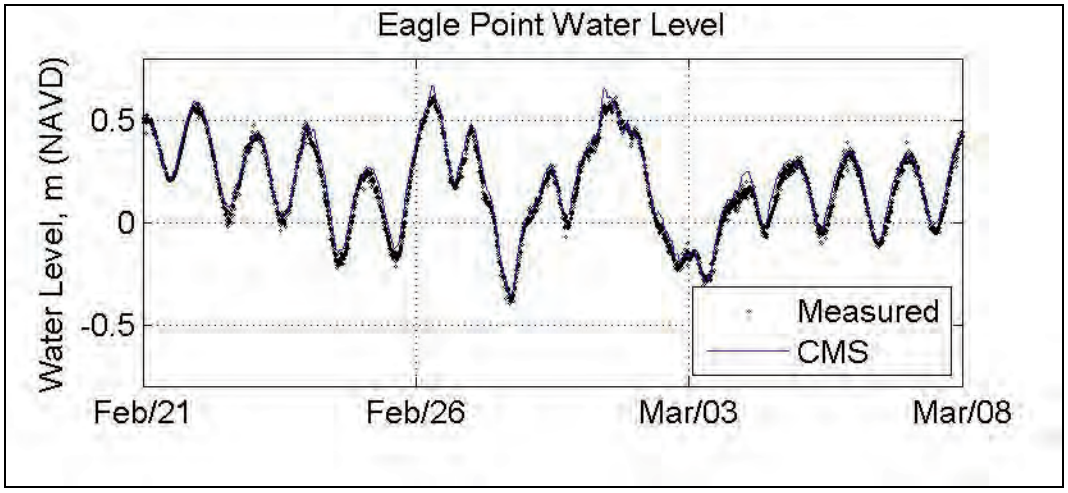

Figure 34. CMS and measured currents along the principal axis at platform A.

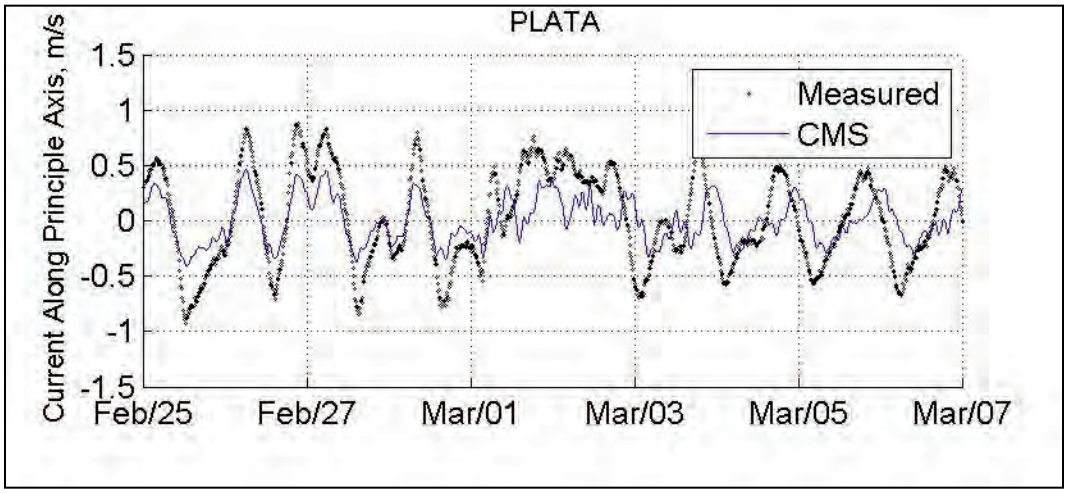

Figure 35. CMS and measured currents along the principal axis at platform D.

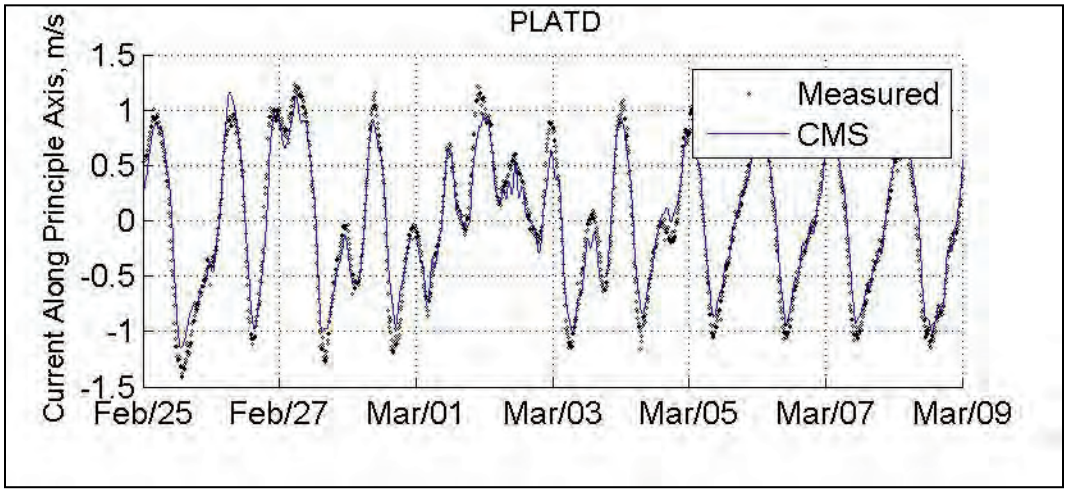

Table 16. Goodness-of-fit statistics for currents and water level for calibration.

Station	NRMSE	NMAE	R^2	Bias
PLAT A	36%	30%	63%	–0.01 m/s
PLAT B	39%	28%	45%	0.01 m/s
PLAT C	39%	32%	26%	0.01 m/s
PLAT D	7%	5%	98%	0.00 m/s
Eagle Point	4%	3%	99%	0.03 m
Pier 21	3%	3%	99%	0.00 m

Figure 36. *x*- and *y*-axis components of velocity at Platform A.

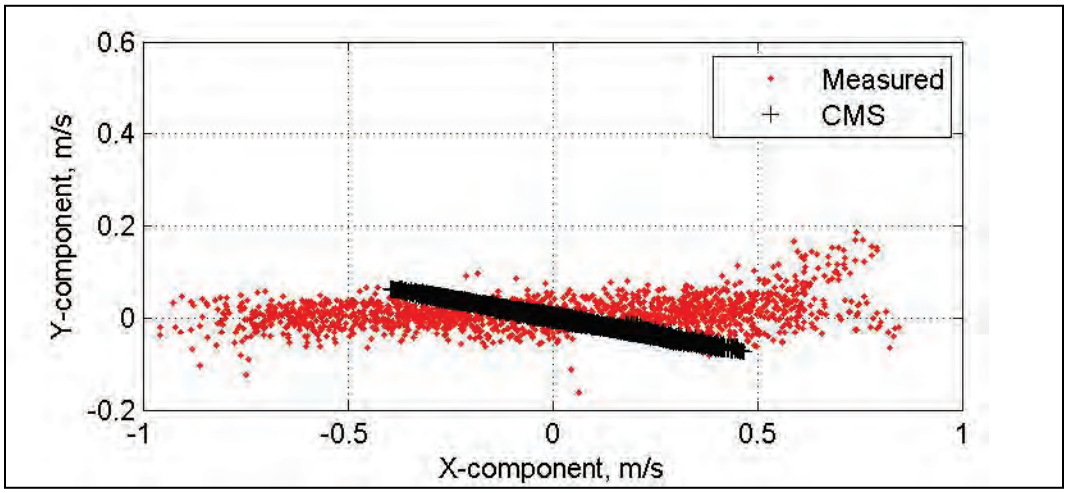

Figure 37. *x*- and *y*-axis components of velocity at Platform D.

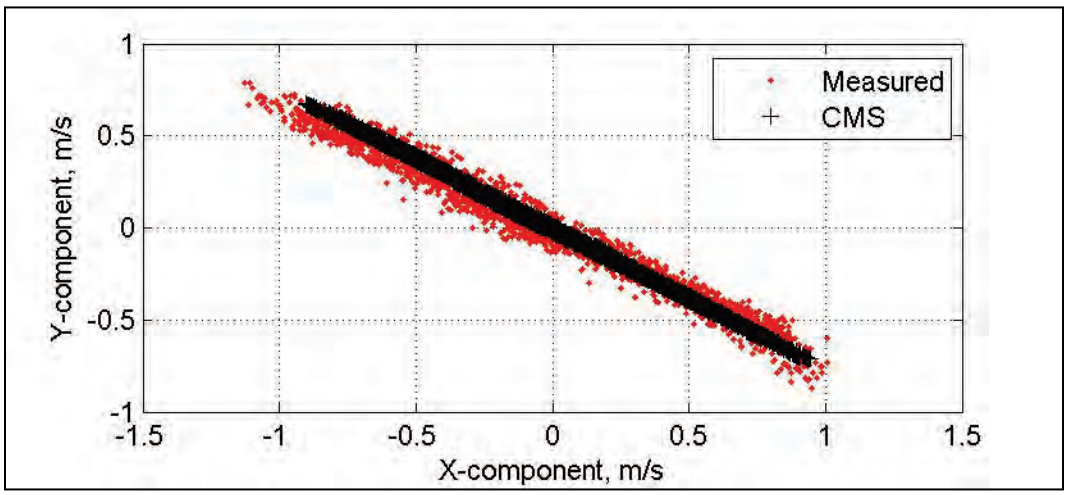

Figure 38. Comparison between CMS and measured water level at Eagle Point.

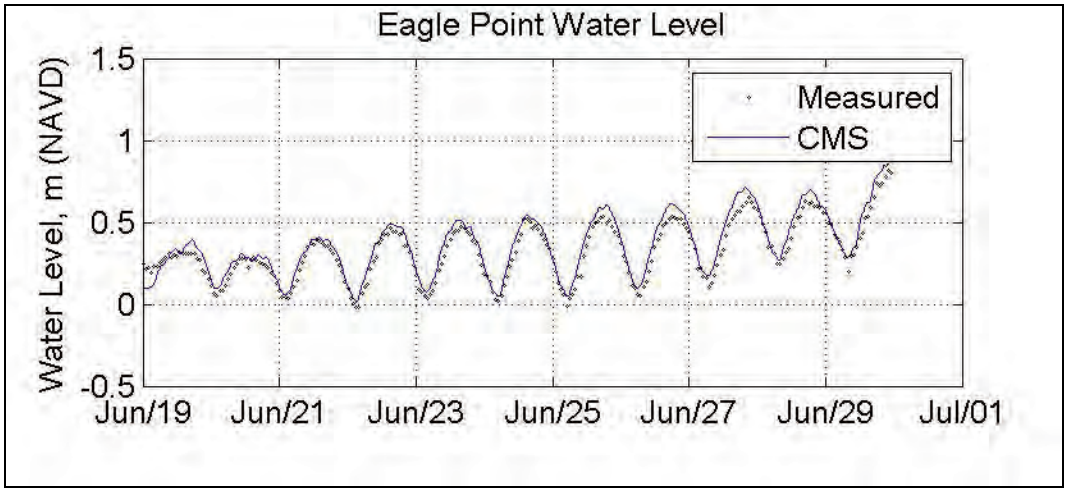

Figure 39. CMS and measured current speed at POD3.

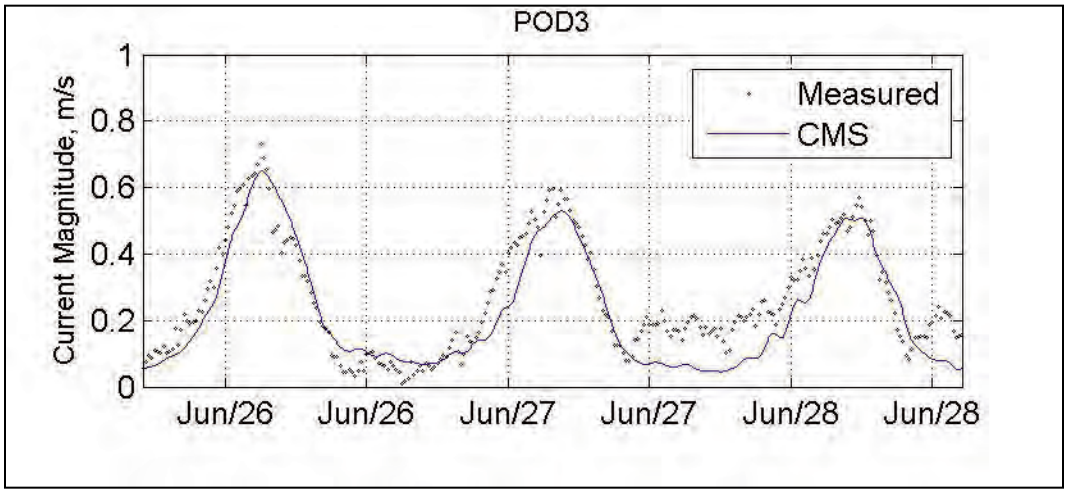

Figure 40. *x*- and *y*-components of velocity at POD 3.

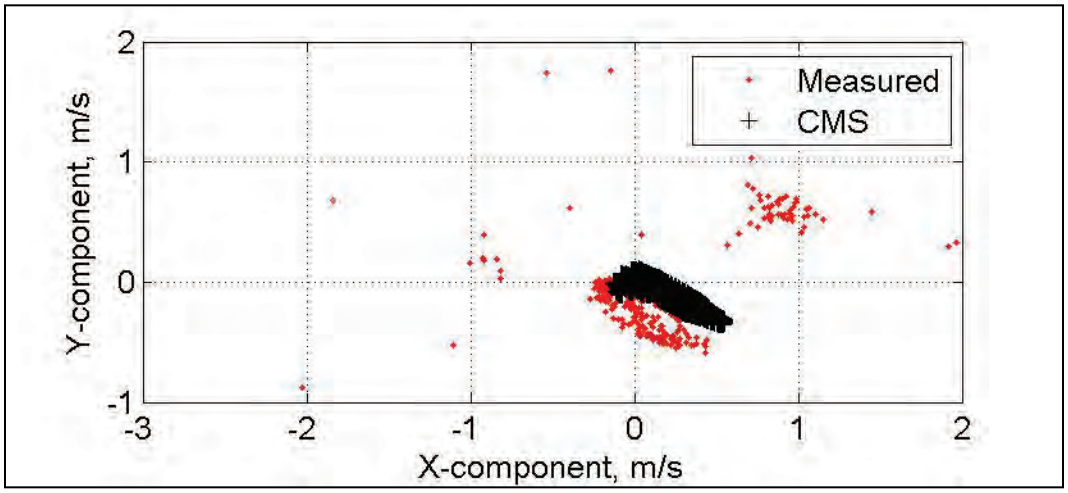

Table 17. Goodness-of-fit statistics for verification.

Station	NRMSE	NMAE	R^2	Bias
POD 3	12%	10%	92%	–0.04 m/s
Eagle Point	19%	15%	58%	0.01 m
Pier 21	17%	14%	80%	0.04 m

Sand transport modeling

The validated model previously discussed was used to compare measured and modeled sediment concentration in the Galveston Entrance Channel. Data used in the analyses are from the period of 27–29 June 2010. The CMS code was applied to calculate sediment concentration and sand transport in Galveston Bay, TX, in the vicinity of the Entrance Channel. The Entrance Channel is characterized by primarily sandy sediment, although shell hash is often observed (Figure 14). Measured data, described in the following, were compared to model results to calibrate the model. Many sediment transport formulations exist, and the best fit is often location specific, so it is common to test multiple formulations when developing a model. Two transport formulae were used to model sand transport and concentration: LUND-CIRP and Van Rijn. The results were then compared to measured data. Additional CMS runs were performed using varying grain sizes to determine model sensitivity to the particle size used for sediment data in the entrance channel and to evaluate the effect of grain sizes on model results.

Sediment transport measurement and modeling

Measured sediment transport data were acquired by CHL. Data collection was described in Chapter 3. These data included measurements along each range at varying depths. Sediment flux across transects was measured in units of kilograms per second (kg/s). Observed transport was determined from the data in two ways:

- **Method 1**: Calculated by taking the ADCP discharge from each bin and multiplying by the total suspended mass (TSM) calculated from the ADCP backscatter for the corresponding bin. Those values were then summed to give the transport flux.
- **Method 2:** Calculated by taking the average of the TSM values obtained from the bottle samples and multiplying that average by the flow discharge.

The LUND-CIRP and Van Rijn methods were selected for sensitivity analysis based on initial unpublished runs with this model grid and results of previous model studies (Sanchez et al. 2011b). Sediment transport data were extracted from CMS using the methods outlined on the CIRP wiki (http://cirpwiki.info/wiki/Main_Page).

Sediment flux measurement and modeling

Sediment flux measured in June 2010 is compared to CMS calculated flux in this section. Field-measured data and CMS calculations are presented in units of kg/s. Figures 41 through 45 graphically present measured and modeled sediment transport data for the Galveston Entrance Channel at the range locations shown in Figure 12. The figures show that the LUND-CIRP formula generally better represents the sediment transport data at most measurement locations. Van Rijn often over- and underpredicts, as supported in the figures.

Figure 41. Range 1 sediment flux measured values and model calculations.

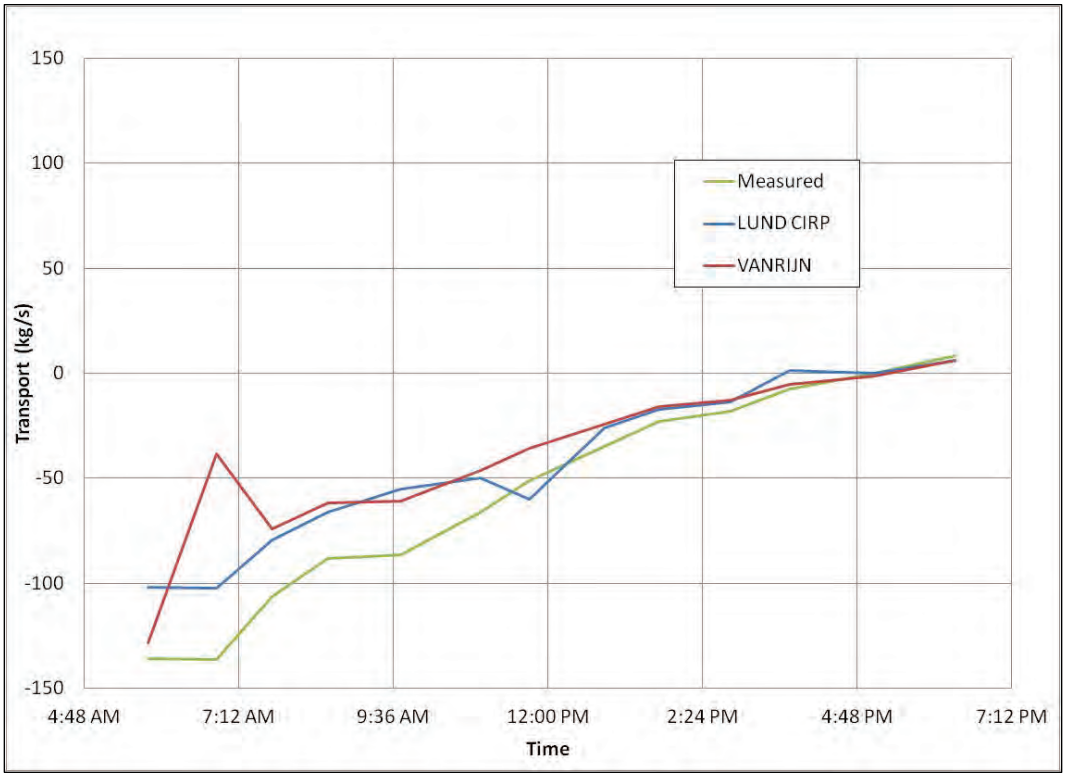

Figure 42. Range 2 sediment flux measured values and model calculations.

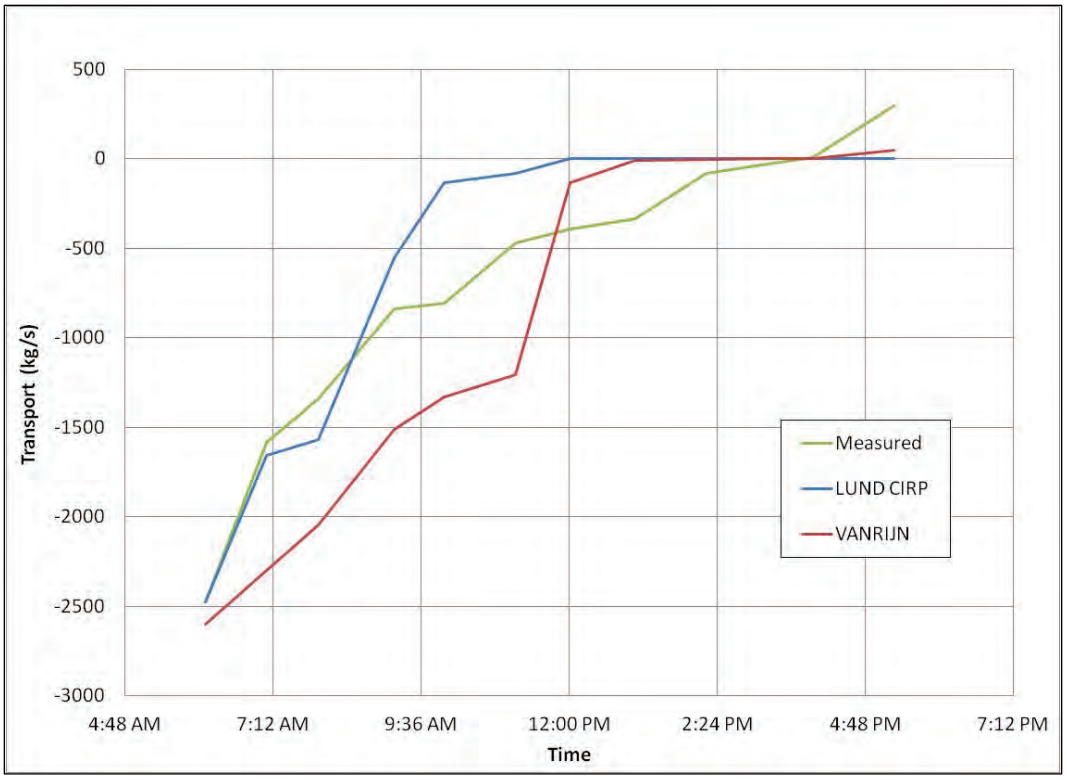

Figure 43. Range 4 sediment flux measured values and model calculations.

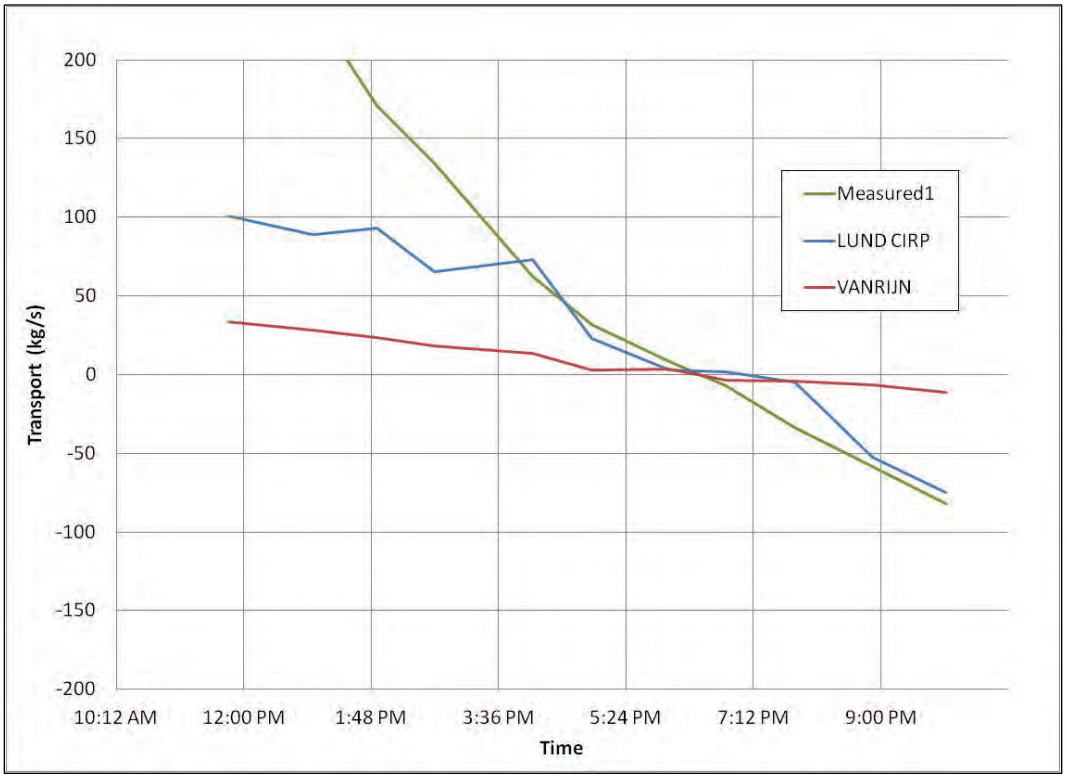

Figure 44. Range 5 sediment flux measured values and model calculations.

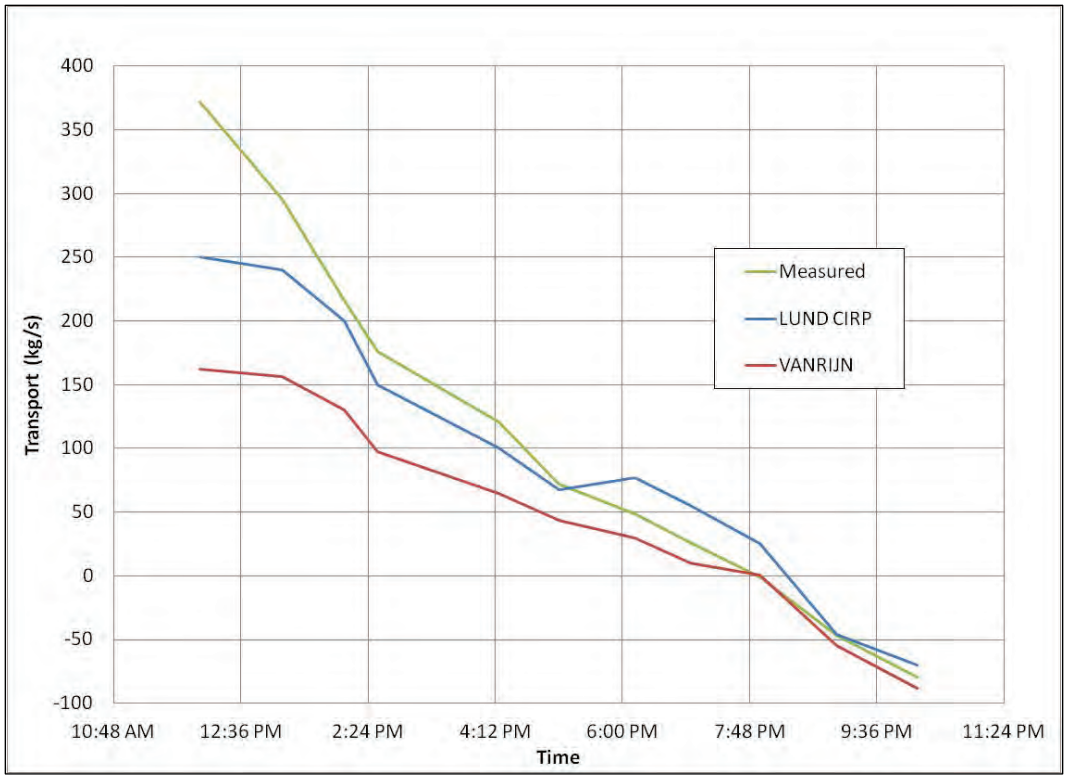

Figure 45. Range 6 sediment flux measured values and model calculations.

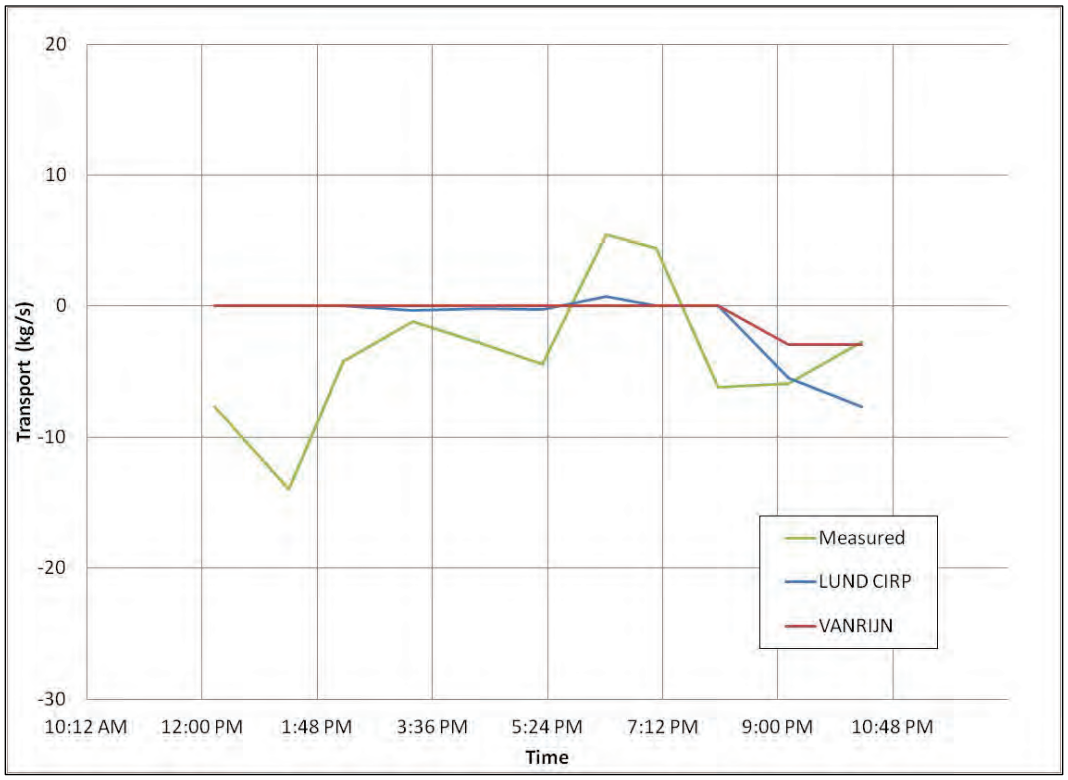

The model was also run for variable sand sizes to determine the effect on estimated sediment concentration and transport. In addition to running the CMS model with a constant D_{50}, runs were performed using additional maximum and minimum sediment sizes. The transport estimates based on a constant D_{50} produced changes in sediment transport model estimates of between 1% and 2%. Using these data, it was determined the transport estimates from the model were not significantly sensitive to varying D_{50}.

Sediment concentration measurement and modeling

Measured sediment concentration data were collected by CHL. In the previous section, measured sediment flux across the range line was presented. Concentration measurements were taken on 27–28 June 2010. Field-measured data were provided in mg/L.

CMS was used to calculate sediment concentration for comparison to field-measured data. The Van Rijn and LUND-CIRP formulas were used in the CMS model. Figure 46 through Figure 50 graphically display the sediment concentration data for June 2010 compared to model results.

Figure 46. Range 1 SSC measured values and model estimates.

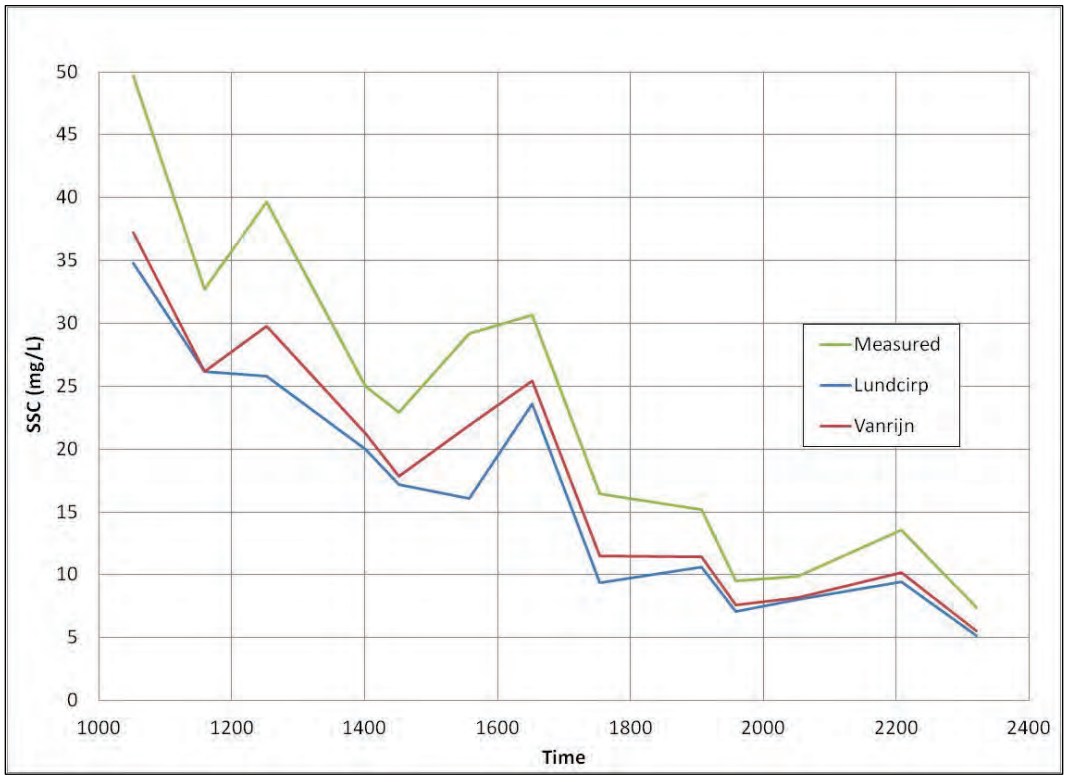

Figure 47. Range 2 SSC measured values and model estimates.

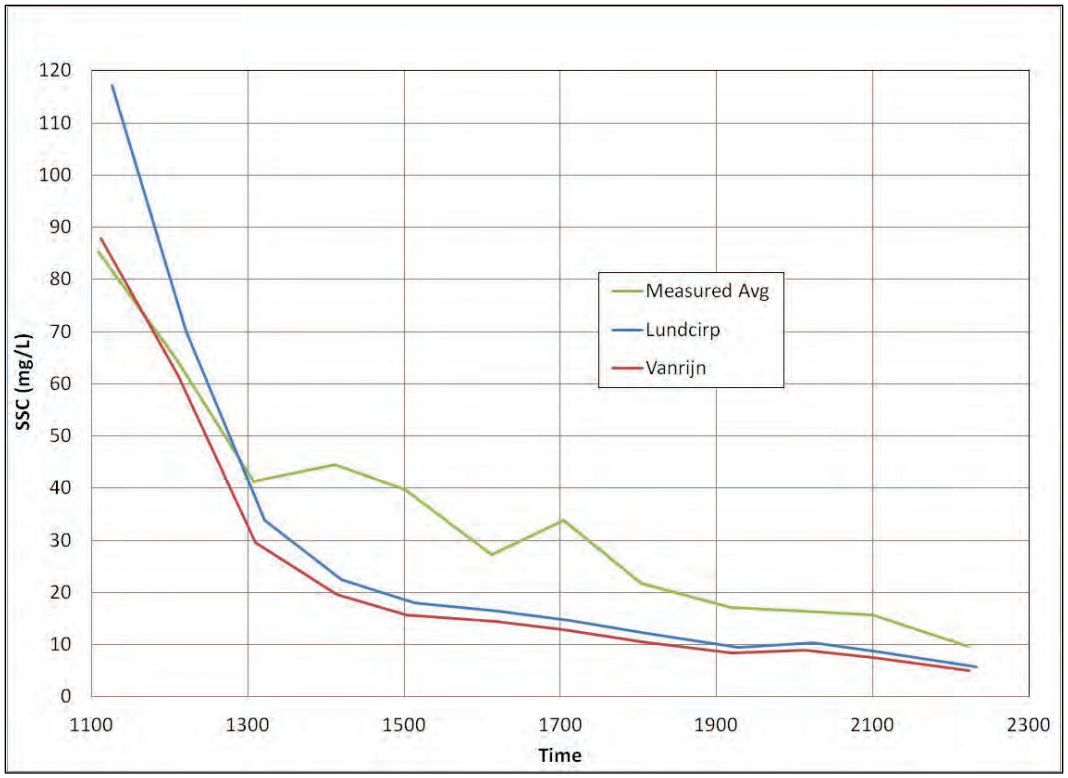

Figure 48. Range 4 SSC measured values and model estimates.

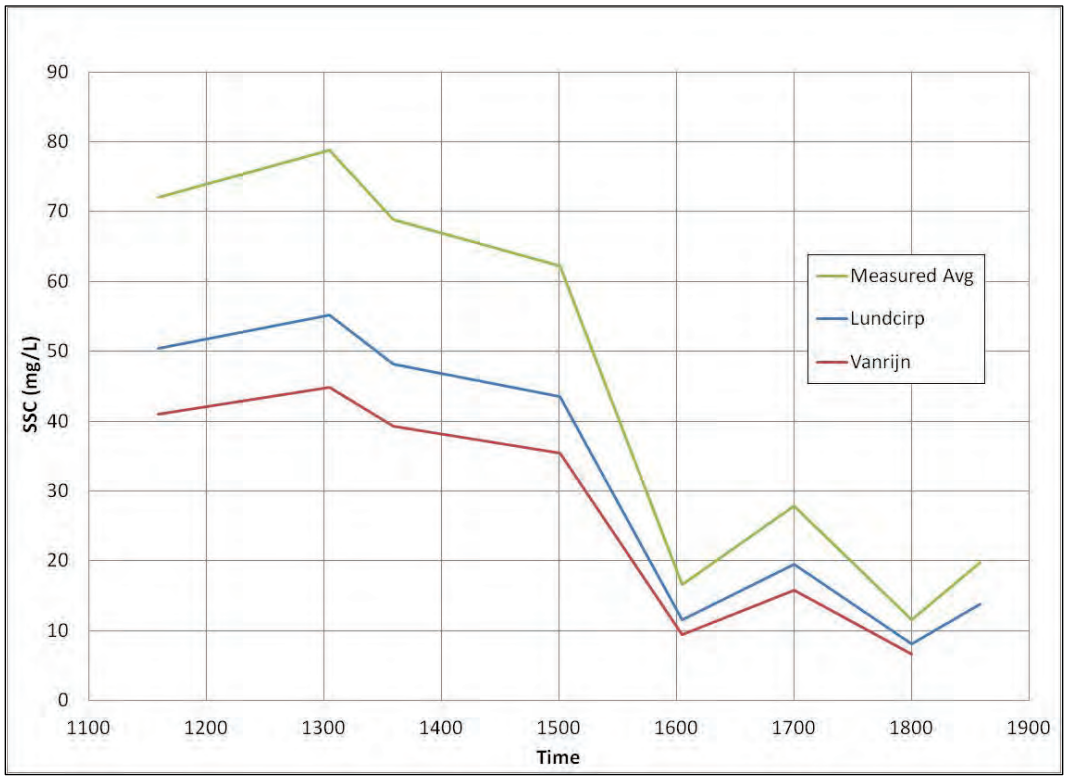

Figure 49. Range 5 SSC measured values and model estimates.

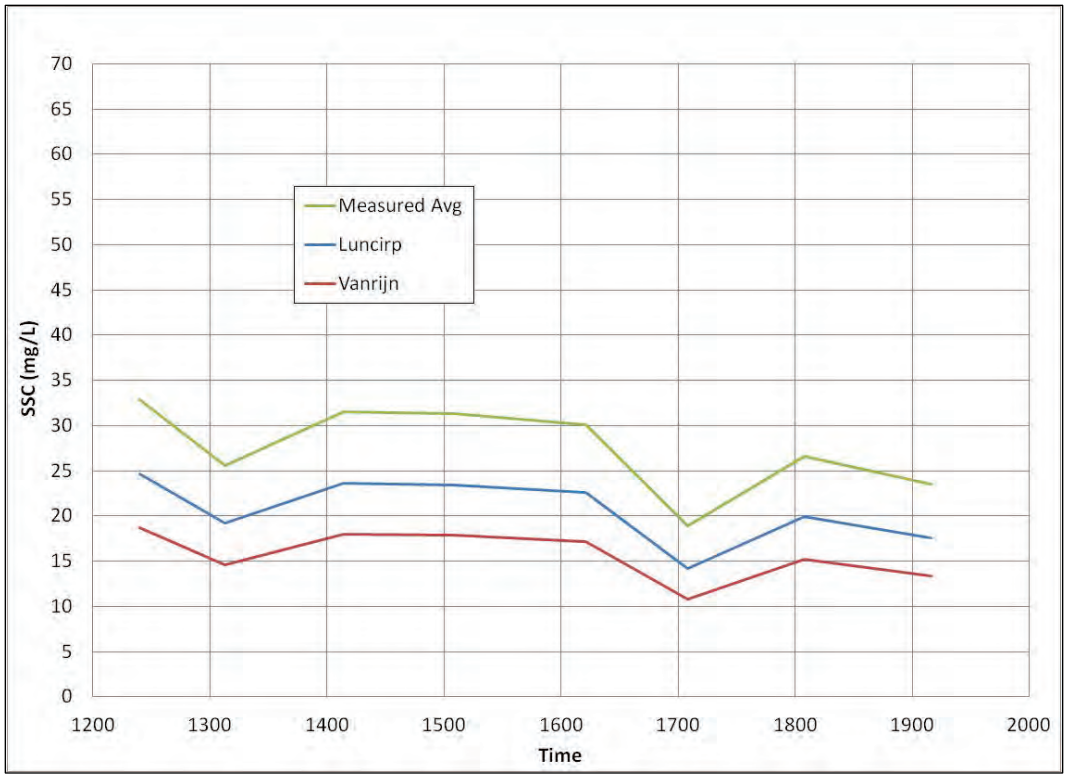

Figure 50. Range 6 SSC measured values and model estimates.

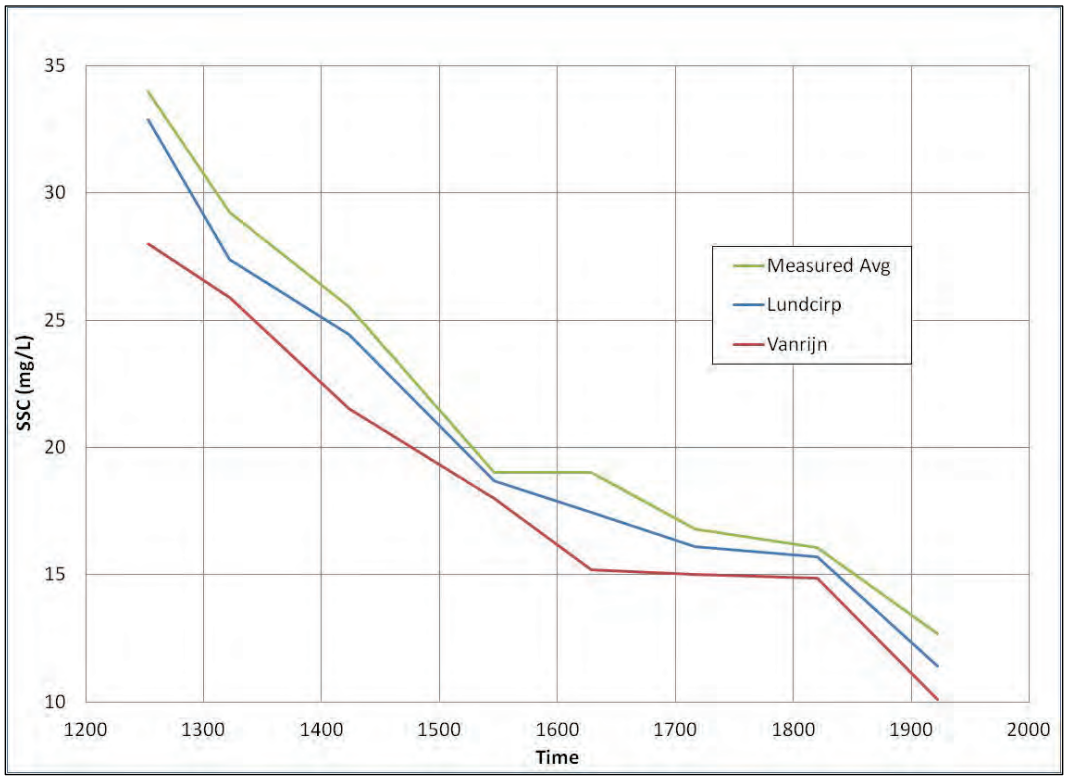

Modeled suspended sediment concentration (SSC) results versus measured were compared for both LUND-CIRP and Van Rijn formulas. These comparisons are shown in Figures 45 through 49 for the different range locations (Figure 12). Van Rijn consistently underestimated concentrations as is often the case. LUND-CIRP-based calculations better represented the measured concentration data.

Conclusions

Data collected during two time periods in 2010 were applied to validate the CMS for circulation and sand transport. Measurements of water level and currents were compared with CMS-computed results at multiple locations including the Galveston Entrance Channel, the channel between Galveston and Pelican Islands, Mid-Bay, and the Gulf of Mexico outside the inlet. CMS was run using default settings, except for the Manning's coefficient (n = 0.015 s/m$^{1/3}$), which was varied for calibration. Water level was well represented by the model at all measurement locations as quantified in Tables 16 and 17. Measured currents compare well to modeled currents (quantified in Tables 16 and 17), except within the channel between Galveston and Pelican Islands. Between the islands, velocity magnitude is reproduced; however, flow direction and phase are not. Increased resolution in the channel and accounting for the presence of large vessels may improve results in this physical area. When applying this CMS model in the future, model accuracy quantified in this section should be used to help characterize potential accuracy of model results.

Recommendations for practical applications

The following recommendations are offered based on lessons learned during this model application:

- Spatially constant wind forcing may be applied over bay-scale domains, even when it is an important process. Although not specifically demonstrated for this case, it is important to test this assumption for each time period by comparing observed winds at multiple stations across the domain. Model results will be less accurate as the winds become less constant in space.
- Poor resolution over complex topography could result in locally less accurate results; however, lower resolution is often desired away from the area of interest to increase computational speed.

- Manning's roughness was varied for calibration. In general, the value for this parameter should always be based on comparison of model results to measurements.
- LUND-CIRP-based calculations better represented the measured concentration and sediment transport data than the Van Rijn formula, making LUND-CIRP the best option for additional sediment simulations.

Bay channel model

The bay channel model incorporated several factors to compute sediment movement in the bay. The model included hydrodynamic drivers such as tides, river inflows, and winds. Because this area experiences high volumes of vessel traffic daily, the effect of this traffic on the sedimentation is important. Included in the sediment model was also the effect of average daily vessel transit. A single day of vessel traffic was repeated for each day and included in the sediment model simulation.

The TABS-MDS code was used for the estuarine modeling performed for this study. TABS-MDS is a 2D/3D, finite-element code that simulates hydrodynamics, salinity, and sediment transport. The code solves the basic physics of hydrodynamics and salinity transport through the use of the laws of mass and momentum conservation. A similar version of this code was used in a previous study of the HSC (Tate et al. 2008). The current work builds on the previous studies. This code has been used successfully on many estuarine systems, including the Cape Fear River, the Lake Pontchartrain–Lake Borgne area, New York Harbor, and San Francisco Bay.

The sediment modeling was also performed using TABS-MDS. This modeling was performed uncoupled from the hydrodynamics (i.e., the sediment model results do not impact the hydrodynamic results).

The vessel simulations were performed using Adaptive Hydraulics (AdH). This is a 2D code that allows for the movement of a vessel—based on its size, draft, and speed—to impact the surrounding waterway. This same tool was used in the vessel modeling described in Chapter 4. The shear stresses from the daily vessel simulations are incorporated into the sediment model so that the effects of the vessel movement and the effects of the hydrodynamics are both included in the sediment transport predictions. The sediment model was checked qualitatively under the

present study due to limited field data for the period of simulation, so the parameters as set in Tate et al. (2008) were maintained.

Boundary conditions

Inflow

The Texas Water Development Board (TWDB) uses TxBlend (TWDB 1999) to forecast salinity in the bay for their purposes. They determine freshwater inflows from a watershed model that they maintain. The TWDB freshwater flow data were used in the TABS-MDS model to ensure that the most recent rainfall/runoff predictions were being used. The model included freshwater inflows at nine places as shown in Figure 51. The daily data for the rivers are shown in Figure 52, and the ungaged inflows are shown in Figure 53.

Figure 51. Bay model inflow locations.

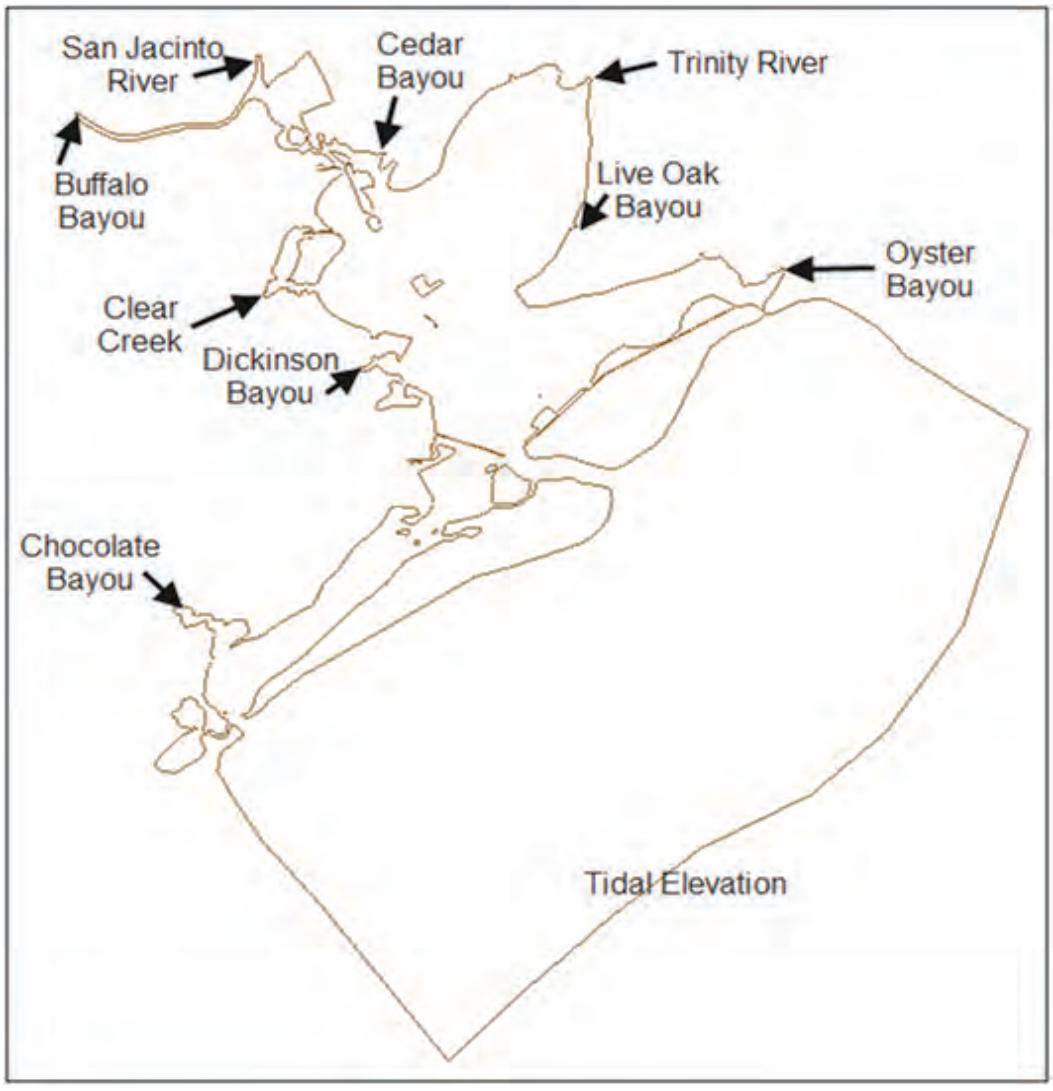

Figure 52. San Jacinto and Trinity River inflows from TWDB.

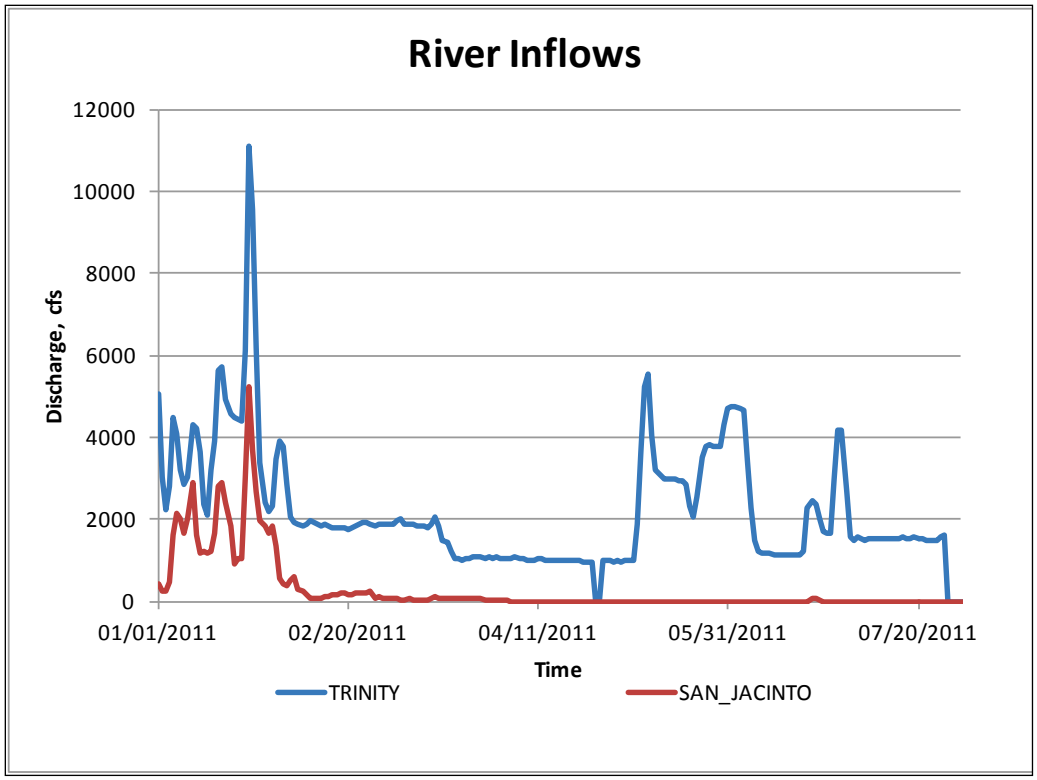

Figure 53. Ungaged freshwater inflows from TWDB.

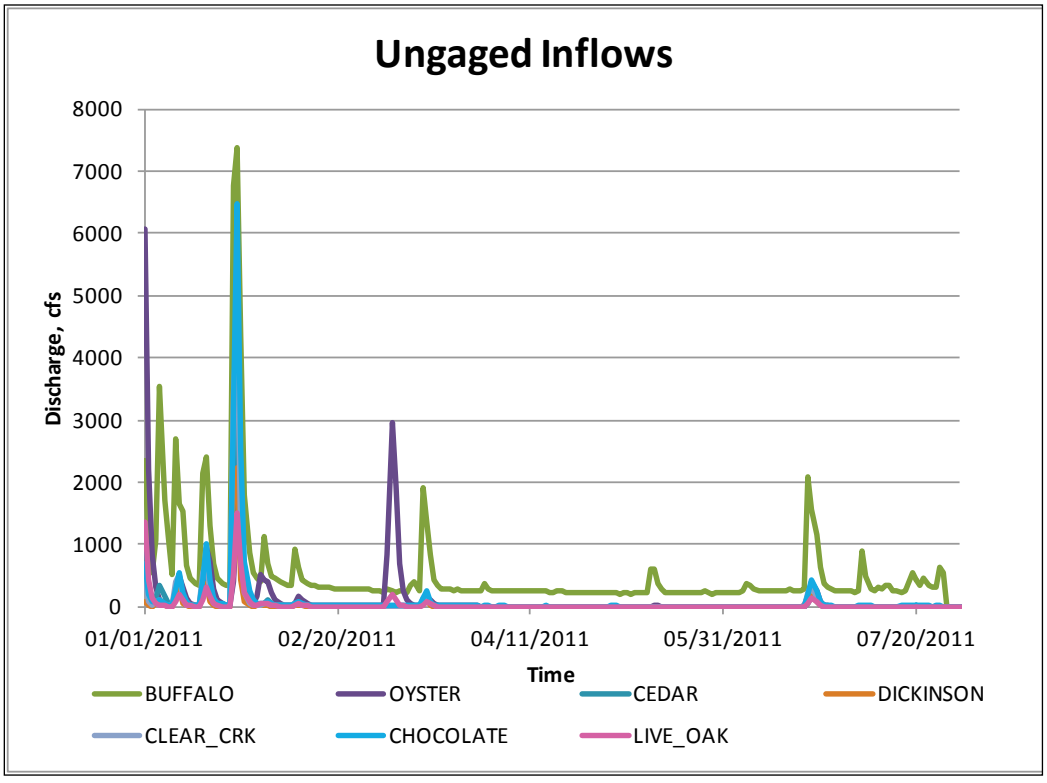

Wind

Wind data used in the 1990 and 2000 efforts were taken from the Houston Intercontinental Airport on the north side of Houston, TX. These data were then shifted based on a correlation made to a short-term gage that had been located in the bay during the 1990 study data collection (Tate et al. 2008). Rather than manipulate wind data from miles away, for this study wind data from Eagle point (shown in Figure 54) were used to drive wind-induced currents in the model. Figure 54 shows the time-varying wind data used.

Figure 54. Wind speed and direction from Eagle Point

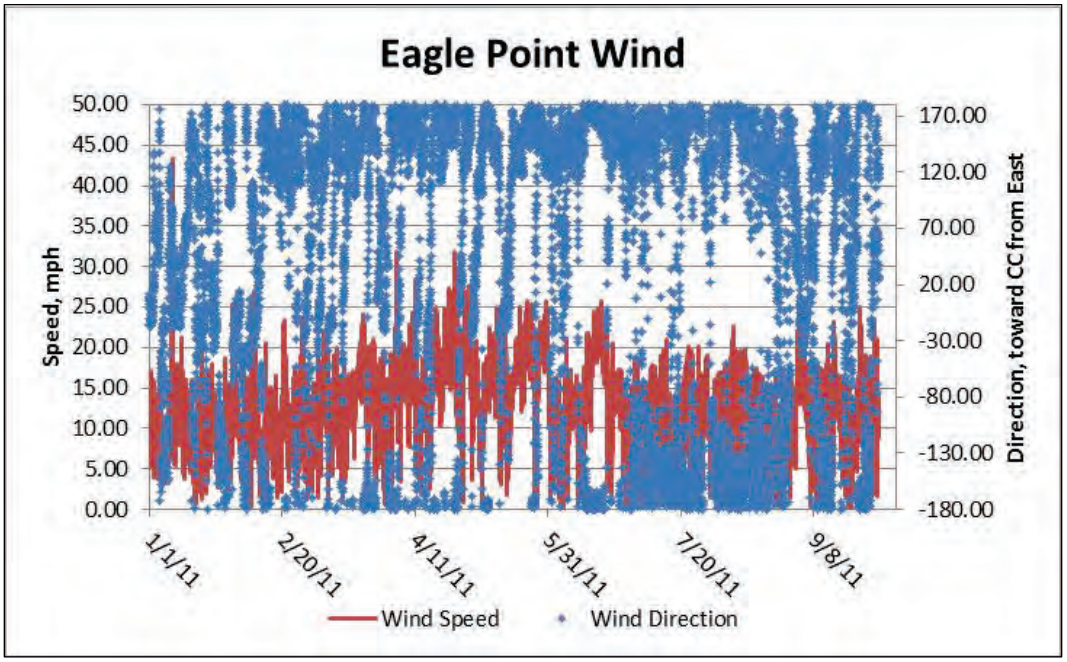

Salinity

Although new wind stations were available for the recent work, new Gulf of Mexico salinity data stations were not available. Previous studies used monthly averages from a 19 yr data set for the model's salinity boundary condition (Tate et al. 2008). It is known that the spring freshwater Mississippi and Atchafalaya River flows, located to the east of Galveston, are transported westward along the coast, dropping the salinity in the Gulf of Mexico at Galveston. Salinity test simulations were performed with the model using the monthly average salinity boundary condition, a constant salinity boundary condition, and a salinity boundary condition correlated to Mississippi River flows. The best comparison to the field data came from the Mississippi River correlation. The correlation was determined from the

previously used monthly average gulf salinity values and Mississippi River flows for the same period such that recent salinity values could be predicted. Given the lack of field-measured data on the gulf side of Galveston, this method was a reasonable alternative. The salinity boundary condition for the Gulf of Mexico model boundary is shown in Figure 55.

Figure 55. Mississippi River correlated salinity boundary condition.

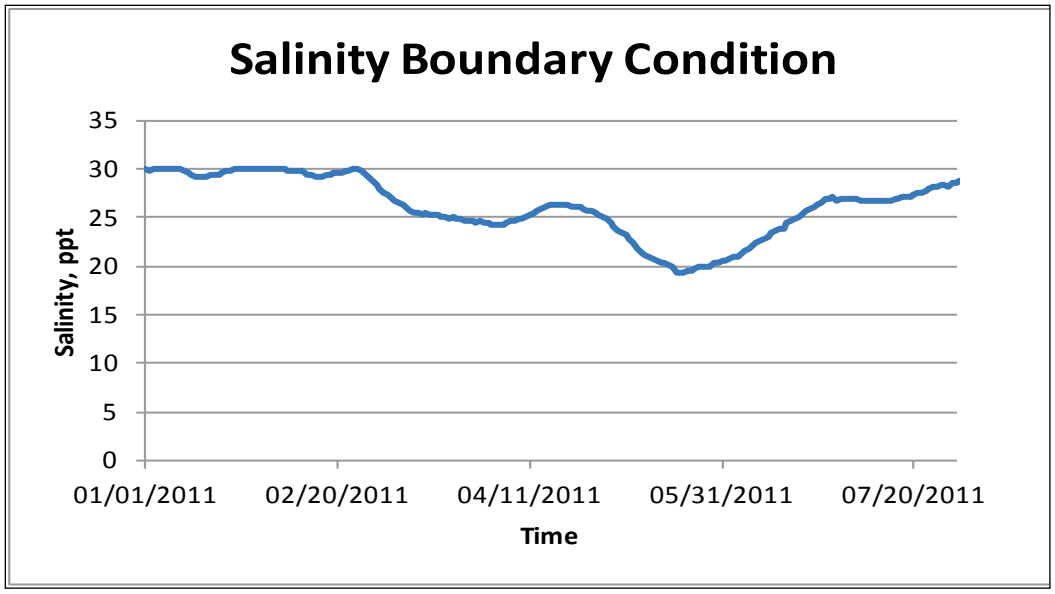

Sediment

The sediment model is driven by the estuarine and vessel motion hydrodynamic modeling results. The boundary conditions for the sediment modeling include grain characteristics, bed definitions, and sediment loads. The same conditions established from the previous sediment model validation (Tate et al. 2008) were used, and the inflow sediment and bed materials are divided into 50% silt material and 50% cohesive material. The sediment-specific parameters are listed in Table 18.

Table 18. Sediment parameters and values

Parameter	Value
Critical shear for deposition of the cohesives	0.05 Pa
Critical shear for erosion of the cohesives	0.1 Pa
Settling velocity of the cohesives	0.05 mm/s
Particle erosion constant for the cohesives	3.84×10^{-5}
Critical shear for deposition of the silts	0.1 Pa
Critical shear for erosion of the silts	0.67 Pa
Settling velocity of the silts	0.22 mm/s

Sediment loads are applied to the two major rivers in the area, the Trinity River and the San Jacinto River. These loads are determined from a rating curve correlating discharge with concentration generated using data from the U.S. Geological Survey (USGS) as documented in Tate et al. (2008). The sediment loads for each river for this 2011 simulation period are shown in Figure 56.

Figure 56. Sediment concentration for the Trinity and San Jacinto Rivers.

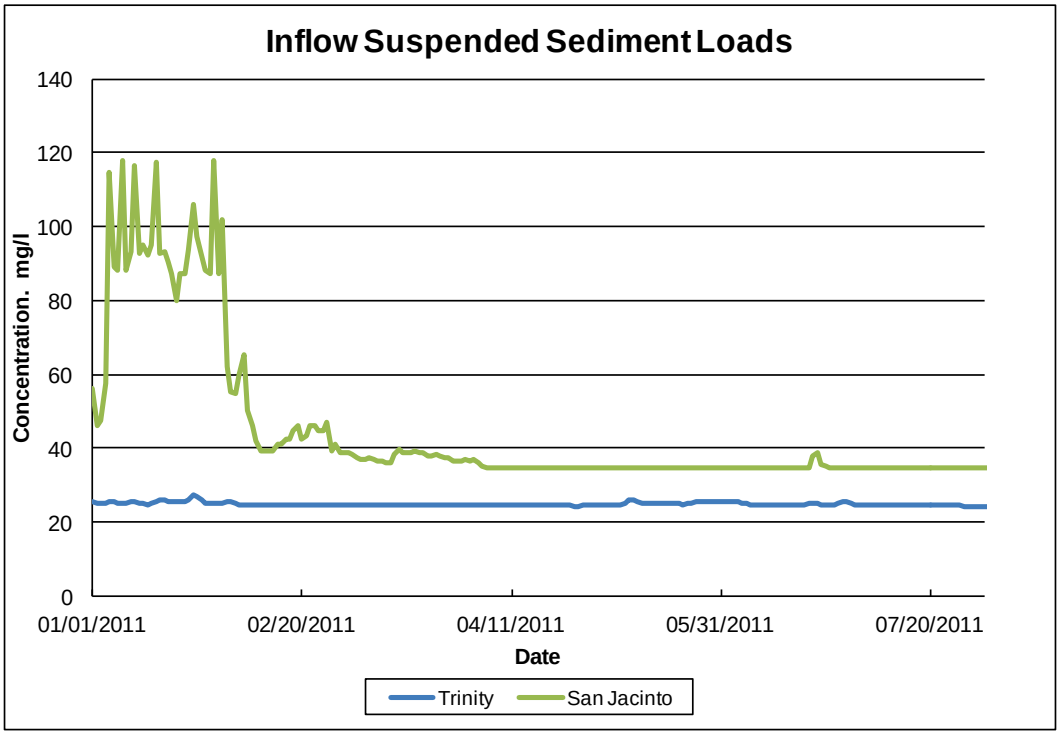

Vessels

The vessel modeling performed using AdH for the sediment portion of this study consisted of a single day of vessel traffic. This representative day was repeated daily in the sediment model. The AdH simulation includes only the bay portion of the model domain and does not have any boundary conditions (i.e., no tide or inflow conditions). The only effects on the water body are due to vessel movement. This is acceptable since all other necessary hydrodynamic effects are modeled in the TABS-MDS hydrodynamic simulations. Forty-eight vessels of different dimensions and paths were included in these simulations. These are the same vessel definitions used in the previous sediment studies in the HSC area (Tate et al. 2008). Table 19 lists the range of dimensions for the 48 vessels simulated. The numerical model mesh used for vessel modeling contains much more resolution than the TABS-MDS model mesh due to the necessity of having several elements

overlap a single vessel. The added base resolution, along with the automatic mesh adaption (refinement) that occurs during the model run, ensures appropriate resolution for calculating the ship waves. In order to correctly compute the actual speed and progression of the wave, and therefore the bed shear stresses, the time-step size is also much smaller for these simulations. Again, details of the vessel inclusion in the sediment model validation can be found in Tate et al. (2008).

Table 19. Vessel characteristics.

Parameter	Value
Draft	15–38 ft
Length	300–900 ft
Beam	50–140 ft
Speed	15–25 ft/s
Travel path	Starting and ending at Sea, Bayport, Barbour's Cut, and Baytown

The movement of the vessel generates a return current that moves out and around the vessel and returns to the channel behind the vessel. The return currents alone can be significant enough to cause erosion of the channel, and the resulting long waves that move into the shallows can cause erosion of those areas as well. The AdH simulation generates the velocity pattern around the vessel caused by the return current and into the surrounding shallows. As the long wave generated by the vessel propagates into the shallows, it will form a bore. This occurs where the vessel speed is greater than the free surface wave speed. This wave speed is approximately $\sqrt{(gh)}$. Here g is the acceleration associated with gravity, and h is the water depth. In shallow water, this free-surface wave speed, or celerity, is slower than in deeper water, thus resulting in a bore. These simulations with moving vessels are only appropriate for the areas immediately outside of the channel and beyond. The solutions directly in the channel are not accurate because the vessel propeller effects are not included, and the model is hydrostatic. Modeled results of water levels produced by a moving vessel as compared to field-measured data are given in Chapter 4.

These AdH simulations provide the vessel-induced shear stress on the bed. This stress field can then be applied to the TABS-MDS sediment model so the shear stresses caused by the vessels are included with those generated by the hydrodynamics, including freshwater flow, tide, and wind. Therefore, the TABS-MDS hydrodynamic model is run, and the AdH vessel model is

run, then the hydrodynamic results and the additional vessel shear stresses are used to drive the TABS-MDS sediment model.

Mesh modifications

The 1990 modeling efforts included a planned condition. Since this time, the planned condition for the Mid-Bay Marsh site has been modified, and additional dredge disposal sites were added to Atkinson Island. The mesh geometry was updated based on aerial images, and available bathymetry data to ensure the most up-to-date domain representation were used. In addition, a previous Bayport study performed for SWG showed a need for a storage area in the upper section of the domain (Tate and Ross 2012). This area is representative of small channels or wetland type areas that may store water under certain events but not contribute to the main flow pathways. These areas are important to obtain accurate tidal storage and thereby accurate flow directions in the ship channel. Figure 57 shows the updated model domain and the location of the wind data at Eagle Point.

Figure 57. Updated HGNC model domain.

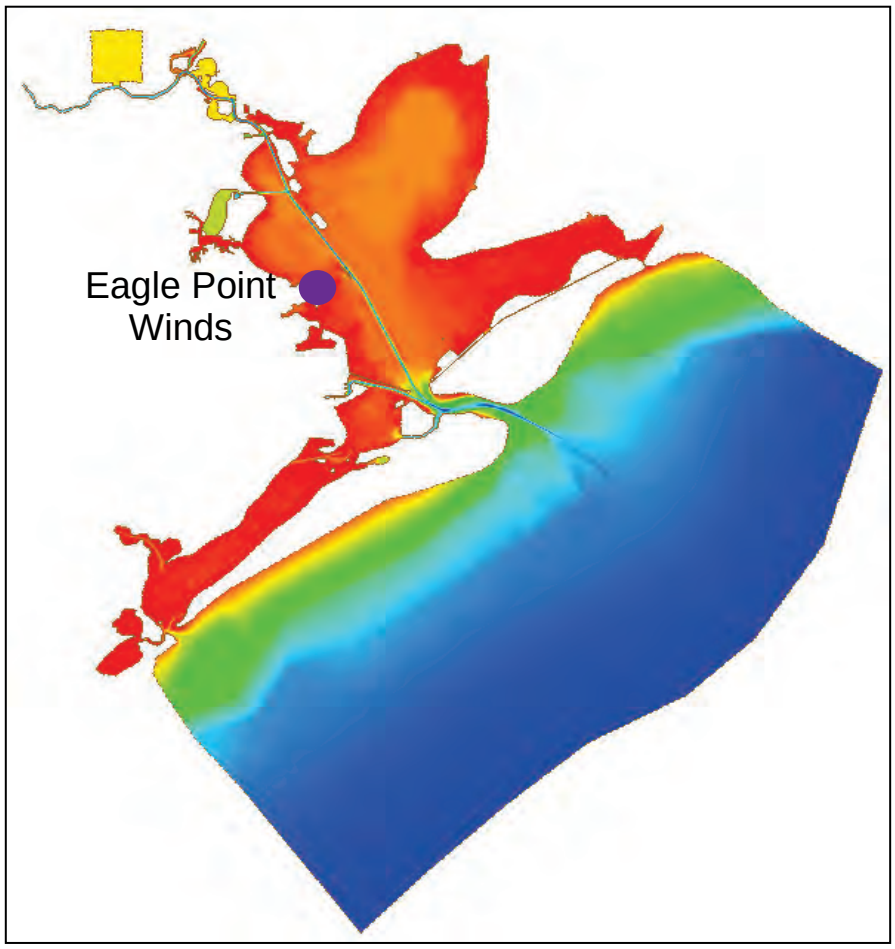

Model/Field comparisons

2010 Field data

If the tidal storage is not sized correctly, the direction of the flow along the channel may not be correct. To ensure the correct storage area was included in the model domain, field data taken for another project in 2010, of velocity and discharge cross sections around the Bayport Flare, were used (Tate and Ross 2012). These cross sections are located across the HSC upstream and downstream of the flare as well as across the Bayport Channel, as shown in Figure 58. The discharge comparisons for cross sections 1, 2, and 3 are shown in Figure 59 through Figure 61 as solid lines for the modeled results and points for the field data.

Figure 58. Discharge cross section locations.

Figure 59. Discharge comparison for cross section 1.

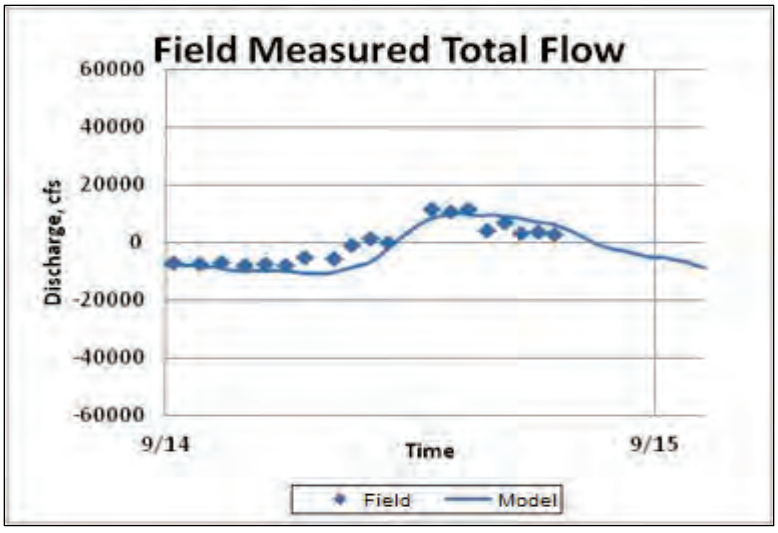

Figure 60. Discharge comparison for cross section 2.

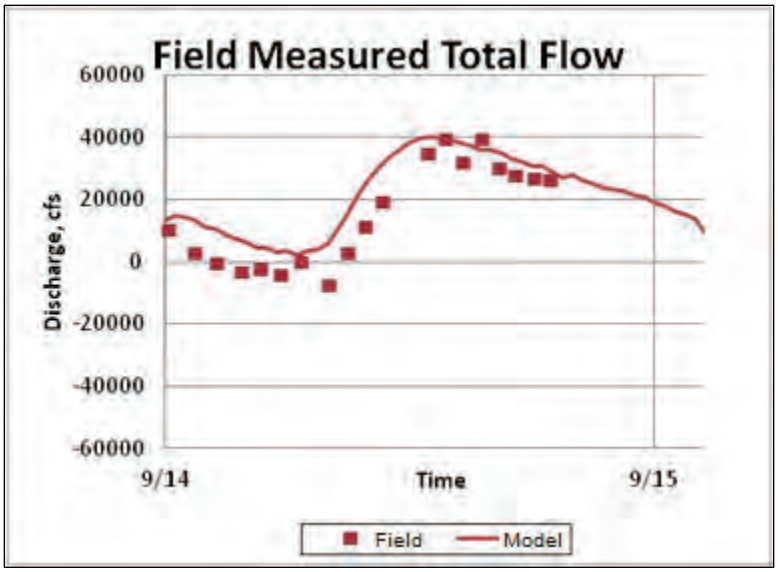

Figure 61. Discharge comparison for cross section 3.

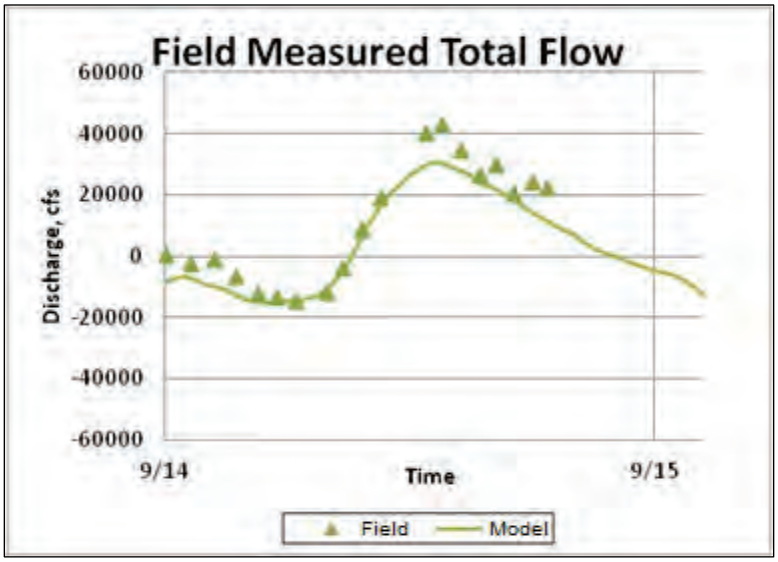

2011 Field data

Model comparisons to 2011 velocity and salinity field data were made at three of the four AWAC locations shown in Figure 20–AWACs 1, 2, and 4. Since several gages had data gaps or biofouling issues, a limited overlap period was available for all sample locations. A 10-day period from 6 June to 16 June 2011 is shown at each site for both surface and bottom velocity and salinity (four plots for each site) in Figure 62 through Figure 73. For all plots, the field data are shown in blue, and the model data are shown in red. Velocity data are positive for flood (directed inland) and negative for ebb (directed toward the gulf).

Figure 62. Bottom velocity comparison at Site 1.

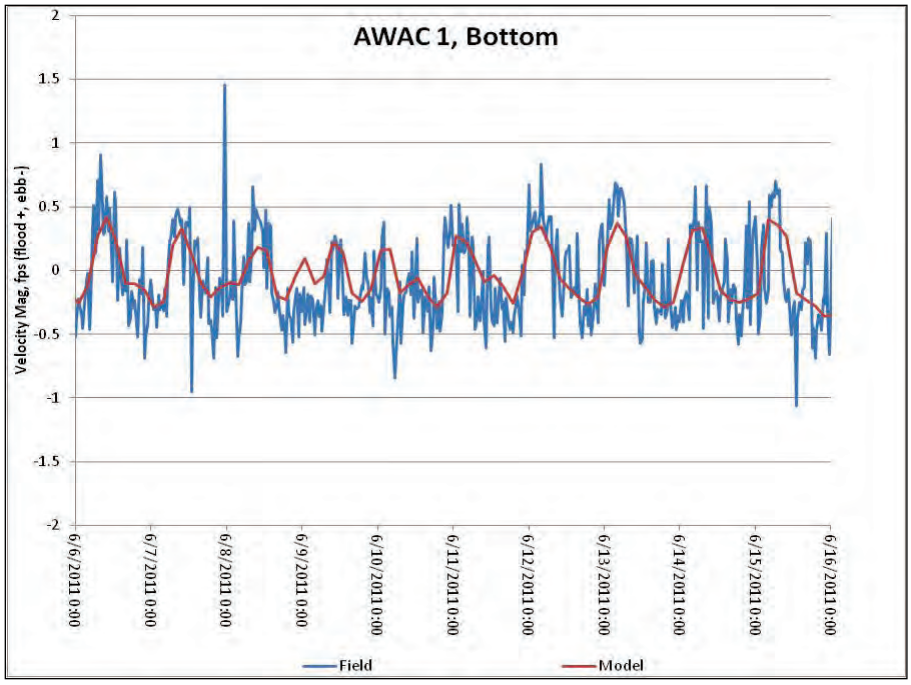

Figure 63. Bottom salinity comparison at Site 1.

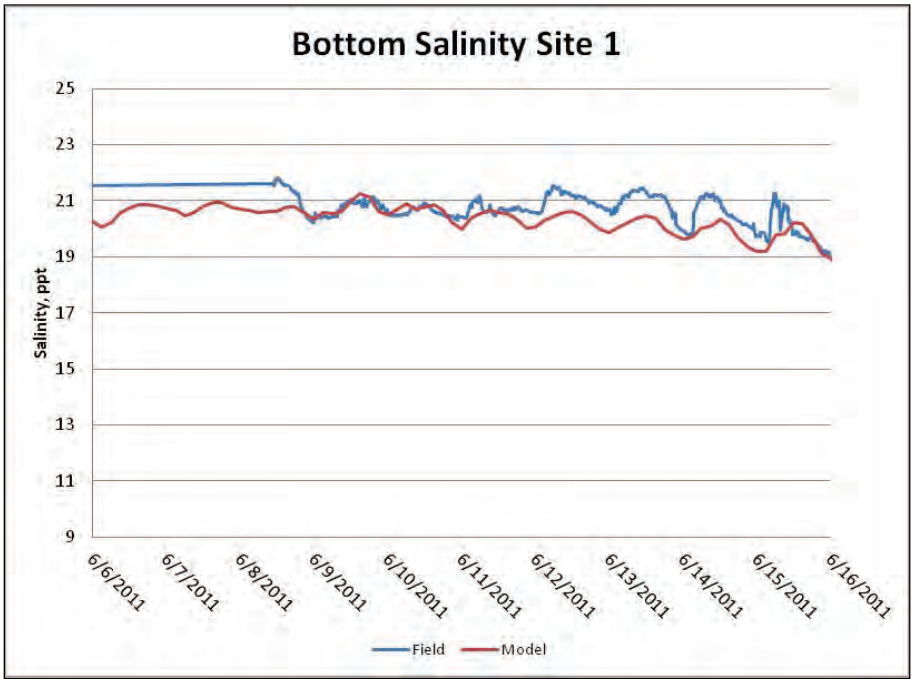

Figure 64. Surface velocity comparison at Site 1.

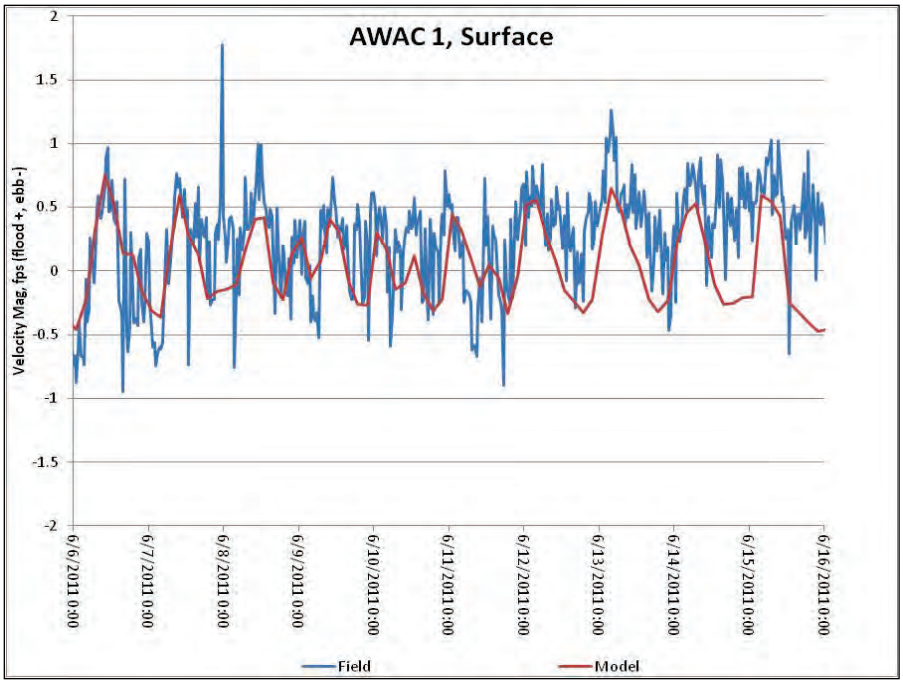

Figure 65. Surface salinity comparison at Site 1.

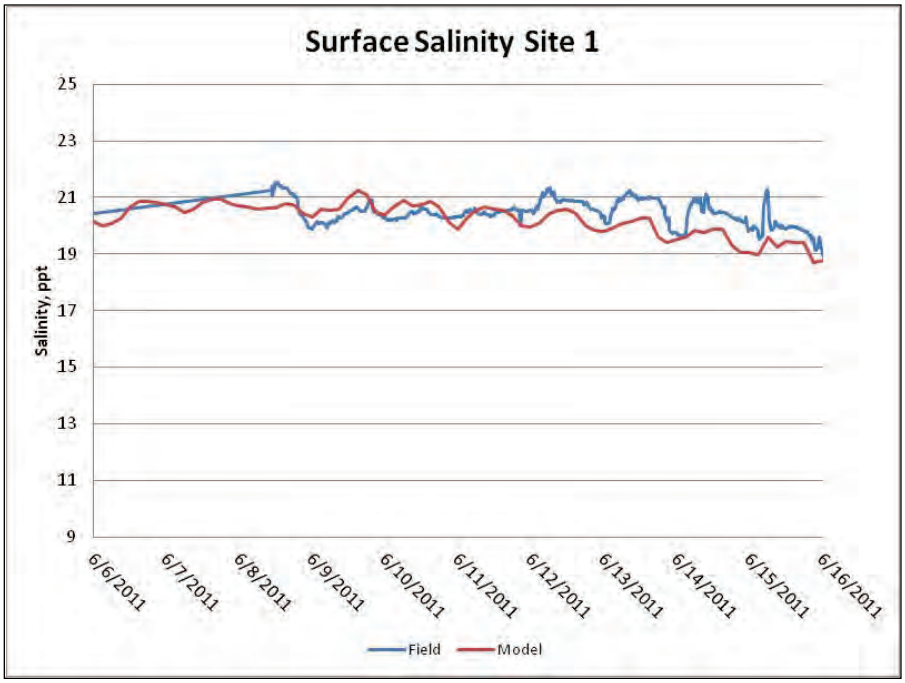

Figure 66. Bottom velocity comparison at Site 2.

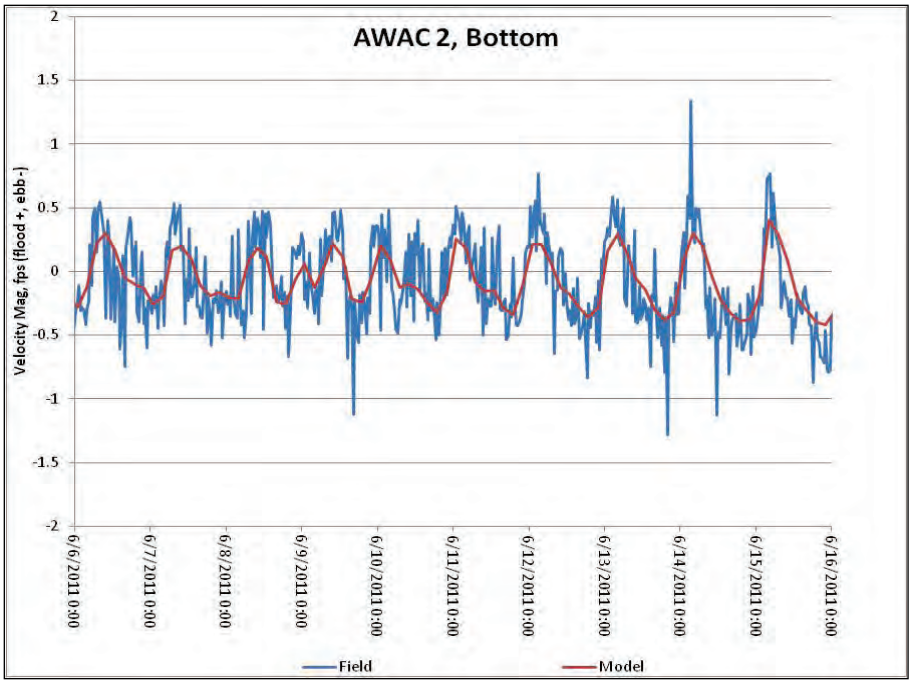

Figure 67. Bottom salinity comparison at Site 2.

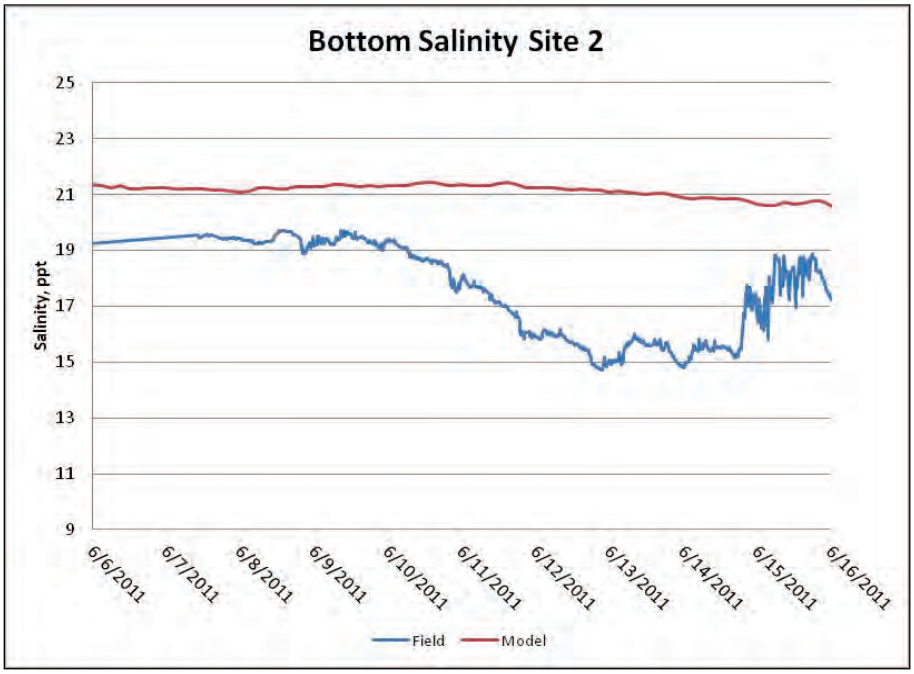

Figure 68. Surface velocity comparison at Site 2.

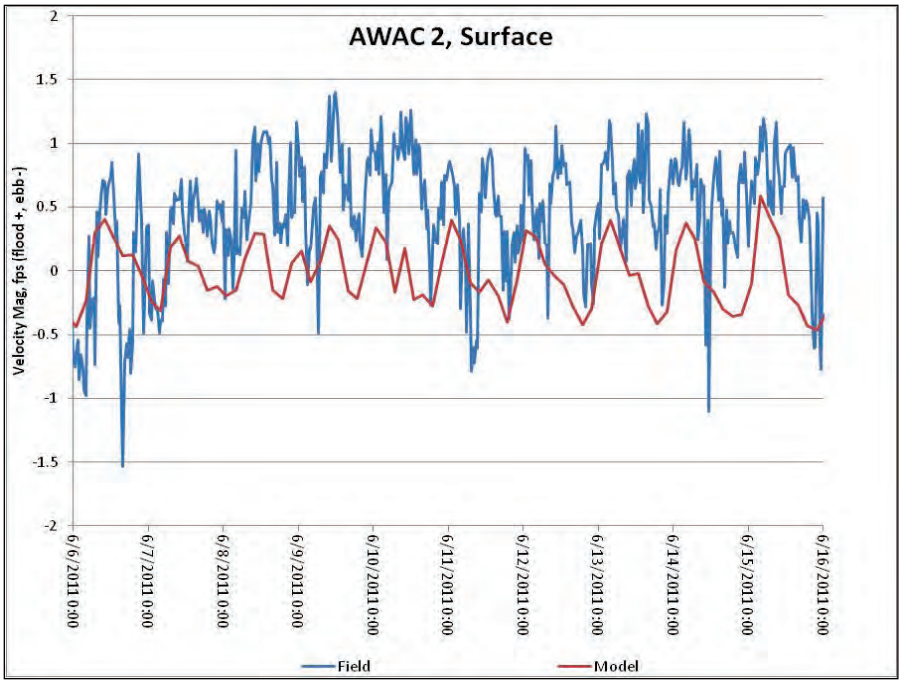

Figure 69. Surface salinity comparison at Site 2.

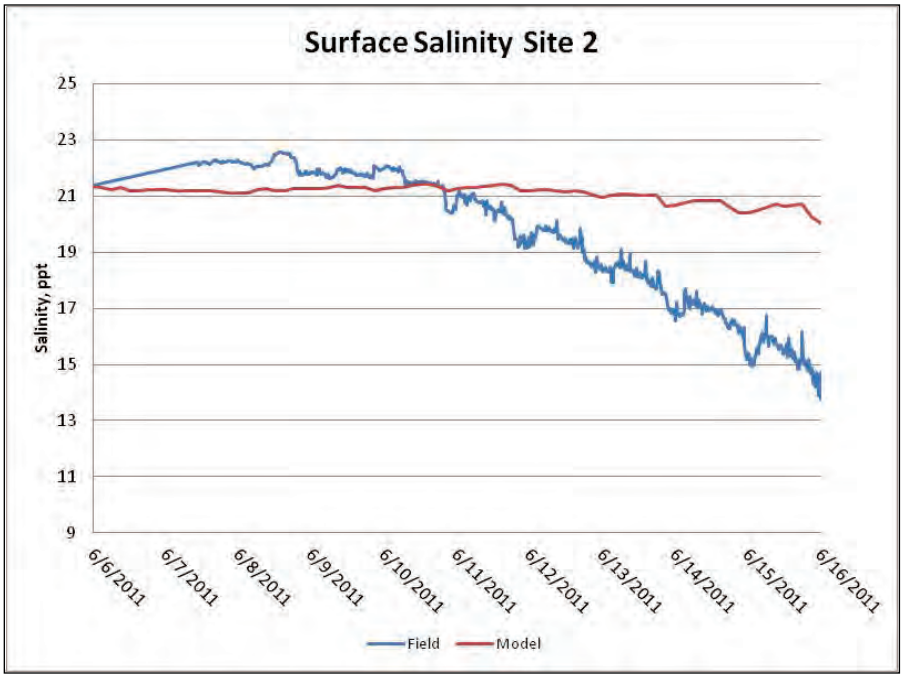

Figure 70. Bottom velocity comparison at Site 4.

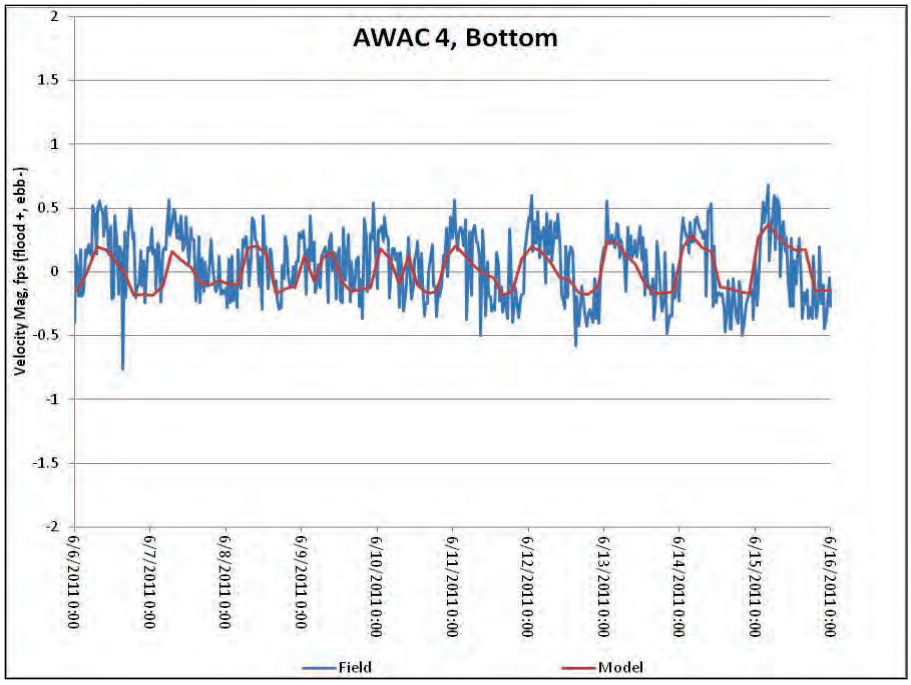

Figure 71. Bottom salinity comparison at Site 4.

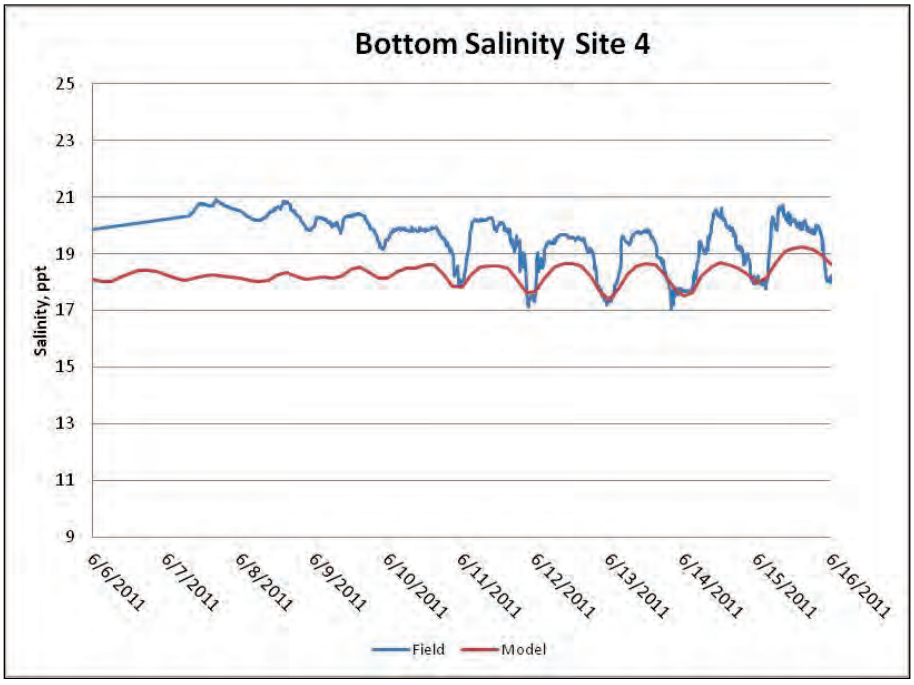

Figure 72. Surface velocity comparison at Site 4.

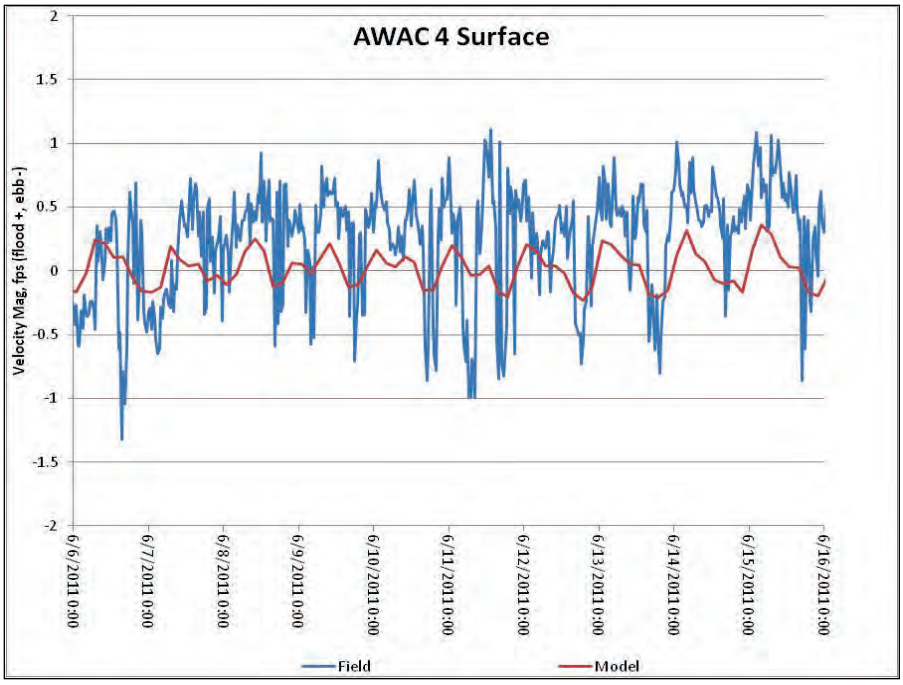

Figure 73. Surface salinity comparison at Site 4.

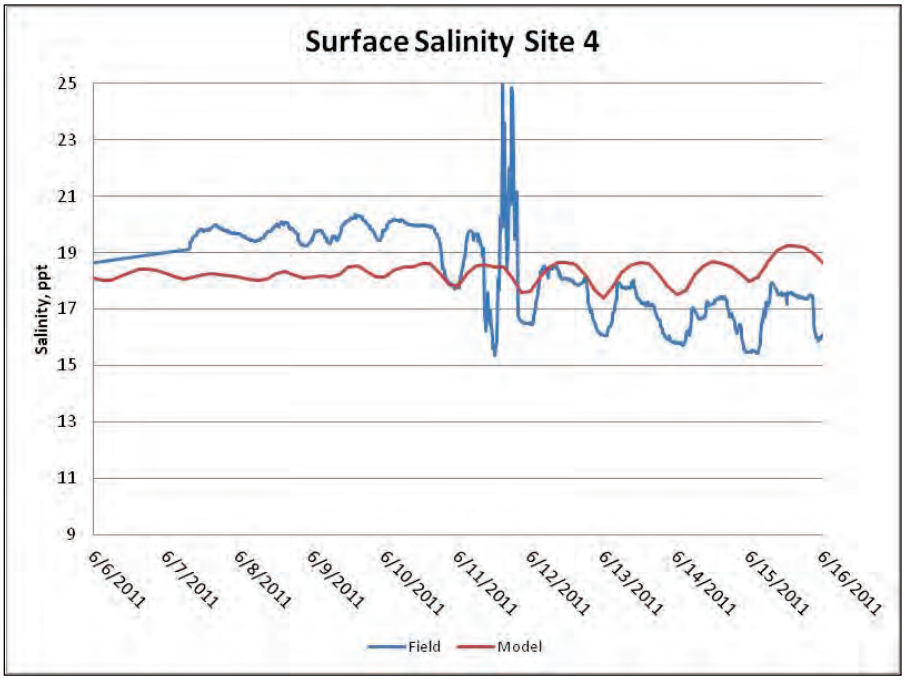

The velocity magnitude data were less than 1.5 fps for most sites, limiting the accuracy of the measurement device such that small fluctuations and noise can have a large impact on the data comparison. It is evident in the plots that there is noise in the field data. However, the model comparison to the field data shows the same pattern and very similar magnitudes. The

peaks of the data are not reproduced, and the surface velocity comparisons are not as good as the bottom comparisons.

The salinity data are best replicated in the model at Site 1. The field data contain some noise, but the tidal pattern is observed by the regular rising and falling of the magnitudes. At Site 1, the salinity data begin to drop during the comparison period, and this is replicated in the model results at both the surface and bottom. At Site 2, the model differs from the field data by approximately 2 ppt. The bottom field data for Site 2 shows a rapid decline in the salinity, a common indicator of biofouling, especially since this trend is not observed at the other sites. The Site 2 surface data drop as well but then recover near the end of the comparison period. If this is a real event, then it is caused by a property not included in the model, such as shrimp trawling operations. At Site 4, the low salinity magnitudes are matched by the model, but the model-computed peaks are lower than the field. However, at the bottom, the model data is higher than the field by approximately 2 ppt. For magnitudes of 20 ppt, a difference of 2 ppt equates to 10%. Salinity comparisons on this order of agreement are considered acceptable.

Sediment

The sediment field data recorded by the AWACs were not correlated to sediment mass due to a lack of sediment load during the low-flow period of the 2011 data collection. Although the sediment model was run with conditions as set by previous work (Tate et al. 2008), a comparison to field data for suspended sediment or channel deposition was not possible. An analysis of the channel shoaling was performed, though, and is shown in Figure 74. This plot shows the volume of material in the HSC from Morgan's Point (0 m) to Bolivar Roads (30,000 m). SWG has noted that since the channel deepening, the shoaling moved southward toward Red Fish Reef. Based on the 2011 hydrodynamic data and the 2005–2006 sediment data, the sediment model indicates that the shoaling is largest just upstream of Red Fish Reef and then decreases toward the Gulf of Mexico. This is a sediment model result, not a field comparison.

Figure 74. Model-computed shoaling volume along the HSC.

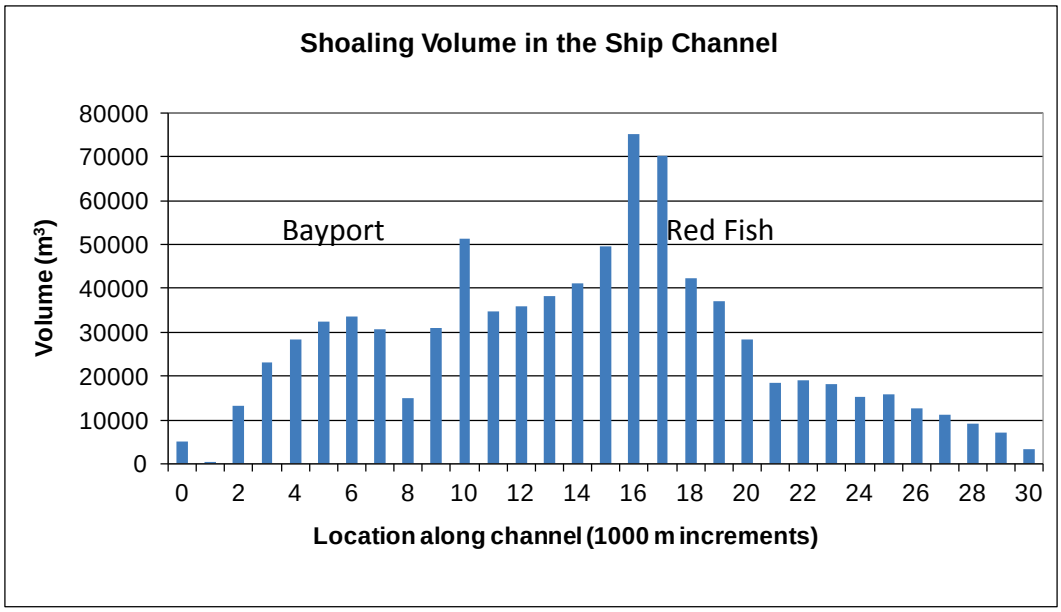

Recommendations for practical applications

The following recommendations are offered based on lessons learned during this model application:

- Boundary condition data should be as accurate as possible. Salinity, river inflow, wind, and tidal elevation data are necessary for the bay model. Incorrect hydrodynamic results will be obtained if the driving boundary condition data are not accurate.
- The model is very sensitive to the sediment load data. Incorrect sediment loads or sources can negatively impact the results.
- The model should be updated such that the bathymetry and roughness parameters are appropriate to match field data. Validation and sensitivity simulations should be performed prior to using the model with new input data.

6 Results and Recommendations

Using the field data and developed numerical models, each of the nine hypotheses for potential causes of increased shoaling (as stated in Chapter 1) were investigated.

Galveston Entrance Channel

Three possible sediment sources that may cause shoaling in the entrance channel and vicinity were hypothesized. Using available field data and numerical models, each of the hypotheses for potential causes of increased shoaling were investigated.

Dispersion of the beneficial use berm (Hypothesis 1)

Beneficial use berms are located to the west of the channel outside the jettied area. The easternmost site is regularly used and receives large quantities of dredged material from the channel reach between Redfish Reef and Bolivar Roads. One possible source of shoal material is from these berms as the material may migrate back into the channel.

To evaluate sediment moving after placement, a particle tracking model (PTM) was applied over a period of 30 days, with particle generation occurring over the first 5 days only. This enables investigation of the fate of those particles over the next 25 days. A PTM also enables investigation of altering, relocating, or creating new placement areas which may reduce shoaling in the channel. A PTM was set to simulate neutrally buoyant particles that move with the flow of water. The investigation did not include the effects of waves. This approach does not directly simulate sediment transport, but it does allow qualitative assessment of transport trends by providing knowledge of the trends in water flow.

Figures 75 through 80 show the distribution of particles originating from six points over the first 5 days (black dots in the figures). The two areas outlined with black boxes indicate the location of the two offshore placement areas, the easternmost of which is identified previously in this report as the “beneficial use berm.” The westernmost placement area has not been utilized in recent dredging placement operations. Particles generated at each point are specified with a different color to enable visual tracking of particle fate.

Figure 75. Particle location after 0.5 days.

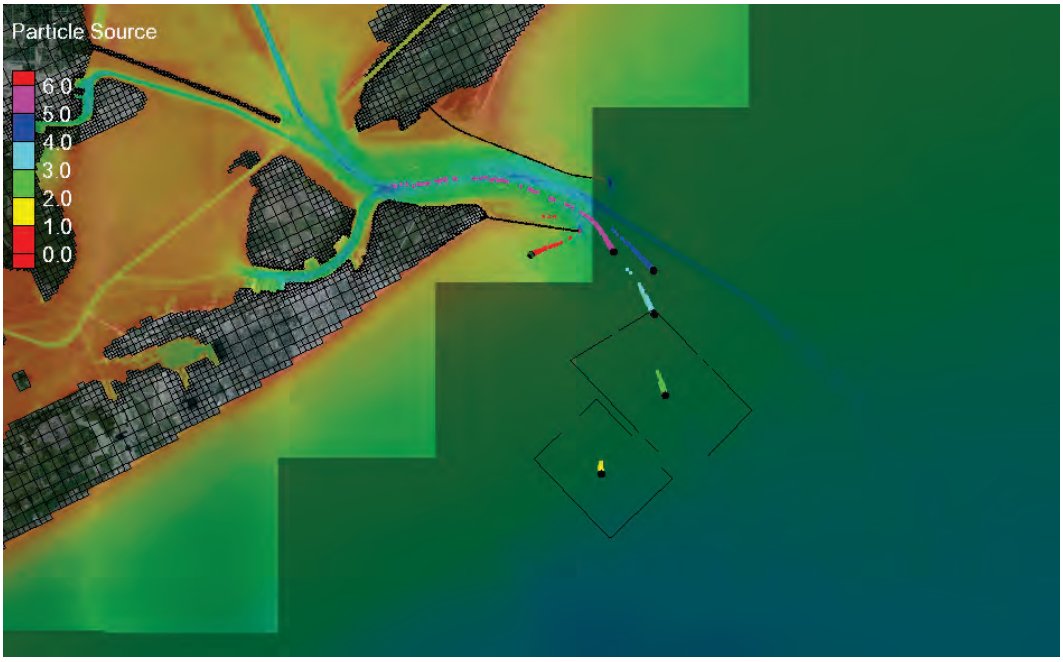

Figure 76. Particle location after 0.75 days.

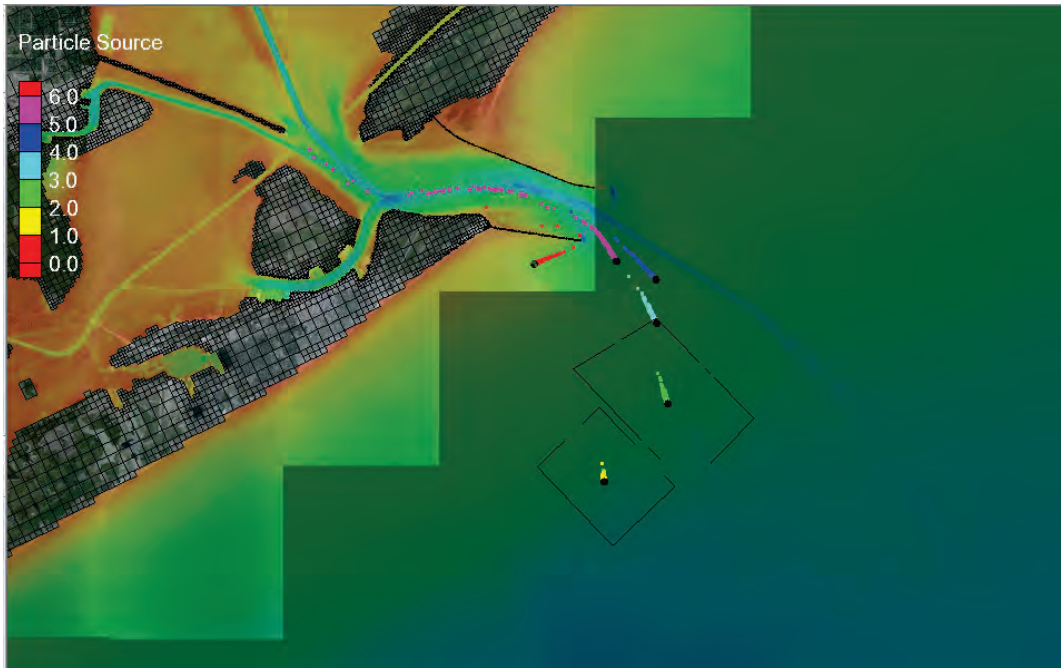

Figure 77. Particle location after 1.25 days.

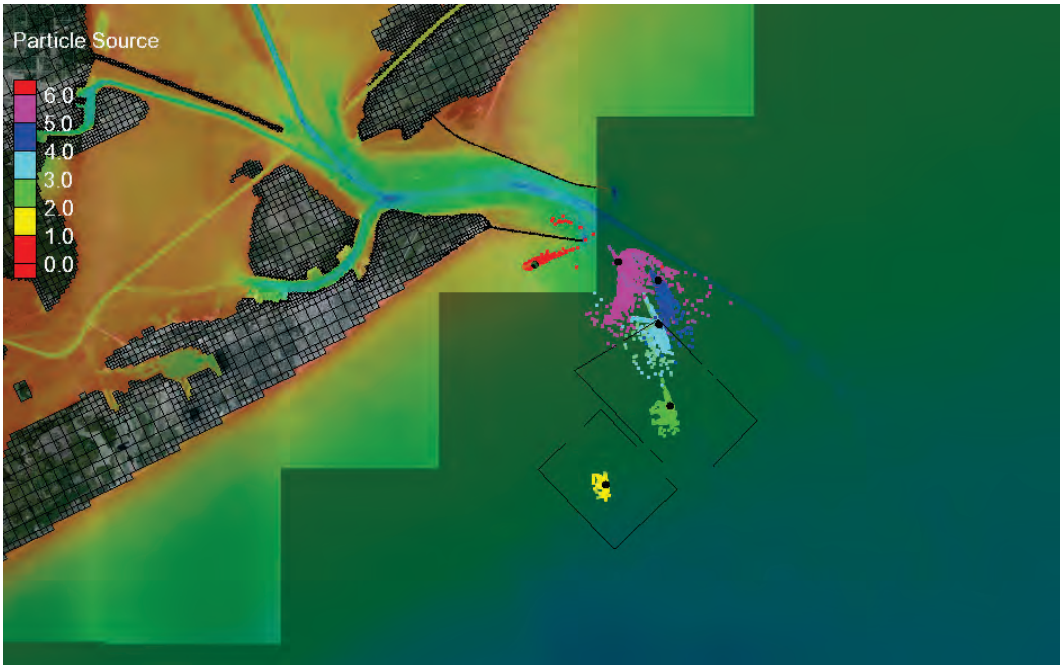

Figure 78. Particle location after 2.5 days.

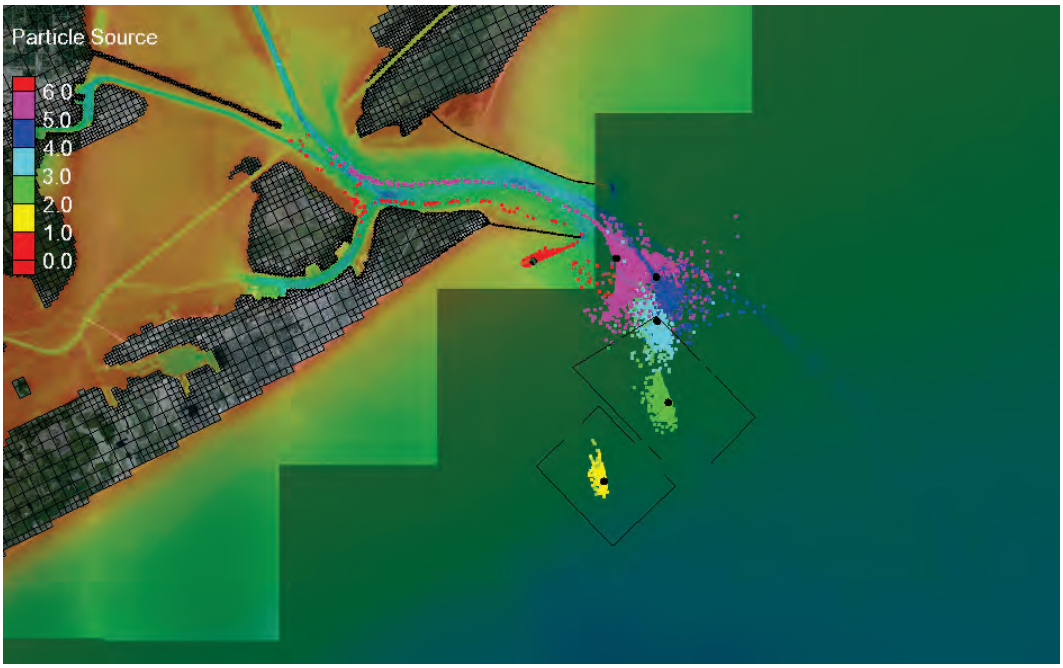

Figure 79. Particle location after 4 days.

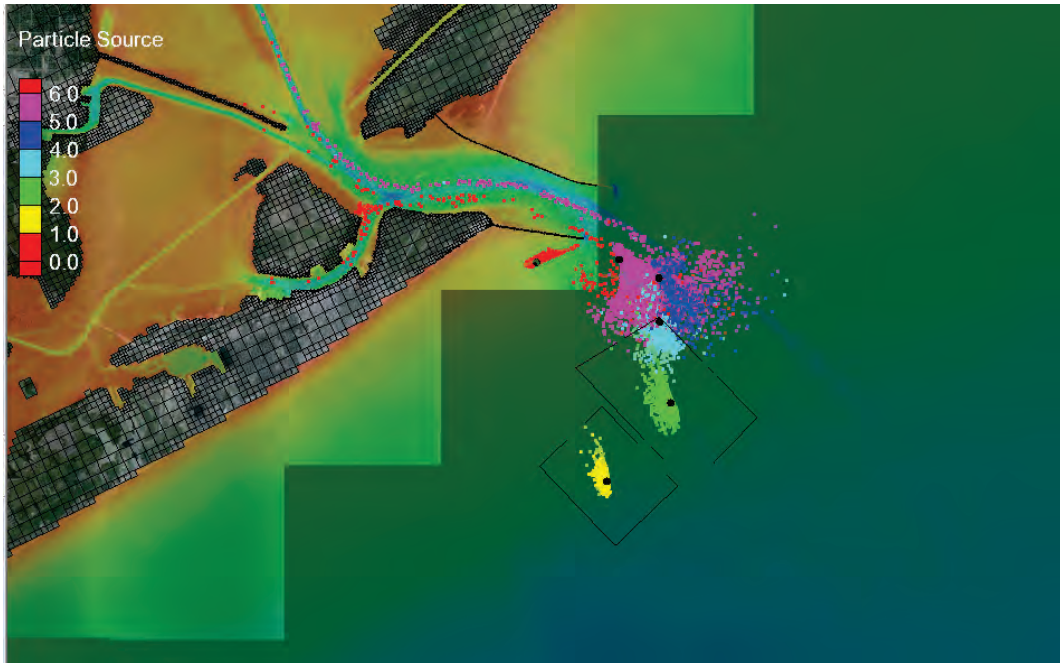

Figure 80. Particle location after 5 days (the end of new particle generation).

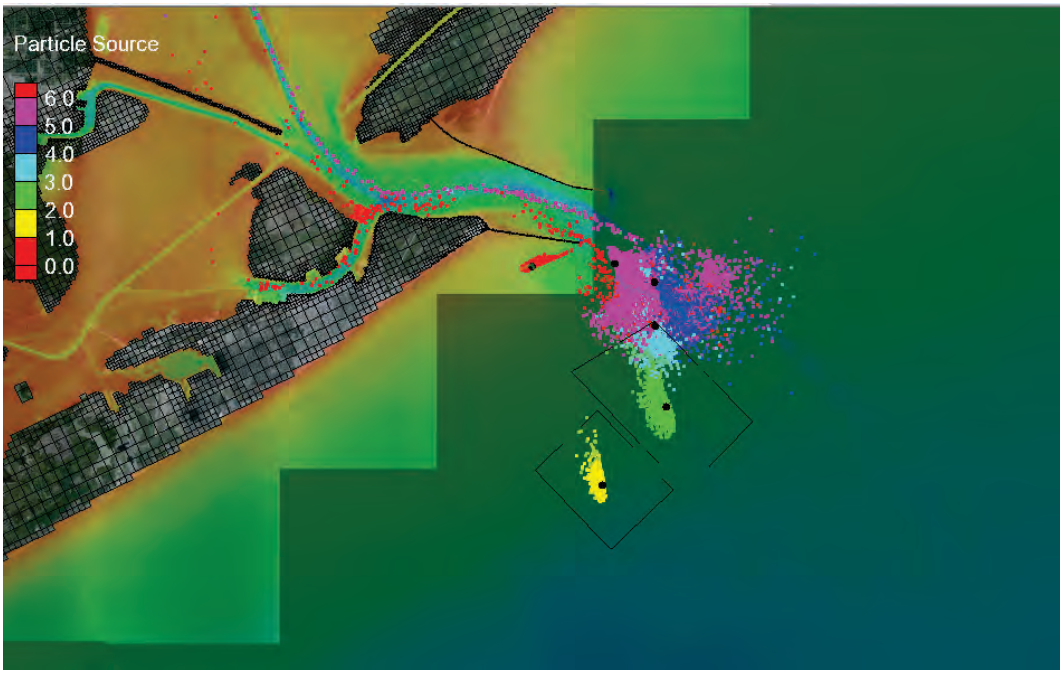

Analysis of PTM results visualized in Figures 75 through 80 suggests the following conclusions:

- Material placed in the beneficial use berm will disperse when bottom stresses are sufficient to mobilize sediments (i.e., finer sediments are

routinely dispersed, and coarser sediments may not be dispersed except under more energetic waves). A more detailed study would be required to refine the exact conditions under which sediments are mobilized.

- Finer sediment (sediments easily eroded) placed in the eastern part of the beneficial use berm will likely migrate to the channel within a few days.
- Sediment placed closer to the channel or on the southern side of the east jetty would be more likely to deposit in the navigation channel; therefore, it would not be advisable to place sediment in close proximity to the channel.

Figure 81 shows the distribution of particles after 10 days, or 5 days after cessation of placement activities. By this time, the particles have reached an approximate equilibrium position. Figure 82 shows the distribution of particles after 30 days at a larger scale. The distribution is approximately the same after 30 days as it was after 10 days. The following general conclusions can be drawn from the results:

- When bottom stress is sufficient to mobilize sediments on the beneficial use berm, some sediment will migrate back into the navigation channel. Sediments placed farther away from the channel in the berm are less likely to be transported back to the channel.
- Over the longer term, sediment may tend to accumulate in an ebb shoal feature.

Figure 81. Particle location after 10 days.

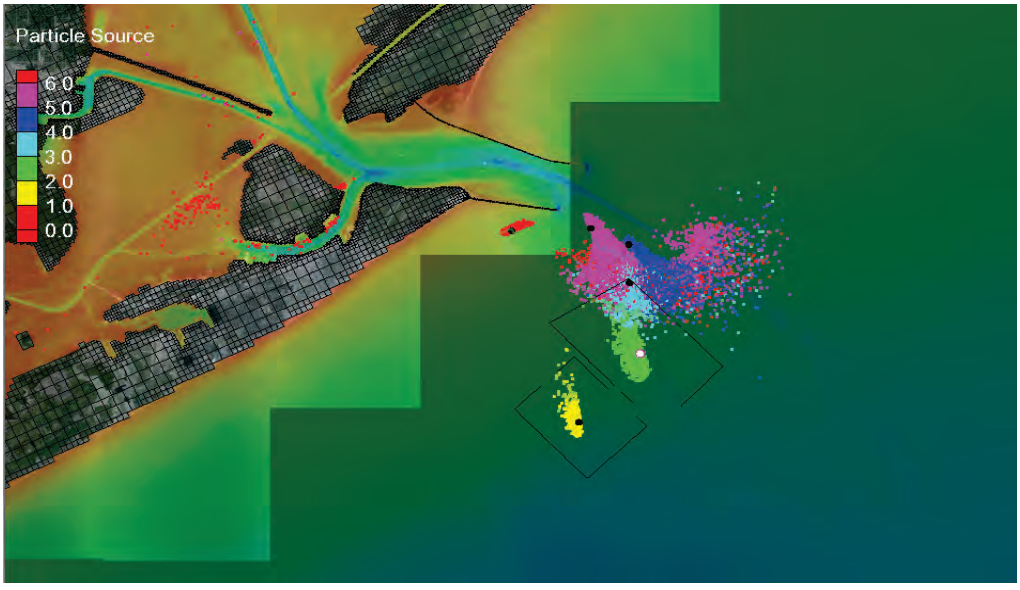

Figure 82. Particle location after 30 days.

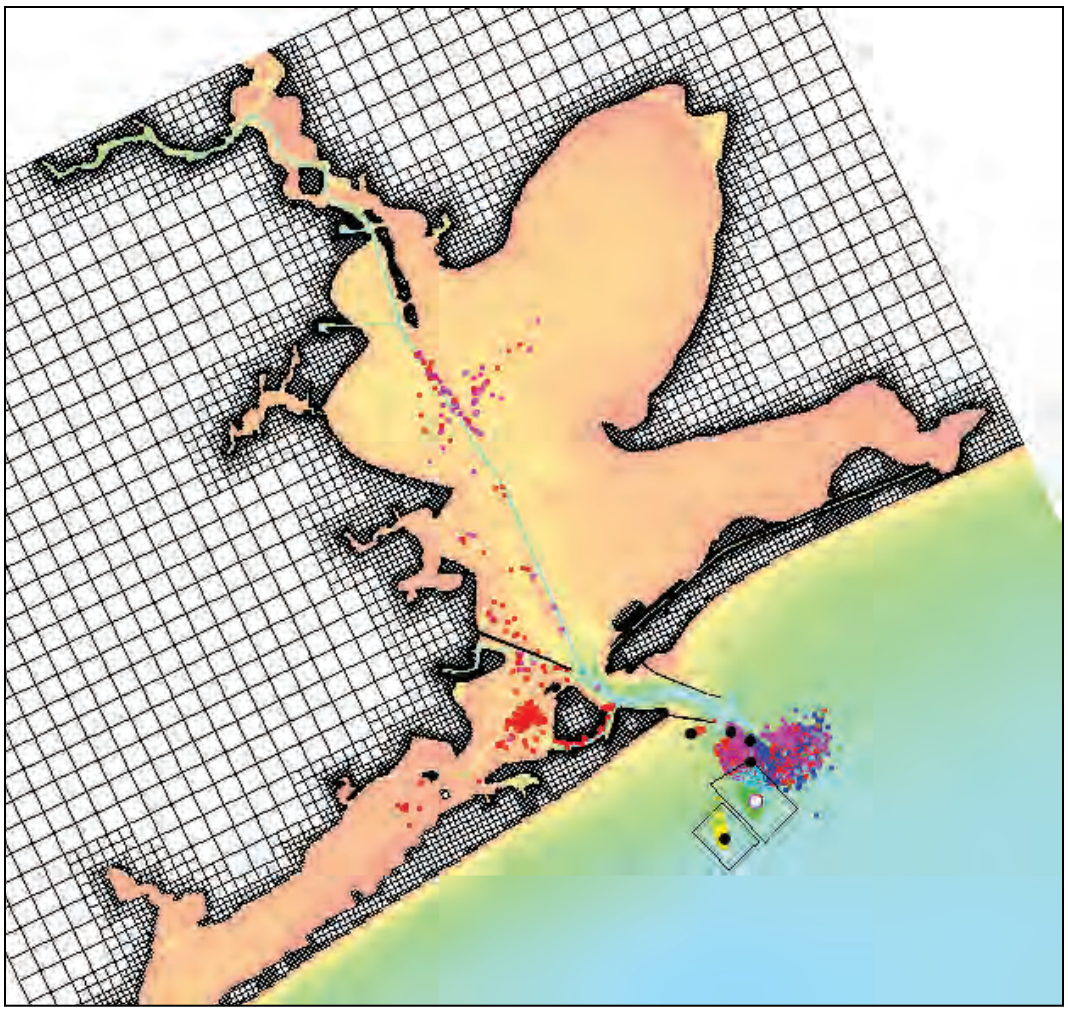

Sand transport through, over, or around the jetties (Hypothesis 2)

Another potential source of sediment causing shoaling in the entrance channel is beach sand from Galveston Island passing over, through, or around the south jetty. The following mechanisms of transport may result in increased channel shoaling:

- Wind may blow beach sediments from East Beach to Big Reef and into the channel (locations shown on Figure 1).
- The jetties are porous, allowing sand to be carried through the stone by water.
- Large waves may allow transport of sand over the jetty during storms.
- Sediment deposited along the beach side of the jetty by longshore transport may be transported around the jetty into the navigation channel.

Morang (2006) calculated sediment transport in the vicinity of the Entrance Channel using the Sediment Budget Analysis System (SBAS) (Figure 83). SBAS is a program that provides visual characterization of and simple calculations associated with a sediment budget. Labels in Figure 83 show transport rate in cubic meters per year (m^3/yr). The analysis indicated that approximately 149,000 m^3/yr (0.195 myd^3/yr) is transported from East Beach into the Entrance Channel to balance the sediment budget. The analysis did not quantify amount transported per potential pathway.

Figure 83. Sediment budget for Galveston Entrance Channel.

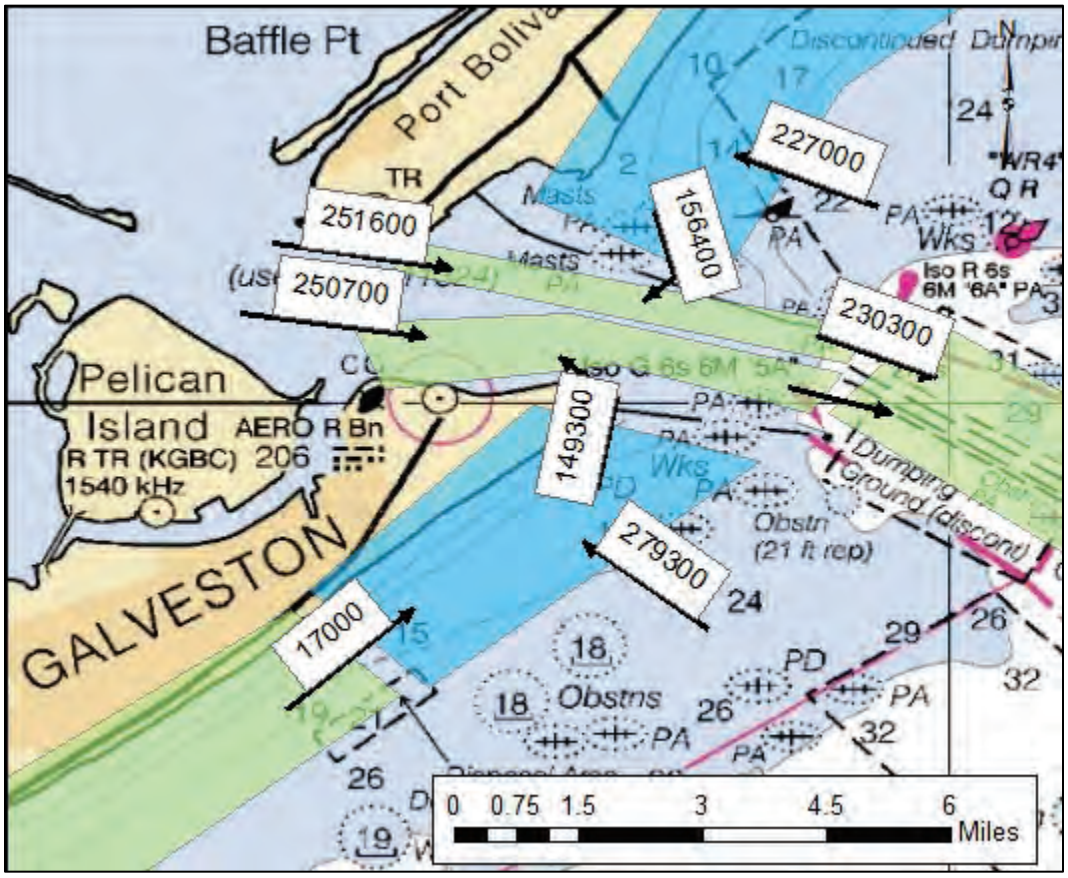

Morang (2013[1]) calculated potential wind-blown sediment transport from East Beach towards Big Reef into the Entrance Channel. Calculations following the USACE Coastal Engineering Manual (USACE 2002) indicated that northward transport could be between 10,000 and 20,000 m^3/yr.

[1]Andrew Morang, ERDC/CHL, personal communication regarding ongoing work for the Regional Sediment Management program, 15 September 2013.

Because of the nature of these calculations and the uncertainty in the input data, actual transport could be as much as an order of magnitude different.

Figure 75 through Figure 82 show potential transport pathways of sediment adjacent to the south jetty. Although the amount of transport has not been quantified, the plots clearly indicate that sediment on East Beach could be transported around the jetties into the navigation channel when bottom stresses are high enough to mobilize sediments (i.e., during periods of energetic waves). Because of the depth of the navigation channel, it is not likely that sand-sized particles would be able to escape the channel naturally once trapped.

Visual observation of the condition of the jetties indicates that sediment transport through the jetty is likely; however, no data are immediately available to estimate the amount. Numerical models have not been applied specifically to attempt to quantify this process since data were not available to calibrate them.

Although data are not available to conclusively quantify the amount of sediment being transported by each pathway, the analysis presented here and by others suggests the total amount is over 100,000 m^3/yr with as much as 20% of that being attributed to Aeolian (i.e., wind-blown) transport. Regional Sediment Management and Planning Assistance to States Projects are currently building on the results of this MCNP project to provide the insight needed to help reduce total transport along these paths into the navigation channel.

Sand transport through Bolivar Roads (Hypothesis 3)

Hypothesis 3 proposes that significant volumes of sand are moving through Bolivar Roads into the estuary. The PTM model results (Figure 81) show that water is transported from the beach into the estuary, supporting this possibility. CMS model results also verify that transport of sand into the estuary occurs. Figure 84, below, shows the percent sand measured in grab samples taken by SWG along the reaches shown in red, prior to dredging. The data show that there is more sand in Bolivar Roads with decreasing percentage of sand moving into the estuary. Recall that Figure 14 showed locations of greater percent sand in the entrance and offshore, illustrating the variation in sampling techniques and locations.

Figure 84. Percent sand measured in the navigation channel.

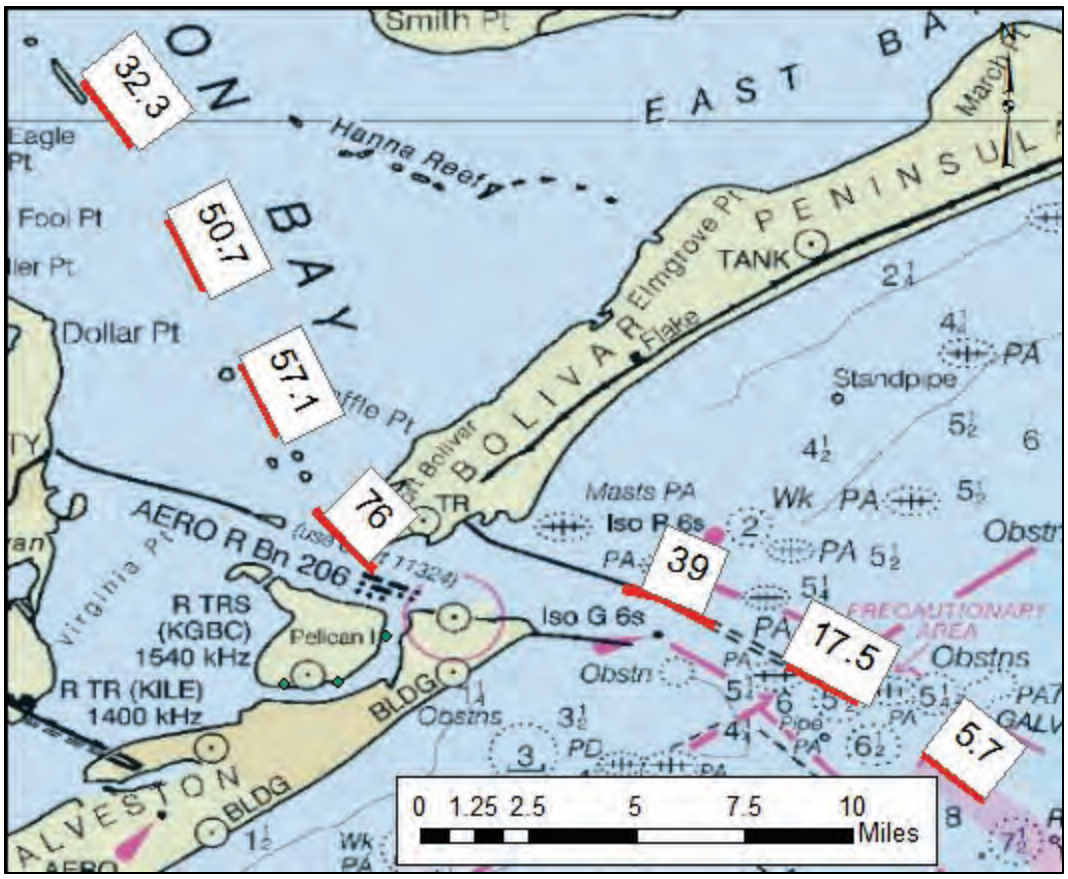

The data and model results support the hypothesis that sand from the beaches is trapped in the estuary, with the highest percentage being trapped and dredged from Bolivar Roads. Note that the sediment budget currently assumes a net transport of sediment towards Bolivar Roads from the Bay. More detailed analysis and data collection would be required to attempt to calculate the exact percentage of sand in the estuarine portion of HSC that should be attributed to beach sources.

Houston Ship Channel

Wind-generated sediment resuspension (Hypothesis 4)

Previous CHL studies included a data collection effort during a period of high wind on 7 December 2005 (Tate et al. 2008). These winds were from the north/northeast at 5–10 meters per second (m/s) (11–22 miles per hour). Samples taken during this time showed fairly clear suspended sediment samples, indicating that the bed material had not been stirred up due to these winds. The shorelines did exhibit areas of bank erosion, but these are much shallower areas than the average 2–3 meters (6–9 ft) of

the bay. The modeling performed here and in previous studies indicates that the bay material does not resuspend due to typical wind conditions in the area (Figure 6 in Chapter 2 illustrates this point). Wind waves have a relatively short wavelength and therefore do not penetrate very deep into the water column.

Field data, however, do indicate that material is eroded from the bed due to large storm events such as tropical storms and hurricanes. Bed material samples from 2005 showed a weak layer on top of a firm layer, whereas samples from 2004 had the firm layer at the surface. Hurricane Rita made landfall in the area in September 2005 and may be the cause of bed material resuspension and this weak surface layer. Therefore, material does consolidate into a firm surface over time. It is possible that new, fresh deposits have a lower critical shear stress for erosion such that wind waves may have a higher erosive impact during some periods of the year when the bed material is weaker. Additional bed material data are necessary to fully support this theory.

Vessel-induced shoaling (Hypothesis 5)

Research on the effects of vessel-induced waves and bores that travel into the shallow regions along a navigation channel were limited until the early 2000s. Much of the previous work was focused in riverine environments. Schroevers et al. (2011) presents a field data collection and analysis of ship-induced waves and sediment erosion in a tidal flat in Europe. Ravens and Thomas (2008) collected ship-induced wave data and shoaling observations in a small creek along the western shore of Trinity Bay in the HGNC system. These data sets indicate the importance of understanding the influences of vessel movements in an area where they are dominant, such as in the HGNC.

Previous studies documented in Tate et al. (2008) indicated that the majority of the material settling to the HSC bed comes from the San Jacinto River load. This previous analysis investigated the influence of the two river loads and the shoreline/bed erosion individually on the amount of material that deposited in the ship channel. As an update of the previous analysis, the 2011 bay model was used to analyze the impacts of the vessel-induced shoaling, the river-load shoaling, and the hydrodynamic-induced shoaling (including tides and winds).

The model was run for 1 January–15 April 2011. Given that this is a low-flow year, the sediment loads on the Trinity River and San Jacinto River are low along with the total flow into the system. The vessel data were the same as the "typical day" as indicated in Tate et al. (2008). Figure 85 shows the shoaling along the HSC from Morgan's Point at zero to Bolivar Roads at 40,000 m. The Bayport Channel enters the HSC at approximately 7,000–8,000 m, and Red Fish Reef is in the area of 20,000–21,000 m. The plot has two scales—the vessel-induced shoaling volume is plotted in red and measured with the scale on the right; the river inflow and hydrodynamic-induced shoaling volume are plotted in green and orange, respectively, and measured with the scale on the left. The red grid lines are for the right-hand scale and the black grid lines are for the left-hand scale.

Figure 85. Shoaling along HSC due to individual components.

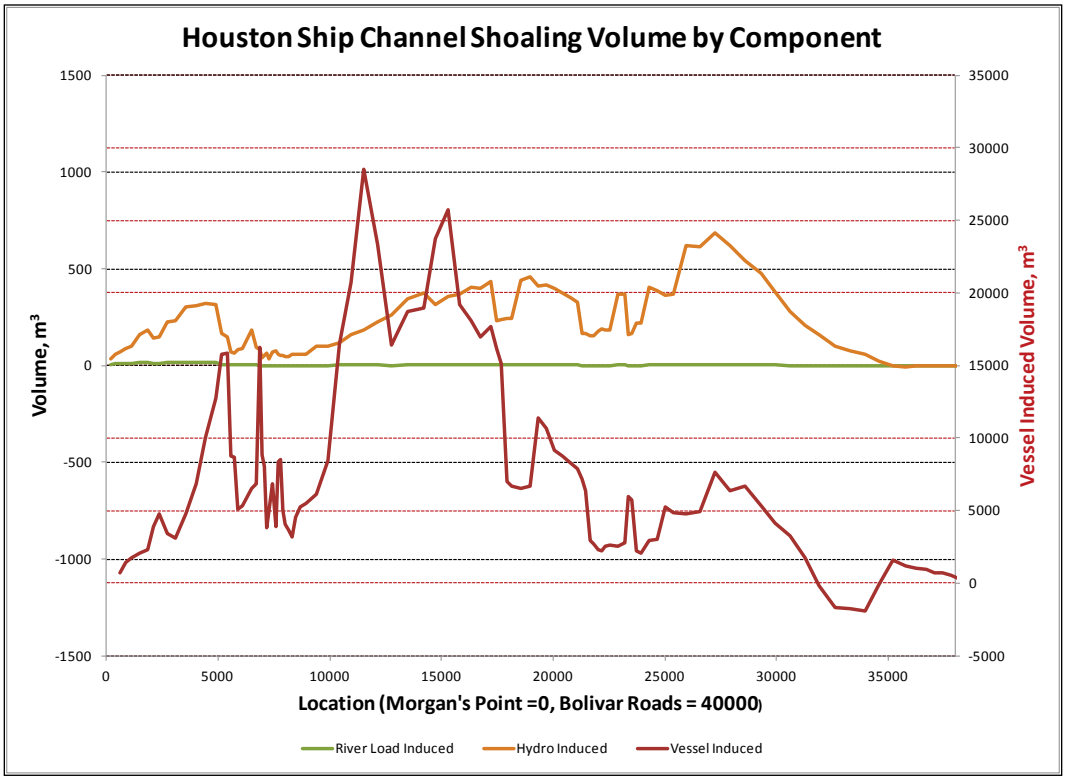

The results of this analysis indicate that the vessel-induced shoaling is the primary contributor to sediment deposition in the ship channel. When the vessels are removed from the simulation, the shoaling drops from a maximum of ~28,000 m^3 to less than ~750 m^3. The total volume of shoaled material during this 3.5-month period is given in Table 20. This volume varies between 738,000 m^3 for the vessel-induced deposition and 330 m^3 for the river-load induced deposition (recall the river loads are extremely

low for 2011). The hydrodynamic-induced deposition is approximately 3% of the vessel-induced shoaling, indicating that the vessels are the key contributor to the need to dredge the ship channel. It is possible, however, that the impact of the vessels is skewed due to the low freshwater flows and sediment loads entering the system for 2011, the year simulated in this analysis.

Table 20. Total volume deposited along HSC by component.

Load	Total Volume (m^3)
Vessel	738,184
Hydro	21,984
River	331

Subsidence (Hypothesis 6)

During 1943–1973, up to 10 ft of subsidence in the Houston-Galveston region occurred because of groundwater removal and oil and gas extraction (Coplin and Galloway 1999; Holzer 1989; Harris-Galveston Subsidence District 2010). Within the HGNC, subsidence was a maximum near Morgan's Point and decreased towards Bolivar Roads (Figure 86). Subsidence of the navigation channel would have increased the navigable depth, reducing the dredging requirement. However, calculation of the increased volume within the channel over this 30 yr period resulted in only 120,700 yd^3/yr additional capacity, and the decrease from pre-1948 to post-1948 rates was of the order 1.6 myd^3/yr (Table 1). It is concluded that Hypothesis 6 is a potential contributor to the decrease in channel shoaling that was observed from 1948 through 1995, but is not sufficient to explain the magnitude.

Atkinson Island impacts (Hypothesis 7)

Based on results from previous studies (Tate and Ross 2009), it appeared that the modification of the shape of Atkinson Island may generate changes in the flow distribution around the island and therefore sediment transport in the area. Disposal sites have been developed on the eastern side of Atkinson Island as indicated by the M1–M8 sites in Figure 87 (red-outlined areas). These cells have been developed over time with the initial four cells (M1—M4) necessary for the enlargement of the HSC.

Figure 86. Subsidence in HGNC by channel stationing from Morgan's Point to Bolivar Roads.

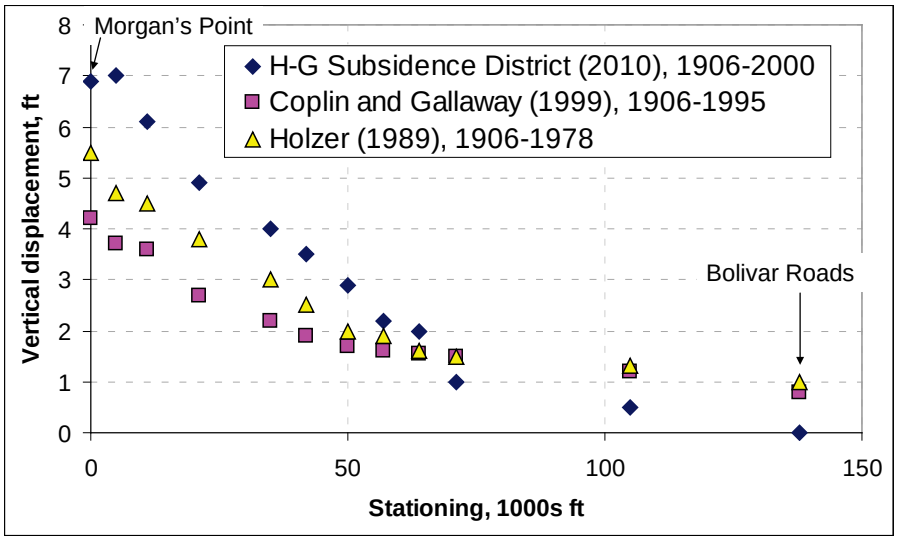

Figure 87. Disposal site plans for Atkinson Island.

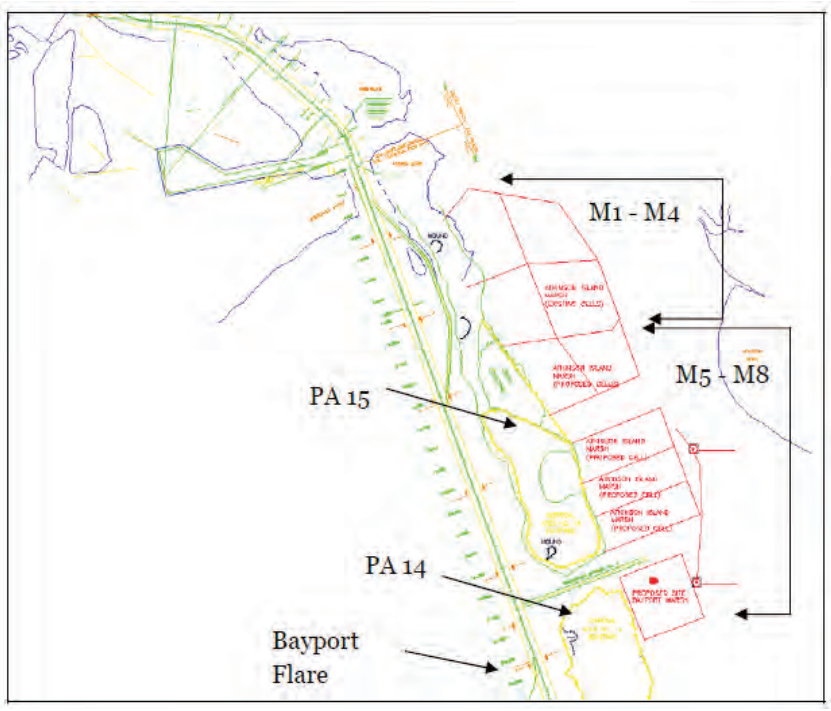

The prechannel-enlargement island size and shape as modeled is shown in Figure 88A, and the enlarged island with some of the disposal sites is shown in Figure 88B.

Simulations of plan configurations in the previous studies indicated that the increased area of the island may be affecting the discharge and sediment transport. A focused test of this hypothesis was developed to

investigate the impact of the initial enlargement of the island. Both island configurations were modeled using the 45 × 530 ft HSC and the 1994–1995 boundary conditions as documented in Tate and Ross (2009).

Figure 88. Atkinson Island as modeled—A: pre-enlargement, B: postenlargement.

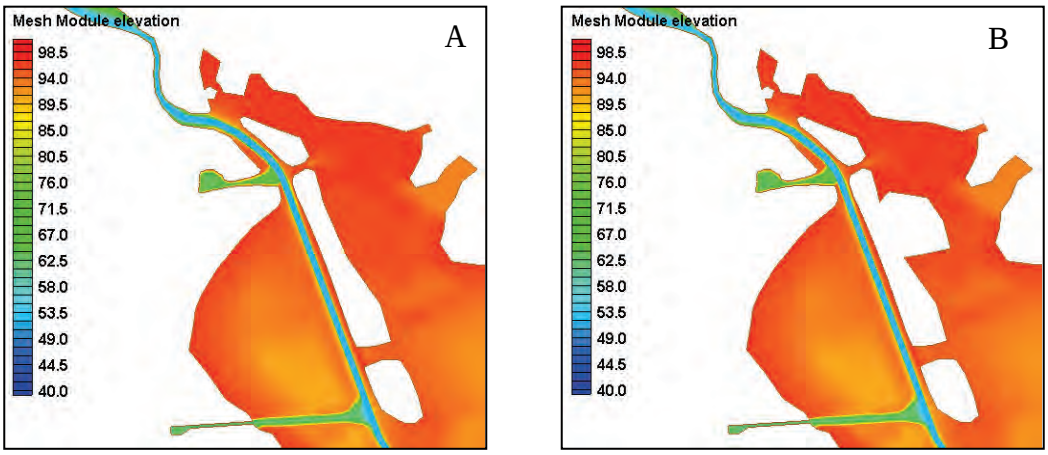

The hydrodynamic results were analyzed to determine how the discharge around Atkinson Island changes when the island is enlarged. A vessel simulation is coupled with the hydrodynamic results in order to compute actual suspended and bed sediment changes that may be generated by the island enlargement.

Hydrodynamic impacts

Discharge and shear stress values were used to initially gauge the impact of the enlarged island footprint. Figure 89 shows four cross-section locations (arcs) where the discharge (flux) is compared for both island configurations. Arcs 1 and 2 provide the information for the west and east side of Atkinson Island at its northernmost tip, respectively. Arcs 3 and 4 provide data for the two pathways through the island, although these sections transport less flow than Arcs 1 and 2. The arrows indicate the direction of positive discharge.

Figures 90 through 93 show the discharge in cubic feet per second for the large (after the HSC enlargement) and the small (prior to HSC enlargement) island configuration during a 60-day period of the simulation. Positive values represent flood-directed flows for sections 1 and 2 and eastward-directed flows for sections 3 and 4. Negative values represent the opposite flow direction—ebb, or southerly, flows for sections 1 and 2 and westward flows (toward the ship channel) for sections 3 and 4.

Figure 89. Discharge comparison locations (arcs).

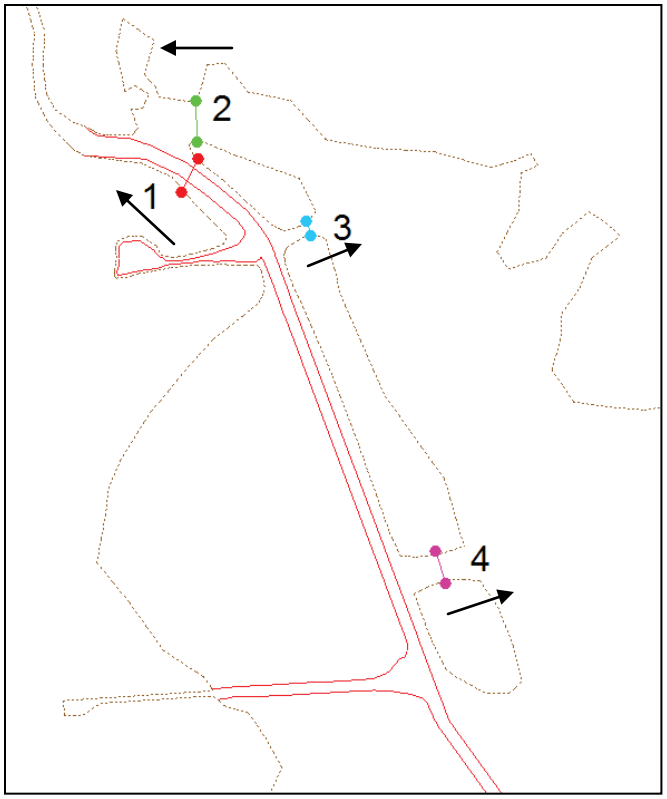

Figure 90. Atkinson Island Arc 1 discharge comparison (cfs).

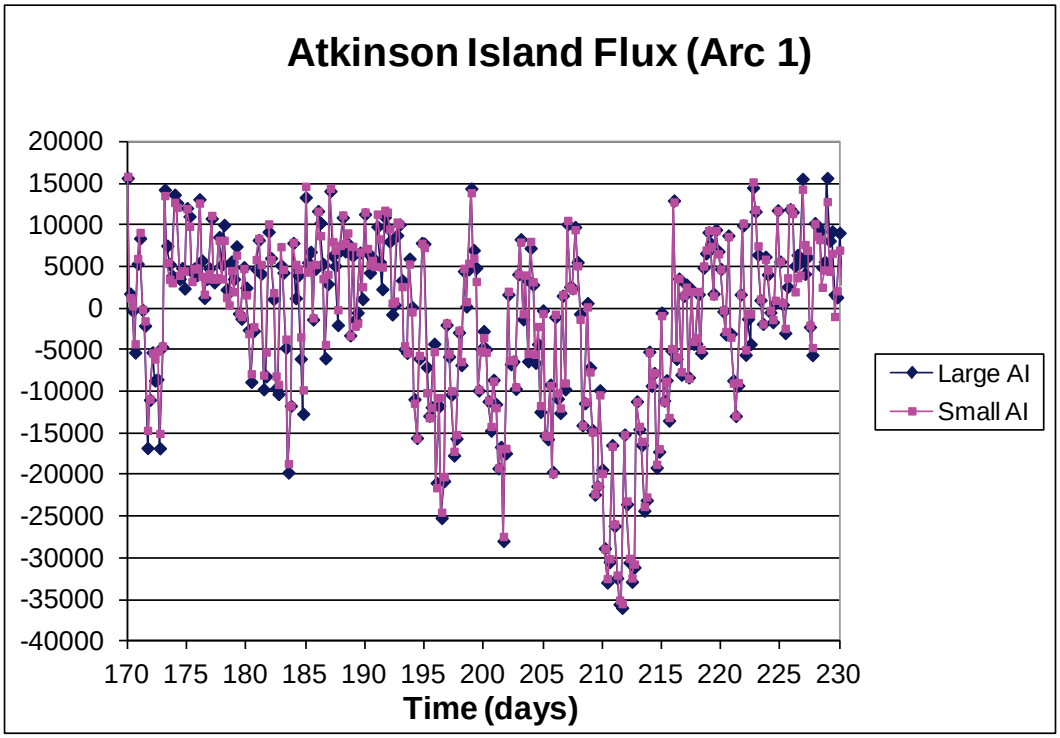

Figure 91. Atkinson Island Arc 2 discharge comparison (cfs).

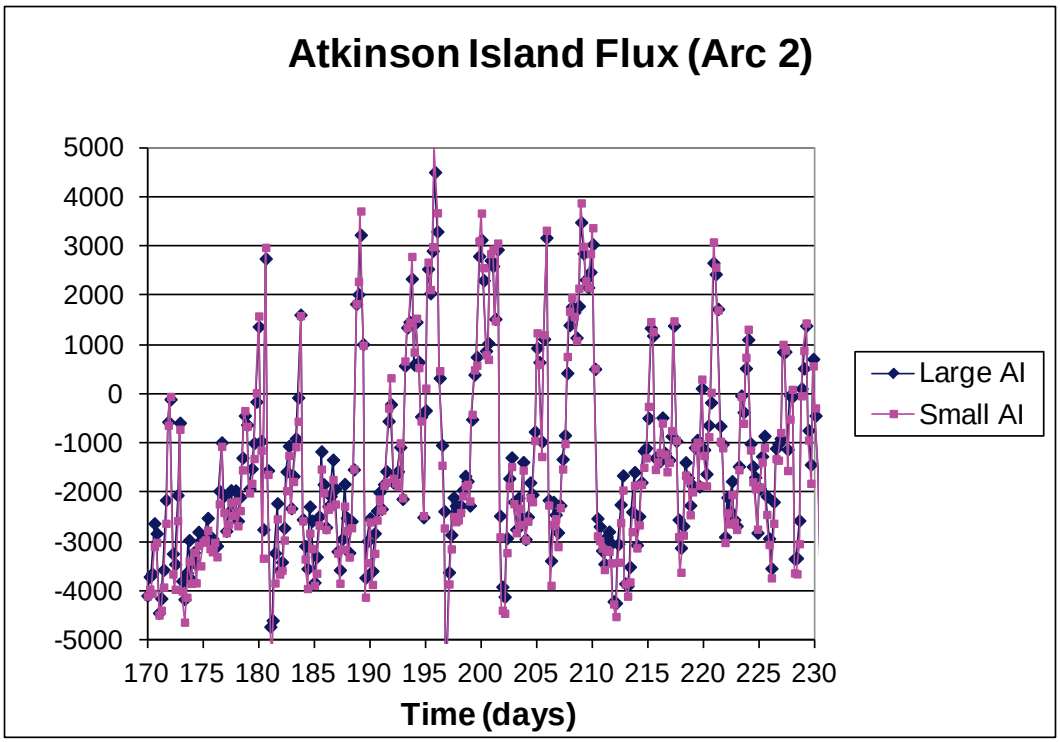

Figure 92. Atkinson Island Arc 3 discharge comparison (cfs).

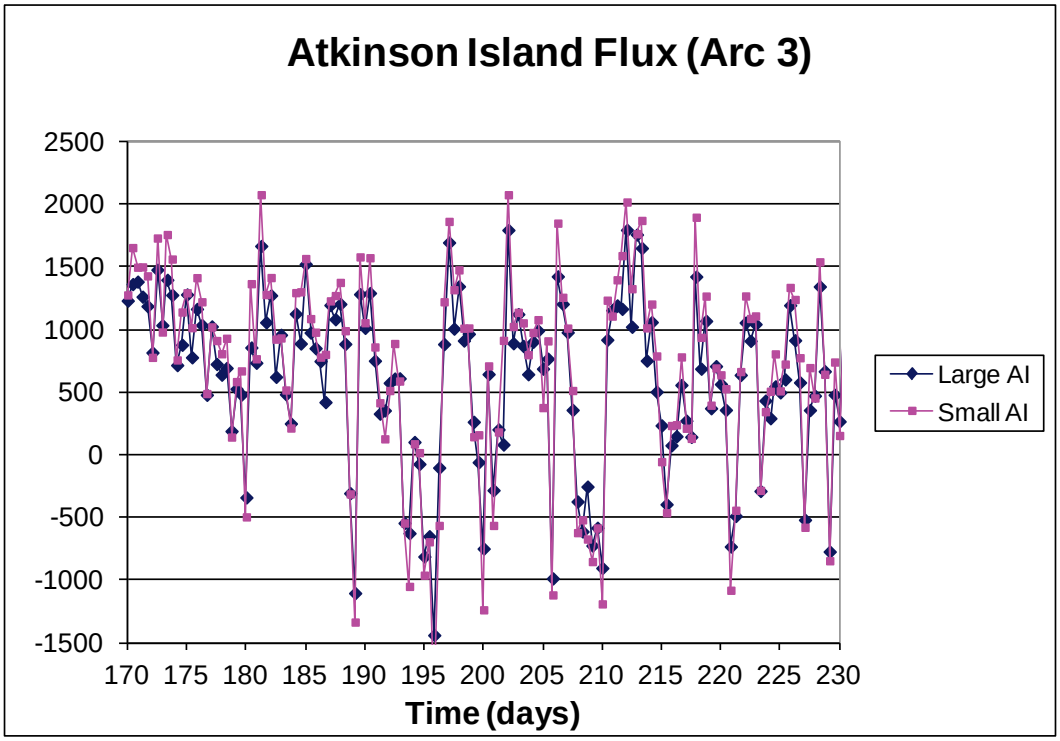

Figure 93. Atkinson Island Arc 4 discharge comparison.

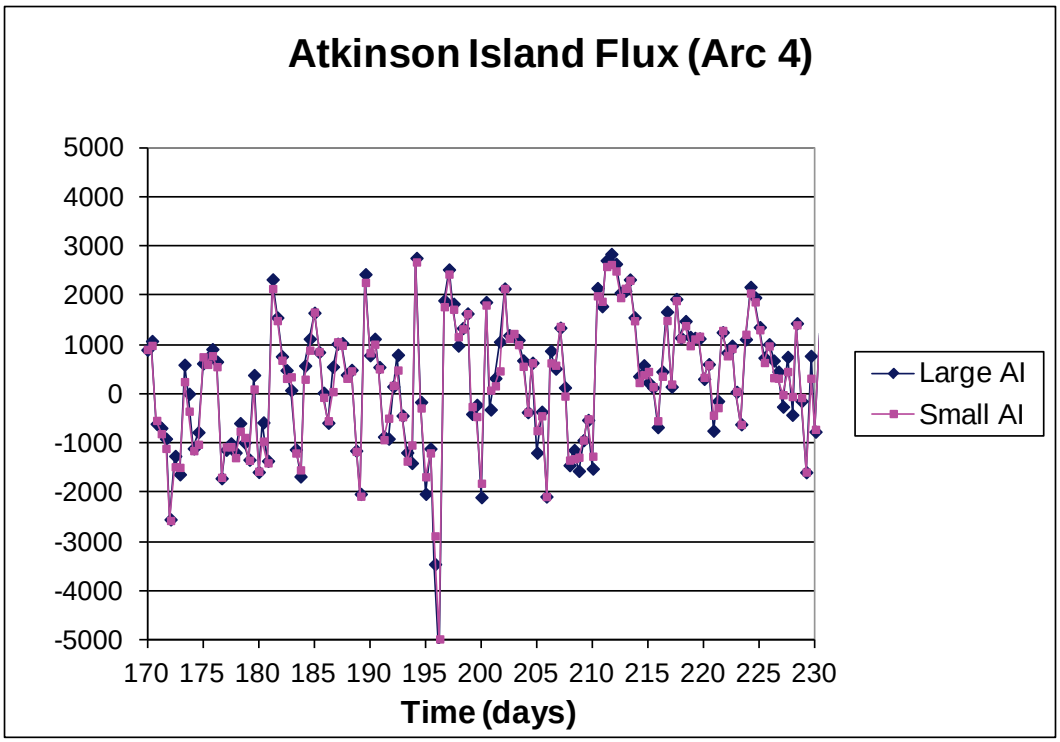

The discharge comparisons are not drastically different between the island configurations. However, at Arc 1 on the HSC side of the island, the discharge increased slightly at times with the enlarged island. Also, at Arc 2 on the eastern side of the island (the side with the increased island area) the discharge decreased due to the larger island size and therefore smaller flow area on the back side of the island. The discharge comparison at Arc 3 near the northern end of the island indicates that the larger island prevents some flow through this pathway. The island enlargement is just downstream from the Arc 3 analysis location. Arc 4, however, shows a small increase in the discharge between the central portion of the island and the southernmost placement area. It is likely that the reduction of flow through the northern pathway is being compensated for at the southern pathway. Also note that there are some times of high velocity on the eastern side of the enlarged Atkinson Island that are lower in the previous island condition. Depending on the sediment properties and the magnitude of these velocities, bed material that was not eroded previously may be eroded due to the enlarged island, providing additional sediment for transport.

An indicator of erosion potential is the shear stress produced by the flow conditions. For the grain sizes defined during the field data collection processes and included in the model, the critical shear stress for erosion is

set to 0.67 Pascals (Pa) for the noncohesive material. Shear stresses greater than the critical value for erosion will generate erosion of the bed material. Shear stresses less than the critical value for erosion will not erode the bed of sandy material but will hinder deposition until the shear stress is less than the critical value for deposition—in this case 0.1 Pa. The critical shear for erosion of the cohesive grain class is 0.1 Pa, so the fine grain material has the potential to erode much sooner than the sands.

Figure 94 shows three locations on the eastern side of Atkinson Island where the shear stress is compared, and Figure 95 through Figure 97 show the shear stress values over the same 60-day period. These plots are shown with a maximum of 0.7 Pa in order to reference the 0.67 Pa critical shear stress for erosion of the noncohesive material. The general trend is that Point 1 has an increased shear stress due to the additional size of the island. Points 2 and 3 show small variations at times but not an overall change in the shear stress magnitudes above or below the pre-enlarged condition. The magnitude of the shear stress at these locations does not indicate a large potential for bed erosion, but it does indicate a greater likelihood that material from the rivers or upstream may remain in suspension longer as it travels along the eastern side of the island, giving it the ability to move farther down the system.

Figure 94. Shear stress comparison locations.

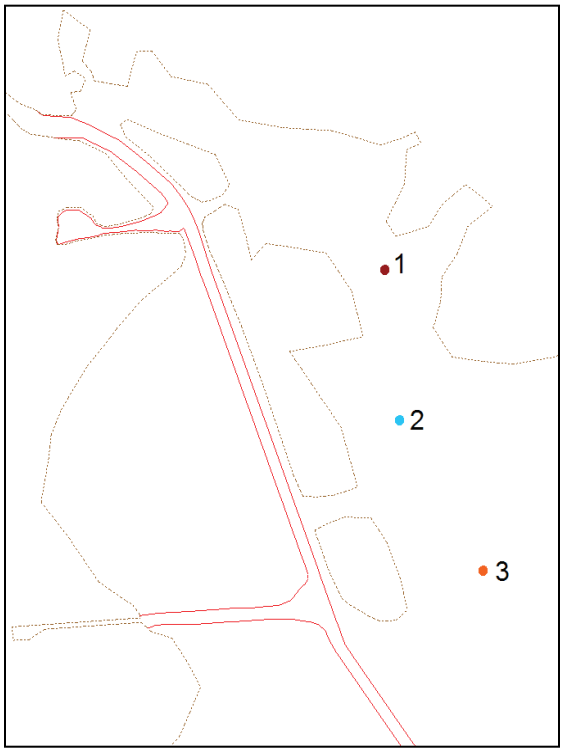

Figure 95. Shear stress comparison for Point 1.

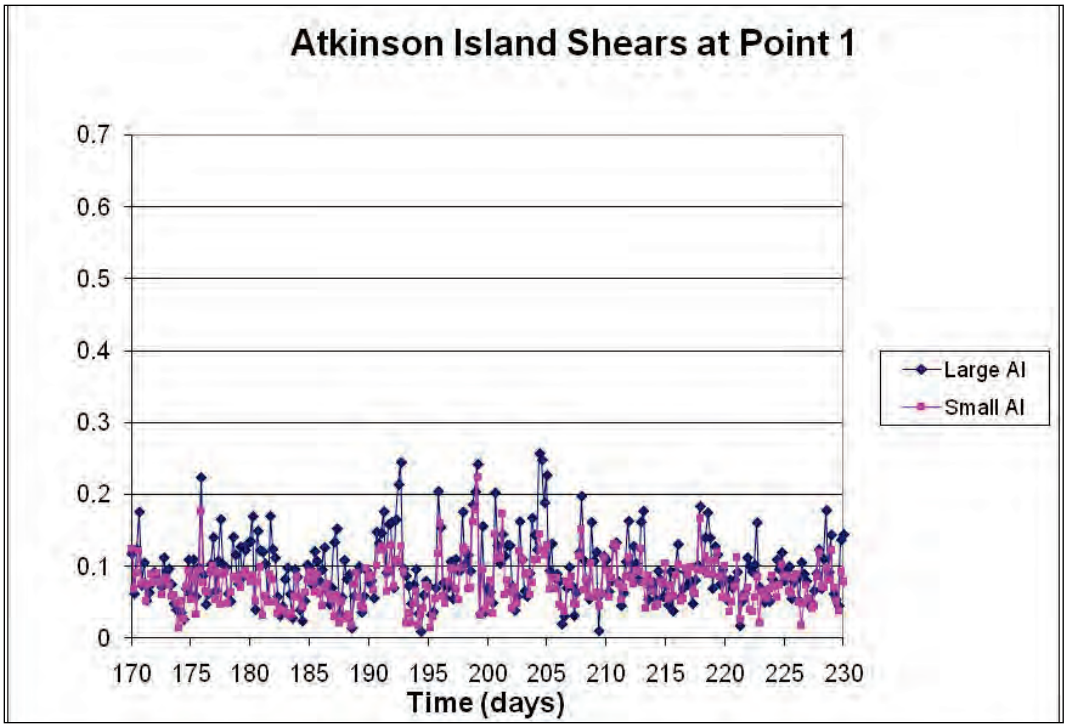

Figure 96. Shear stress comparison for Point 2.

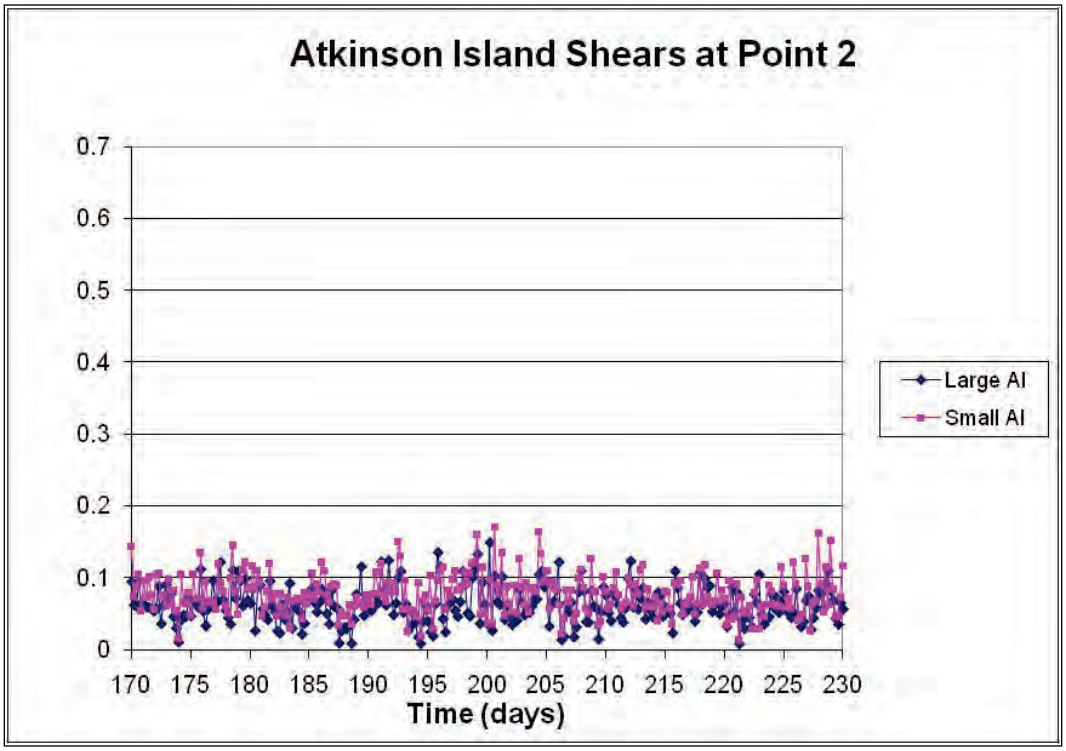

Figure 97. Shear stress comparison for Point 3.

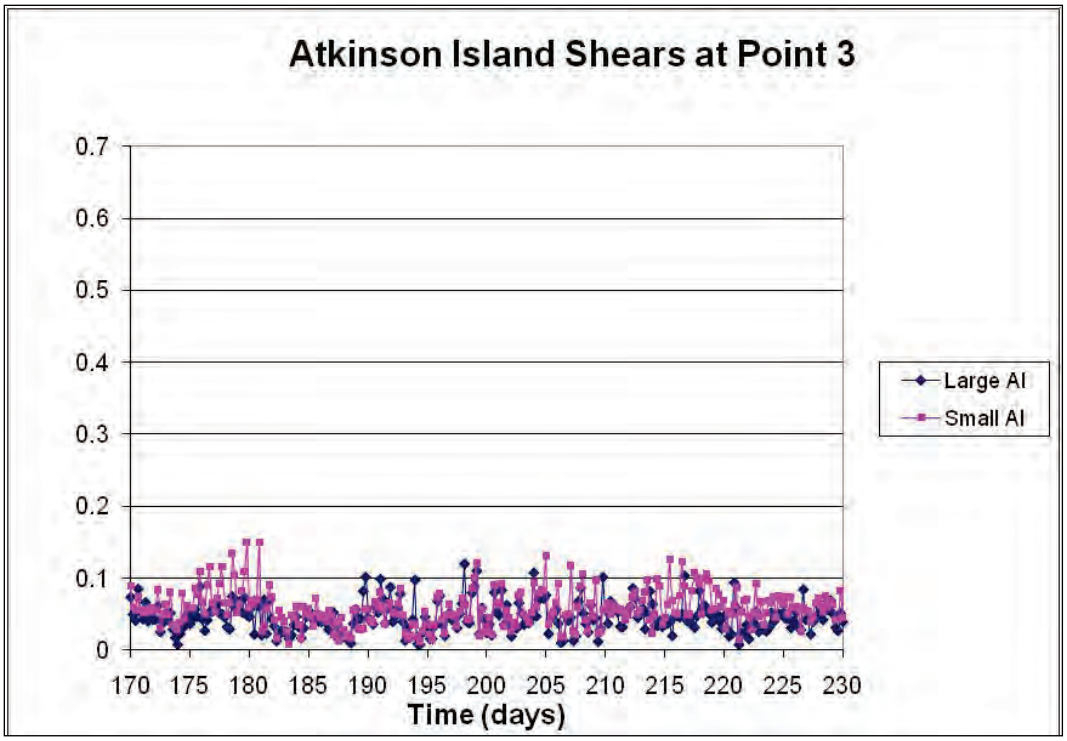

Shoaling impacts

The sediment model run with the inclusion of vessel effects and the bed displacement is compared for the two island configurations (Figures 98 and 99). The shoaling varies on the order of 2–4 centimeters (cm) in the western shallows. The eastern side of Atkinson Island shows approximately 6 cm of deposition in the location of the added disposal site. The circled areas indicate sections of the HSC where the deposition magnitudes change due to the size of the island. Some of the areas shaded in red in the smaller island configuration are actually reduced when the island is enlarged. However, the total volume in a reach is actually increased. In the HSC along Atkinson Island, the larger island increases the total deposition in the channel area by 4%. In the section from the Bayport Flare to the marsh site, the channel deposition increases by 10%.

From this focused analysis of the hydrodynamic and sediment transport impacts due to changes in the footprint of the island, and therefore the cross-sectional area behind the island, the impact on the channel shoaling of the planned disposal areas can be negative. More sediment is settling in the channel when the supply and available bed material are unchanged. It is imperative to consider the impacts of any geometric changes, especially those near the ship channel where vessels impact the flows and

sedimentation. By placing dredged material on the back side of the island, the shoaling rates along the island and southward are increased.

Figure 98. Atkinson Island with additional disposal sites.

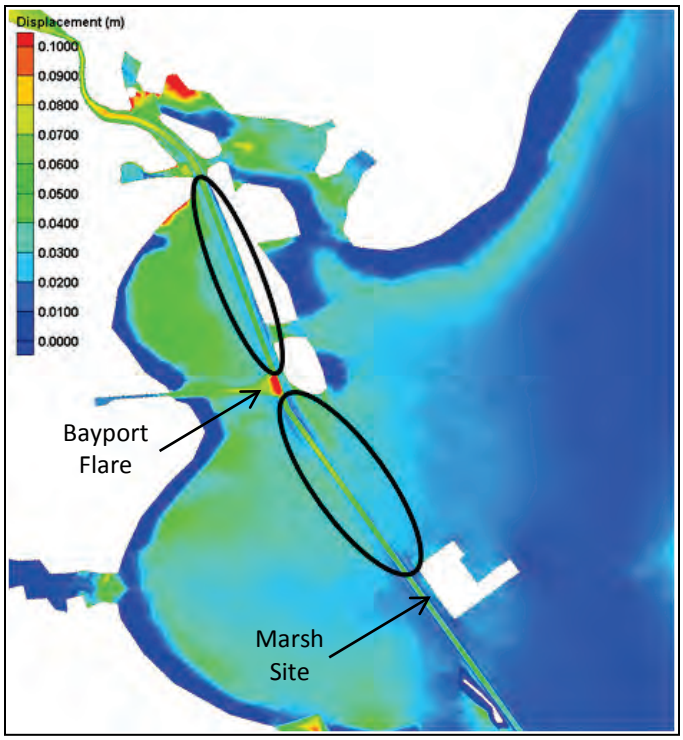

Figure 99. Atkinson Island prior to enlargement.

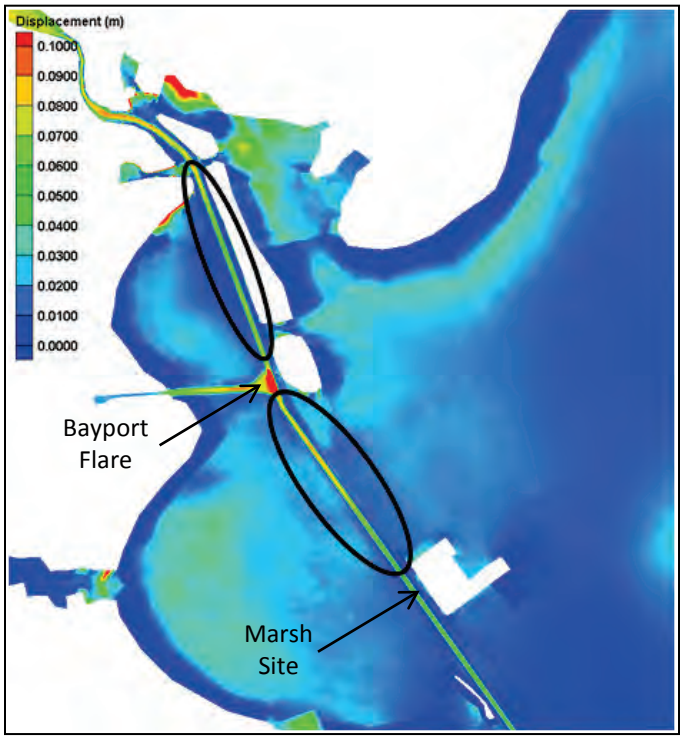

Fluid mud (Hypothesis 8)

The May 2012 data collection effort included a fluid mud component. However, no fluid mud was found in the area of the bay or channel between Barbour's Cut and the Mid-Bay Marsh site. The indication from all who have detected fluid mud in the system is that it is sporadic and not a regular or cyclic occurrence. It is still possible that some event pushes this fluid material into the channel such that it is a source of large deposition volumes, but presently this hypotheses cannot be confirmed.

Spring sediment properties (Hypothesis 9)

Based on previous research, data collection efforts, and modeling studies, it is known that changes occur in the HGNC system during the spring high-flow events. Salinity drops in the Gulf of Mexico causing the residual flow direction in the bay to reverse. It is also known that high-flow events are drivers for high sediment loads and freshly deposited material. CHL has collected sediment data in September and December but not in the spring or early summer months. The MCNP effort included a spring data collection effort to determine bed material properties for new deposits as well as sediment loads from the rivers that enter the bay. However, the 2011 data collection effort did not yield these data due to low rainfall and drought conditions in south-central Texas. The sediment properties and inflows for a spring flow event remain uncertain, and this hypothesis remains untested.

Recommendations

Based on the field data collection efforts, numerical modeling of the entrance channel and estuarine portion of the HSC, and the related analyses, three major recommendations are provided.

Dredge database standards

Determining the actual amount of shoaled material along the HSC was difficult due to the many conflicting sources of dredged quantity. The USACE Annual Reports, the district dredge quantity database, and the after-work dredge surveys provided varying quantities. This issue is not limited to the HSC area but is found in many USACE districts. Numerical models and future estimates cannot be verified if there is little confidence in the dredge quantity that is being estimated. A set of dredge database standards should be developed so all USACE-regulated navigation

channels record the same type of information. This information should be measured/computed in a standard way in all districts. If there are various quantities based on multiple documenting methods, all of these sources should be included in the dredge database.

A set of MATLAB functions was developed to look at raw dredge quantity data and plot the data for specific channel reaches. These tools read tabular data, including time, station, and dredge volume. Output included plots of dredging quantities over time for a section or along the channel at specified times. The functions allow for interactive plotting and manipulation of large sets of dredge quantity data. Utility codes of this type can be combined into a dredge quantity database analysis tool for visualization and computation of dredged quantities.

Vessel analysis data

A large volume of vessel data was collected for the HGNC area. Although all hypotheses could not be verified with the data available, a good initial set of data as well as insight into better collection methods for vessel impact tracking was obtained. Additional data collection in other navigable waterways can expand the sampling set such that more general and national conclusions can be drawn. The data presented in this study aid in the understanding of the effects of large vessels that travel a channel surrounded by shallow bays, but currently it is not known if these same effects occur along all navigable channels of this type.

The Vessel Data Analysis GUI was developed during this study and is a good tool for consolidating several data types into one picture. Velocity data, tide data, concentration data, vessel speeds and sizes can be sorted and linked to get a *big picture* understanding of the impacts produced under certain conditions. This tool is not specific to the HSC area and can be used to look at AWAC and ADV data from any project.

Numerical models

Numerical models are excellent tools to help district engineers analyze modifications in geometry and flow conditions of a given area. Under this study, two numerical models were developed and updated for current conditions. The entrance channel model was set up for use with the CMS by ERDC and USACE SWG personnel. The estuarine portion of the model was updated from previously developed TABS-MDS and AdH models by

ERDC. These tools are available for future analysis that the USACE district would like to perform.

Ideally, a model is developed and validated by experts in numerical modeling such that the model is applicable for a wide range of scenarios. Once a model is developed, it can be passed to the district engineer with specific instructions and analysis tools specific to need. This handoff would include a short training session as well as instruction documentation. Model maintenance can be included to ensure that the model maintains usability over time and to cover later assistance with using the model or training new personnel.

7 Conclusions

The Monitoring Completed Navigation Projects Program, Houston-Galveston Navigation Channel Shoaling Study, included investigation into historical data and prior studies of the area, collection of new hydrodynamic and sediment data, and numerical modeling of the entrance and bay sections of the HGNC network. Over 100 yr of dredge data records were analyzed. Three data collection efforts were undertaken. Three numerical models were developed—one for the entrance at Bolivar Roads, one for the estuarine portion of the bay, and another for the ship effects in the bay.

The study uncovered uncertainties in the dredge data record keeping and inconsistent data among sources. Without knowing what the true shoaling values are, it is difficult to know if new methods of estimation or modeling are accurate and adequate for the USACE district needs. It is apparent from additional studies involving other districts and agencies that this is not a localized issue.

Due to drought conditions during the MCNP-supported data collection effort, suspended sediment and bed material sampling is still needed during the time of spring high-flow events to determine accurate riverine sediment loads and new-deposit bed properties. With additional data, the estuarine sediment model may be able to be further improved. The hydrodynamic model has been upgraded based on recent data and is available for analysis of system changes.

A large volume of vessel data was collected and analyzed to determine trends in vessel impacts on the shoaling potential in the ship channel and in the shallow areas of the bay. The data collection effort provided insight and verified some hypotheses about how the vessels impact the shoaling. However, additional collection efforts are necessary to further develop the conclusions made in this study.

Two numerical models were developed to help analyze the shoaling potential in the HSC and possible causes. The CMS model focuses on the entrance channel and jetties. The TABS-MDS /AdH model focuses on the portion of the HSC through Trinity Bay. Each model is intended to be used

to investigate proposed system changes or answer questions posed, and each is optimized for its focus area.

Based on the many analysis methods included in this study, several recommendations were provided. These include developing dredge database standards, utilizing the developed numerical models, and expanding on the vessel data collection. Several analysis tools were developed and should also be utilized when appropriate to help ease the data manipulation and improve overall understanding of the data as a collection.

Based on these and other study results, present-day HGNC navigation channel shoaling is exacerbated by the following processes and/or anthropogenic activities:

Entrance Channel

- Placement of fine-grained sediment in the beneficial use berm, which can be mobilized during periods with sufficient forcing conditions.
- Sand transport over, through, and around the south jetty.
- Net flood-directed transport of sediments into the bay throughout the tidal cycle.

Houston Ship Channel

- Suspension and transport of freshly deposited bay sediment during tropical storms and hurricanes.
- Transit of vessels that induce a surge and subsequent drawdown of water in the shallow bay adjacent to the navigation channel.
- Configuration of the larger footprint of Atkinson Island, a dredged material placement site, which increases shoaling by 4%–10%.

References

Alperin, L. M. 1977. *Custodians of the coast: History of the U.S. Army Engineers at Galveston*. Galveston, TX: Galveston District, U.S. Army Corps of Engineers.

Berger, R. C., R. T. McAdory, W. D. Martin, and J. H. Schmidt. 1995a. *Houston-Galveston navigation channels, Texas Project. Report 3, three-dimensional hydrodynamic model verification*. Technical Report HL-92-7. Vicksburg, MS: U.S. Army Engineer Waterways Experiment Station.

Berger, R. C., R. T. McAdory, J. H. Schmidt , W. D. Martin, and L. H. Hauck. 1995b. *Houston-Galveston navigation channels, Texas Project. Report 4, three-dimensional numerical modeling of hydrodynamics and salinity*. Technical Report HL-92-7. Vicksburg, MS: U.S. Army Engineer Waterways Experiment Station.

Carrillo, A. R., M. S. Sarruff, and R. C. Berger. 2002. *Effects of adding barge lanes along Houston Ship Channel through Galveston Bay, Texas.* ERDC/CHL TR-02-23. Vicksburg, MS: U.S. Army Engineer Research and Development Center.

Coplin, L. S., and D. Galloway. 1999. Houston-Galveston, Texas, Managing coastal subsidence. In *Land Subsidence in the United States*, ed. D. Galloway, D. R. Jones, and S. E. Ingebritsen, 35–48. U.S. Geological Survey Circular 1182. Reston, VA: U.S. Department of the Interior, U.S. Geological Survey.

Gahagan & Bryant Associates. 2008. *Houston Ship Channel sedimentation study*. Draft report submitted to the Port of Houston Authority. November 2008

Galveston Bay Estuary Program. 2002. *The state of the bay: A characterization of the Galveston Bay ecosystem*, 2nd Ed. Ed. J. Lester and L. Gonzalez. Austin, TX: Texas Commission on Environmental Quality.

Harris-Galveston Subsidence District. 2010. http://www.hgsubsidence.org/.

Headquarters, U.S. Army Corps of Engineers (USACE). 1944–2002. *USACE annual reports*. Washington, DC: Headquarters, U.S. Army Corps of Engineers.

———. 2002. *Coastal engineering manual part III – Chapter 4: Wind-blown sediment transport*. EM 1110-2-1100. Washington, DC: Headquarters, U.S. Army Corps of Engineers.

Holzer, T. L. 1989. State and local response to damaging land subsidence in United States urban areas. *Engineering Geology* 27: 449–466.

Maynord, S. T, J. E. Hite, Jr., and M. J. Sanchez. 2006. *Atkinson Island mooring basin alternatives, Houston Ship Channel*. ERDC/CHL TR-06-19.Vicksburg, MS: U.S. Army Engineer Research and Development Center.

McNeil, J., C. Taylor, and W. Lick. 1996. Measurements of erosion of undisturbed bottom sediments with depth. *Journal of Hydraulic Engineering* 122: 316–324.

Morang, A. 2006. *North Texas sediment budget*. ERDC/CHL TR-06-17. Vicksburg, MS: U.S. Army Engineer Research and Development Center.

National Oceanographic and Atmospheric and Association (NOAA). 2014. *Tides and currents, Galveston Pier 21, Station ID 8771450*. Washington, DC: National Oceanic and Atmospheric Administration.

Ravens, T. M., and R. C. Thomas. 2008. Ship wave-induced sedimentation of a tidal creek in Galveston Bay. *Journal of Waterway, Port, Coastal, and Ocean Engineering* 134(1): 21–29, January/February 2008.

Sánchez, A., W. Wu, T. M. Beck, H. Li, J. Rosati, R. Thomas, J. D. Rosati, Z. Demirbilek, M. Brown, and C. Reed. 2011a. *Verification and validation of the Coastal Modeling System: Report III, CMS-flow hydrodynamics*. ERDC/CHL-TR-11-10. Vicksburg, MS: U.S. Army Engineer Research and Development Center.

Sánchez, A., W. Wu, T. M. Beck, J. D. Rosati, Z. Demirbilek, H. Li, and M. E. Brown. 2011b. *Verification and validation of the Coastal Modeling System: Report IV, CMS-flow sediment transport and morphology change*. ERDC/CHL-TR-11-10. Vicksburg, MS: U.S. Army Engineer Research and Development Center.

Schroevars, M., B. J. A. Huisman, M. van der Wal, and J. Terwindt. 2011. Measuring ship induced waves and currents on a tidal flat in the Western Scheldt Estuary. In *Proceedings of the IEEE/OES/CWTM Tenth Working Conference on Current Measurement Technology*, 20–23 March 2011. Monterey, CA.

Solis, R. S., W. L. Longley, and G. Malstaff. 1994. Influence of inflow on sediment deposition in delta and bay systems. In *Freshwater inflows to Texas bays and estuaries*, ed. W. L. Longley, 56–70. Austin, TX: Texas Water Development Board.

Tate, J. N., and R. C. Berger. 2006. *Houston-Galveston navigation channels, Texas Project: Navigation channel sedimentation study, phase 1*. ERDC/CHL TR-06-8. Vicksburg, MS: U.S. Army Engineer Research and Development Center.

Tate, J. N., R. C. Berger, and C. G. Ross. 2008. *Houston-Galveston navigation channels, Texas Project: Navigation channel sedimentation study, phase 2*. ERDC/CHL TR-08-8. Vicksburg, MS: U.S. Army Engineer Research and Development Center.

Tate, J, N., and C. G. Ross. 2009. *Houston-Galveston navigation channels, Texas Project: Navigation channel sedimentation study, phase 2 plan simulations*. ERDC/CHL TR-09-6. Vicksburg, MS: U.S. Army Engineer Research and Development Center.

Tate, J. N., and C. G. Ross. 2012. *Bayport Flare hydrodynamic study for ship simulation*. ERDC/CHL TR-12-13. Vicksburg, MS: U.S. Army Engineer Research and Development Center.

Texas Water Development Board (TWDB). 1999. *User's manual for the Texas Water Development Board's hydrodynamic and salinity model: TxBLEND*. Austin, TX: Texas Water Development Board.

Trawle, M. J. 1981. *Effects of depth on dredging frequency: Report 2, methods of estuarine shoaling analysis*. Technical Report H-78-5. Vicksburg, MS: U.S. Army Engineer Waterways Experiment Station.

URS. 2010. *Implementation of bathymetric survey plan and sampling and monitoring plan–Galveston Ship Channel, Galveston, Texas*. Prepared for USACE Galveston District, Galveston, TX. Tallahassee, FL: URS Corporation Southern.

U.S. Army Corps of Engineers (USACE), Galveston District. 1995. *Engineering supplement to limited reevaluation report, vol. 1 and 2*. U.S. Army Corps of Engineers, Galveston District.

U.S. Coast Guard. 2006. *State of the waterway–2005*. Vessel Traffic Service, Houston-Galveston. New Orleans, LA: U.S. Coast Guard, District 8.

Ward, G. H., and N. E. Armstrong. 1993. *Water and sediment quality of Galveston Bay*. Galveston Bay National Estuary Program Conference 1993.

White, W. A., R. A. Morton, and C. W. Holmes. 2002. A comparison of factors controlling sedimentation rates and wetland loss in fluvial-deltaic systems. Texas Gulf Coast. *Geomorphology* 44: 47–66.

Appendix A: Vessel Data and Plots

This appendix includes the complete set of LOMA vessel characteristic data for 12 May 2012 in Table 21 through Table 24. This dataset includes time at Position 1, the call sign, vessel type, beam (width), length, draft, speed, and travel direction. Also included are plots of drawdown at AWAC 1 as compared to specific vessel characteristics.

Table 21. Vessel characteristics for 12 May 2012.

POS1 (hh:mm:ss)	Vessel call sign	Type of ship	Beam (m)	Length (m)	Draft (m)	Speed (m/s)	Direction
0:07:10	V7NF9	Cargo	32	294	12	5.72	DOWN
20:36:20	A8AP6	Tank	44	250	9	5.42	UP
14:05:11	S6NK2			247	9	5.10	UP
2:11:51	3FXG7	Cargo	33	245	11	6.77	UP
20:26:08	3FXG7	Cargo	33	245	11	6.63	DOWN
19:45:42	3FUU	Tank	42	229	9	5.30	DOWN
6:23:42	SZLF	Tank	32	228	13	5.90	UP
18:01:07	A8WO6	Cargo	32	228	12	6.12	DOWN
22:48:47	V7NE6	Tank	36	228	12	6.68	UP
18:15:44	C6JT8	Cargo	32	225	7	4.92	UP
3:41:43	3EXG9	Cargo	32	199	9	7.07	DOWN
13:42:16	P3DJ9	Cargo	32	189	12	5.43	DOWN
16:17:20	2DBR8	Tank	32	188	8	5.49	UP
12:51:45	LAUU4			188	5	5.86	DOWN
7:00:02	ICLK	Tank	27	184	11	5.97	DOWN
3:49:18	LAJB7	Tank	32	183	12	6.41	DOWN
9:36:59	9HSR8	Tank	32	183	12	5.97	UP
14:00:02	9VVN2	Tank	32	183	11	6.37	DOWN
4:19:01	LACQ7	Tank	32	183	10	5.96	UP
16:25:23	9VVD9	Tank	32	183	8	6.36	UP
9:30:27	ELUZ4	Tank	20	182	8	5.79	UP
15:53:07	3EYS7	Tank	33	182	8	6.17	UP
15:06:40	FNFI	Tank	32	180	12	6.05	DOWN
0:35:31	V7HP3	Tank	28	179	11	6.24	UP
19:42:24	OZGS2	Tank	28	177	7	6.33	UP

POS1 (hh:mm:ss)	Vessel call sign	Type of ship	Beam (m)	Length (m)	Draft (m)	Speed (m/s)	Direction
12:51:48	ZCSP5	Tank	31	176	12	6.38	UP
19:51:49	VRGP3	Cargo	28	175	8	6.41	UP
1:06:29	9VHS2	Tank	25	158	11	6.66	UP
1:15:23	9V9577			141	10	6.28	DOWN
11:53:13	3EPE8	Tank	24	141	9	6.24	DOWN
2:59:02	V2OU6	Container	22	139	9	7.07	UP
23:02:25	PEAD	Cargo	16	135	8	6.59	DOWN
3:50:23	WDC9931			126	6	4.19	UP
14:27:47	V7MU3			124	9	6.33	DOWN
19:12:20	WDF4929	Cargo	20	120	7	6.88	DOWN
19:17:17	V2JO1	Cargo	20	120	7	7.47	UP
6:15:20	V2ED			86	6	5.79	DOWN
12:26:45	WDC2462			36	3	3.96	UP
20:47:12	WDD3759			35	2	7.16	UP
16:00:55	WDE2477			33	3	3.79	UP
12:58:59	WDF4879			32	3	0.059	UP
14:15:08	WBE9251			31	3	4.51	UP
9:33:36	WCZ9961			30	5	5.65	UP
19:03:28	WDD5964			29	3	3.35	UP
10:09:24	WDF3017			28	3	2.74	DOWN
7:29:15	WDC2706			27	4	1.88	UP
2:20:55	WDD4289			27	3	0.056	DOWN
10:41:04	WYQ8975			27	0	6.05	DOWN
15:47:41	WDF9302			27	0	4.46	DOWN
17:02:21	WYR6530			24	9	2.61	UP
6:46:08	WDF2365			24	3	3.82	UP
8:28:15	WDC5757			24	3	0.050	UP
8:28:15	WDD7994			24	3	0.082	UP
15:05:35	WDC3914	Towing	8	24	3	0.055	UP
15:58:37	WDC3747			24	2	0.055	UP
3:12:44	WDC3771			23	3	4.34	UP
3:12:44	WDD2725			23	3	0.086	DOWN
3:12:44	WDD5264			23	3	0.057	DOWN
10:17:39	WDE4207			23	3	3.73	DOWN
10:17:39	WDE6036			23	3	0.30	DOWN
16:27:28	WDC2785			23	3	4.21	UP

POS1 (hh:mm:ss)	Vessel call sign	Type of ship	Beam (m)	Length (m)	Draft (m)	Speed (m/s)	Direction
16:27:28	WDC2789			23	3	0.13	UP
21:19:25	WDC2818			23	3	4.10	UP
2:44:43	WDF9141			23	2	0.091	UP
2:44:43	WDF2418			23	0	3.21	DOWN
20:01:01	WDC4554			22	3	3.24	UP
0:18:50	WCZ6032			20	3	0.13	DOWN
1:04:16	WDC3290			20	3	3.20	UP
15:58:37	WDF2416			20	3	3.76	UP
16:54:49	WDC2640			20	3	0.065	UP
0:18:50	WDC7687			20	2	3.13	UP
4:12:43	WDB3169			18	3	0.069	UP
13:11:28	WDD4550			18	3	3.87	DOWN
12:19:41	WDF2901			18	0	4.28	DOWN
16:43:18	WCY7080			17	3	2.59	DOWN
16:43:18	WDF2142			17	3	0.065	UP
22:28:18	WDC2624			17	0	3.35	UP
21:45:16	WDC2639			16	3	3.36	UP
0:20:40	WCX9475			15	3	3.88	UP
0:20:40	WDA4660			15	3	0.48	UP
11:28:13	WDC2715			12	2	0.13	UP
22:03:16	SXVZ			0	8	5.65	UP
22:03:16	V20X4			0	8	0.066	UP
18:21:23	WDF9089			0	3	4.60	DOWN
18:33:32	WDC3740			0	2	3.26	UP
20:49:53	WDC6777			0	2	7.17	UP
1:34:48	WDA7892			0	0	3.72	UP
12:07:57	WDE3911			0	0	1.73	DOWN
19:10:59	WDB5626			0	0	1.84	UP

Table 22. Vessel characteristics for subset of events used in the analysis.

POS1 (hh:mm:ss)	Vessel call sign	Beam (m)	Length (m)	Draft (m)	Speed (m/s)	Direction	Event
0:07:10	V7NF9	32	294	12	5.72	DOWN	1
0:35:31	V7HP3	28	179	11	6.24	UP	2
1:06:29	9VHS2	25	158	11	6.66	UP	3
2:11:51	3FXG7	33	245	11	6.77	UP	4
2:59:02	V2OU6	22	139	9	7.07	UP	5
3:41:43	3EXG9	32	199	9	7.07	DOWN	7
3:49:18	LAJB7	32	183	12	6.41	DOWN	8
4:19:01	LACQ7	32	183	10	5.96	UP	9
6:23:42	SZLF	32	228	13	5.90	UP	10
7:00:02	ICLK	27	184	11	5.97	DOWN	11
9:30:27	ELUZ4	20	182	8	5.79	UP	12
9:36:59	9HSR8	32	183	12	5.97	UP	13
11:53:13	3EPE8	24	141	9	6.24	DOWN	14
12:51:48	ZCSP5	31	176	12	6.38	UP	15
13:42:16	P3DJ9	32	189	12	5.43	DOWN	16
14:00:02	9VVN2	32	183	11	6.37	DOWN	17
14:05:11	S6NK2	8	247	9	5.10	UP	18
15:06:40	FNFI	32	180	12	6.05	DOWN	19
15:53:07	3EYS7	33	182	8	6.17	UP	20
16:17:20	2DBR8	32	188	8	5.49	UP	21
16:25:23	9VVD9	32	183	8	6.36	UP	22
18:01:07	A8WO6	32	228	12	6.12	DOWN	23
18:15:44	C6JT8	32	225	7	4.92	UP	24
19:12:20	WDF4929	20	120	7	6.88	DOWN	25
19:17:17	V2JO1	20	120	7	7.47	UP	26
19:42:24	OZGS2	28	177	7	6.33	UP	27
19:45:42	3FUU	42	229	9	5.30	DOWN	28
19:51:49	VRGP3	28	175	8	6.41	UP	29
20:26:08	3FXG7	33	245	11	6.63	DOWN	30
20:36:20	A8AP6	44	250	9	5.42	UP	31
22:48:47	V7NE6	36	228	12	6.68	UP	33
23:02:25	PEAD	16	135	8	6.59	DOWN	34

Table 23. Vessel drawdown at AWACs 1–3 for events used in the analysis.

Event	AWAC 1 (m)	AWAC 2 (m)	AWAC 3 (m)
1	0.15	0.075	0.05
2	0.25	0.175	0.125
3	0.24	0.2	0.15
4	0.11	0.28	0.09
5	0.15	0.15	0
7	0.4	0.32	0.09
8	0.23	0.16	0
9	0.295	0.215	0.13
10	0.37	0.26	0.16
11	0.11	0	0
12	0.12	0.14	0.08
13	0.29	0.18	0.12
14	0.075	0.07	0.05
15	0.355	0.31	0.11
16	0.09	0.04	0
17	0.16	0.18	0
18	0.175	0.06	0
19	0.09	0.05	0.06
20	0.19	0.23	0.09
21	0.34	0.12	0.085
22	0.27	0.23	0.09
23	0.28	0.275	0.115
24	0.08	0.275	0.115
25	0.19	0.185	0.08
26	0.095	0.12	0.08
27	0.14	0.195	0.085
28	0.17	0.16	0
29	0.125	0.16	0.08
30	0.325	0.275	0.09
31	0.31	0.175	0.07
33	0.395	0.25	0.085
34	0.09	0.085	0

Table 24. Vessel concentration at AWACs 1–3 for events used in the analysis.

Event	AWAC 1 (mg/L)	AWAC 2 (mg/L)	AWAC 3 (mg/L)
1	0	125	0
2	65	190	0
3	0	125	0
4	0	80	55
5	0	0	0
7	120	250	0
8	0	165	0
9	0	0	0
10	40	80	0
11	0	0	0
12	0	385	0
13	0	0	0
14	0	0	0
15	100	50	105
16	99	0	0
17	0	90	0
18	0	0	0
19	0	0	0
20	0	125	0
21	80	0	0
22	0	100	0
23	50	210	0
24	0	163	0
25	75	90	0
26	0	0	0
27	35	55	205
28	0	0	0
29	0	0	0
30	160	170	0
31	0	0	0
33	140	350	0
34	0	0	0

Comparison plots of vessel characteristics and drawdown at AWAC 1 are shown in Figure 100 through Figure 102. These were developed to determine if any trends were observable, but the data appear well scattered.

Figure 100. Drawdown at AWAC 1 versus beam for drafts 7–13 m.

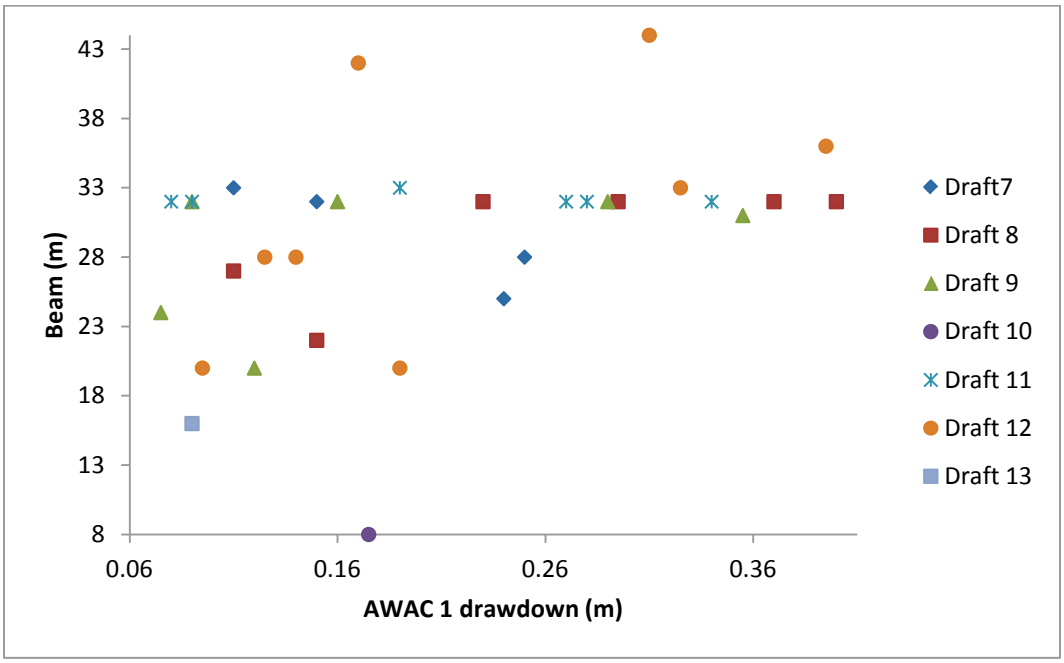

Figure 101. Drawdown at AWAC 1 vs. length for drafts 7–13 m.

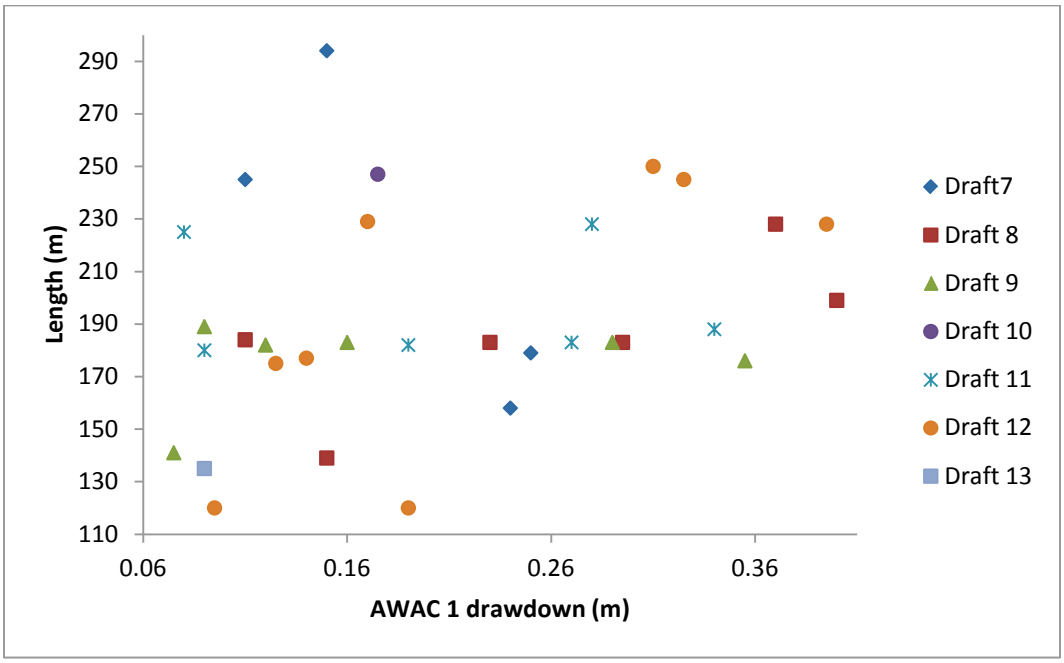

Figure 102. Drawdown at AWAC 1 vs. speed for drafts 7–13 m.

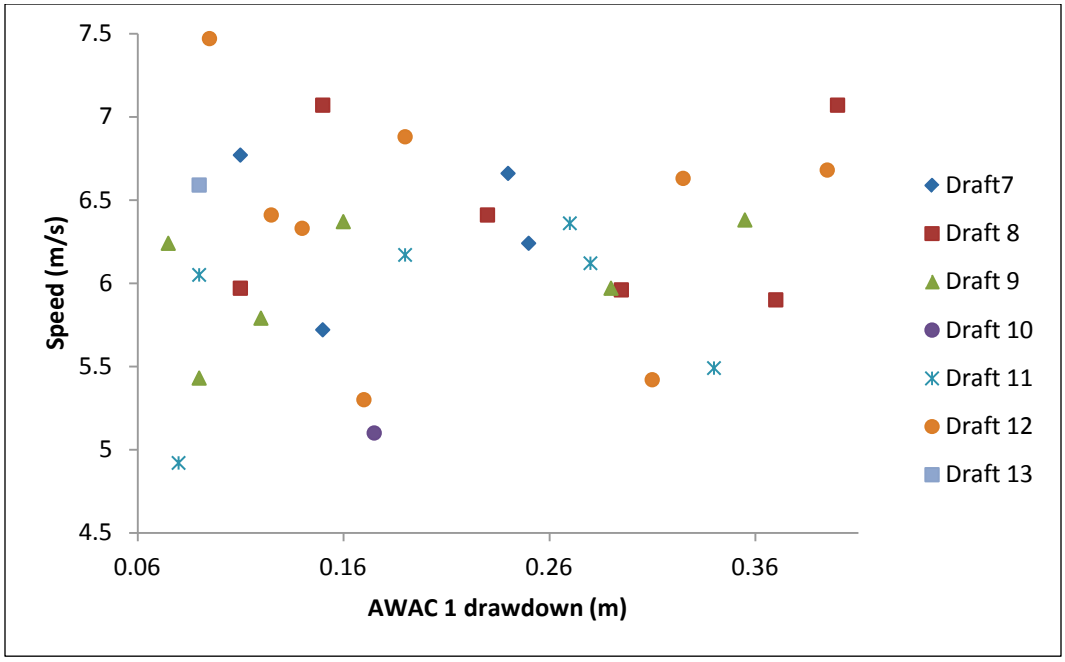

The depth and concentration time series for the full 24 hr period of 12 May 2012 are given in Figure 103 through Figure 110. Plots are provided for each of the four AWACs for both depth and concentration. Vessel passages are indicated by the spikes in the data. The plot titles list a ship and its characteristics, but the data provided include the effects of all vessel passages for this 24 hr period.

Figure 103. Depth at AWAC 1 on 12 May 2012.

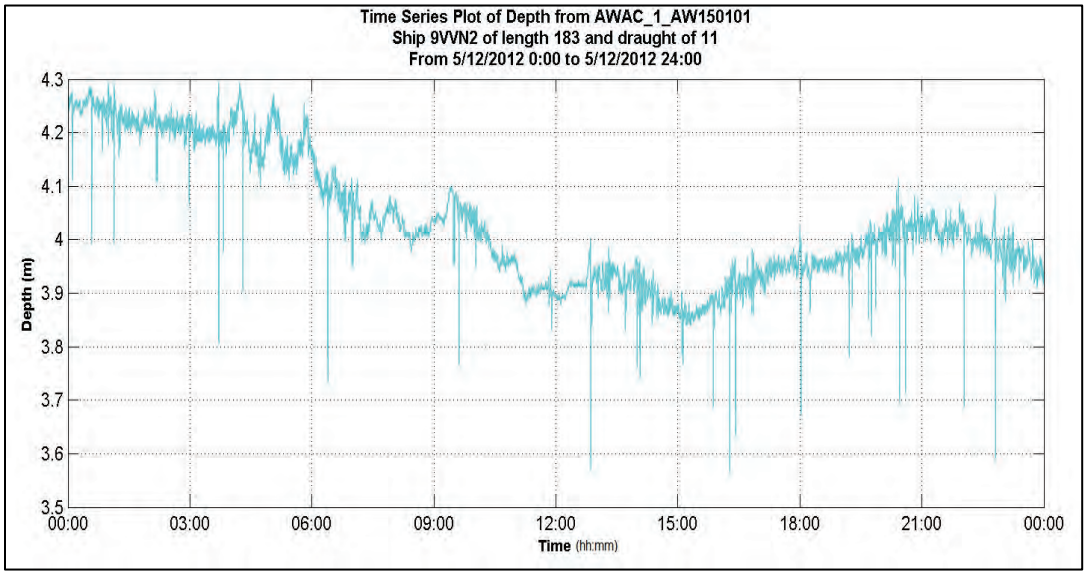

Figure 104. Depth at AWAC 2 on 12 May 2012.

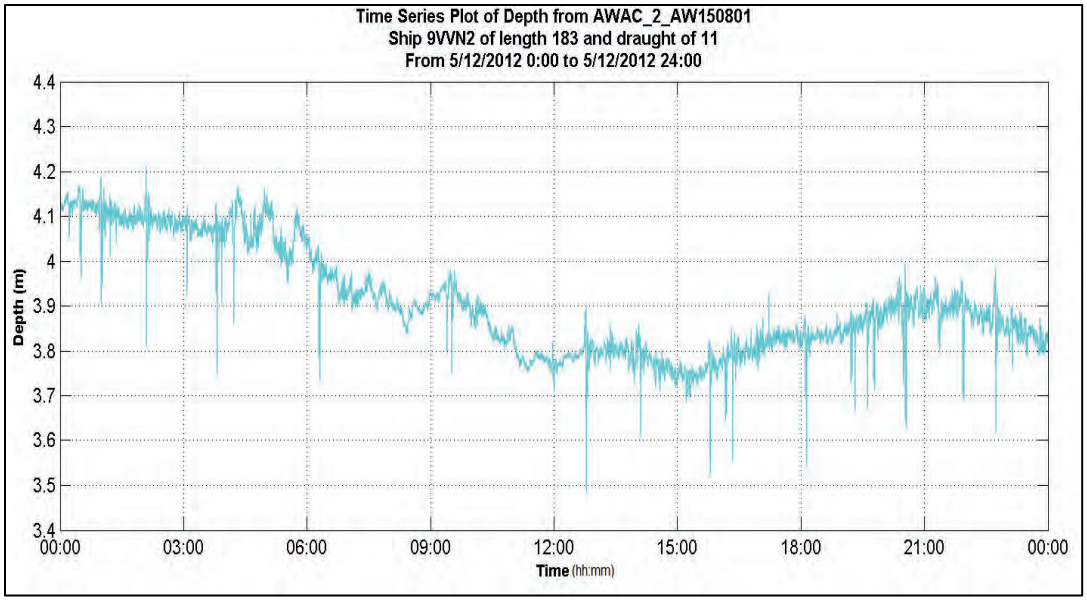

Figure 105. Depth at AWAC 3 on 12 May 2012.

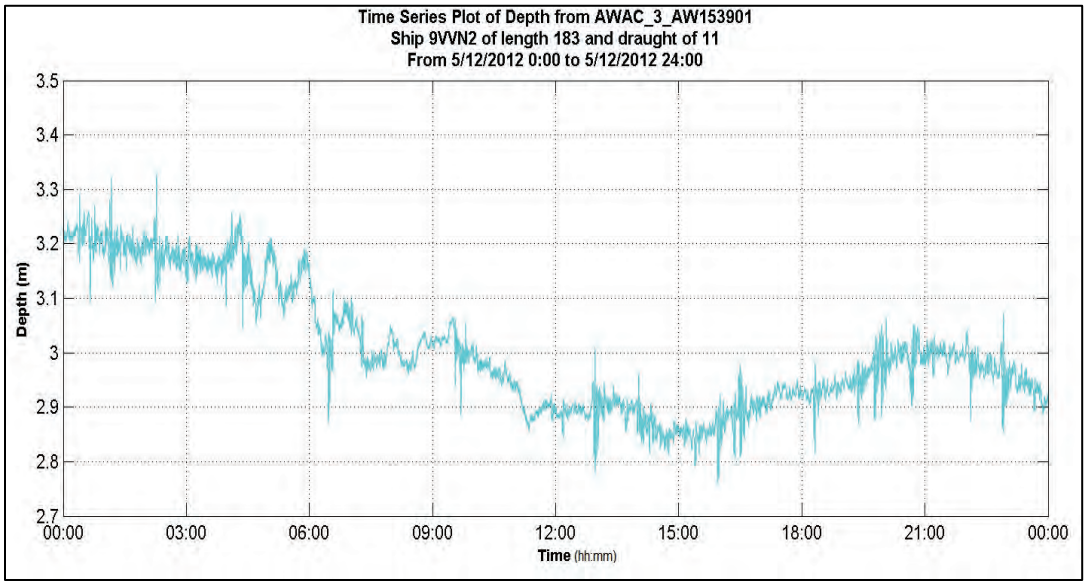

Figure 106. Depth at AWAC 4 on 12 May 2012.

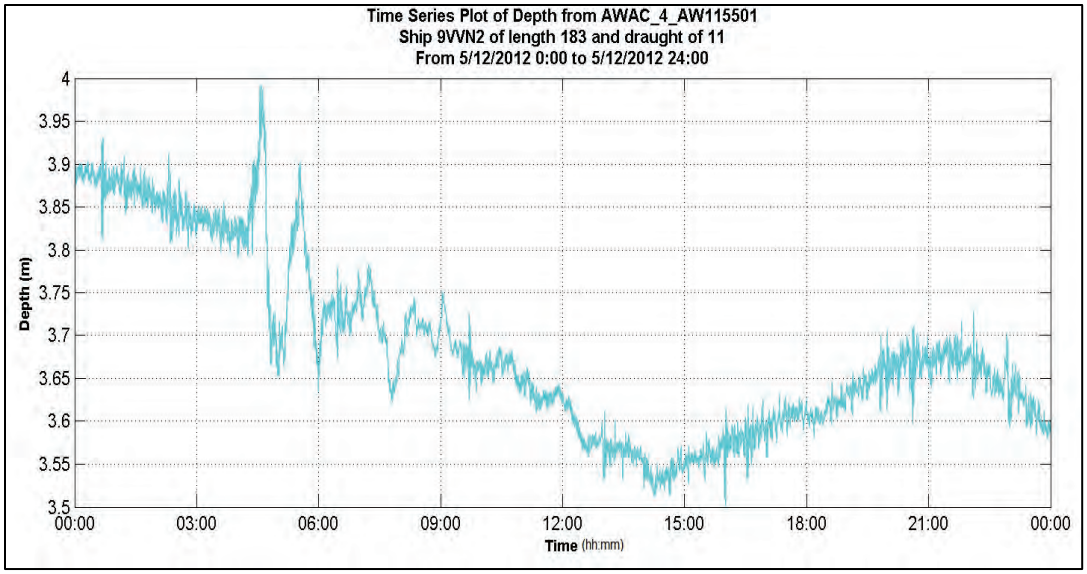

Figure 107. Concentration at AWAC 1 on 12 May 2012.

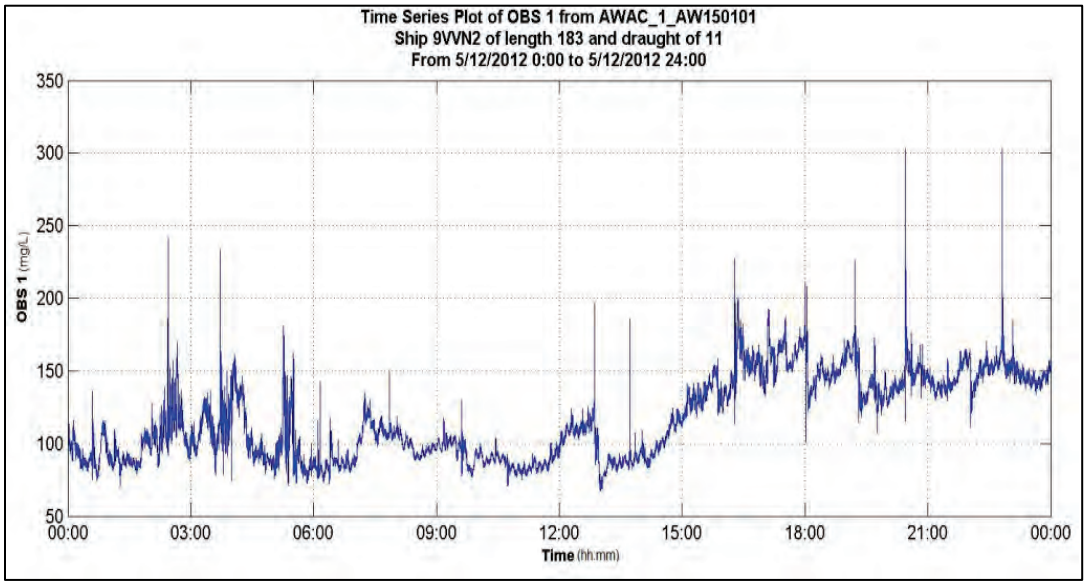

Figure 108. Concentration at AWAC 2 on 12 May 2012.

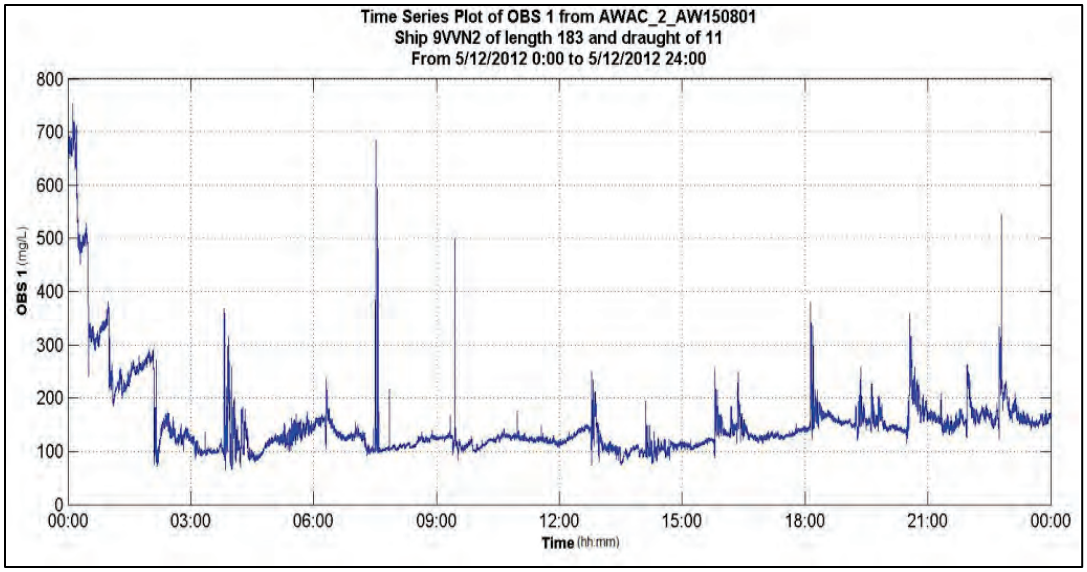

Figure 109. Concentration at AWAC 3 on 12 May 2012.

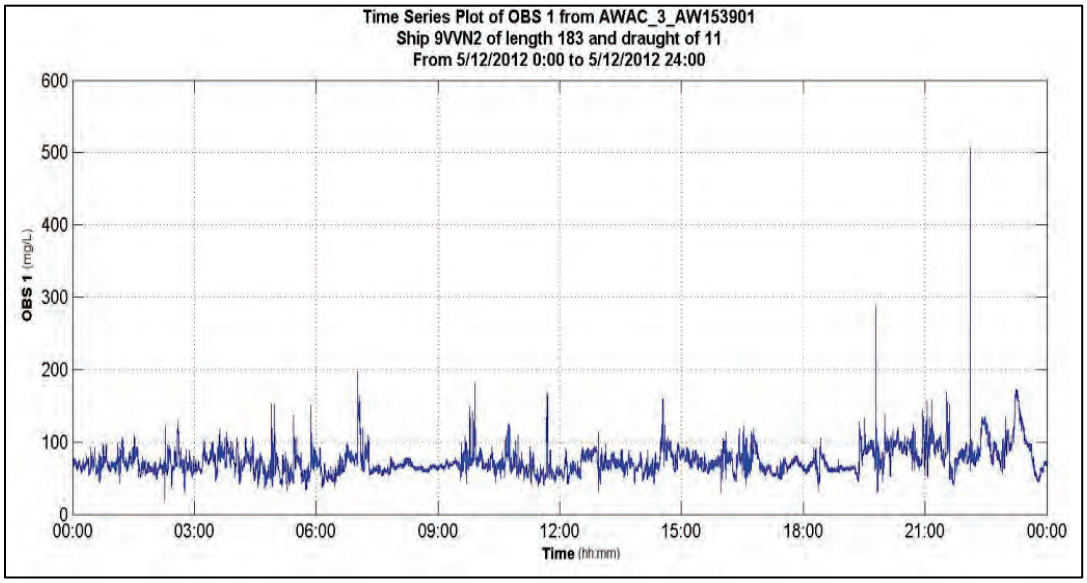

Figure 110. Concentration at AWAC 4 on 12 May 2012.

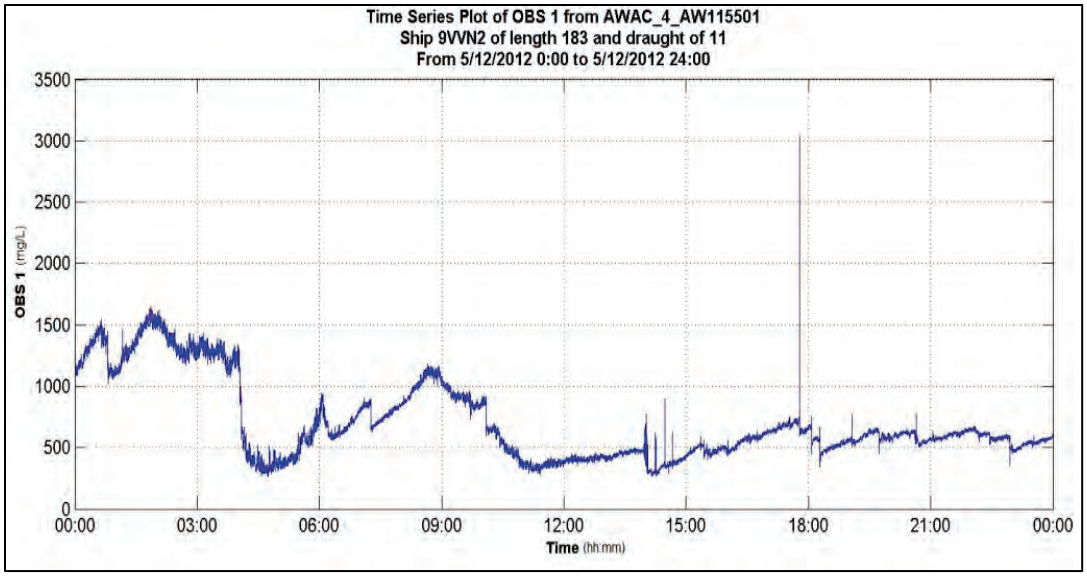

Appendix B: Graphical User Interface (GUI) Analysis Tool

A MATLAB GUI was created to simplify organizing the data for analysis. Figure 111 through Figure 120 exhibit the different applications that can be performed through the GUI. Figure 111 is an overall view of the entire GUI separated into sections that are explained below.

Figure 111. Overview of GUI.

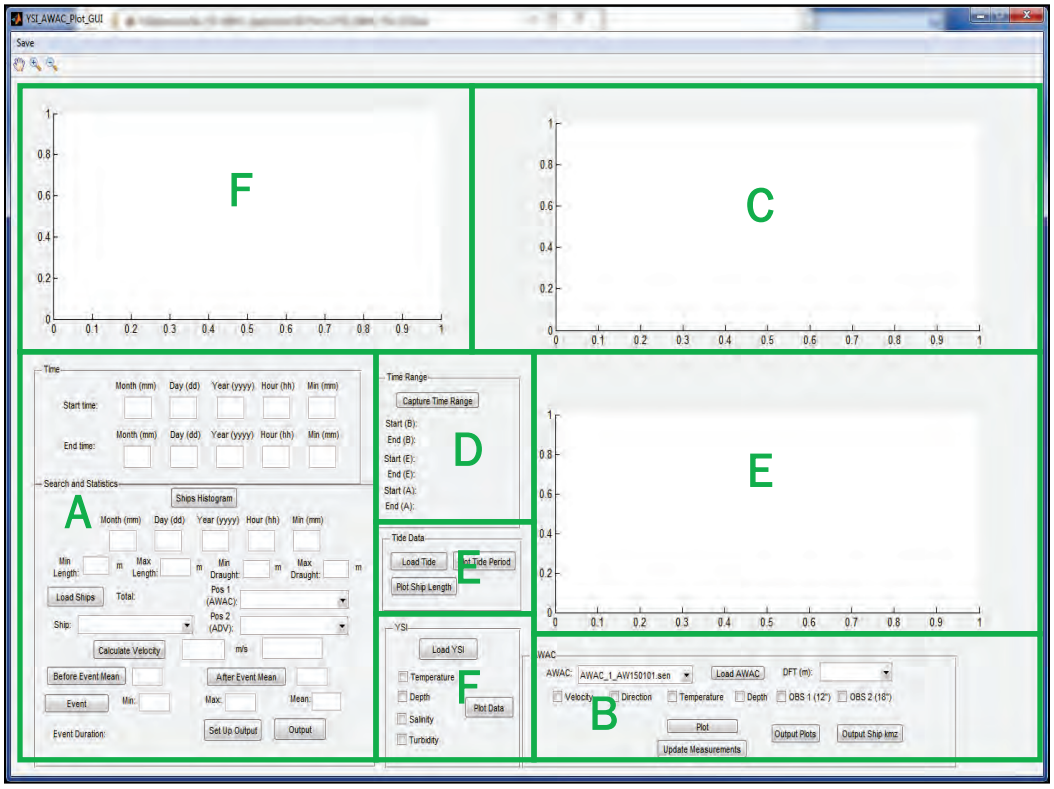

The characteristics of the vessels may be specified to search for a certain range (such as the length and draft for the classes stated earlier) and date as shown in Figure 112 (Section A).

Figure 112. Section A: Search by characteristics.

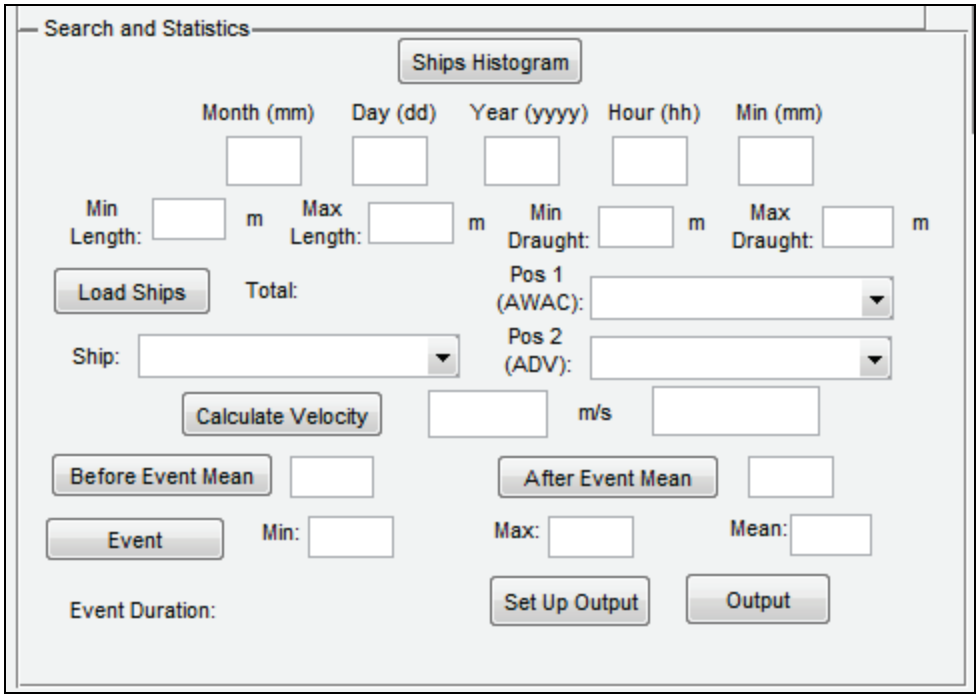

For instance, when conducting the analysis, all vessels within the range of length 0–300 m and draft (draught in the GUI) 5–30 m on 12 May 2012 were selected to capture all vessels for that day. A time must also be entered, and the GUI searches within ±30 minutes of this time. The characteristics of these vessels along with the time were then documented.

Figure 113 shows that after entering the search restrictions, the ships with those characteristics appear in a drop-down menu. A ship is chosen from the drop-down, and the POS1 and POS2 appear for that ship as seen in Figure 114.

Figure 113. Section A: Vessel search results example.

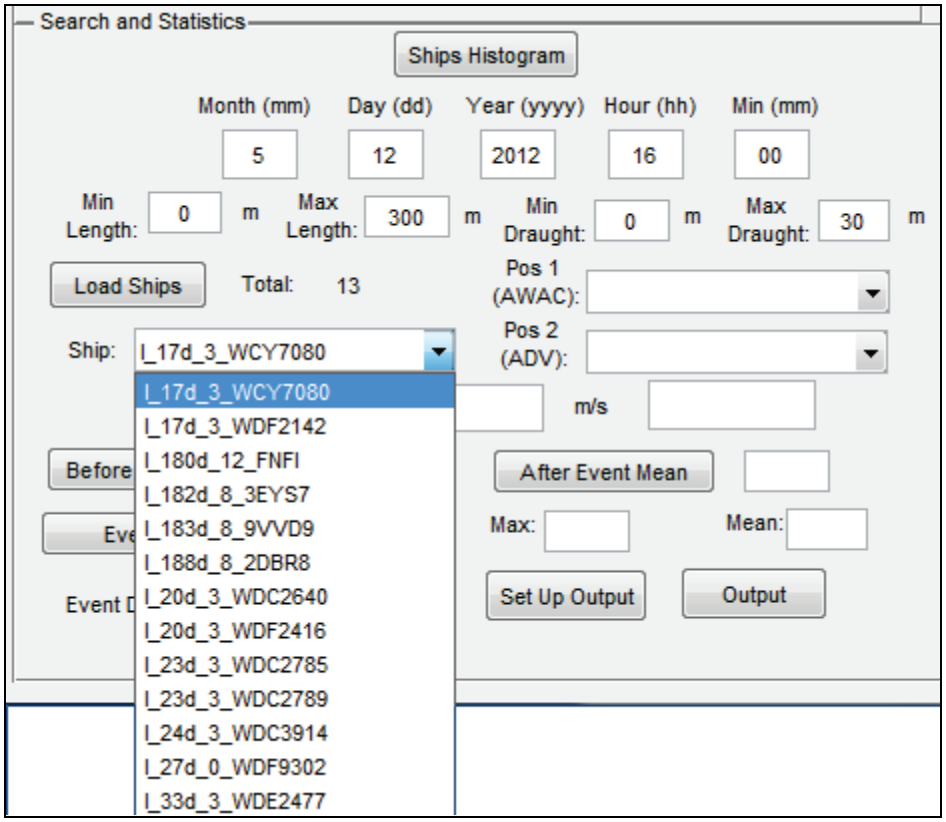

Figure 114. Section A: Vessel with POS1 and POS2, velocity, direction, and time frame of plot.

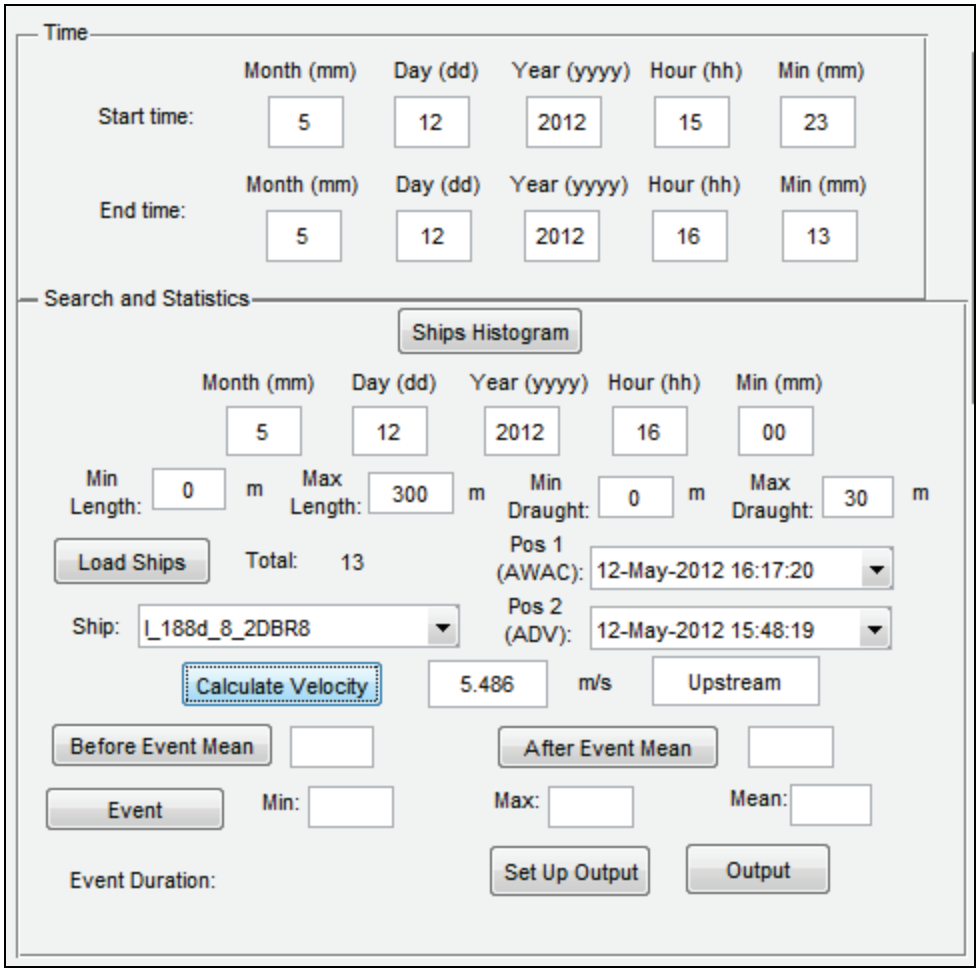

Some vessels make numerous trips per day causing multiple POS1 and POS2 for a single vessel and date. Since more than one POS1 and POS2 may exist for a vessel, the desired time must be chosen, and then the velocity can be calculated between those positions along with the direction in which the vessel is traveling (upstream or downstream). The next step is to choose the AWAC to analyze as shown in Figure 115 (Section B).

Figure 115. Section B: Choosing and loading AWAC to analyze.

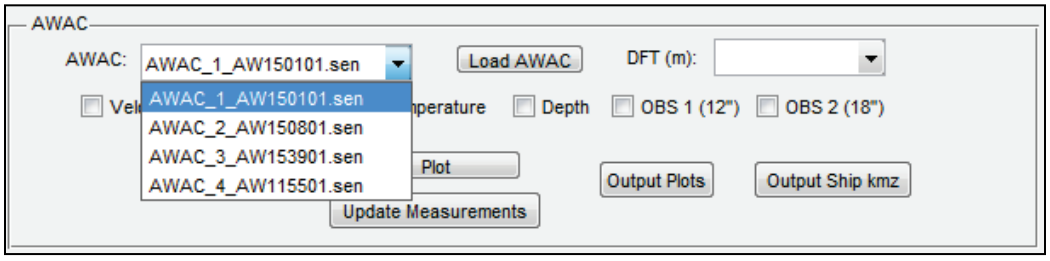

After choosing the AWAC and loading it, the data for water velocity, direction, temperature, depth (from the water surface to the top of the instrument), and total suspended material concentration (OBS1) may be plotted on the *y*-axis with time on the *x*-axis. For instance, in Figure 116, the velocity observed at AWAC1 at a depth of 2.2 m is chosen to plot.

Figure 116. Section B: The velocity at depths of 1.2, 2.2, 3.2, or 4.2 may be plotted.

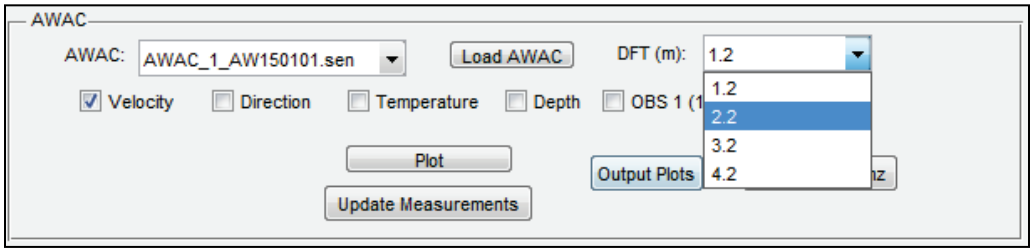

An automatic time range of 50 minutes is used for the data plot after selecting the vessel, but this may be changed. The time on the *x*-axis of the plot is specified by inputting in the boxes shown in Figure 117, followed by an example plot in Figure 118 (Section C). This example plot shows the automatic 50-minute period.

Figure 117. Section A: Specified time range for plot.

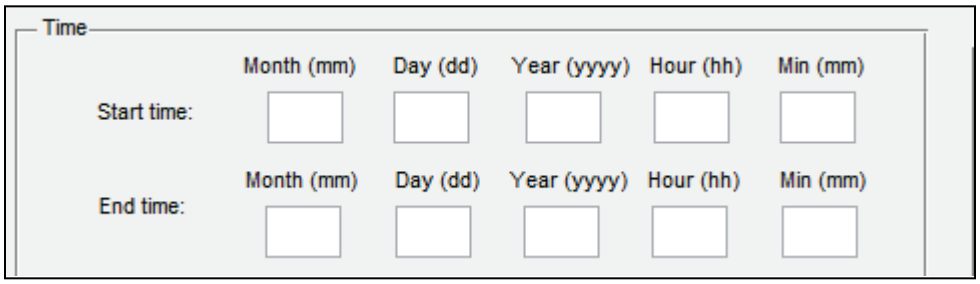

Figure 118. Section C: Plot of specified characteristic in automatic 50-minute time range.

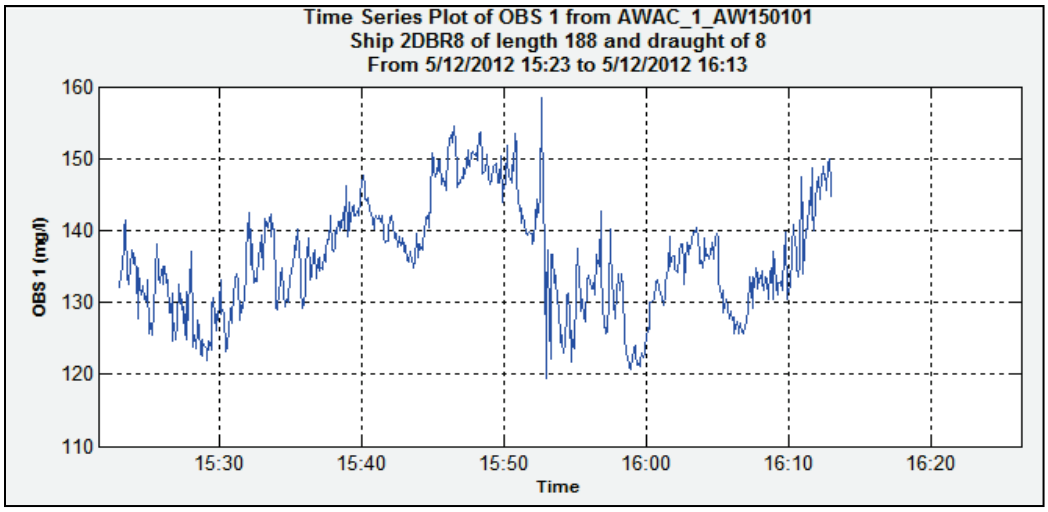

Time ranges may then be specified to capture events as shown in Figure 119 (Section D). The data within the event time range is then used for calculations shown in Figure 120 by selecting "Update Measurements" in Section B. These results may then be output to a file. Sections E and F in Figure 101 allow the tide and YSI data—temperature, specific conductivity, salinity, and turbidity—collected from the ADV to be uploaded and analyzed. Analysis of the YSI data was not done for the present study.

Figure 119. Section D: To capture events, a time range may be specified.

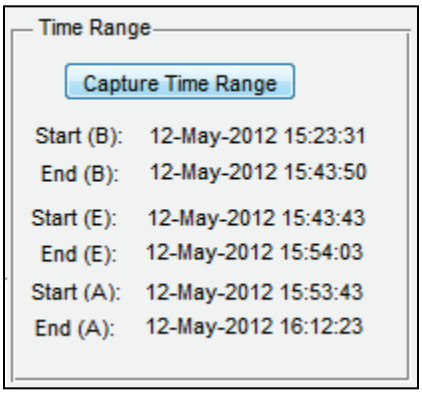

Figure 120. Section A: The calculations for the event period.

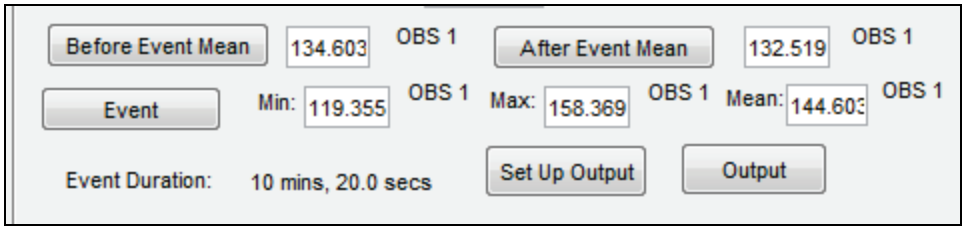

Appendix C: ADCP Concentration Plots

The following are plots of the ADCP concentration and vessel characteristic data that were collected behind passing vessels on 12 May 2012.

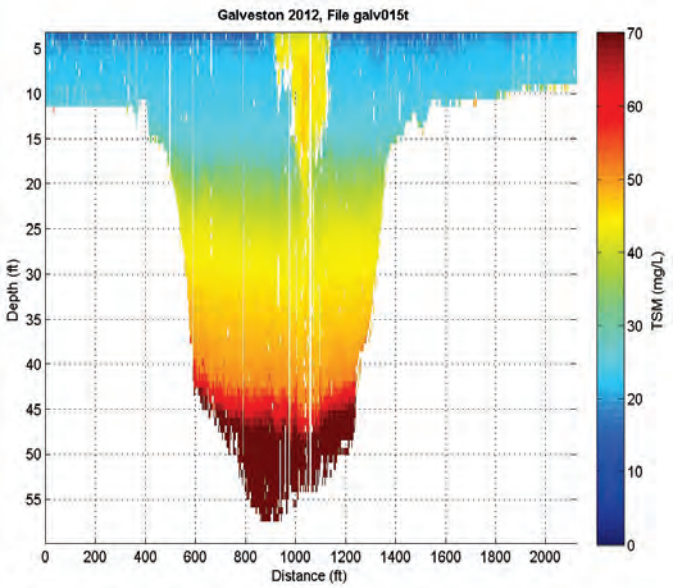

Vessel	NA
Type	NA
Length(m)	NA
Beam(m)	NA
Draft(m)	NA
Speed(avg, m/s)	NA

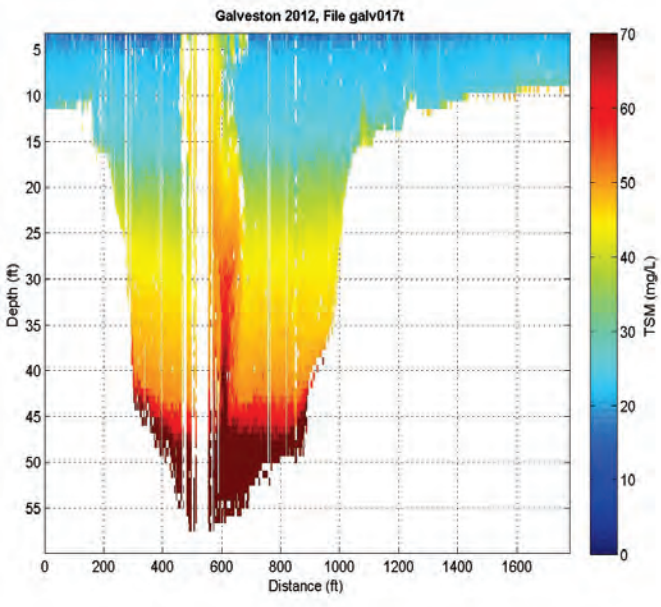

Vessel	*Eagle Matsayama*
Type	Oil tanker
Length(m)	182
Beam(m)	33
Draft(m)	12
Speed(avg, m/s)	6.33

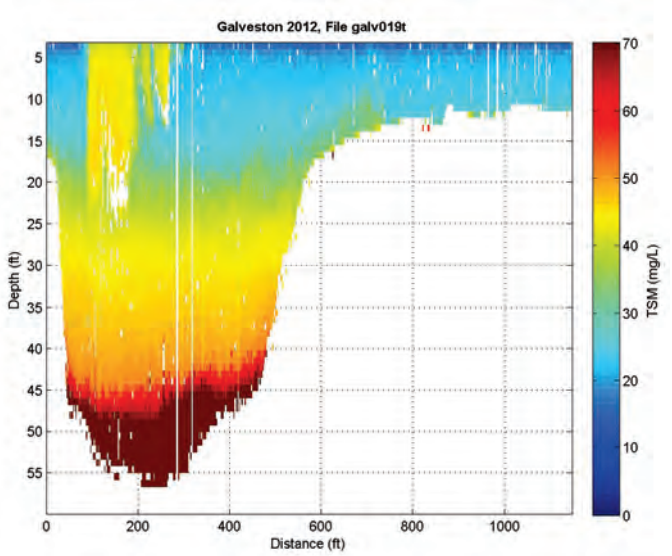

Vessel	*MSC Brianna*
Type	Container ship
Length(m)	245
Beam(m)	33
Draft(m)	7
Speed(avg, m/s)	5.61

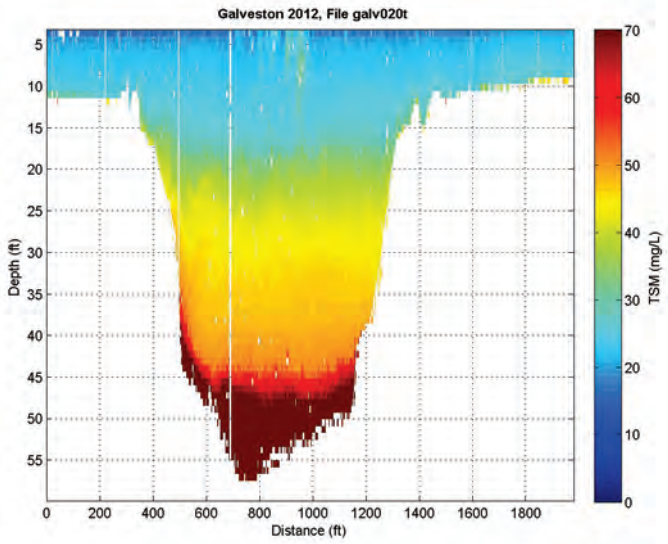

Vessel	NA
Type	Single tow; Double tow
Length(m)	NA
Beam(m)	NA
Draft(m)	NA
Speed(avg, m/s)	NA

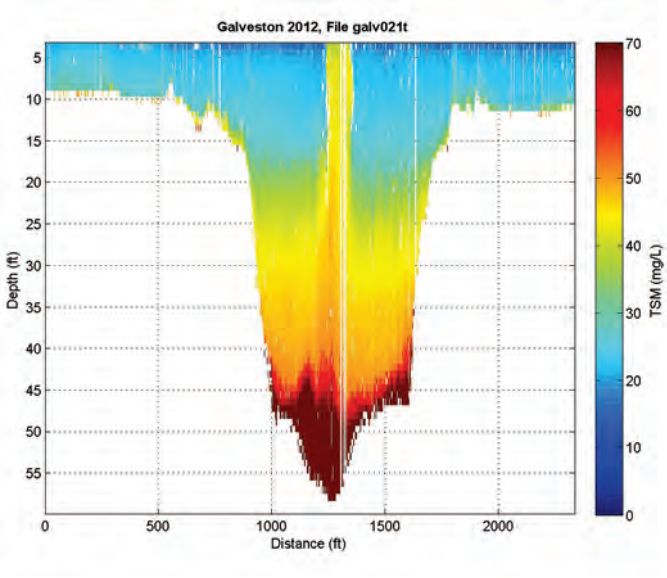

Vessel	NA
Type	NA
Length(m)	NA
Beam(m)	NA
Draft(m)	NA
Speed(avg, m/s)	NA

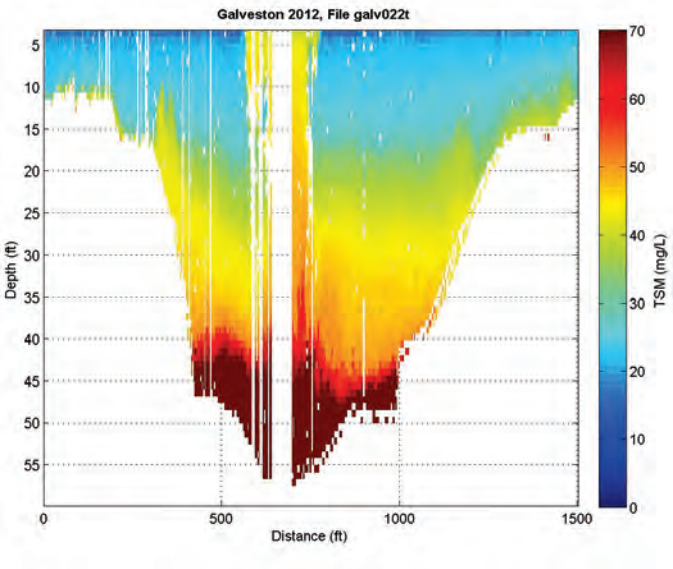

Vessel	*Pigeon Point; FSL Hamburg; Corpus Christi*
Type	Chemical tanker; Oil tanker; Pusher tug
Length(m)	188; 183; 184
Beam(m)	32; 32; 22
Draft(m)	12; 9; 9
Speed(avg, m/s)	7.46; 5.97; 5.35

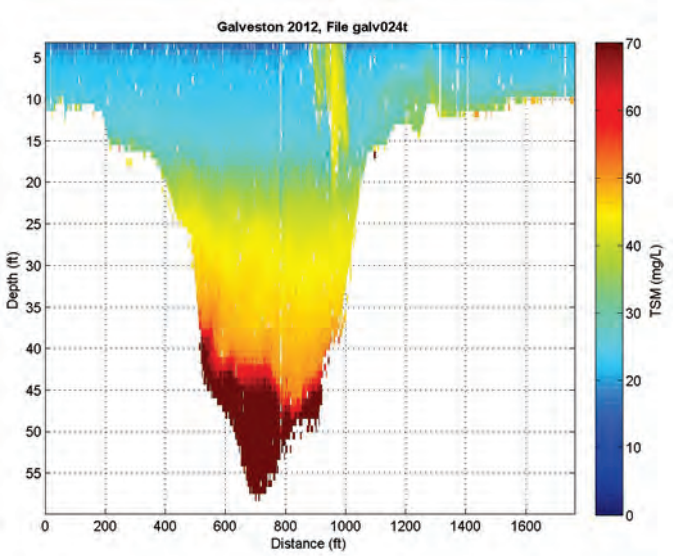

Vessel	NA
Type	NA
Length(m)	NA
Beam(m)	NA
Draft(m)	NA
Speed(avg, m/s)	NA

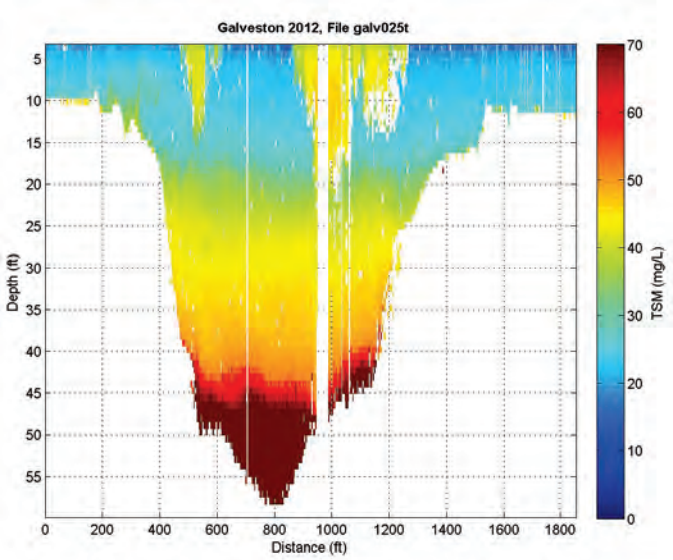

Vessel	*Cernia Crosby*
Type	Single tow
Length(m)	NA
Beam(m)	NA
Draft(m)	NA
Speed(avg, m/s)	NA

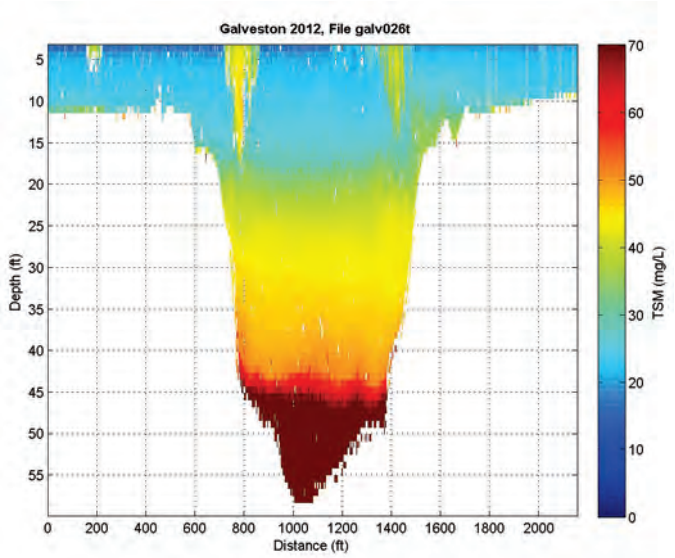

Vessel	*Buckskin; Endurance*
Type	Tug; Container ship
Length(m)	20; 135
Beam(m)	8; 22
Draft(m)	3; 9
Speed(avg, m/s)	3.65; 8.49

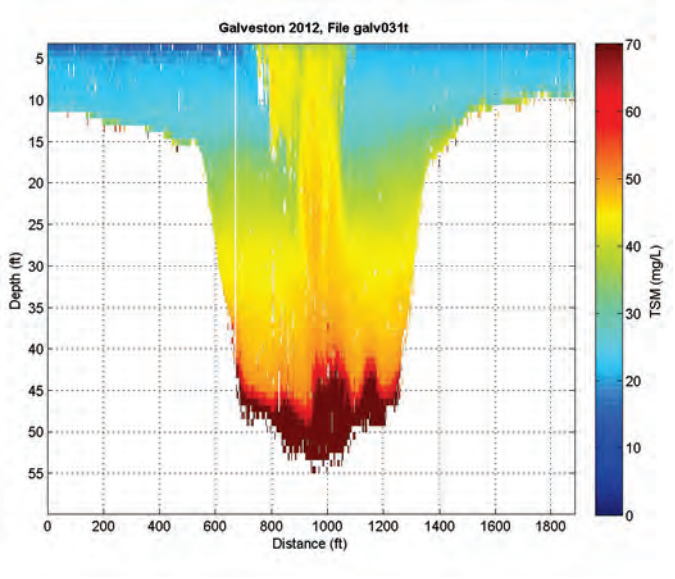

Vessel	*George Tut; Ladylin*
Type	Container ship
Length(m)	264;
Beam(m)	32;
Draft(m)	11;
Speed(avg, m/s)	7.56;

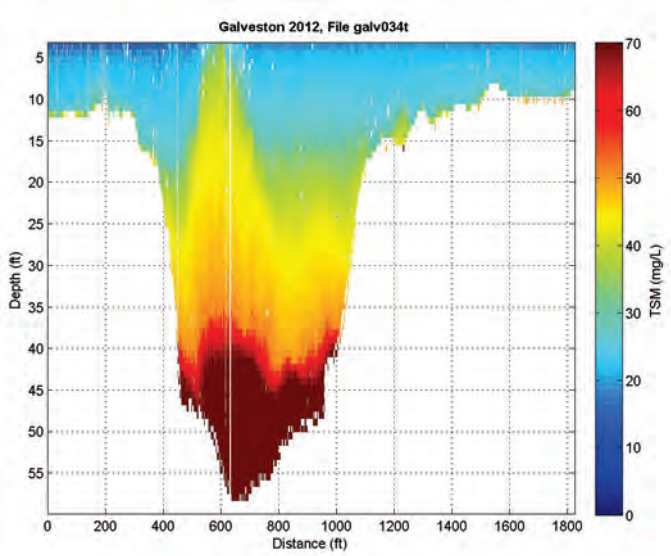

Vessel	*Box Trader*
Type	Container ship
Length(m)	228
Beam(m)	32
Draft(m)	10
Speed(avg, m/s)	4.48

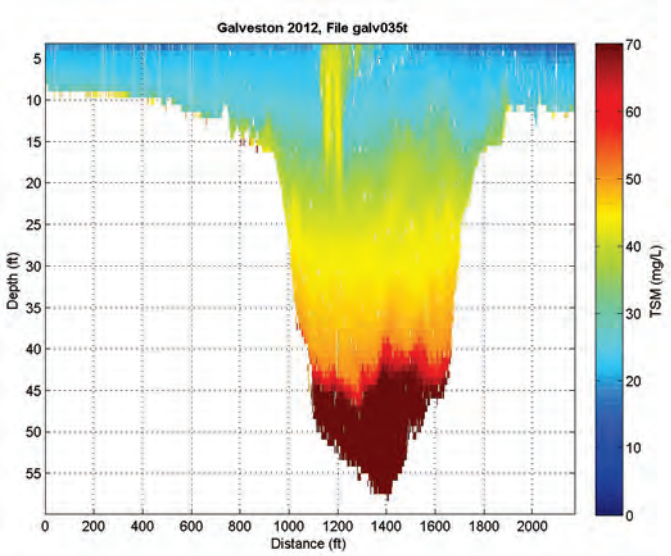

Vessel	*WH Blount*
Type	Bulk carrier
Length(m)	225
Beam(m)	32
Draft(m)	8
Speed(avg, m/s)	6.58

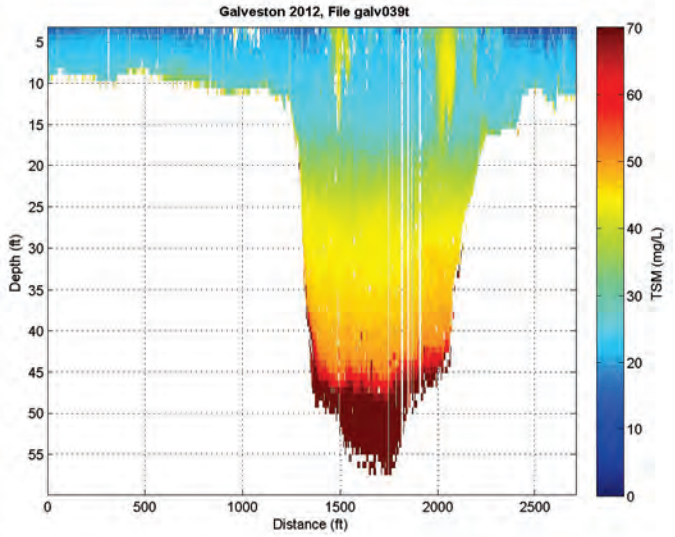

Vessel	*San Bernard*
Type	Oil/Chemical tanker
Length(m)	106
Beam(m)	16
Draft(m)	5
Speed(avg, m/s)	5.71

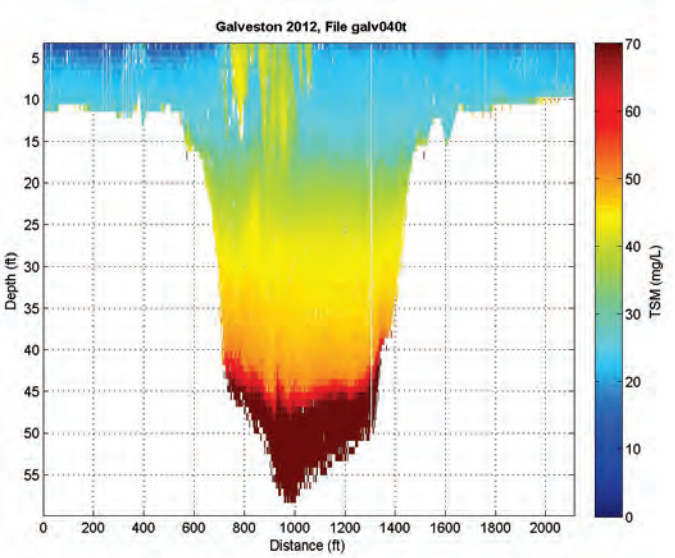

Vessel	*Ocean Crescent; Carol Brent; Eagle Dewall; Martin Navigator; Industrial Century*
Type	General cargo; NA; NA; Tug; General cargo
Length(m)	120; NA; NA; NA; 120
Beam(m)	20; NA; NA; NA; 20
Draft(m)	6; NA; NA; NA; 6
Speed(avg, m/s)	4.99; NA; NA; NA; 6.02

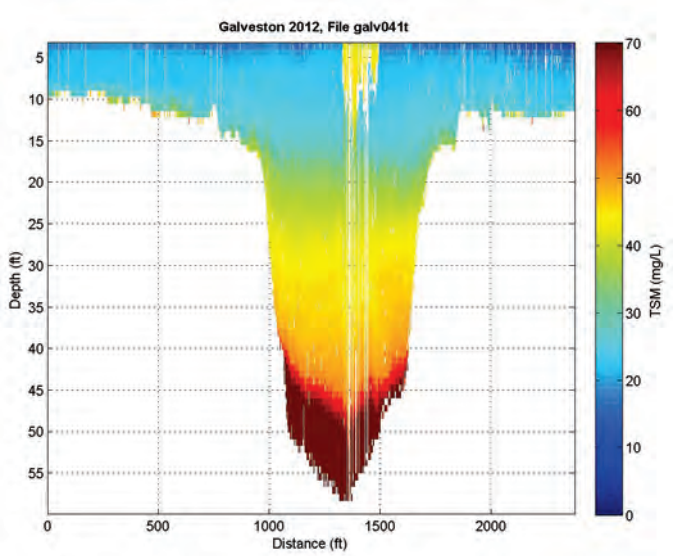

Vessel	NA
Type	NA
Length(m)	NA
Beam(m)	NA
Draft(m)	NA
Speed(avg, m/s)	NA

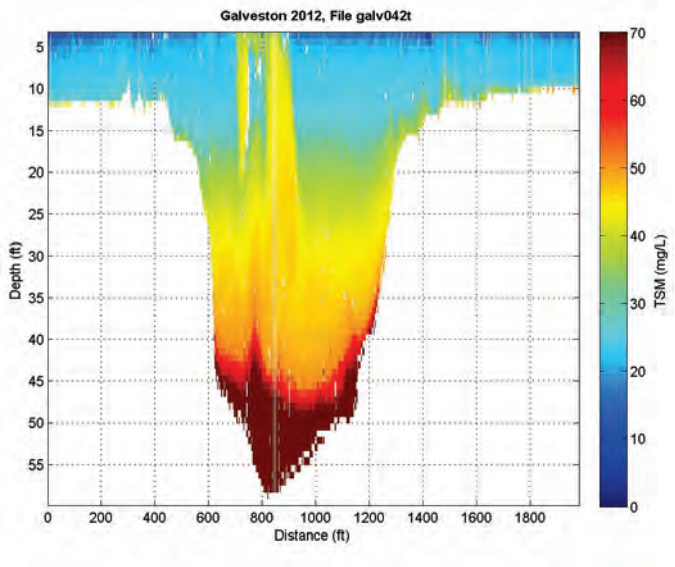

Vessel	*Donnie Sonier*
Type	Tug
Length(m)	22
Beam(m)	10
Draft(m)	0
Speed(avg, m/s)	2.98

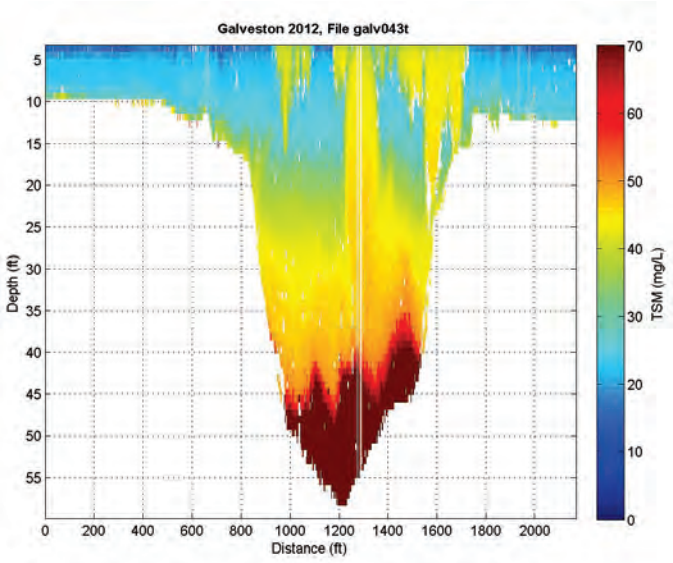

Vessel	*Eagle Sydney; Frida Maersk*
Type	Oil tanker; Oil/Chemical tanker
Length(m)	229; 177
Beam(m)	42; 28
Draft(m)	9; 9
Speed(avg, m/s)	6.02; 6.89

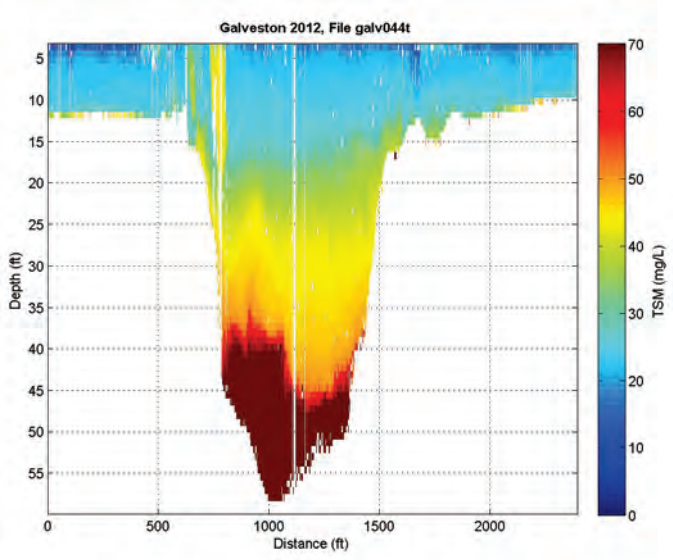

Vessel	*The Rock; Maersk Wolfsburg; Marquette*
Type	Oil/Chemical tanker; Container ship; NA
Length(m)	184; 175; NA
Beam(m)	27; 28; NA
Draft(m)	10; 8; NA
Speed(avg, m/s)	6.33; 7.92; NA

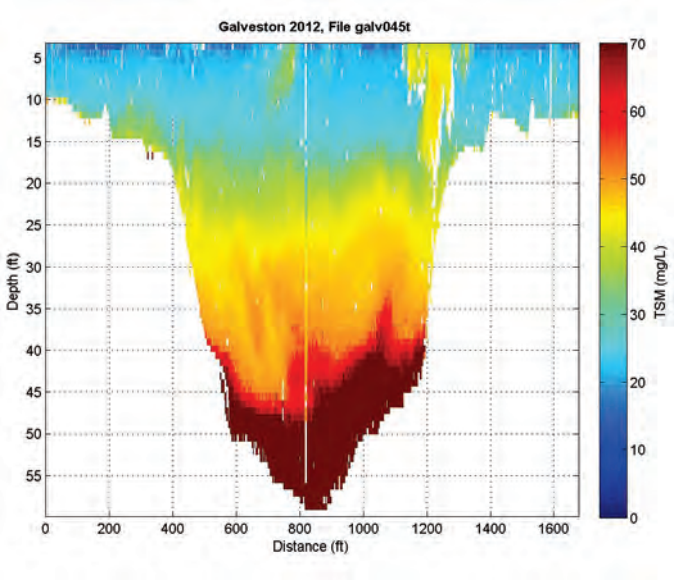

Vessel	*Lorette*
Type	Pusher tug
Length(m)	20
Beam(m)	8
Draft(m)	3
Speed(avg, m/s)	3.6

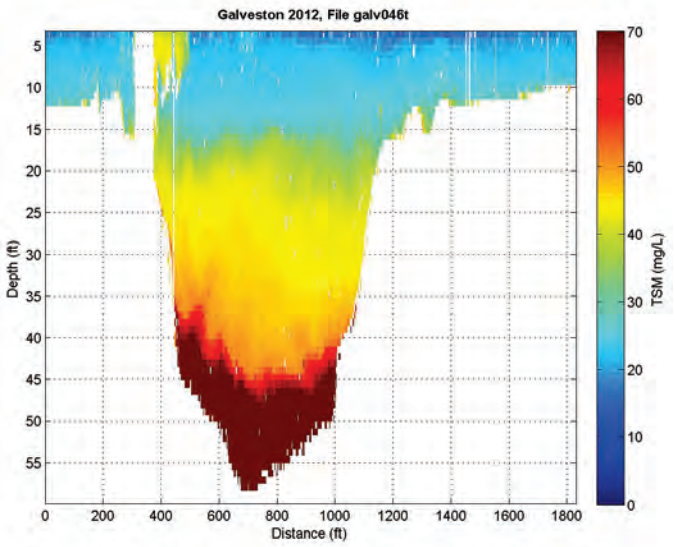

Vessel	*Cove Point*; NA
Type	Tug; Double tow
Length(m)	22; NA
Beam(m)	7; NA
Draft(m)	3; NA
Speed(avg, m/s)	2.98; NA

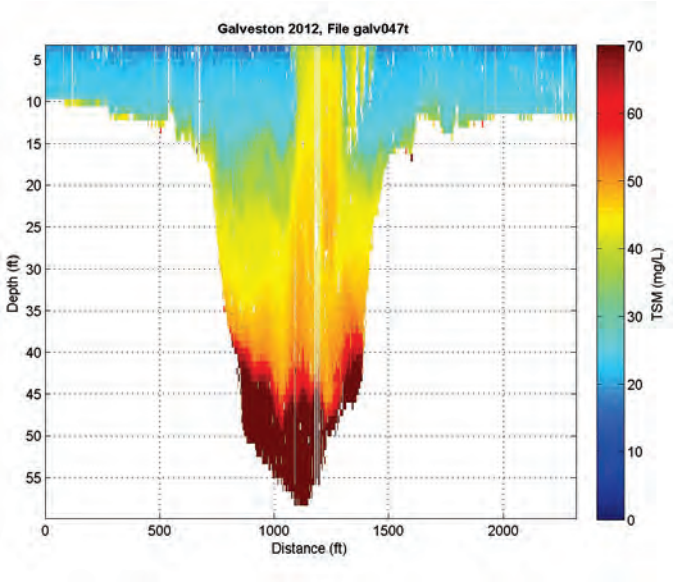

Vessel	*T.H. Kelly*
Type	Tug
Length(m)	27
Beam(m)	10
Draft(m)	3
Speed(avg, m/s)	3.76

REPORT DOCUMENTATION PAGE

Form Approved
OMB No. 0704-0188

1. REPORT DATE	2. REPORT TYPE	3. DATES COVERED *(From - To)*
December 2014	Final Report	Oct. 2009 – Sept. 2012

4. TITLE AND SUBTITLE

Houston-Galveston Navigation Channel Shoaling Study

5a. CONTRACT NUMBER

5b. GRANT NUMBER

5c. PROGRAM ELEMENT NUMBER

6. AUTHOR(S)

Jennifer Tate, Brittany Gunkel, Julie Rosati, Eric Wood, Alejandro Sanchez, Rob Thomas, Naveen Ganesh, and Thad Pratt

5d. PROJECT NUMBER

5e. TASK NUMBER

5f. WORK UNIT NUMBER

7. PERFORMING ORGANIZATION NAME(S) AND ADDRESS(ES)

U.S. Army Engineer Research and Development Center
Coastal and Hydraulics Laboratory
3909 Halls Ferry Road
Vicksburg, MS 39180

8. PERFORMING ORGANIZATION REPORT NUMBER

ERDC/CHL TR-14-14

9. SPONSORING/MONITORING AGENCY NAME(S) AND ADDRESS(ES)

10. SPONSOR/MONITOR'S ACRONYM(S)

11. SPONSOR/MONITOR'S REPORT NUMBER(S)

12. DISTRIBUTION/AVAILABILITY STATEMENT

Approved for public release; distribution is unlimited.

13. SUPPLEMENTARY NOTES

14. ABSTRACT

The Monitoring Completed Navigation Projects (MCNP) program evaluates the performance of civil works navigation projects to advance coastal and hydraulic engineering technology and guidance. Monitoring is designed to understand how well projects are achieving their design goals to ultimately develop more accurate and cost-effective engineering solutions for US Army Corps of Engineers (USACE) coastal and hydraulic problems. Through the MCNP, design criteria and methods, construction practices, and Operation and Maintenance (O&M) techniques are improved. The monitoring program also identifies where present technology is inadequate or where additional research is required. The Houston-Galveston Navigation Channel (HGNC) MCNP study was initiated in 2009 to determine the causes of an unanticipated increase in channel shoaling, which occurred after deepening and widening was completed in 2005. Commercial traffic in Galveston Bay began in 1837 through a shallow natural channel. Recent deepening and widening of the Houston-Galveston Navigation Channel was authorized to accommodate larger vessels and meet safety and efficiency requirements of the Port of Galveston and Port of Houston. When designing the most recent channel improvement, the USACE Galveston District calculated future shoaling and the associated required placement area capacity based on historical O&M data. The District anticipated that the trends from 1948-1995 would continue and the only increase in O&M dredging would be caused by the lengthening of the channel offshore. The final design estimated 1.42 Million cubic yards (Mcy) per year maintenance dredging for the 45 ft x 530 ft channel, whereas the actual has been estimated by some methods to be much more. Nine hypotheses were developed to explain the unanticipated increase in navigation channel shoaling after channel improvements. These hypotheses were tested through historical analysis, field data collection, and numerical modeling. Goals of the study were to determine why the HGNC is shoaling more than anticipated by the pre-enlargement analysis and planned disposal practices as well as to develop standards to aid future channel enlargement O&M plans. These methods were based on analytical computations, modeling, and field data analysis.

15. SUBJECT TERMS		
Monitoring Completed Navigation Projects (MCNP)	Coastal Modeling System (CMS)	Navigation channel shoaling
Adaptive Hydraulics (AdH)	Particle Tracking Model (PTM)	Dredge disposal
	Houston Ship Channel (HSC)	

16. SECURITY CLASSIFICATION OF:			17. LIMITATION OF ABSTRACT	18. NUMBER OF PAGES	19a. NAME OF RESPONSIBLE PERSON
a. REPORT	b. ABSTRACT	c. THIS PAGE			
UNCLASSIFIED	UNCLASSIFIED	UNCLASSIFIED	UNLIMITED	154	19b. TELEPHONE NUMBER *(Include area code)*